

CHARACTERIZATION OF THE SPATIAL VARIABILITY OF MILL  
TAILINGS HYDRAULIC PROPERTIES:  
A STATISTICAL AND GEOSTATISTICAL ANALYSIS

by

Gary D. Johnson

Submitted in Partial Fulfillment of  
the Requirements for the Degree of  
Master of Science in Hydrology

New Mexico Institute of Mining and Technology  
Socorro, New Mexico

March, 1987

Geotechnical  
Information Center

N.M. BUREAU OF MINES  
AND MINERAL RESOURCES  
SOCORRO, N.M. 87801

## ACKNOWLEDGEMENTS

I wish to thank my advisor, Dr. Allan Gutjahr, for his help and direction which enabled this study to occur. In addition, I would like to thank Dr. Daniel Stephens for his guidance on the data collection aspect of this study.

The author also wishes to thank the United States Bureau of Mines, Mineral Institute Waste Treatment and Recovery Generic Center for providing the funding for this project. In addition, I express my thanks to ASARCO for allowing us to perform research on their tailings impoundment.

Special thanks goes to my partner Ken Harris for helping to keep me going during rough periods and also, by helping to enable these combined projects to be a success. In addition, I would like to thank the people who helped us in the field (and also at La Tasa's Drive In): Barb Kickham, Debra McElroy, Marcy Leavitt, Warren Cox, Jeff' Havelena, Greg Little, and Deena Stanley. Also, I thank our invaluable lab assistants Todd Stein, Tracy McFarland, Mary Stollenwertz, and Robert Mace.

Very special thanks goes to my parents and family for their understanding and support over the last few years. I would also like to thank my good friend Tim Brooks for helping me to retain my sanity at least part of the time. Finally, I would like to thank the friendly folks who brew and distribute Coors beer throughout the great Southwest. Enjoy.

ABSTRACT

In order for a more representative estimate of seepage through a tailings impoundment to be formulated, the spatial variability of the hydraulic properties in the mill tailings must be addressed. Tailings impoundments are far from homogeneous environments and should not be considered such when forming predictions on seepage.

This study was performed on an abandoned lead/zinc tailings impoundment in west-central New Mexico. The method of tailings deposition at this site was an upstreaming peripheral discharge system. Generally, this type of system produces a sedimentary structure that coarsens vertically upward and fines laterally away from the emitters.

The use of galvanized, thin wall samples (shelby tubes) recovered with the aid of a drilling rig was the most advantageous method of sampling. The samples were obtained from a cross section made up of horizontal transects at 2 given depths and 6 vertical transects. Hydraulic parameters tested included  $K(\text{sat})$ , porosity, moisture content/pressure head relationships ( $\theta/\psi$ ), and particle size. In situ moisture content was measured with a neutron-probe moisture meter. Problems were encountered using this device in tailings.

Particle size decreased towards the central portion of the cross section but was fairly constant with depth. Porosity increased slightly towards the center and exhibited a general decrease with depth.  $K(\text{sat})$  decreased both towards the central portion of the cross section and with depth. The decrease in  $K$  and  $n$  with depth is believed to be the result of matrix compaction due to increased overburden. The upper 50 cm of the tails throughout the cross section were found to be compositionally and structurally different from the tails at greater depths.

The calculation of sample statistics (mean, standard deviation, range) for the horizontal and vertical transects was an effective method of delineating the variability along each sampling line. This method, however, relayed no information about the structure of this variability.

Regression analyses were employed in an attempt to characterize trends in the data throughout the cross section. 2-D regression equations were formulated for the variables  $K(\text{sat})$ ,  $n$ ,  $\theta_{1.5}$ , and  $d_{10}$  with good success. This method, however, was not able to effectively characterize discontinuities in the data that are common in such a layered system.

Construction of variograms showed that  $\theta_{1.5}$  was the only variable that retained any structure after the trends had been removed. Kriged estimates of the  $\theta_{1.5}$  distribution were formulated throughout the cross section. This type of analysis appears to be the most representative method of characterization. However, due to the lack of structure in all but one variable, only a limited amount of information could be gained using variogram and kriging analyses.

Correlation coefficients were determined between various data distributions. The greatest correlation with each dependent

variable was noted for the moisture content  $\theta_{1.5}$  and grain size parameter  $d_{34}$ . Predictive equations were developed using multiple regression analyses.



TABLE OF CONTENTS

ACKNOWLEDGEMENTS .....	i
ABSTRACT .....	ii
TABLE OF CONTENTS .....	iv
LIST OF TABLES .....	vi
LIST OF FIGURES .....	vii
I. INTRODUCTION .....	1
Previous Work .....	4
II. SITE DESCRIPTION .....	5
Field Site History .....	7
Waldo/Graphic Mine .....	7
Waldo Mill .....	9
Tailings Impoundment .....	11
Chemical Analyses .....	17
III. DATA COLLECTION .....	19
Sampling Locations .....	19
Shelby Tubes .....	19
Neutron Access Tubes .....	27
Sampling Procedures .....	29
Obtaining Undisturbed Sample Cores .....	29
Installation of Neutron Access Tubes .....	36
Laboratory and Field Procedures .....	37
Hydraulic Conductivity .....	37
Sample Extrusion .....	37
$\theta/\psi$ Relationships .....	38
Particle Size Analysis .....	40
Neutron Probe .....	40
Presentation of Data .....	40
Particle Size Distribution .....	41
Pore Size Distribution .....	52
Hydraulic Conductivity Distribution .....	60
In situ Moisture Content .....	68
IV. METHODS OF CHARACTERIZATION .....	71
Introduction .....	71
Sample Statistics .....	72
Results .....	72
Conclusions .....	77
Regression Analyses .....	82
Theory .....	82
1-D Horizontal .....	87
1-D Vertical .....	102
2-D Cross Section .....	110
Conclusions .....	120
Geostatistical Analyses .....	121
Previous Work .....	121
Variogram Analysis .....	122
Theory .....	122

	Analysis .....	125
	Fitting Variogram Models .....	129
	Kriging Analysis .....	131
	Theory .....	131
	Analysis .....	133
	Kriging Variance .....	134
	Validation .....	136
	Conclusions .....	139
V.	SUMMARY .....	141
VI.	RECOMMENDATIONS FOR FUTURE WORK .....	145
	Predictive Equations .....	146
	REFERENCES .....	150
	APPENDIX .....	153
	List of Appendices .....	154

LIST OF TABLES

Table 1.	Water chemistry analyses .....	17
Table 2.	Horizontal transects statistics .....	72
Table 3.	Vertical transects statistics .....	73
Table 4.	Statistical Values from the Van Stone lead/zinc tailings impoundment .....	75
Table 5.	Least squares regression statistics, 1-D horizontal .....	88
Table 6.	Least squares regression statistics, 1-D vertical .....	103
Table 7.	Least squares regression statistics, 2-D cross section .....	110
Table 8.	Correlation coefficients between the various data distributions .....	147
Table 9.	Final predictive equations using multiple regression analyses .....	149
Table A1.	Output from hydraulic conductivity program MANOMET .....	A-5
Table J1.	Sample statistics for layer 1 .....	A-63
Table J2.	Sample statistics for the underlying soil .	A-64

LIST OF FIGURES

1.	Locations within the United States of mining and processing wastes .....	2
2.	Location map of field site .....	6
3.	Geology of the field site area .....	"
4.	Blueprint of the mill-site, 1916 .....	10
5.	Topographic map of the Waldo Mill tailings impoundment .....	12
6.	Diagram of the upstream method of tailings disposal .....	15
7.	Conceptual model of material variation within a tailings deposit .....	20
8.	Topographic map of the Waldo Mill tailings impoundment .....	21
9.	Locations of sampling transects and neutron probe access tubes .....	23
10.	Conceptual model of material variation along the cross section .....	24
11.	Cross section showing position of shelby tube samples .....	26
12.	Cross section showing position of vertical transects .....	28
13.	Cross section showing position of neutron access tubes .....	30
14.	Photograph of 'slime' sample core .....	34
15.	Locations of permeability and particle size samples within a shelby tube .....	39
16.	Plot of the range in grain size curves exhibited throughout the cross section .....	42
17.	Soil textural triangle comparing particle size extremes from the cross section .....	42
18a.	$d_{10}$ distribution laterally at 205 cm depth .....	44
" b.	$d_{10}$ distribution with depth for each transect .....	"
" c.	" " " " " " " " " " " " " " .....	"
19a.	$d_{50}$ distribution laterally at 205 cm depth .....	45
" b.	$d_{50}$ distribution with depth for each transect .....	"
" c.	" " " " " " " " " " " " " " .....	"
20a.	$d_{84}$ distribution laterally at 205 cm depth .....	46
" b.	$d_{84}$ distribution with depth for each transect .....	"
" c.	" " " " " " " " " " " " " " .....	"
21.	Diagram showing possible reason for the grain size discontinuity at 62 m .....	49
22a.	UC distribution laterally at 205 cm depth .....	50
" b.	UC distribution with depth for each transect .....	"
" c.	UC " " " " " " " " " " " " " " .....	"
23.	Plot of the range in grain size curves for the underlying soil .....	53
24.	Soil textural triangle comparing particle size extremes from the underlying soil .....	53
25.	Plot of the range in pore size distribution for the cross section .....	54
26a.	Porosity distribution laterally at 205 cm depth ...	56
" b.	Porosity distribution with depth for each transect .	"
" c.	" " " " " " " " " " " " " " .....	"

27a.	$\theta_{1.5}$	distribution laterally at 205 cm depth	58
" b.	$\theta_{1.5}$	distribution with depth for each transect	"
" c.	$\theta_{1.5}$	" " " " " "	"
28a.	$\theta_{15}$	distribution laterally at 205 cm depth	59
" b.	$\theta_{15}$	distribution with depth for each transect	"
" c.	$\theta_{15}$	" " " " " "	"
29.	log K	distribution laterally at 28 cm depth	61
30.	"	" " " 41 cm "	"
31.	"	" " " 54 cm "	62
32.	"	" " " 165 cm "	"
33.	"	" " " 179 cm "	63
34.	"	" " " 192 cm "	"
35.	"	" " " 205 cm "	64
36.	log K	distribution with depth, transect V11	"
37.	"	" " " " , transect V10	"
38.	"	" " " " , transect V75	65
39.	"	" " " " , transect V47	"
40.	"	" " " " , transect V7	"
41.	"	" " " " , transect V6	"
42.		Range in hydraulic conductivity values for the cross section	67
43.	$\theta_F$	distribution with depth, tube #6	70
44.	$\theta_F$	" " " , tube #9	"
45.	$\theta_F$	" " " , tube #10	"
46.	$\theta_F$	" " " , tube #11	"
47.		Mean and standard deviation values of $d_{50}$ for each transect	76
48.		Mean and standard deviation values of $\theta_{1.5}$ for each transect	76
49.		Mean and standard deviation values of log K for each transect	76
50.		Mean vs. standard deviation values for $d_{10}$ from the vertical transects	78
51.		Mean vs. standard deviation values for $d_{50}$ from the vertical transects	78
52.		Mean vs. standard deviation values for $d_{34}$ from the vertical transects	79
53.		Standard deviations of $d_{50}$ vs. $\theta_{1.5}$ from the vertical transects	79
54.		Standard deviations of $d_{50}$ vs. log K from the vertical transects	81
55.		Standard deviations of $\theta_{1.5}$ vs. log K from the vertical transects	81
56a.		Regression fits to the $d_{30}$ data, 205 cm depth	90
" b.		Normality plot for figure 56a ( $d_{30}$ , all data, 205cm)	"
" c.		" " " " 56a ( $d_{30}$ , data deleted, 205 cm)	91
57a.		Trends in $\theta$ at the 205 cm depth ( $n$ , $\theta_{1.5}$ , $\theta_{15}$ )	"
" b.		Normality plot for figure 57a ( $n$ , 205 cm)	93
" c.		" " " " 57a ( $\theta_{15}$ , 205 cm)	"
58a.		Regression fits to the $\theta_{1.5}$ data, 205 cm depth	94
" b.		Normality plot for figure 58a ( $\theta_{1.5}$ , all data, 205cm)	"
" c.		" " " " 58a ( $\theta_{1.5}$ , data deleted, 205 cm)	96

59a. Regression fit to the log K data, 28 cm depth ..... 96  
 " b. Normality plot for figure 59a (log K, 28 cm) ..... 97  
 60. Regression fit to the log K data, 179 cm depth ..... "  
 61a. Trends in log K at various depths ..... 98  
 " b. Normality plot for figure 61a (log K, 54 cm) ..... "  
 " c. " " " " 61a (log K, 165 cm) ..... 100  
 " d. " " " " 61a (log K, 179 cm) ..... "  
 " e. " " " " 61a (log K, 192 cm) ..... 101  
 " f. " " " " 61a (log K, 205 cm) ..... "  
 62a. Scaled log K vs. depth, 0-450 cm ..... 104  
 " b. Normality plot for figure 62a (scaled log K, 0-450cm) 106  
 63a. Scaled log K vs. depth, 0-375 cm ..... 104  
 " b. Normality plot for figure 63a (scaled log K, 0-375cm) 106  
 64a. Scaled log K vs. depth, 50-375 cm ..... 104  
 " b. Normality plot for figure 64a (scaled log K, 50-375 cm) ..... 107  
 65. Scaled log K vs. depth, 0-50 cm ..... 104  
 66a. Scaled n vs. depth, 0-375 cm ..... 107  
 " b. Normality plot for figure 66a (scaled n, 0-375 cm) . 109  
 67. Scaled  $\theta_{1.5}$  vs. depth, 0-375 cm ..... 107  
 68. Scaled  $d_{10}$  vs. depth, 0-375 cm ..... 109  
 69a. Contoured cross section of the 2-D regression fits to the log K data (0-50 cm & 50-400 cm) ..... 113  
 " b. Normality plot for figure 69a (2-D, log K, 0-50 cm) 114  
 " c. " " " " 69a (2-D, log K, 50-400cm) "  
 70a. Contoured cross section of the 2-D regression fit to the log K data (0-400 cm) ..... 113  
 " b. Normality plot for figure 70a (2-D, log K, 0-400 cm) 115  
 71a. Contoured cross section of the 2-D regression fit to the porosity data ..... 117  
 " b. Normality plot for figure 71a (2-D, n) ..... "  
 72a. Contoured cross section of the 2-D regression fit to the  $\theta_{1.5}$  data ..... 118  
 " b. Normality plot for figure 72a (2-D,  $\theta_{1.5}$ ) ..... "  
 73a. Contoured cross section of the 2-D regression fit to the  $d_{10}$  data ..... 119  
 " b. Normality plot for figure 73a (2-D,  $d_{10}$ ) ..... "  
 74. Example of an exponential variogram ..... 124  
 75. Example of a pure nugget effect variogram ..... "  
 76. Variograms of detrended log K values from the cross section ..... 126  
 77. Variograms of detrended porosity values from the cross section ..... 126  
 78. Variograms of detrended  $\theta_{1.5}$  values from the cross section ..... 128  
 79. Variograms of detrended  $d_{10}$  values from the cross section ..... 128  
 80. Example of fitting an exponential variogram ..... 130  
 81. Variogram models for  $\theta_{1.5}$  ..... "  
 82. Contoured cross section of the  $\theta_{1.5}$  kriged distribution (variogram model 1) ..... 135  
 83. Contoured cross section of the  $\theta_{1.5}$  kriged distribution (variogram model 2) ..... 135  
 84. Contoured cross section of the kriging standard

	deviation distribution for $\theta_{1.5}$ (variogram model 1) .....	137
85.	Contoured cross section of the kriging standard deviation distribution for $\theta_{1.5}$ (variogram model 2) .....	137
A1.	Diagram of the shelby tube permeameter .....	A-2
A2.	Example of fluctuations in K over time .....	A-4
C1.	Schematic diagram of Vertiject device .....	A-9
E1.	Diagram of hanging column apparatus .....	A-13
E2.	Diagram of a volumetric pressure plate extractor ..	"
L1.	Variograms of detrended log K values from the cross section (0-50 cm) .....	A-71
L2.	Variograms of detrended log K values from the cross section (50-400 cm) .....	A-71

I) INTRODUCTION

Mining has been an important industry to this country for the last century. This is especially true in the western states with the discovery of gold, silver, copper, and most recently uranium. The first discoveries found rich deposits which had little need for processing. However, as time has passed, the ore grades being mined have decreased resulting in the production of more and more waste. Several mills in this country process in excess of 100 million tons of waste daily (Kealy, 1979).

Various processes have been developed over the years for extracting ore from the surrounding waste rock. This extraction process basically entails a series of crushing and chemical treatments. The resultant by-products are referred to as mill tailings. In the past, mill tailings were disposed of as quickly and as cheaply as possible with little concern for the environment. This invariably meant depositing the tailings directly onto the native soil.

Mining activity in this country has declined substantially within the last decade. However, tailings impoundments from previous operations still remain and are common throughout the country. Locations of major mining and processing wastes as mapped by the Department of Transportation are shown in figure 1. In addition, many smaller operations are not represented on the map.

A tailings impoundment is invariably different in chemical composition from the naturally occurring soil upon which it



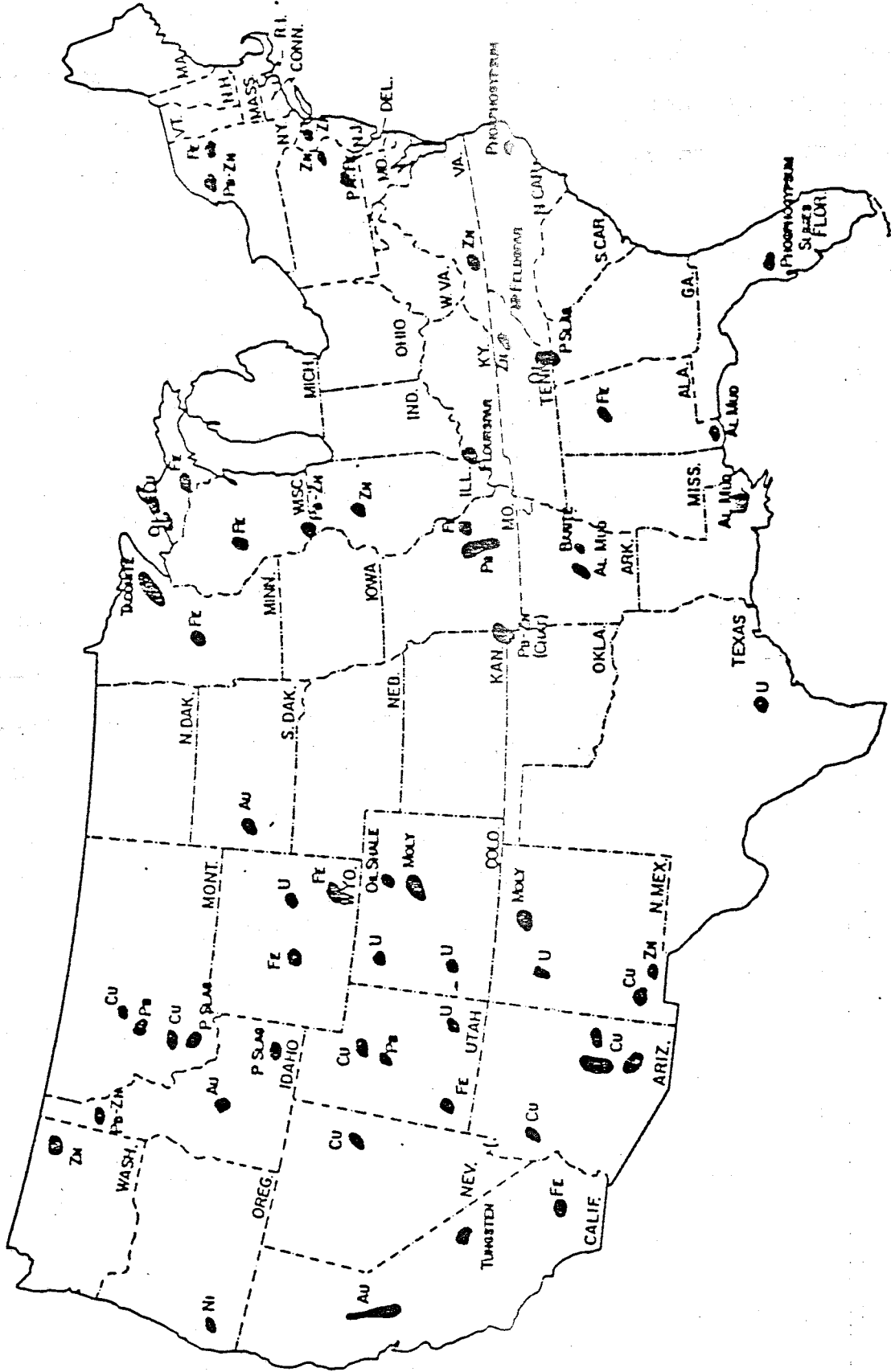


Figure 1. Locations of mining and processing wastes.

rests. If appreciable seepage through a tailings site occurs, it is possible that the underlying groundwater can be adversely affected. Accurate estimation of seepage at an individual site would aid in reclamation decisions. Various studies have been done in the past in an attempt to predict seepage from tailings impoundments. Almost all considered the impoundments as near homogeneous environments with little or no heterogeneity. However, a tailings impoundment is an extremely heterogeneous environment because of the method by which it is deposited. The effect that this variability has on seepage predictions has yet to be addressed.

The following research is the first of a 2 part study funded by the U.S. Bureau of Mines under the Mineral Institute Waste Treatment and Recovery Generic Center, University of Nevada at Reno. The emphasis of this study covers the different methods which can be used to characterize the spatial variability of hydraulic properties in mill tailings. The benefits and shortcomings of each method will be discussed. The second part of this study is being performed by Ken Harris, who is also a Hydrology graduate student at NMIMT. Harris' research concentrates on the effects that variability in the input data have on seepage prediction using the numerical model UNSAT2 (Davis & Neuman, 1983). The main emphasis of this combined study is to determine what effect the degree of characterization has on seepage estimates. For the results of the modeling study, I refer the reader to the Independent Study in Hydrology by Ken Harris.

### Previous Work

The majority of research on mill tailings in the past has dealt with identifying and improving the stability of embankment dams. Studies by Soderburg and Busch (1975), Hightler and Vallee (1980), and others view tailings from a soils engineering standpoint. The primary concern in such research was to develop methods to prevent such occurrences as flow slides and liquefaction. The presence of water in, and seepage through, tailings in such studies was more important from a stability standpoint than from a seepage/contaminant standpoint.

More recently, research on the prediction of seepage through impoundments has been performed by McWhorter and Nelson (1980), Isaacs and Hunt (1981), and others. However, the incorporation of spatial variability of the tailing's hydraulic properties into these predictive models has been all but absent.

Much information is available on the use of geostatistics for characterizing the spatial variability of hydraulic properties in soils. The use of geostatistical procedures in tailings, however, has been quite limited. At the introduction of each geostatistical methods section, an overview of previous work relating to that section will be presented.

## II) SITE DESCRIPTION

The field site for this study is an abandoned lead-zinc tailings impoundment 1.5 miles south of Magdalena, New Mexico (figure 2). The tailings impoundment and accompanying mill predominantly serviced the Waldo-Graphic mine located 1 mile to the east in the Magdalena Mountains.

The mill site foundation is at an elevation of 6890 feet above sea level. The impoundment is located to the west of the mill on a gradual hillslope that dips 4 degrees to the north, north-west. The tails were deposited directly on the native soil which is a very-poorly sorted silt-loam. This soil is the upper boundary of the alluvial fill that rests atop the Tertiary rhyolite bedrock (figure 3) of Hop Canyon (Austin, 1960). The depth to water in the area ranges from 260-300 feet below land surface.

The semi-arid climate of Hop Canyon is indicative of the climate of west-central New Mexico. The average yearly rainfall equals 11.49 inches with the wettest months being July, August, and September. The average yearly temperature in 1985 equaled 53.9°F. The temperature extremes ranged from a low of 6°F in December to a high of 100°F in July.

The tailings surface is completely void of vegetation. The vegetation surrounding the impoundment is classified as a pinon, juniper savannah woodland with pinon pine, juniper, prickly pear and cholla cactus, and grama grasses common (Morgan, 1986).

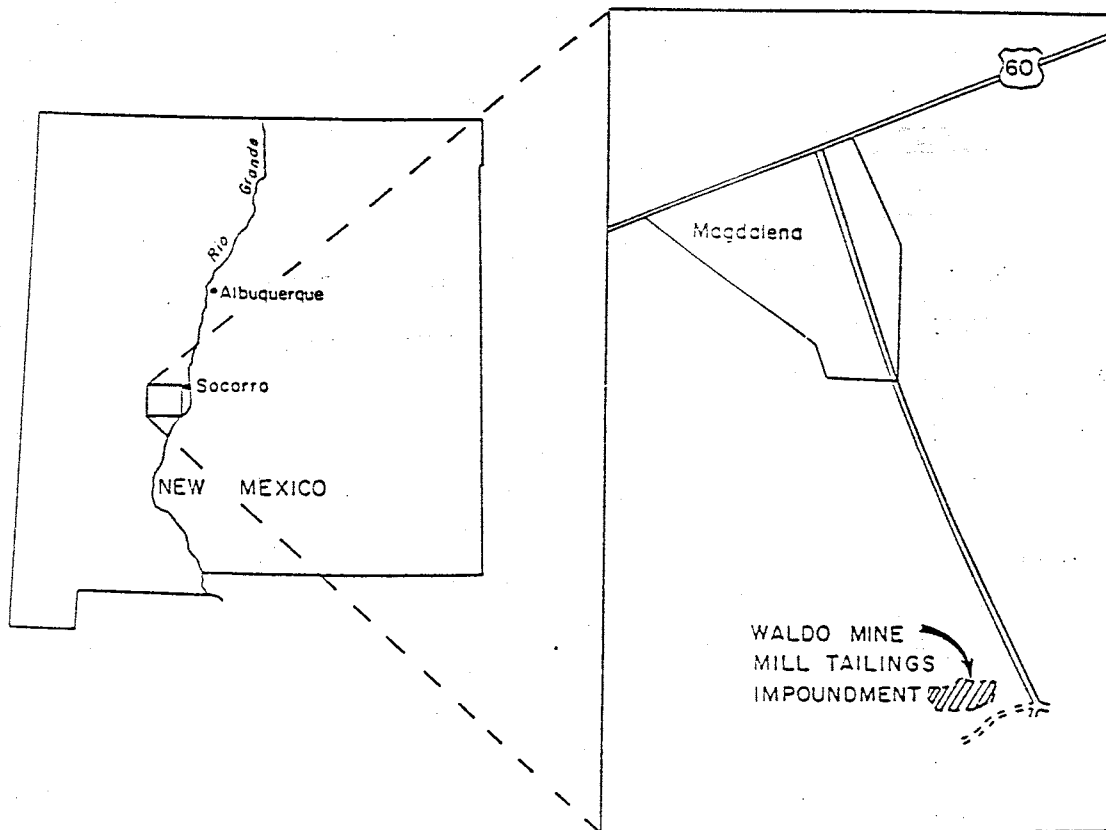


Figure 2. Location map of the Waldo Mill tailings impoundment.

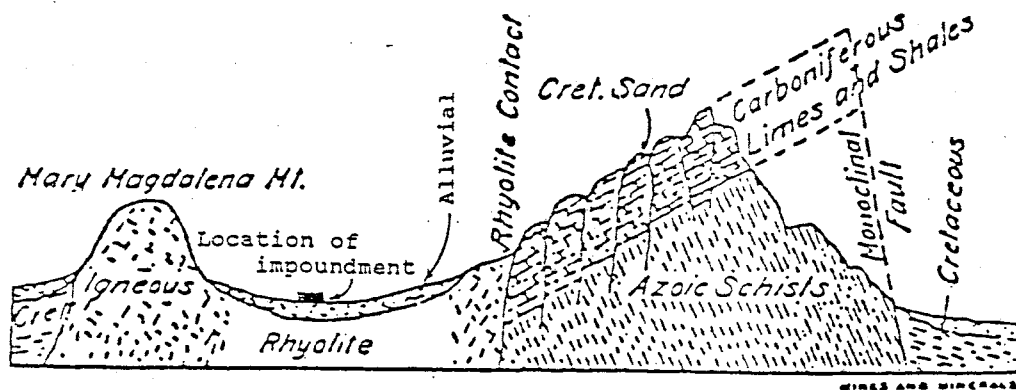


Figure 3. Geology of the field site area. Cross section of the Magdalena Range looking north.

## FIELD SITE HISTORY

### Waldo/Graphic Mine

The Magdalena-Kelly mining district was at one time one of the leading lead and zinc producing districts in New Mexico and even throughout the United States. This district has yielded over 40 million dollars in zinc, lead, copper, silver, and gold (Lusk, 1948). Mining in the area began in 1866 with the first discovery of cerussite (lead carbonate) by Col. J. S. Hutchason. It was then that he filed the first claims for the Graphic and Juanita sites.

Mining in the early years (1866-1878) centered around copper and silver. According to the New Mexico Minerals Yearbook (1917), gold was also present in the district but only in minor amounts (highest yearly production total for district: 1917, 2186 oz.).

In 1878, large bodies of cerussite ore were discovered at the Graphic mine. This ore was initially sent for processing to the Rio Grande smelter in Socorro by numerous mule teams. This smelter, however, closed in 1893. As a result, the 100-ton Graphic smelter was constructed in 1896 at the site of the present day Waldo mill foundation. This smelter operated intermittently until 1902 when the Graphic's deposit of lead carbonates were exhausted (Dabney, 1946).

In 1903, smithsonite (zinc carbonate), previously considered a worthless by-product of the Graphic mine, was found to be profitable. The Sherwin and Williams Paint Company, needing zinc

for their paint manufacturing, purchased the Graphic mine in 1904 for \$150,000. Sherwin Williams then turned over the mine operation to its subsidiary, the Ozark Smelting and Mining Company (Dabney, 1946). Mining in the Magdalena-Kelly district remained prosperous until 1920. In the 20 years that followed this date, mining activity in the district was scarce due to a decline in lead and zinc prices.

On April 10, 1943, American Smelting and Refining Company (ASARCO) purchased the Waldo/Graphic mine. The Waldo mining claim, which is due west of the Graphic, was initially separate from the Graphic claim. However, as mining in this area increased, many of the tunnels from these two mines were joined. Production of both lead and zinc from these mines increased substantially in 1943 due to the increased demand brought on by World War II. Production remained high throughout the 40's until June 3, 1949 when the mine was closed by ASARCO.

The Waldo/Graphic mine was worked on smaller scales by lessees in 1950 and 1951. In 1953, Robert Chamberlain (currently the caretaker of the mine and mill-site property) mined copper from the Waldo under a lease from ASARCO (Mineral Yearbook, 1953). Mining ceased in the Waldo/Graphic in 1953 and it has remained idle to this day.

The mine is currently used as a research facility for the Mining Engineering Department at New Mexico Institute of Mining & Technology in Socorro. ASARCO currently owns the Waldo/Graphic mine and the surrounding area which includes the mill tailings impoundment to the west.

### Waldo Mill

Before the ore could be shipped to the mill site, it was crushed in a primary crusher located near the mine entrance. As soon as the crushed ore could pass through an 8" mesh screen opening, it was shipped to the mill site along a 5000 foot aerial tramway bucket system (Lusk, 1947). Both the aerial tramway and the 150-ton concentrating mill (figure 4) were constructed in 1913 by the Ozark Smelting and Mining Co. (Lusk, 1948). This mill was used primarily to concentrate lead and zinc ore from the Waldo/Graphic mine.

The mill ran intermittently in the 1920's and early 1930's depending on the status of lead and zinc prices. It was closed from 1937 until April 1941 when the Rashob Mining Interest optioned the mill and reopened it for operation (Minerals Yearbook, 1942). Sherwin Williams then acquired control of the mill on July 1, 1942 and was responsible for its operation until it was sold to ASARCO.

On April 10, 1943, ASARCO purchased the mill and upgraded its production capacity to 200 tons per day (Minerals Yearbook, 1944). The mill ran at full capacity from 1944-1948. In June of 1948, the mill began treating custom ore from the nearby Kelly mine dump in addition to ore from the Waldo/Graphic mine. During this same period, mill tailings from earlier operations at the Waldo impoundment were reprocessed to extract additional lead and zinc. With the closing of the Waldo/Graphic mine in June 1949, the mill continued limited operation by processing custom ores



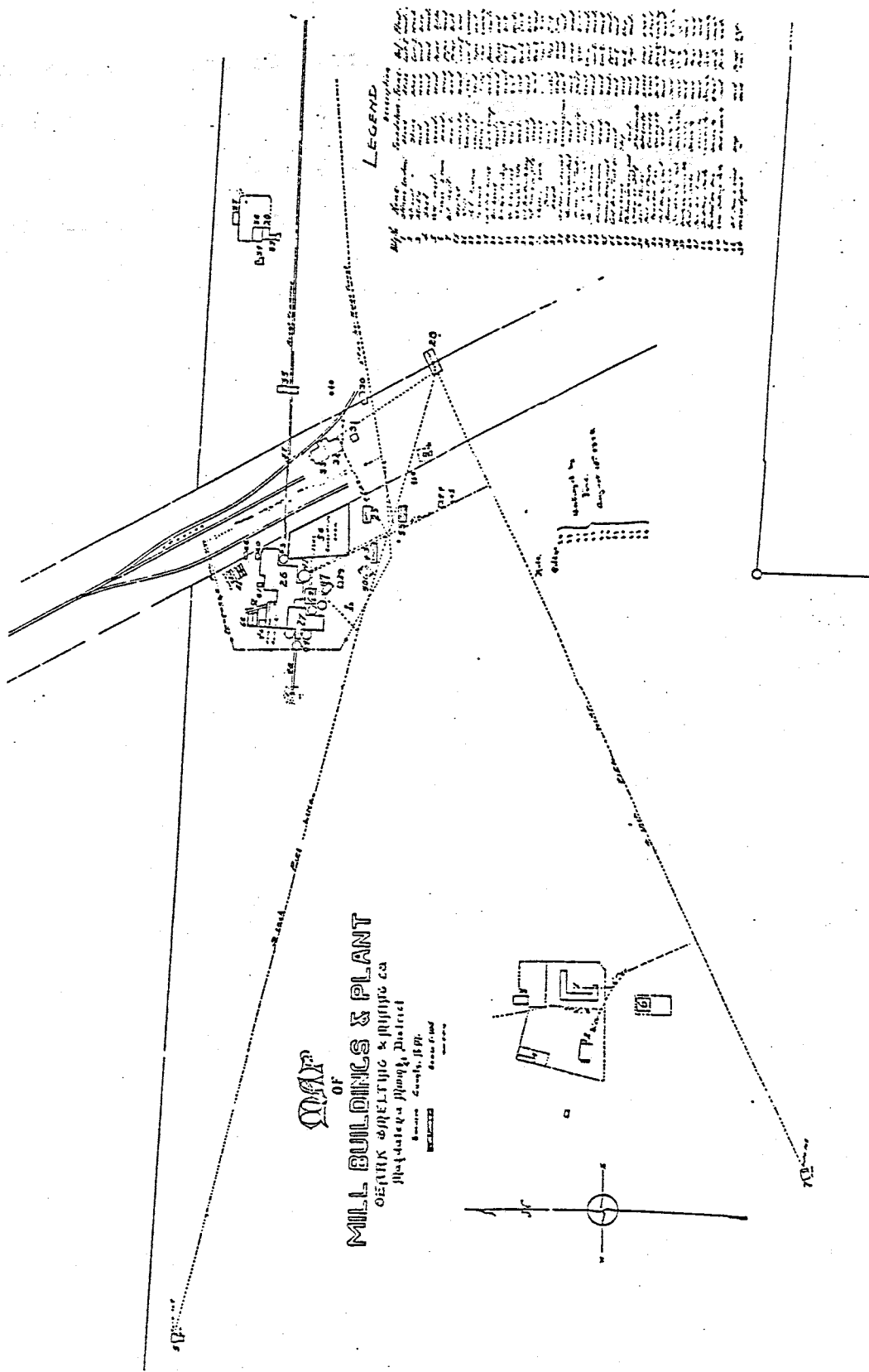


Figure 4. Blueprint of the mill-site and surrounding property, 1916.

from the Kelly, Lynchburg, Witt, Green, Juanita and Maher properties (Minerals Yearbook, 1949). In 1950, the Waldo mill was closed permanently by ASARCO and sold for dismantling. The mill foundation and two of the officer's residences to the west (figure 4) are the only remaining structures at the mill-site area.

The water used in the milling and tailings disposal process was pumped from two wells west of the mill and stored in a 100,000 gallon storage tank (figure 4). To reduce the amount of pumping in these wells, approximately 80% of the water used in the tailings thickener and tailings pond was reclaimed (Lusk, 1947).

#### Tailings impoundment

Not a great deal of information was kept by the mining companies on the history of tailings deposition. However, by using available literature on tailings deposition, aerial photographs, conversations with former employees, and by making careful observations in the field, a reasonable history of deposition can be formulated. With a better understanding of the past depositional processes, choosing locations to sample can be done more effectively.

It is evident from observations that the tailings were deposited in 3 distinct layers. Deposition of the first layer is believed to have begun in 1913 (figure 5). This date coincides with the construction of the Ozark (Waldo) mill. Deposition of this layer was quite simple. The tailings were spigotted from a pipe at the mill onto the native soil and allowed to flow

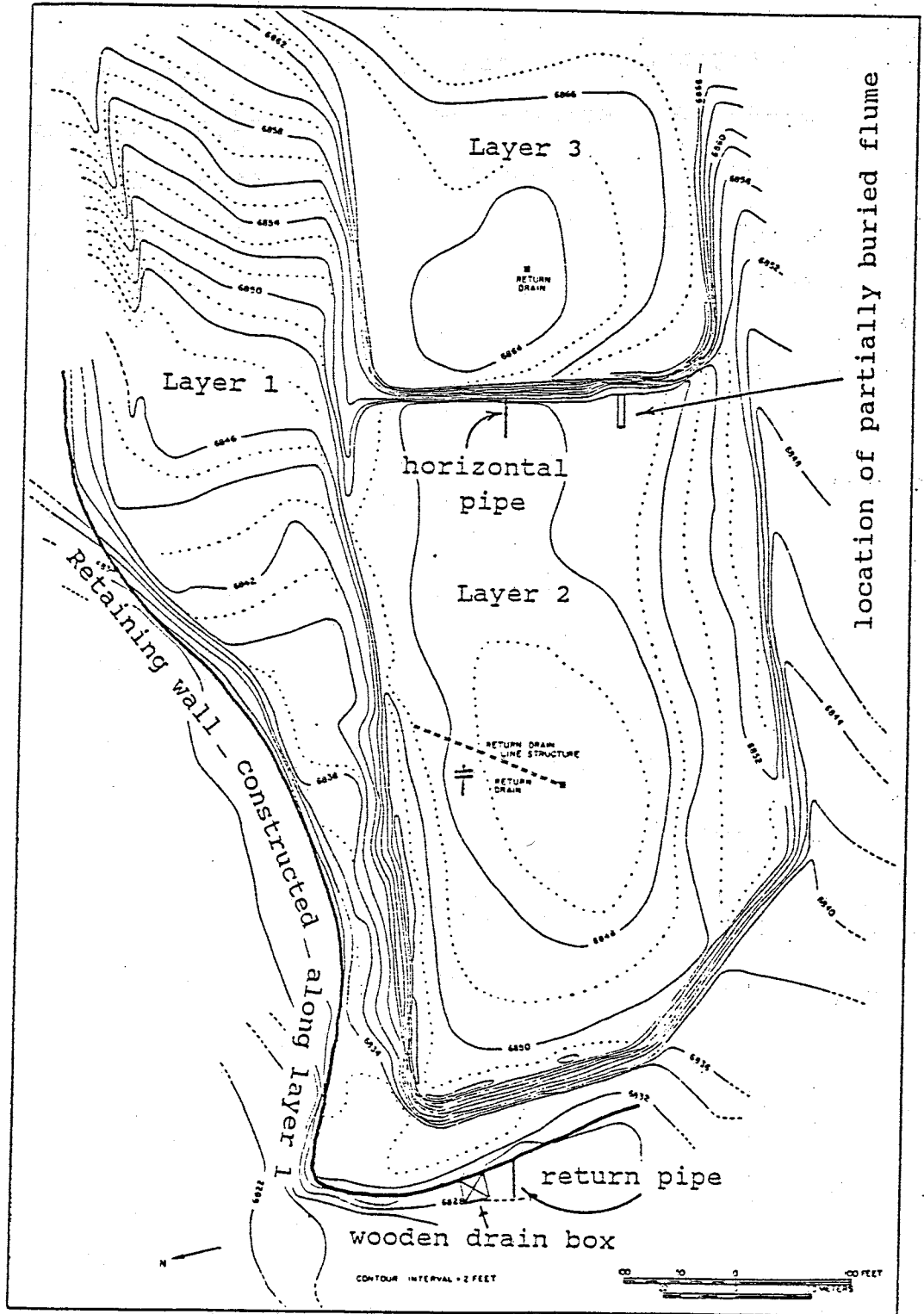


Figure 5. Topographic map of the Waldo Mill tailings impoundment.

down-gradient to the northwest. Sand berms were constructed along the northern and western edges to retain flow. A wooden drain box is present at the western-most edge of the first layer. It is believed that this was used to drain water from the pond that might have formed during deposition. A 10 cm diameter pipe is located at the base of layer 1 near this drain. This pipe may have been used as a water line to return the drainage water back to the mill site for reuse. Analysis of aerial photographs show that this method of deposition was used at least until 1943.

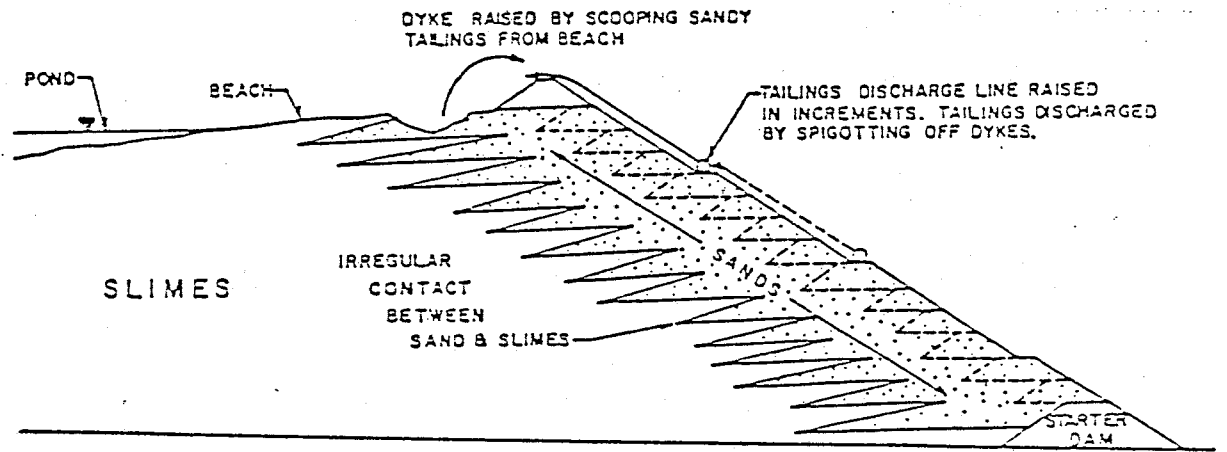
Eroded portions of the retaining walls on the first layer have enabled tailings to flow down-valley to the north and west. Tailings were found in an arroyo 75 meters to the west of the impoundment. To the north, traces of tailings and slag material (up to 1 cm diameter) were found in an arroyo 600 meters from the impoundment. The presence of the coarse slag material is a good indicator that the transport might have occurred during the initial deposition of tailings and is not, therefore, a product of secondary erosion. In both arroyos where the displaced tailings have been found, the vegetation does not appear to be adversely affected.

Advances in the methods of deposition can be seen in the second and third layers. The deposition of layer 2, which is noticeably the largest of the 3 layers, is believed to have begun in 1943. This estimate coincides with the purchase of the mill by ASARCO. Approximately 70% of layer 2 overlies the first layer. The remaining 30% was deposited on native soil.

Sand retaining walls, similar to those of layer 1, were constructed along the northern, western, and southern edges. Unlike the first layer however, 12.7 cm wide wooden flume lines were emplaced on top of the sand berms. These flumes had openings on one side which enabled tailings to flow out towards the center of the pond. When the height of tailings in the pond approached that of the retaining walls, a new sand retaining wall was constructed on top of the previous one. This new barrier was offset slightly towards the center of the pond in a process termed upstreaming (figure 6). It is believed that the flume lines were raised as many as 6 times along the west edge. Here, the second layer reaches a maximum thickness of 5 meters at the northwest corner. Conversely, due to topographic effects, the layer is less than 1 meter along the southeastern edge.

Reclamation of water from the tailings pond was very important due to the scarcity of water in the area. As was previously mentioned, approximately 80% of the water used at the tailings pond and tailings thickener was able to be reclaimed. For this purpose, a decant tower was placed in the center of the pond. The water which drained into this was then piped back to the mill for further use.

A partially buried flume trough was discovered at the base of the third layer where it contacts the surface of layer 2 (figure 5). This flume is 78 meters from the northern edge of the second layer. It is possible that the position of this flume once marked the southern boundary of layer 2. If this is true, the second layer was later widened to the south by 26 meters.



UPSTREAM METHOD OF TAILINGS DAM CONSTRUCTION

Figure 6. Diagram of the upstream method of tailings disposal.

Another explanation regarding this central flume is that it could have been used to deposit tailings to the center portion of the pond near the eastern edge.

A pipe, 5 cm in diameter, extrudes horizontally from the vertical face along the western edge of layer 3. It is possible that this pipe was used as a return line for reclaimed water from layer 2. A partially buried electrical pole can also be found on the northern side of the second layer. At one time this pole was used to support electrical lines from the generation station to the northwest well-house.

Layer 3 was deposited using procedures identical to those for layer 2. Deposition of tailings by flumes occurred along the north, west, and south edges as well. The third layer is approximately  $\frac{1}{3}$  the size of layer 2. This layer, which pinches out along its southeastern border, was greatly affected by the underlying topography. The maximum thickness of layer 3 is 4.5 meters at its northwest corner. A decant tower, identical to the one on layer 2, is also present in the center of layer 3.

A great deal of erosion has occurred along the northern edge of layer 3. Erosion has cut into the tailings embankment up to 7 meters in places forming a canyon-like appearance along the northern edge.

From the eastern edge of layer 3 back to the mill-site, a highly disturbed area of tailings and slag material exists. There appears to be no pattern to the deposition of the waste material in this area. In the northern half of this section, waste heaps (up to 3 meters high) of coarse slag and limestone fragments

exist. Analysis of historical photographs show that waste material such as slag and rock fragments have been deposited in this area since the inception of the mill.

#### CHEMICAL ANALYSES

The following water chemistry analysis is included to familiarize the reader with the possible chemical alterations that can occur when water comes into contact with mill tailings. The findings listed in this section in no way prove or refute the presence of seepage through the Waldo impoundment. Once again, they are included only to point out the possible adverse effects which can occur if appreciable seepage through a mill tailings impoundment exists. This stresses the need to effectively characterize this and similar sites hydraulically in order to formulate an accurate estimation of seepage.

The results from the water chemistry analyses are listed in table 1. The data represents the various ions in solution in parts per million (ppm). Column 1 lists the acceptable values for tap water for the State of New Mexico. The water sample for column 2 was obtained in the laboratory from shelby tube leachate. The third column represents the ion analysis from a water sample obtained from the surface pond at the impoundment. A pH value is also given for this sample. Both water samples (2 & 3) exhibit enormous amounts of Fe, Mn, and Zn in solution. This is not surprising given the composition of the mill tailings.

---

TABLE 1

WATER CHEMISTRY ANALYSIS



(ions in solution, ppm)

<u>ions</u>	(standard)		
	<u>(1)</u>	<u>(2)</u>	<u>(3)</u>
Al	5.0	0.07	178.0
Cr	0.05	0.5	<0.01
Cu	1.0	0.5	11.45
Fe	1.0	1610.0	665.0
Mn	0.2	1225.0	128.0
Pb	0.05	0.82	<1.0
Zn	10.0	2162.0	350.0
(pH)	6-9		2.25

(1) Tap water standard, State of New Mexico (NMWQS, 1981)

(2) Shelby tube leachate from laboratory analysis

(3) Water sample from surface pond at the field site, 10/86

---

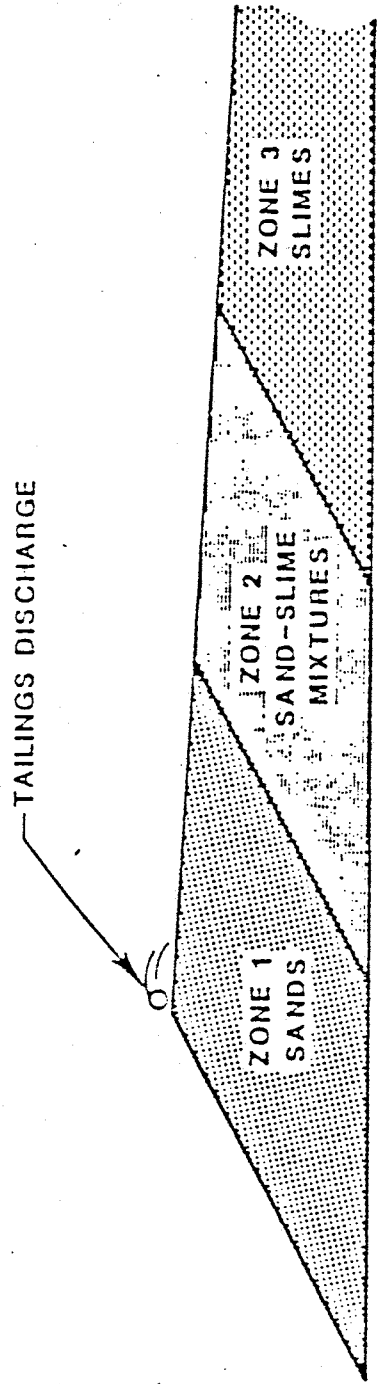
### III) DATA COLLECTION

#### SAMPLING LOCATIONS

##### Shelby tubes

A sedimentary structure that coarsens vertically upward and fines laterally will be produced from an upstreaming, peripheral tailings discharge system. This was the type of discharge system used to deposit layers 2 and 3 at the Waldo impoundment. Figure 7 is a cross-section of such a sedimentary sequence. The coarser-grained particles (sands) will deposit quickly near the discharge point. The finer-grained particles (slimes) deposit in the less turbid waters of the tailings pond located at a greater distance from the discharge point. In between these somewhat distinct 'zones' exists a gradational area of interbedded sand and slimes. The interbedding in this zone is due to fluctuations in discharge velocity from the mill site over time.

To better describe the sample locations within the impoundment, a reliable base map was needed. The scale on the existing USGS topographic map of the area was much too large to describe the impoundment in detail. A base map representing the impoundment was constructed by Ken Harris and myself using a telescopic alidade and plane table (Compton, 1962). Although this method of surveying is somewhat antiquated, it worked well for this study. The contour interval for this map is 2 feet (figure 8) with the dotted lines representing 1 foot intermediate contours. The reference elevation was obtained from a benchmark located approximately 500 meters northeast of the impoundment.



(REF: KEALY & BUSCH, 1971)

Figure 7. Conceptual model of material variation within a tailings deposit.

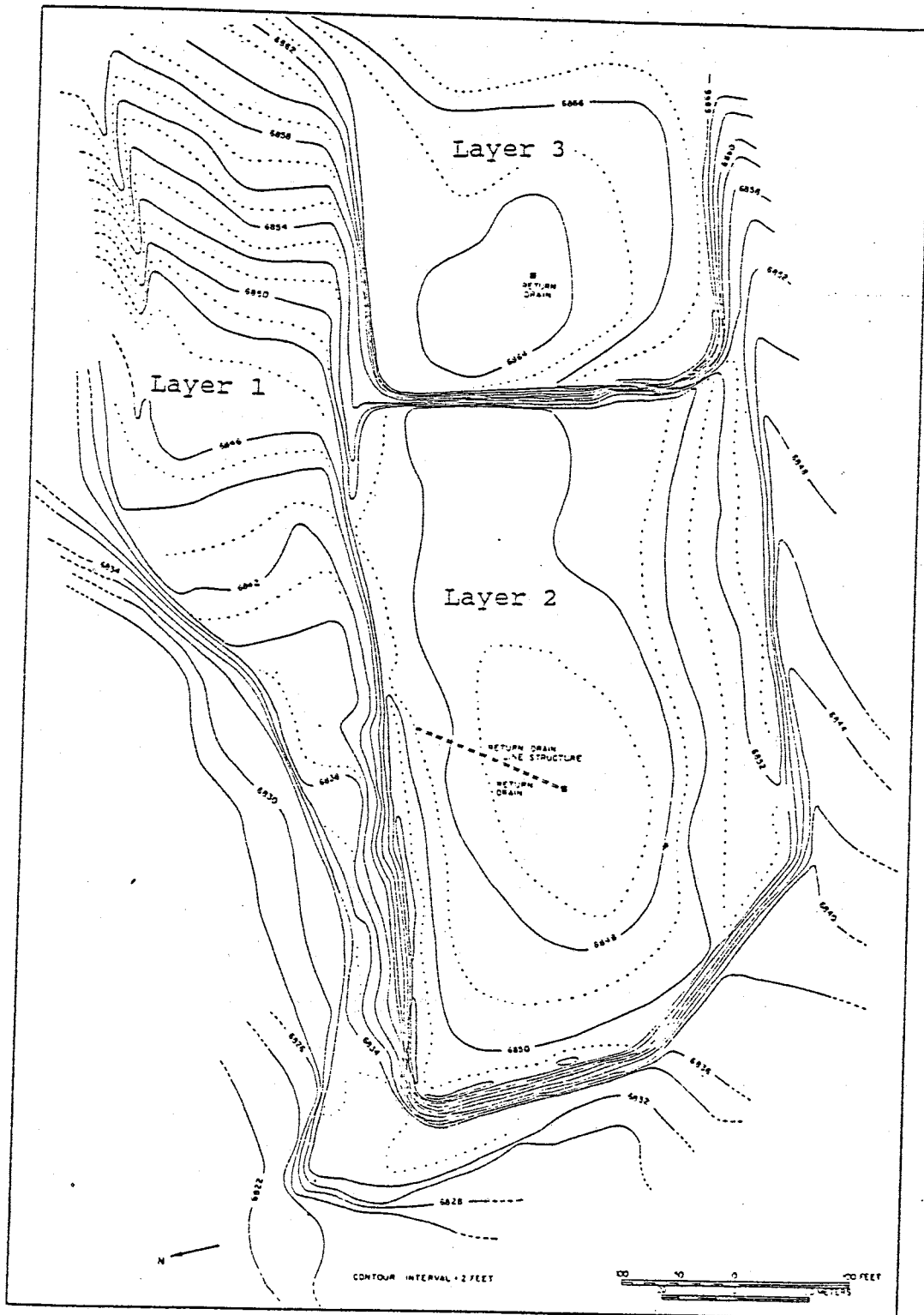


Figure 8. Topographic map of the Waldo Mill tailings impoundment.

This study will concentrate on the tailings from the second layer of the impoundment (figure 8). Layer 2 was chosen over layer 1 due to the methods of deposition involved. The peripheral discharge method used to construct layer 2 is more commonly used in current tailings disposal than the disposal method employed for layer 1 (discharge at the mill site from a non-rotating point source). The depositional methods of the second and third layers were identical. Layer 2, which is approximately 3 times the size of layer 3, was chosen over the third layer because it is more representative of the impoundment as a whole.

The horizontal sampling transect across the second layer is located 3.4 meters due west of the return drain along a trend of N6°W (figure 9). The individual dots along the transect mark the sampling locations of the lower transect at the 152 cm depth. The purpose of this transect was to characterize the entire range of hydraulic properties in the mill tails. The position of this transect accomplishes this over the shortest distance possible. The finest-grained tails should exist near the return drain in the central portion of layer 2. Therefore, the transect was placed as near to the drain as possible. The transect also incorporates both the northern and southern edges where the coarsest tails should exist. Deposition on the second layer occurred from 3 edges (north, west, & south). Along the transect, the majority of deposition is believed to have come from the northern and southern edges. Thus, one would expect the basic structure along the cross-section to reflect that of figure 10.

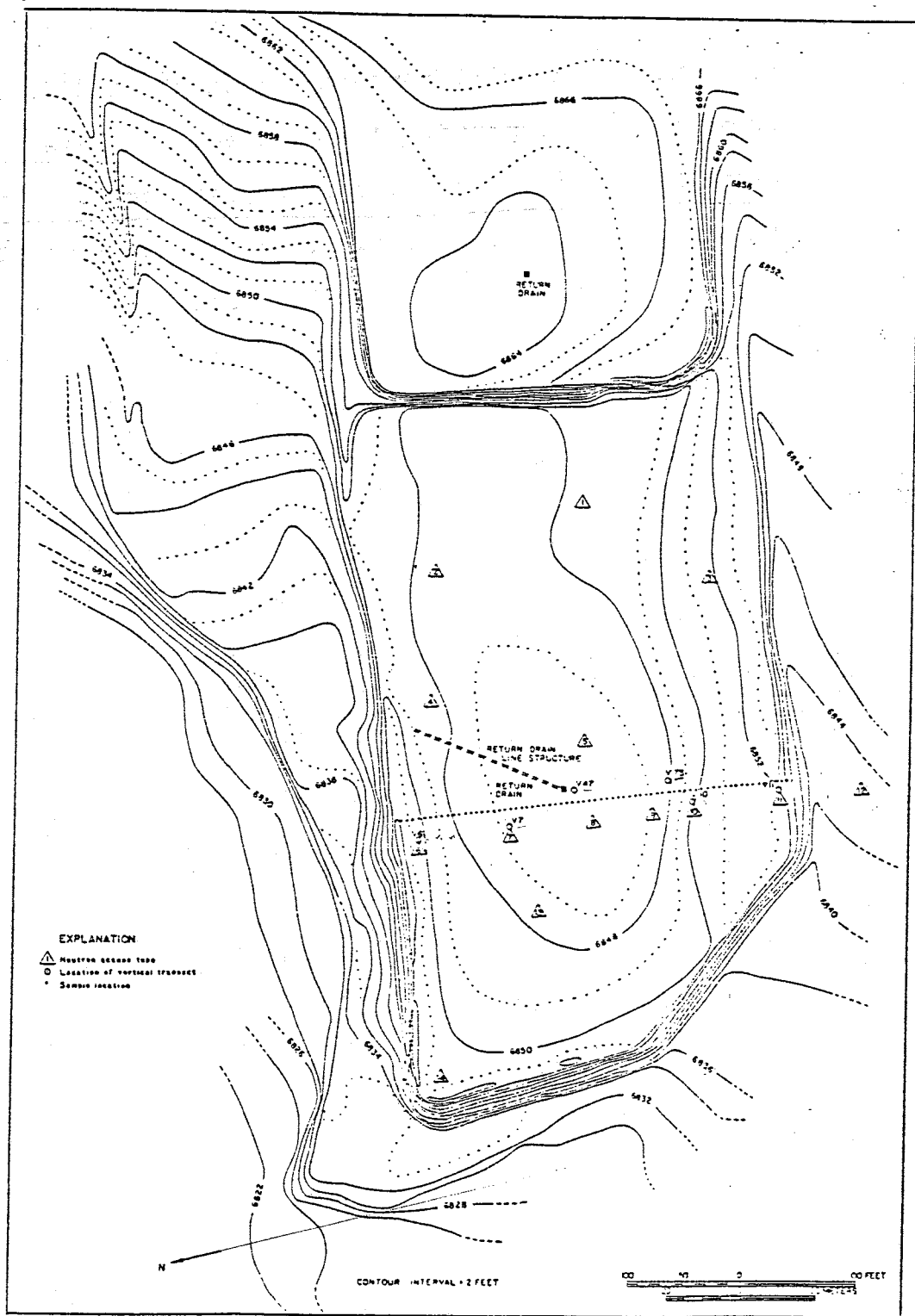


Figure 9. Locations of sampling transects and neutron-probe access tubes.

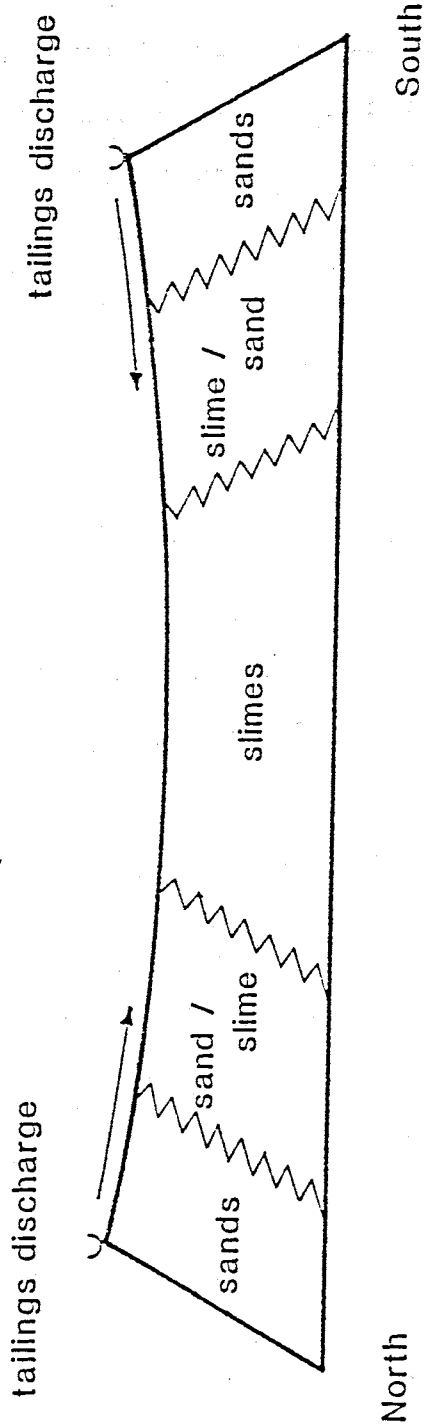


Figure 10. Conceptual model of material variation throughout the cross section.

The first set of samples were taken along the horizontal transect at a depth of 15 cm. Using shelly tubes, samples 52 cm in length were obtained (15-67 cm below surface). This depth was chosen in an attempt to characterize the hydraulic properties of the surface zone. Twenty-three samples were taken at a spacing of 4.56 meters laterally. One additional sample was taken at the northern end of the transect at a horizontal spacing of 3.75 meters. From the crest of the northern retaining wall to the crest of the southern retaining wall, the transect is 104.07 meters in length. The location of the shelly tube samples in cross-section from the upper transect can be seen in figure 11.

A second set of samples were taken along the same transect at a depth of 152 cm. Once again, shelly tubes were used to obtain samples from 152-205 cm below the surface. This depth was chosen because it is approximately the midpoint of the second layer (figure 11). Sixty-seven samples were taken at a spacing of 1.52 meters. Three additional samples were taken at the northern end of the transect at a spacing of 1.25 meters. The length of the lower transect is 104.07 meters as well. The increased number of samples for the lower transect were taken to better characterize the variability of the second layer laterally along the cross-section.

In addition, six continuous vertical transects, totalling 46 samples in all, were taken within 5.5 meters of the horizontal transect. Transects V6, V7, V10, and V11 lie to the west of the horizontal transects (figure 9). Transects V47 and V75 were placed to the east of the horizontal transect due to excavation



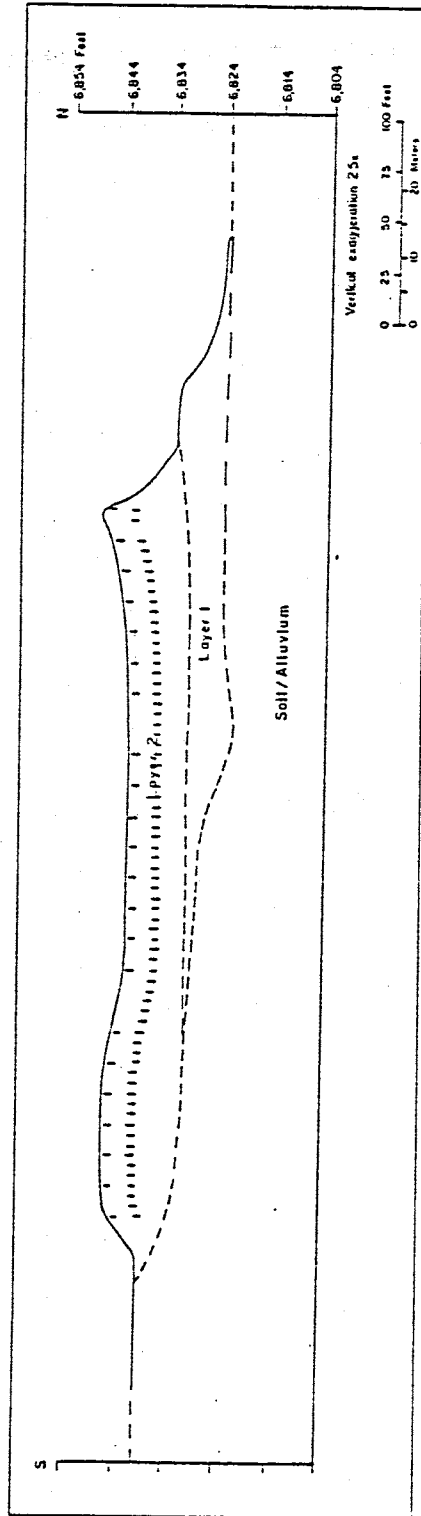


Figure 11. Cross section showing position of shelby tube samples. Length of sample line represents actual length of the sample (note vertical exaggeration).

- through pile #3

of trenches necessary to obtain these samples. The purpose of the vertical transects is to characterize the variability of the tailings at the different locations with depth. Samples along these transects are taken continuously from the surface, through the tailings, and into the native soil. Due to the overlap of layers 1 and 2, 4 of the 6 transects contain samples from layer 1 as well. The extent of the cross-sectional area sampled by the vertical transects is shown in figure 12.

#### Neutron access tubes

Fourteen 5.1 cm diameter neutron-probe access tubes varying in depths from 1.5 to 9.1 meters were installed at various locations in the second layer and surrounding soil. The locations of these tubes are represented by the triangles in figure 9. The locations of these tubes were selected to adequately characterize the in situ moisture contents in the different media throughout the second layer. Six of these tubes were placed 7.5 meters to the west of the drain tower at a trend of N 7.5 W. The access tubes were emplaced prior to sampling at the vertical transect locations. Neutron access tubes 6, 7, 10, and 11 are positioned 2 meters due west of vertical transects V6, V7, V10, and V11 respectively. Neutron access tubes 8 and 9 are located 10.1 and 10.7 meters away from vertical transects V47 and V75 respectively. Samples at V47 and V75 were obtained with the aid of a backhoe. This procedure produced large trenches that were later backfilled. The increased distances between the access tubes (8 & 9) and transects V47 and V75 were necessary so that the disturbance caused by sampling would not effect moisture

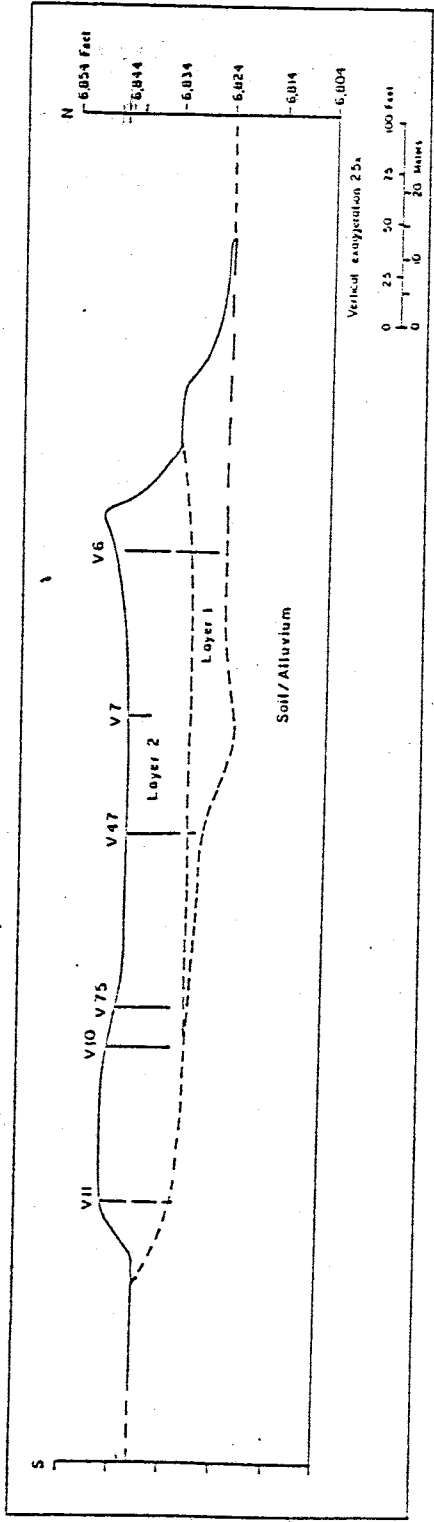


Figure 12. Cross section showing position of vertical transects. Gaps in the lines represent areas in which data was unable to be obtained.

readings at access tube locations 8 and 9. An additional access tube in the native soil was emplaced along the same trend as tubes 6-11. This tube was positioned to provide soil moisture data along the transect to the south of the impoundment.

As previously mentioned, neutron access tubes 6-11 are located near the 6 vertical transects. Their position in cross-section is noted in figure 13.

### SAMPLING PROCEDURES

#### Obtaining undisturbed sample cores

Before a decision could be made on the method of data collection, it was necessary to determine which hydraulic parameters of the tailings would be useful in this study. The hydraulic properties focused on for this study include: saturated hydraulic conductivity (K), porosity (n), volumetric moisture contents at 1.5 and 15 bars pressure ( $\theta_{1.5}$  &  $\theta_{15}$ ), soil moisture characteristics ( $\theta/\psi$  curves), in situ moisture contents ( $\theta_F$ ), and particle-size distributions.

Many field and laboratory methods exist to determine saturated K. Field methods such as the instantaneous profile (IP) test or the double-cylinder permeameter do not characterize variability in a layered media very effectively (Hillel, 1980). Using either of these methods, it is also difficult to obtain K values for the matrix at depths below the surface zone. For these reasons, it was decided that 'undisturbed' sample cores would be taken for use in the laboratory instead of determining the hydraulic properties of the tailings in situ.

Two methods for obtaining 'undisturbed' core samples were

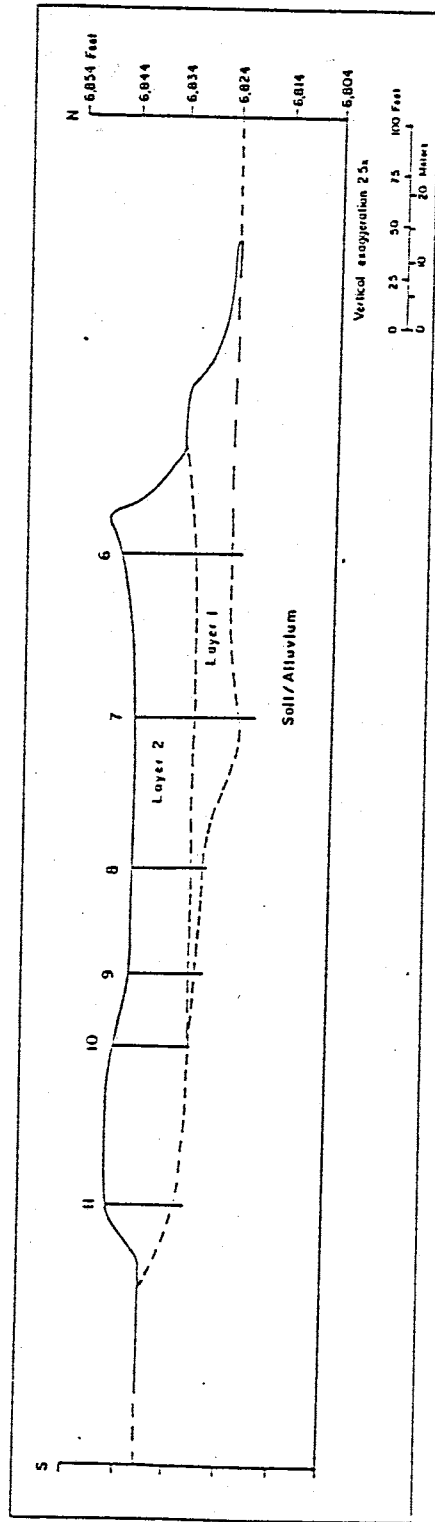


Figure 13. Cross section showing position of neutron-probe access tubes.

available for this study. These methods included the use of 5.1 cm x 5.0 cm diameter 'ring' samples which are obtained using a hand sampler and 61.0 cm x 7.6 cm diameter thin wall samples (shelby tubes) which are obtained with the aid of a drilling rig.

One dozen ring samples were initially obtained to determine the feasibility of this method for sampling tailings. This method, however, was quickly proven ineffective. It was impossible to obtain samples at locations in the coarser-grained, partially cemented sands. The pressure necessary to force the sampler through these resistant layers could not be obtained using a hand sampler.

A problem with sampling in the fine-grained material (slimes) was also encountered. The slimes tend to be very fine-grained (mean particle size = .006 mm) and exhibit a high in situ moisture content ( $\theta \geq 0.35$ ). These two factors make for a very cohesive matrix. When attempting to extract samples from the 'slime zone', it was difficult to break the adhesion at the base of the sample. Many times the adhesion of the base of sample to the original matrix was greater than the friction between the sample and the sample ring wall. Thus, many samples from the slimes could not be extracted from the base of the borehole. Due to these problems, this method of sampling was abandoned.

The alternative method of using shelby tubes was found to be preferable for sampling in tailings. Galvanized steel shelby tubes 61 cm in length were chosen. Galvanized tubes were used due to the corrosive nature of the tailings. Corrosion of

non-galvanized steel tubes occurred after only one use.

The shelby tube samples were obtained with the aid of a Mobile B-30 drilling rig. In attempt to preserve the structure of the original matrix, rotation was not used during sampling. This is common practice in shelby tube sampling. A sample is retained in a shelby tube by 2 forces: 1) friction between the sample and the tube wall, and 2) suction from entrapped air between the top of the sample and the shelby tube adapter. The additional retaining force provided by the suction enabled greater sampling success in the finer-grained material (slimes).

One of the main advantages to using the drill rig was the ease of obtaining shelby tube samples at depth. A borehole, equal in diameter to the shelby tube, could be drilled directly above the sampling location. This procedure enabled samples to be taken at depths up to 10 meters.

The drill rig also enabled samples to be taken in the resistant, partially-cemented 'sand zones'. The pressure supplied by the weight of the rig was enough to cut through these resistant layers in all but a few cases. Due to the extremely dry conditions in these 'sand zones' ( $\theta_f=0.10$ ), an incredible amount of resistance (up to 1200 psi) would build up between the outside wall of the shelby tube and the surrounding matrix. Obtaining a sample under these conditions was made possible by spraying the outside of the shelby tube with tap water prior to sampling. The water acted as a lubricant which resulted in a substantial decrease in resistance.

Another advantage to the shelby tube when compared to a ring

sample is its greater volume. Four conductivity measurements can be determined for a given permeability test within each shelby tube sample. It would require 4 separate ring samples and 4 permeability tests to reproduce these same results.

The shelby tube sampling method, however, was not completely trouble-free. Problems still existed when attempting to recover samples from the fine-grained slimes. Very thin layers (1-2 mm) of silty sand are layered within the 'slime zone'. These sand layers can be seen in figure 14 along the measuring tape at 12, 18, 25, and 31 cm. These layers have little or no tensile strength. This is noted in the photograph by the fact that, upon drying, the slime sample cores invariably separated along the fine sand layers. When attempting to extrude a sample from the slime matrix, the adhesion at the base of the sample was invariably greater than the tensile strength of one of these thin sand layers within the shelby tube. As a result, the bottom portion of the sample below one of these sand layers was commonly unrecoverable. This meant that only a partial sample above the given sand layer could be retained. The arrows and numbers along the left side of the sample core in the photograph represent the interval over which conductivity measurements were obtained.

Many different ideas were tried to combat the sampling problem in the slimes. The first method, which unfortunately proved unsuccessful, involved rotating the shelby tube 1/4 revolution before extruding it from the matrix. The idea here being that the rotation might separate the base of sample from the matrix. Due to the highly pliable nature of the slimes,



TRANSECT NUMBER: V47

PHOTO NUMBER: 4

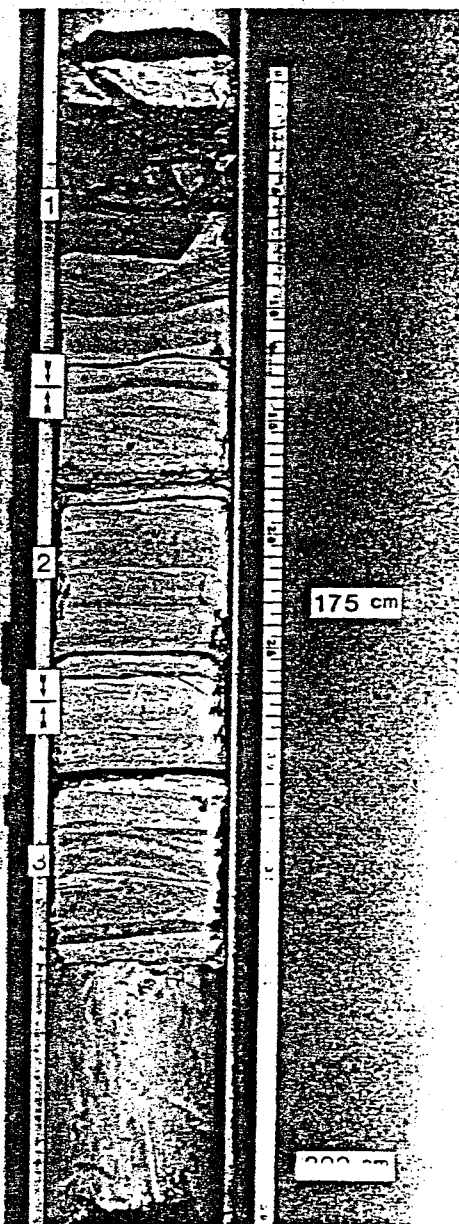


Figure 14. Photograph of 'slime' sample core showing the presence of very thin (1-2 mm) silty-sand layers.

the adhesion between the sample base and the matrix could not be broken using rotation. The next idea was to coat the inside of the shelby tube with coarse sand prior to sampling. The sand was added to increase the friction between the sample and the surface of the tube wall. Unfortunately, this increased friction was not great enough to overcome the adhesion of the slime sample to the matrix. Compacting the sample by overpushing was also tried on the advice of Steve Gray (1985). It was hoped that by compacting the sample throughout the shelby tube, the force between the sample and the tube wall would be increased. Once again, the method proved unsuccessful.

After all other ideas had been exhausted, samples from the 'slime zone' were obtained with the aid of a backhoe. This procedure included pushing the shelby tube as usual using the drill rig. However, instead of lifting the shelby tube from the borehole, a backhoe was used to dig a trench along the side of the shelby tube. The shelby tube could then be capped on the bottom and lifted from the trench. The sample was encased in the shelby tube at all times during excavation with the backhoe. Therefore, it is unlikely that any sample disturbance occurred as a result this method. Eighteen samples from the lower horizontal transect as well as all 17 samples from vertical transects V47 and V75 were obtained using this method.

Difficulties were also encountered when sampling the soil underlying the impoundment. The soil is very poorly sorted with pebbles up to 2 cm in diameter common. Contacting one of these rocks during sampling meant destruction of the shelby tube

cutting edge. Due to the frequency of these pebbles in the soil, it was very difficult to obtain 'full' shelby tube samples.

#### Installation of neutron access tubes

Thirteen neutron access tubes were installed in the second layer. An additional access tube was emplaced in the native soil 21 meters south of the impoundment. These 5.1 cm diameter tubes are made of aluminum with a wall thickness of 1 mm. Boreholes for the access tubes were drilled using 5.1 cm drill stem powered by a Mobile B-30 drill rig. Enlargement of the borehole during drilling to a diameter greater than 5.1 cm occurred. An annular space between the access tube and the borehole wall of approximately 0.5 cm was found to exist when installing the access tubes. This space was carefully backfilled with tailings to prevent piping of water down the outside of the access tube.

The access tubes must be kept water tight between readings. The base of each tube is sealed with a no. 10.5 rubber stopper. In addition, a layer of silicone was applied to the outside of each stopper. The top of an individual tube is sealed in between moisture readings using a no. 10.5 rubber stopper as well.

Due to destruction by vandalism of previously installed in situ apparatus at this site (mercury manometer tensiometers and neutron access probe tubes), each of the neutron access tubes used in this study were buried beneath the surface approximately 5-7 cm. In between moisture readings, a 7.6 cm diameter PVC cap is placed over each of the neutron access tubes. These caps are then buried approximately 1 cm with tailings. The position of the access tubes have been surveyed onto the topographic map.

Their locations in the field are marked by large rocks which are uncommon to the surface of the tailings on the second layer.

### LABORATORY PROCEDURES

Laboratory procedures were performed on the tailings samples to determine:

- saturated hydraulic conductivity		K
- porosity		n
- volumetric moisture content @ 1.5 bars		$\theta_{1.5}$
- " " " @ 15 bars		$\theta_{15}$
- soil moisture characteristics		$\theta/\psi$ curves
- particle size distributions:		
- particle diameter at 10% finer by weight		$d_{10}$
- " " 16% "		$d_{15}$
- " " 30% "		$d_{30}$
- " " 50% "		$d_{50}$
- " " 60% "		$d_{60}$
- " " 84% "		$d_{84}$

Using these particle size parameters, the following particle size distribution parameters were determined:

- geometric mean particle diameter	$GM = (d_{15} \times d_{84})^{0.5}$
- uniformity coefficient	$UC = (d_{60} / d_{10})$
- coefficient of curvature	$CC = (d_{30})^2 / (d_{10} \times d_{60})$
- trask sorting coefficient	$SORT = (d_{34} / d_{10})^{0.5}$
- trask skewness coefficient	$SKEW = (d_{34} \times d_{15}) / (d_{50})^{0.5}$

### Hydraulic conductivity

The first analysis run on the shelby tube samples was the determination of K using the shelby tube permeameter. The operating procedure for the permeameter is listed in appendix A. Three manometers were used in this procedure along with a constant head source. This enabled 4 conductivity measurements to be obtained from each sample.

### Sample extrusion

A smaller sample was needed for use in determining  $\theta/\psi$  relationships. Therefore, a 3.0 x 5.4 cm diameter ring sample

was obtained from the base of each shelby tube sample. To do this, the shelby tube sample was extruded using the Vertiject device (see appendix C for operating procedures).

Along with the ring sample, 3 additional 'grab' samples were retained from the shelby tube every 13.3 cm. These 'grab' samples were retained for particle size analysis. The location of the 'grab' samples within each shelby tube correlates directly to the position of the shelby tube permeameter manometers. Figure 15 is a schematic diagram of the sample locations within a shelby tube.

Using the Vertiject device, intact sample cores were obtained from the shelby tube samples of the vertical transects. These cores were later cut in half and photographed. Selected photographs of these cores taken from various positions in the cross section are presented in appendix D. Once again, a ring sample was taken from the base of each shelby tube sample. In addition, 3 'grab' samples were taken from the discarded half of each shelby tube core.

#### $\theta/\psi$ relationships

The sample rings obtained from the shelby tubes were then used to determine moisture content/pressure head relationships of the tailings. Appendix E describes the methods used to obtain such  $\theta/\psi$  relationships.

The volumetric pressure plate was used to determine the moisture contents of the ring samples at 1.5 and 15 bars. This analysis was performed on all ring samples taken from both horizontal transects.

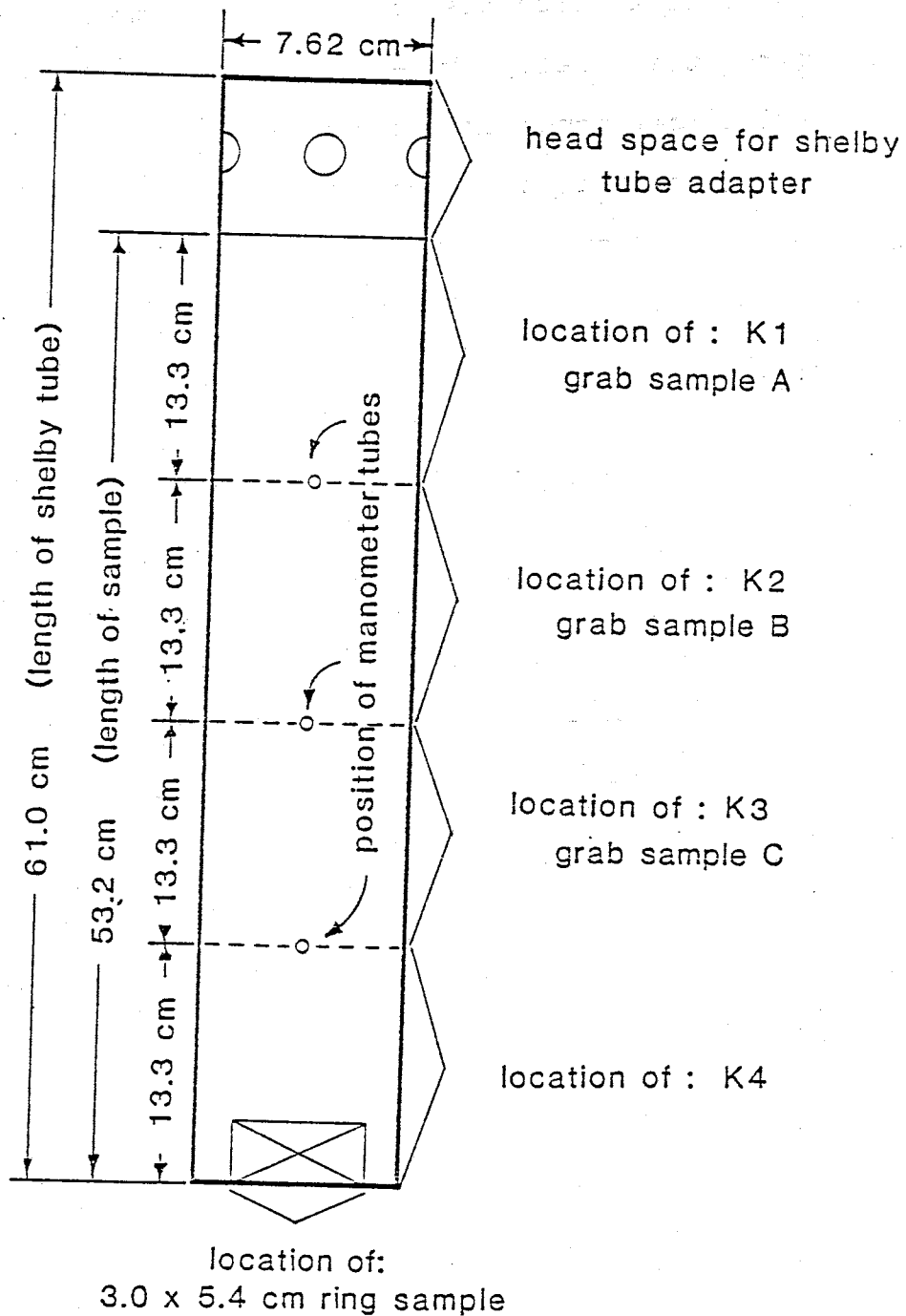


Figure 15. Locations of permeability and particle size samples within a shelly tube.

A more extensive  $\theta/\psi$  analysis was performed on the ring samples from the vertical transects. Using both the hanging column apparatus and the volumetric pressure plate,  $\theta/\psi$  curves were produced for all of the vertical transect rings.

#### Particle size analysis

The final laboratory analysis was the determination of particle size. Due to the fine-grained nature of the tailings, both hydrometer and sieve analyses were used (appendix F for procedures). Sixty one samples from the lower horizontal transect (192-205 cm) and 47 samples from the 6 vertical transects were analyzed using these methods. Using the data from this analysis ( $d_{10}$ ,  $d_{16}$ ,  $d_{30}$ , etc.), the particle size distribution parameters of geometric mean, uniformity coefficient, coefficient of curvature, trask sorting and trask skewness were determined.

#### Neutron probe

In situ field moisture contents were determined using neutron thermalization or neutron scattering. The neutron probe used is manufactured by Campbell Pacific Nuclear, model 503. The radiation source consists of 50 millicuries of americium 241/beryllium. The probe was calibrated to the field site by my partner, Ken Harris. Moisture readings were determined at 30.5 cm intervals in each of the access tubes.

#### PRESENTATION OF DATA

It was mentioned earlier that, due to the methods of deposition, a tailings impoundment is far from a homogeneous environment. One would expect the hydraulic properties of such a

media to vary throughout. The presence of such variability was found to be the case at the Waldo Mill impoundment. The data values described in this study ( $d_{10}$ , ...,  $d_{84}$ ,  $\theta/\psi$ ,  $n$ ,  $\theta_{1.5}$ ,  $\theta_{15}$ ,  $\theta_F$ , &  $\log K$ ) are presented in tabular form in appendix I.

Two basic hypotheses formulated prior to sampling on the variability of the hydraulic properties at the Waldo site were :

- 1) a great deal of variability should exist horizontally across the second layer and
- 2) a lesser degree of variability should be present vertically through the second layer.

The magnitude of the horizontal variability was envisioned due to the gradation of particle-size away from the emitters (flumes). Zones comprised of sand, sand/slimes, and slimes are common as the distance from the discharge point increases (Kealy, 1971). It was believed prior to sampling that a greater degree of homogeneity should exist in the vertical direction (figure 10). Some questions remained, however, about the vertical variability in the 'sand-slime' zone. Interfingering between sand and slime layers would result in a greater degree of variability.

#### Particle size distribution

To begin with, the variability in the particle size distribution will be discussed. Figure 16 represents the particle size extremes along the transect. The plots are a measure of particle diameter versus percent finer by weight. The break in curve A at 75 microns is due to discrepancies in the data produced by the sieve and hydrometer analyses. Sample A, taken from the central portion of the cross section, is composed primarily of silt and clay-sized tails. The coarsest sample, B, was taken near the



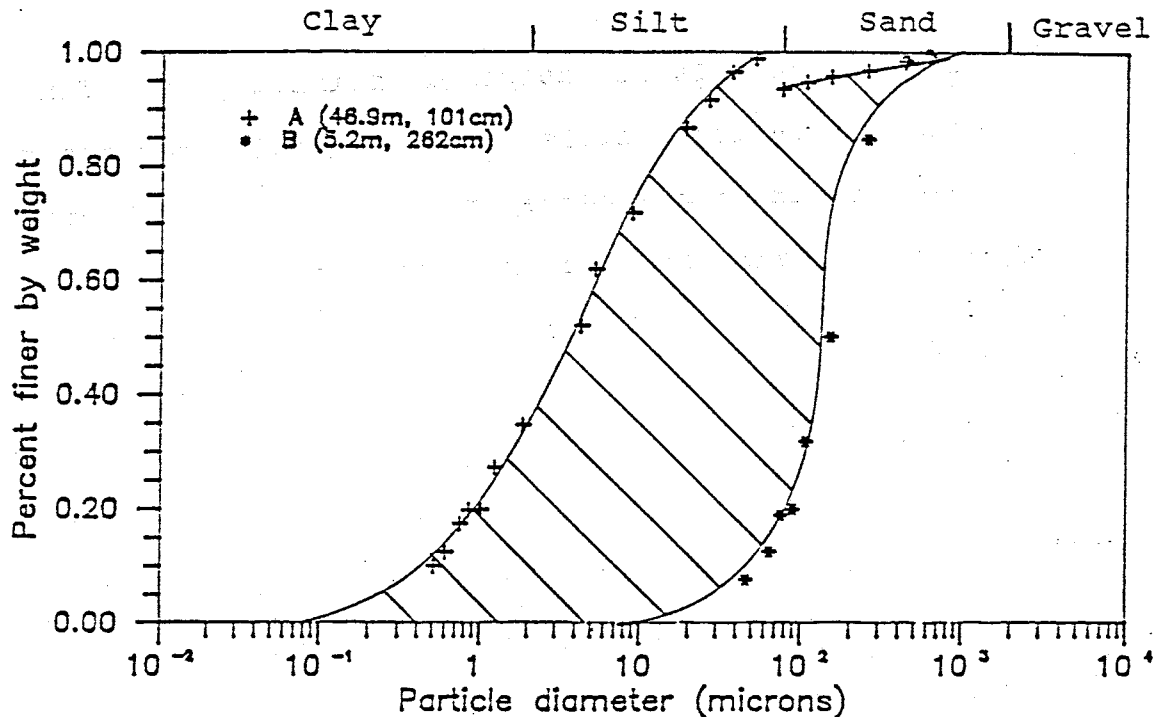


Figure 16. Range in grain size curves exhibited throughout the cross section.

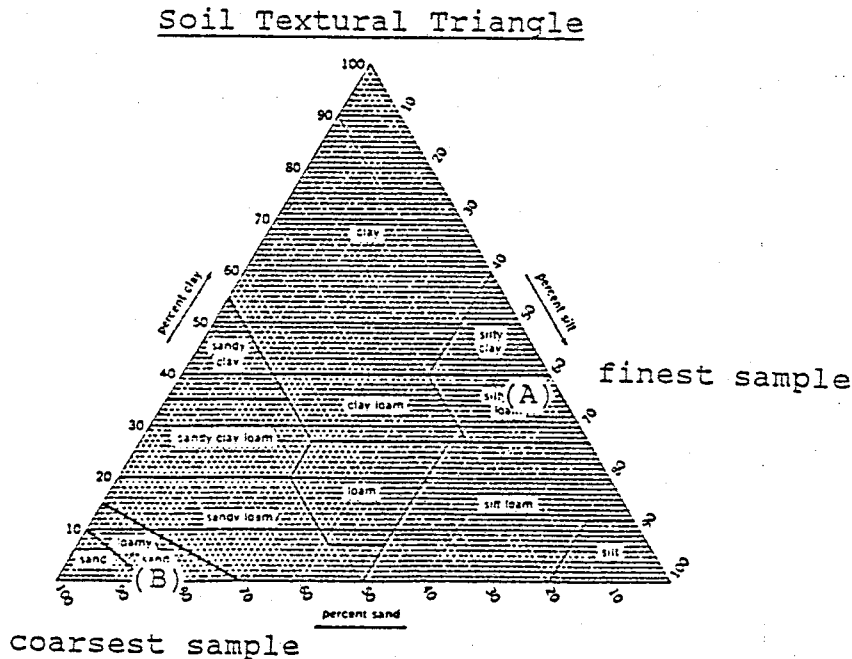


Figure 17. Comparison of particle size extremes to naturally occurring soils.

northern edge. It is composed primarily of fine and medium-grained sand-sized tails. The diagonal lines separating the two curves represent the range of grain sizes which can occur between the edges and the central portion of the cross section. It appears from figure 1 that the majority of the tails are silt-sized particles.

The particle distribution of the tailings can be compared to that of natural occurring soils using a soil textural triangle (figure 17). The finest tailings sample in this case would be classified as a silty clay loam while the coarsest would classify as a loamy sand. Intermediate tailings samples would classify as silt loams, loams, and sandy loams.

The variability in particle size along the transect in the horizontal direction is plotted in figures 18a, 19a, and 20a. These figures represent the particle diameter in microns at 10, 50, and 84 percent finer by weight respectively. Notice the difference in scales along the Y axis for each plot. Prior to sampling, it was assumed that the particle size in the center portion of the transect should be quite uniform both horizontally and vertically. This is definitely the case laterally from 25-62 meters along the transect. This marks the area where the uniform, fine-grained slimes are present. The variability in this zone (25-62 m) is greatest at the 84th percentile. This variability, however, is nowhere near that present in other sections of the transect.

As one moves to either side of the slime zone, the particle size of the tailings increase. This is to be expected with a

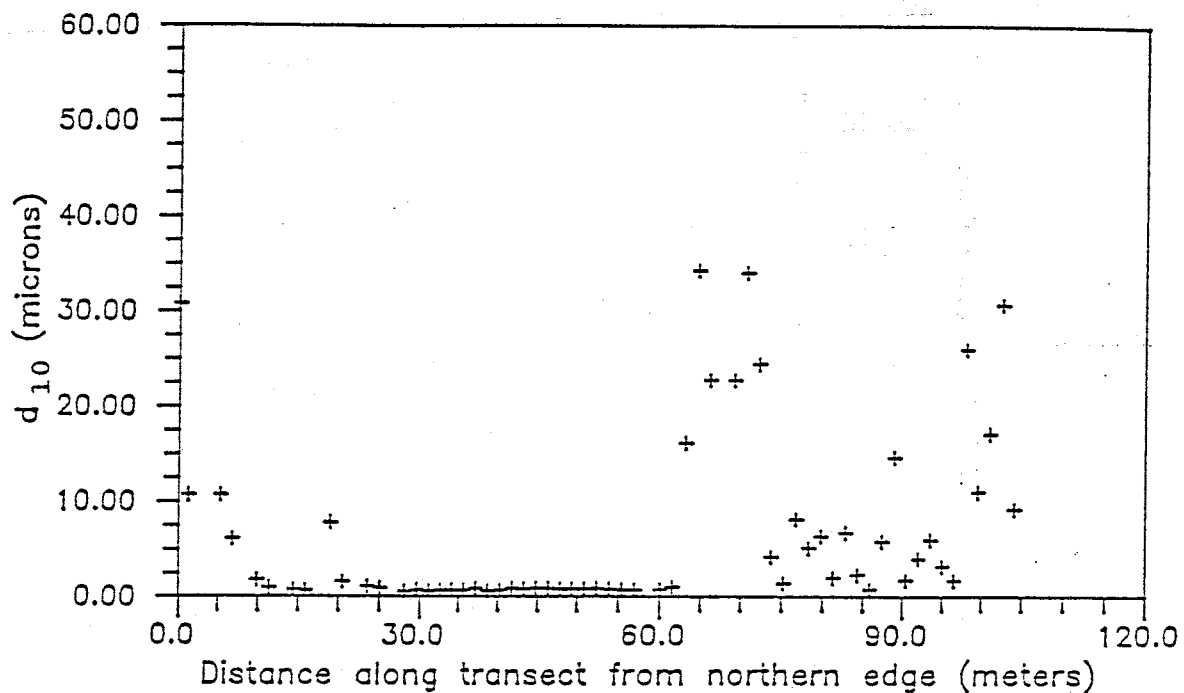


Figure 18a.  $d_{10}$  distribution laterally at 205cm depth.

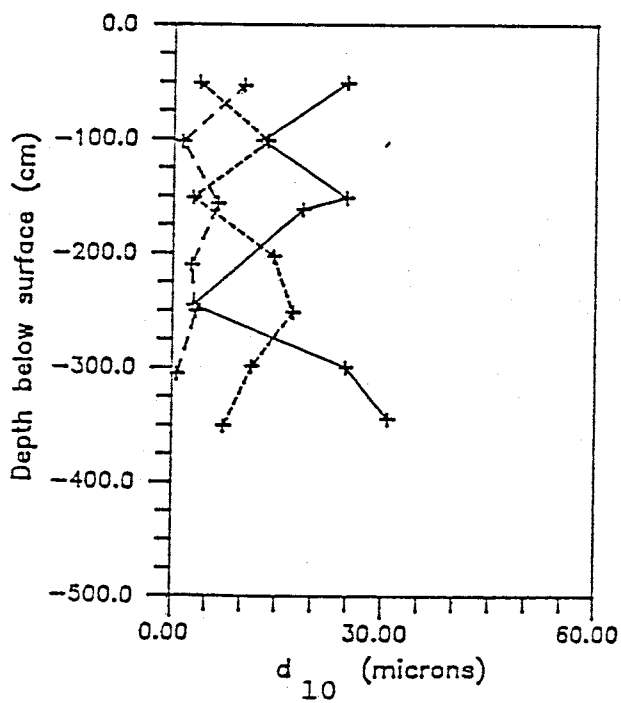


Figure 18b.

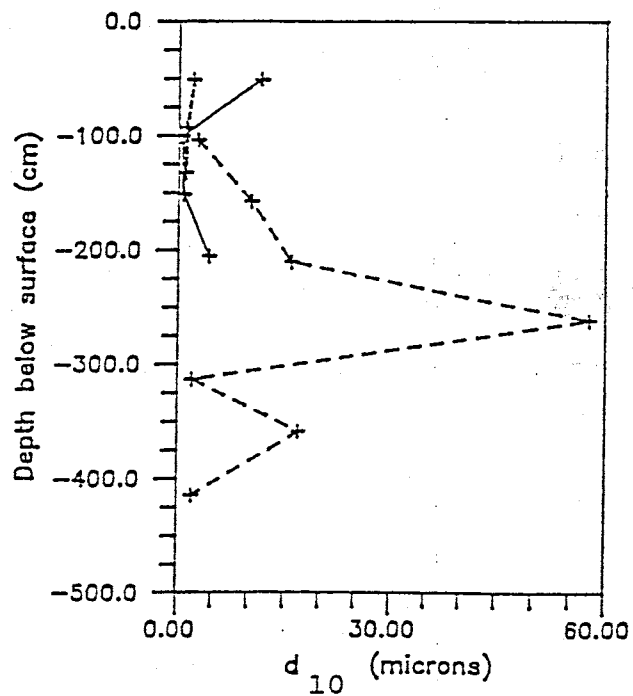


Figure 18c.

$d_{10}$  distribution with depth for each vertical transect.

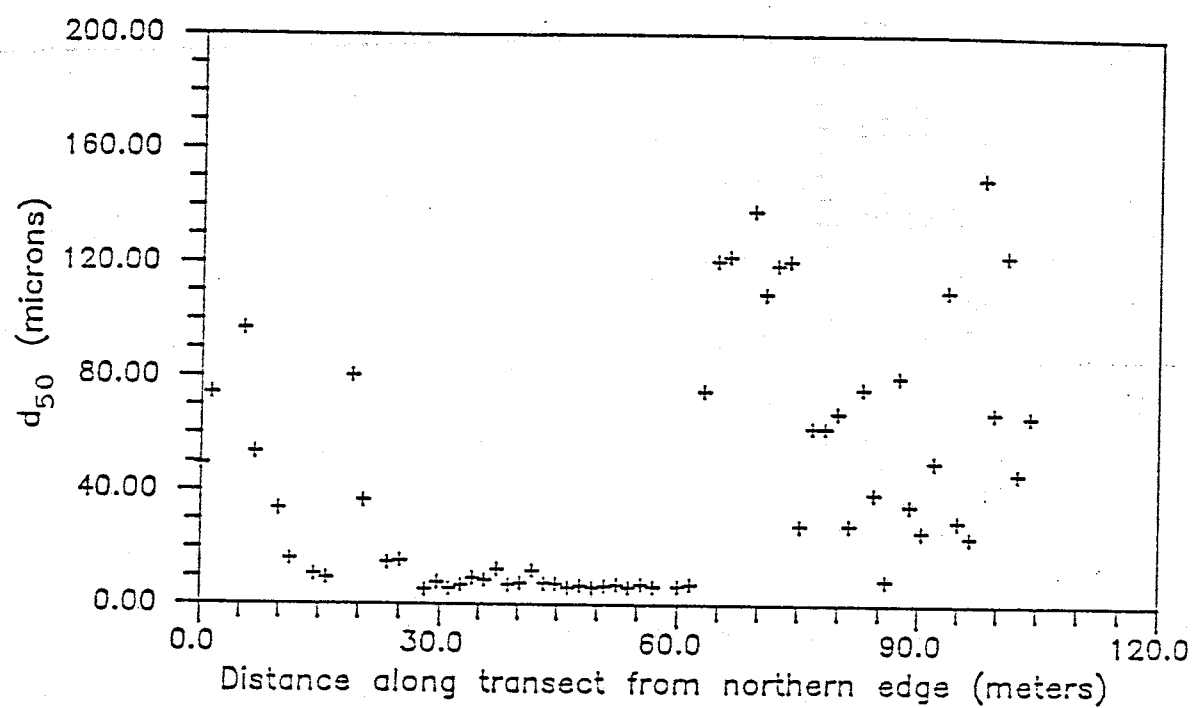


Figure 19a.  $d_{50}$  distribution laterally at 205cm depth.

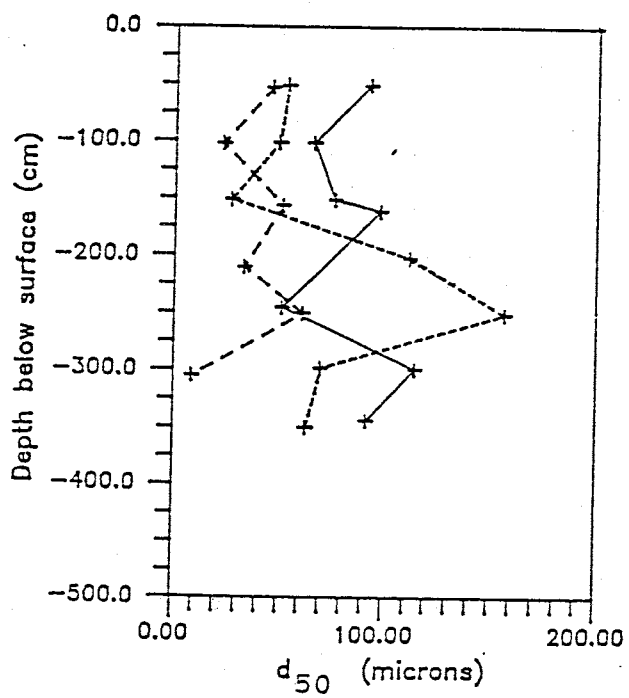


Figure 19b.

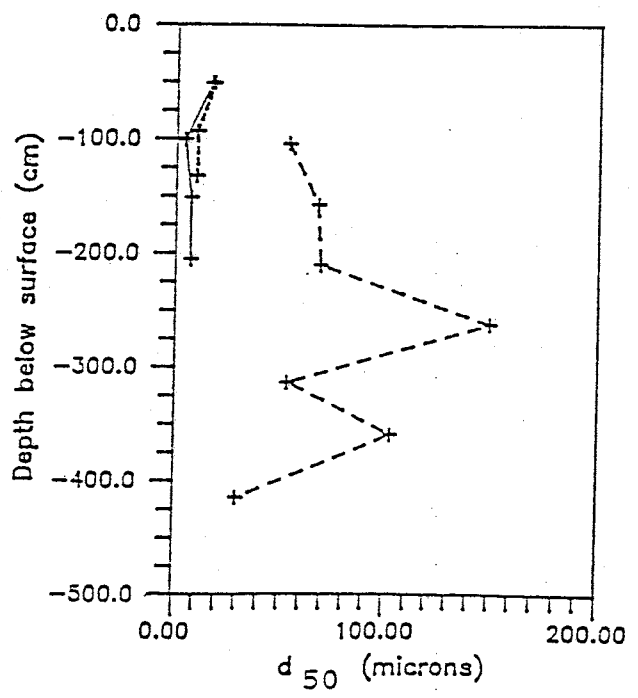


Figure 19c.

$d_{50}$  distribution with depth for each vertical transect.

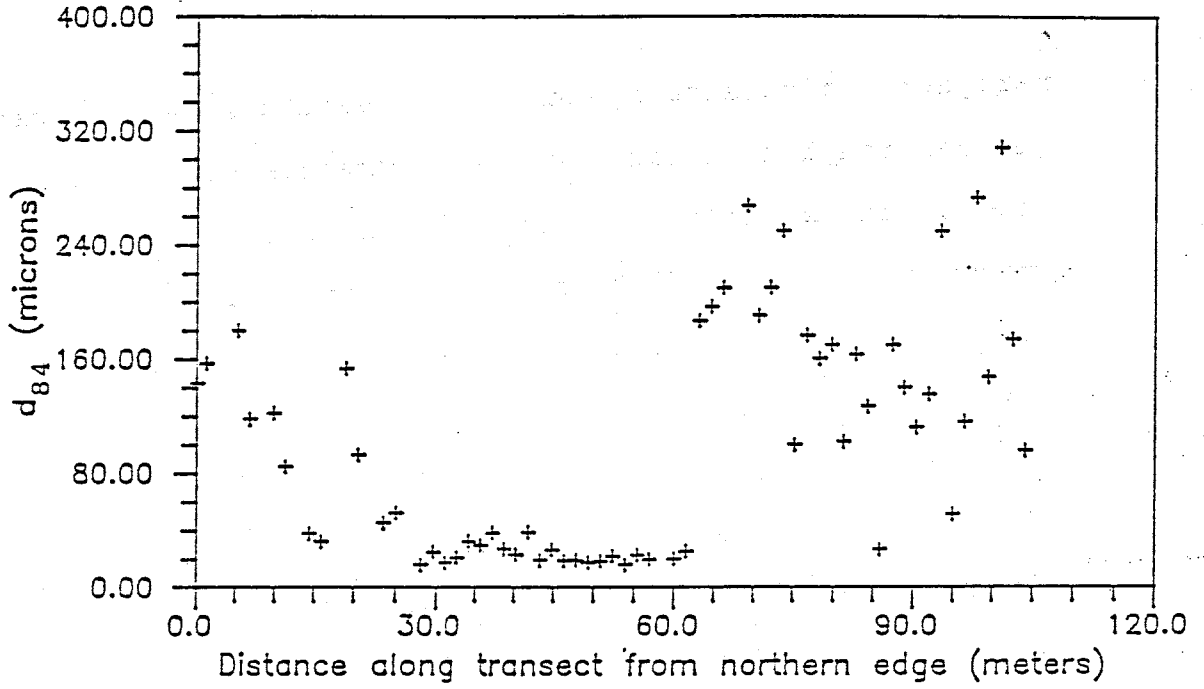


Figure 20a.  $d_{84}$  distribution laterally at 205cm depth.

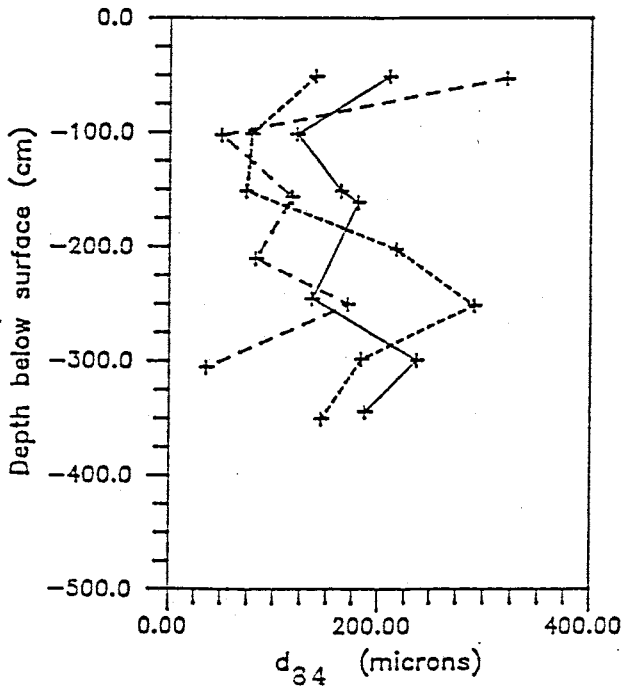


Figure 20b.

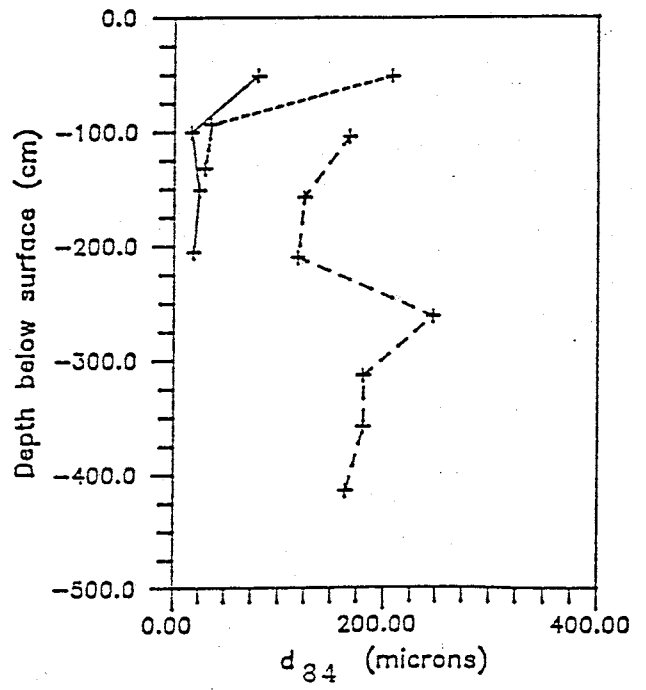


Figure 20c.

$d_{84}$  distribution with depth for each vertical transect.

peripheral discharge system. The variability in particle size between sampling locations also increases substantially to either side of the slime zone. The particle size near the edge of the impoundment is a function of the particle size coming from the mill house. The degree of crushing at the mill site was dependent on the ore content in the rock. Thus, the waste material produced by the mill would vary in particle size. Near the flumes, the coarser particles would settle out. The fines tended to be carried to the pond in the central portion of the impoundment. Between these 2 areas, layers of coarse and fine-grained tails form depending on the output from the flume. The presence of these layers, many under 1 cm in thickness, cause a great deal of variability in the grain size distribution in areas from 0-25 m and 72-104 m.

A sharp discontinuity in the data exists at 62 meters in figures 18a, 19a, and 20a. In a distance of 1.5 m along the transect, the samples go from the finest encountered to some of the coarsest. The presence of such coarse material over 30 meters from the flume line (southern edge) is very surprising. ? explain

The second layer of the impoundment is somewhat bowl-shaped. The tailings were deposited downslope from the edges. As the pond in the center of the impoundment would begin to fill in, the gradient between the edge and the center decreased. For this reason, the layers of tailings are not always parallel to the surface. Therefore, even though the depth of the samples from the surface was identical (205 cm), chances are that the same layer was not sampled. This is most likely the reason for

the sharp discontinuity at 62 meters. Figure 21 is an example of how such a discontinuity could occur.

Figures 18b & c, 19b & c, and 20b & c exhibit the variability with depth of  $d_{10}$ ,  $d_{50}$ , and  $d_{84}$  respectively. The particle size distributions from the vertical transects in the slime zone (V7 & V47) are the most uniform with depth. This was envisioned previously. On the contrary, the variability at V6 and V11 along the northern and southern edges is very large. Once again, this is due to fluctuations in the output from the mill. The variability with depth in the transition zone, sampled by transects V10 and V75, is much greater in the coarser fractions ( $d_{50}$  and  $d_{84}$ ) than in the finer fraction ( $d_{10}$ ). The large variability is caused by interfingering of coarser-grained layers with the fine-grained slimes.

The particle size at approximately 50 cm depth from the  $d_{84}$  plots for the interior vertical transects V7, V47, and V75 are much coarser than the underlying samples. The reason for this increased particle size at shallow depths in the interior of the second layer could be the result of surface wash. Surface wash would cause coarser particles from the edges to be redistributed towards the center of the transect. This process would be the most effective when the pond is absent from the surface of the second layer.

The uniformity coefficient (UC), as the name suggests, is a measure of how uniform the particle distribution is within a sample. Figures 22a, b, & c are the plots of UC throughout the cross section. In figure 22a, it is found that the most uniform

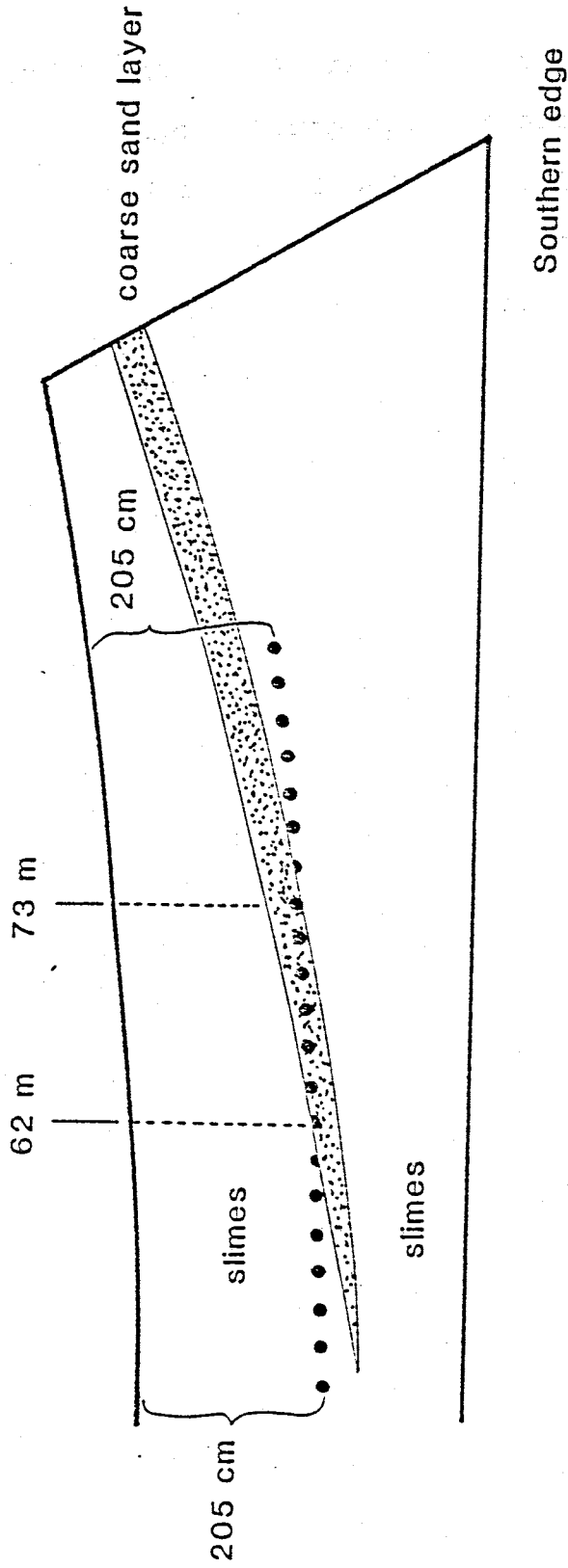


Figure 21. Possible reason for the grain size discontinuity at 62m along the lower horizontal transect.



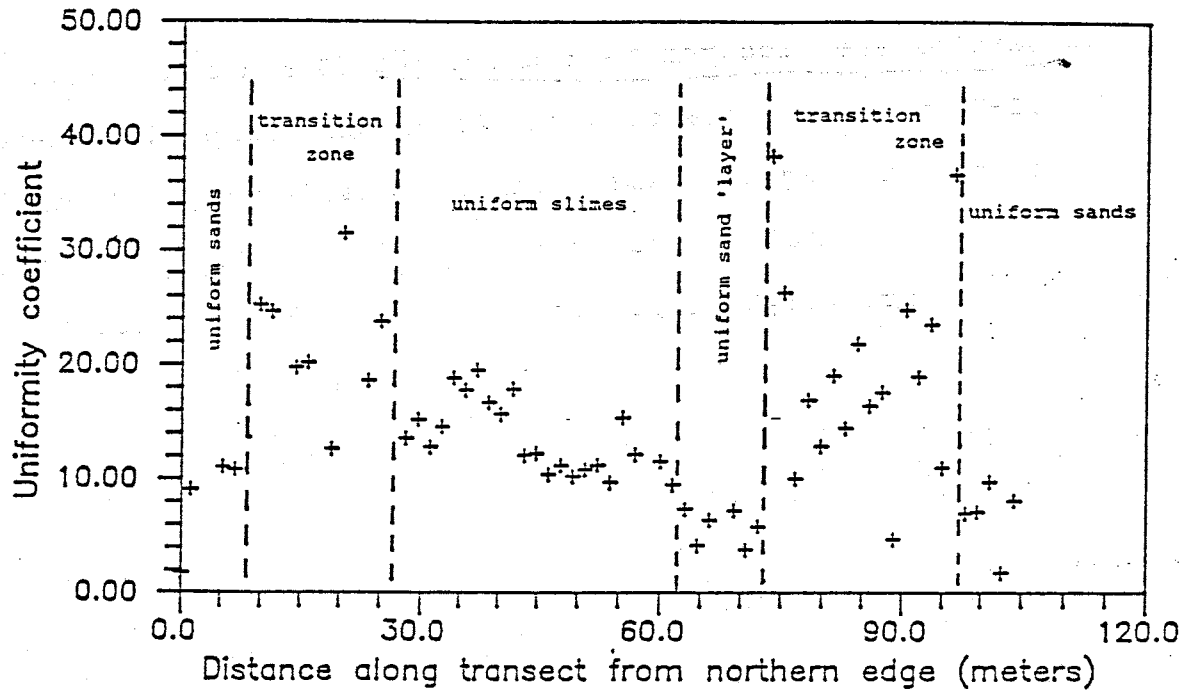


Figure 22a. UC distribution laterally at 205cm depth.

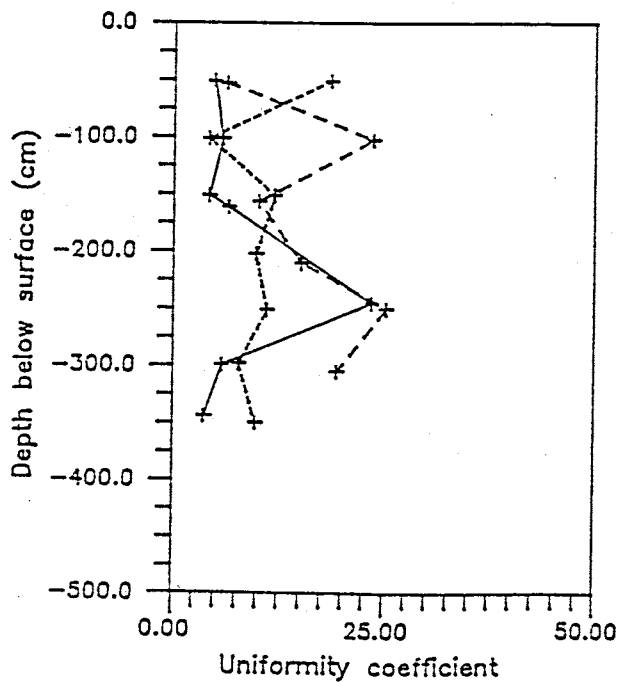


Figure 22b.

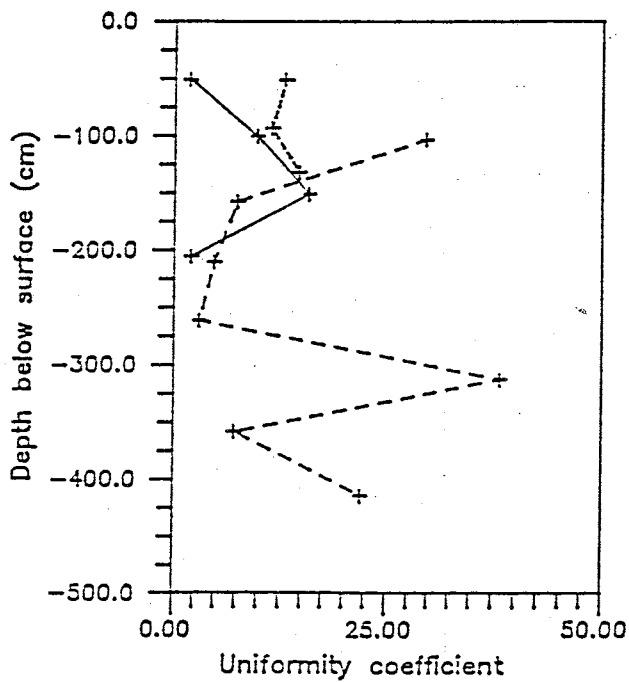


Figure 22c.

UC distribution with depth for each vertical transect.

samples are located near the edges (0-8 m and 96-104 m) and from 62-73 m where a coarse sand layer was sampled. Therefore, even though the grain size varies considerably between layers with depth along both edges, the individual layers (sample thickness = 3 cm) are very uniform in particle size. If more than one layer is sampled within the 3 cm long ring sample, the range in particle size for the sample will increase. Thus, the UC for that sample will also increase. Therefore, a high UC value within a given sample ring is a good indication of layering.

Large fluctuations in the UC from 8-42 m and from 73-96 m are present in figure 22a. This variability is no doubt due to layering of coarse and fine-grained tails as previously mentioned. Lower UC values are present from 42-62 meters. Fine-grained tails predominate in this area with little interlayering of coarser grained particles.

All inferences made using the grain size data from the vertical transects must be done with caution. This is due to the scarcity of data in the vertical direction.

To summarize, it appears that the center portion of the transect (slime zone, 25-62 m) is the most uniform with fine-grained tails predominating. Between the slime zone and the edges (8-25 m & 62-96 m), highly variable transition zones are present. These zones appear to consist of interlayered fine and coarse-grained particles (slimes and sands). Near both edges (sand zones, 0-8 m & 96-104 m) the tailings are coarser grained but still highly variable with depth. In the sand zones, the degree of layering is dependent on the variance of particle size

delivered from the mill.

The range in grain size was also determined for the soil underlying the transect. Figure 23 shows that the range in grain size is much less for the soil than the overlying tailings. Observation of these curves show that the soil is very poorly sorted ranging from clay to gravel-size particles within the same sample. The 2 plots are not the typical smooth, S shaped curves that were seen for the tailings. This is due to the multi-modal distribution of particle sizes present in the soil. Plotting the 2 extreme values on a soil textural triangle (figure 24) shows that the underlying soil ranges from a loam to a silt loam.

#### Pore size distribution

The particle size distribution was just shown to be quite variable throughout the cross section. Therefore, it is likely that the pore size distribution will also vary greatly. Although the particle size distribution is not the only factor influencing pore distribution, it is probably the most important. Other factors influencing pore size distribution include packing structure, particle shape, presence of secondary cementation, and degree of compaction.

The range of the pore size distribution from the cross section through second layer can be seen in figure 25. Both curves represent tailings moisture characteristics ( $\theta/\psi$  curves) upon drying. Each plot was fit to its set of respective data points (not shown) using the regression program VANGNM written by Rien van Genuchten (1978).

The variability between the  $\theta/\psi$  curves A and B in figure 25

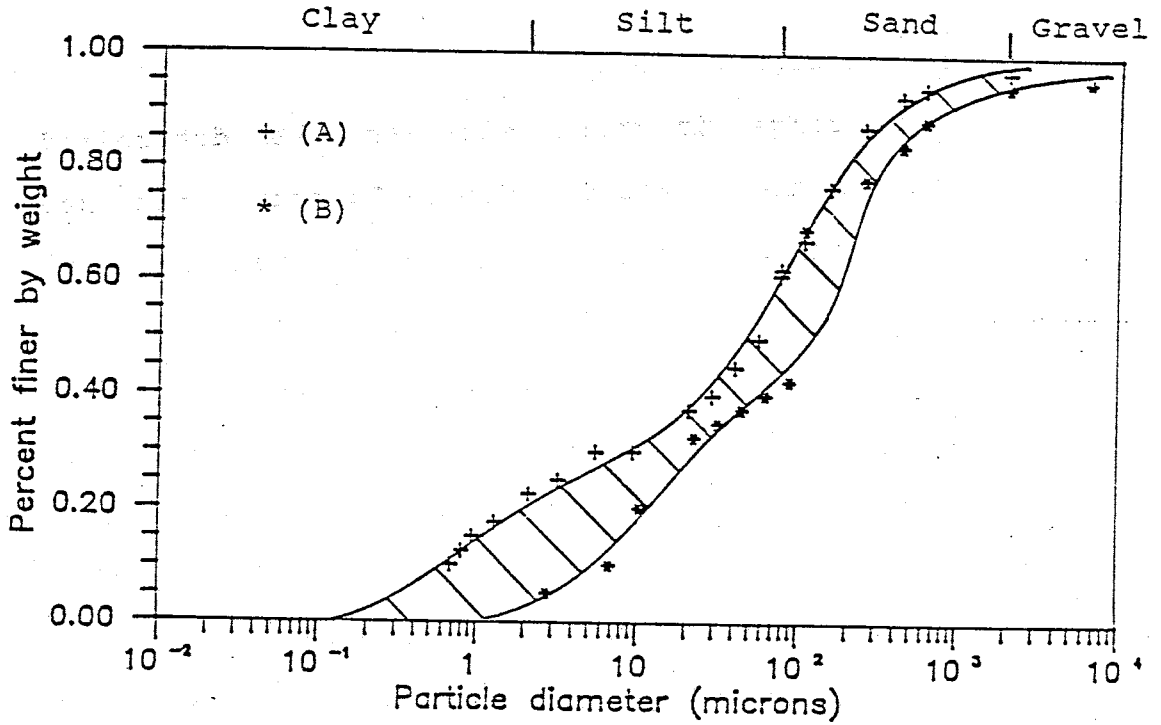


Figure 23. Range in grain size curves for the underlying soil.

Soil Textural Triangle

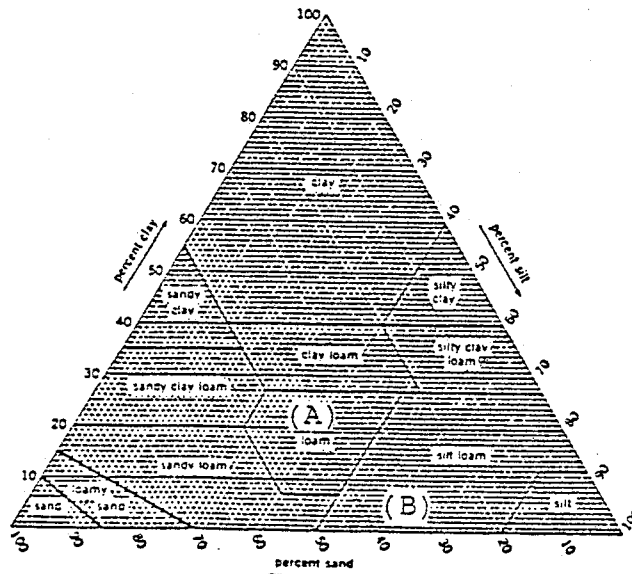


Figure 24. Grain size extremes for the underlying soil.

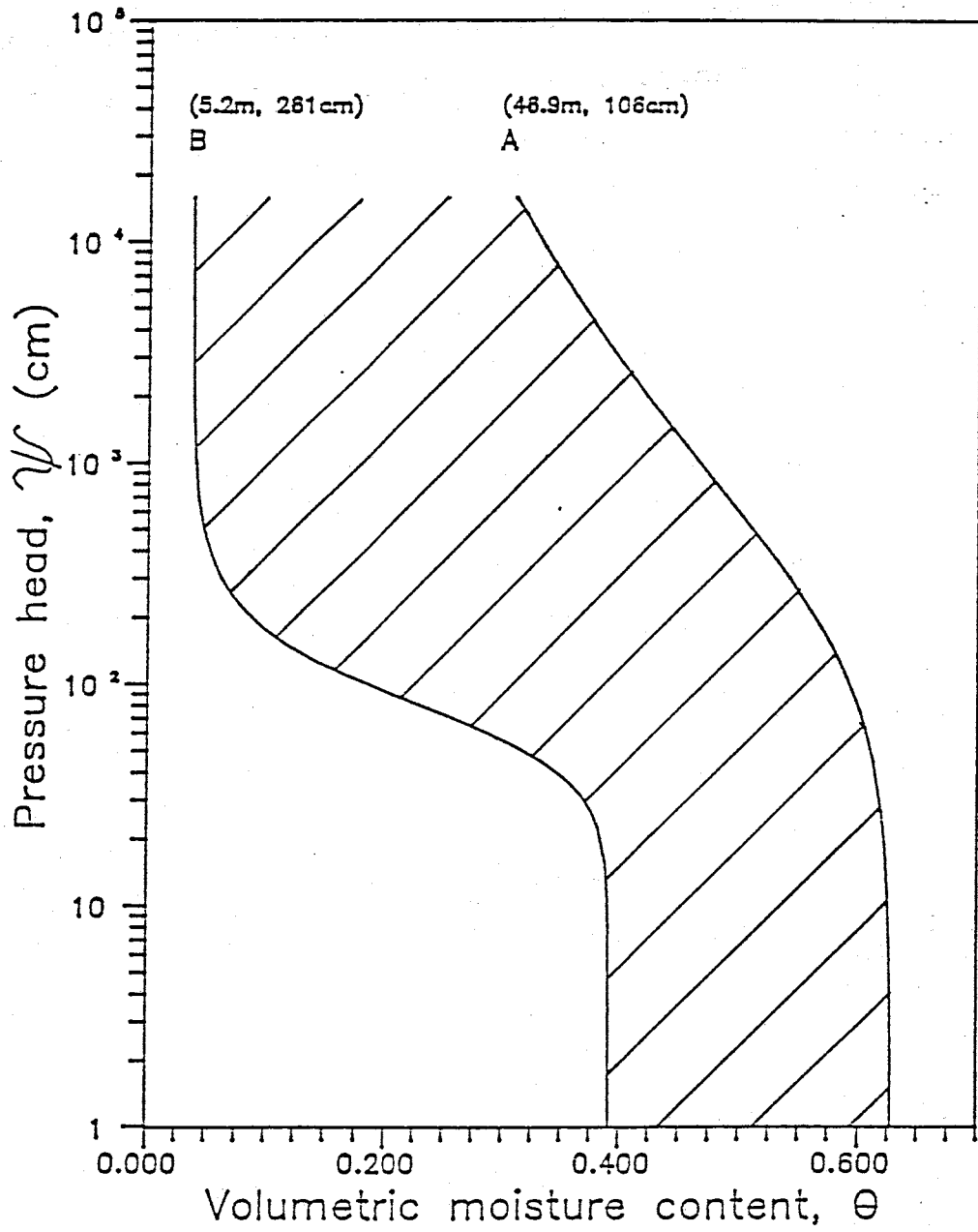


Figure 25. Range in pore size distribution for the cross section.

is similar to the variability between soil moisture characteristics of a clay and a fine-sand. It is not coincidental that the  $\theta/\psi$  relationships developed from samples A and B in figure 25 are based on the same samples as figure 16. The samples (A & B) which mark the particle size distribution extremes in figure 16 also inversely form the pore size distribution extremes in figure 25.

Moisture contents for samples along both the horizontal and vertical transects were determined at saturation (porosity), 1.5, and 15 bars pressure. The moisture content at 15 bars ( $\theta_{15}$ ) was analyzed because at this pressure most of the available water in the sample has been extruded.  $\theta_{15}$  is commonly referred to as the residual moisture content. The moisture content at 1.5 bars ( $\theta_{1.5}$ ) was also analyzed for each sample. This is a very useful intermediate pressure to distinguish between samples with different pore size distributions. Extensive  $\theta/\psi$  relationships, enabling the construction of  $\theta/\psi$  curves, were determined for all soil moisture samples from the vertical transects.

Figure 26a is the porosity distribution along the lower horizontal transect (205 cm). The range in porosity values along this transect is quite extensive (0.38 to 0.68). The porosity distribution is the most uniform in the slime zone (25-62 m). Here, the values only range from 0.52 to 0.62. Aside from this zone, porosity values throughout the rest of the transect are highly variable. This variability is no doubt due to the layering in the coarse-grained fractions.

In the vertical direction (26b & c), porosity appears to

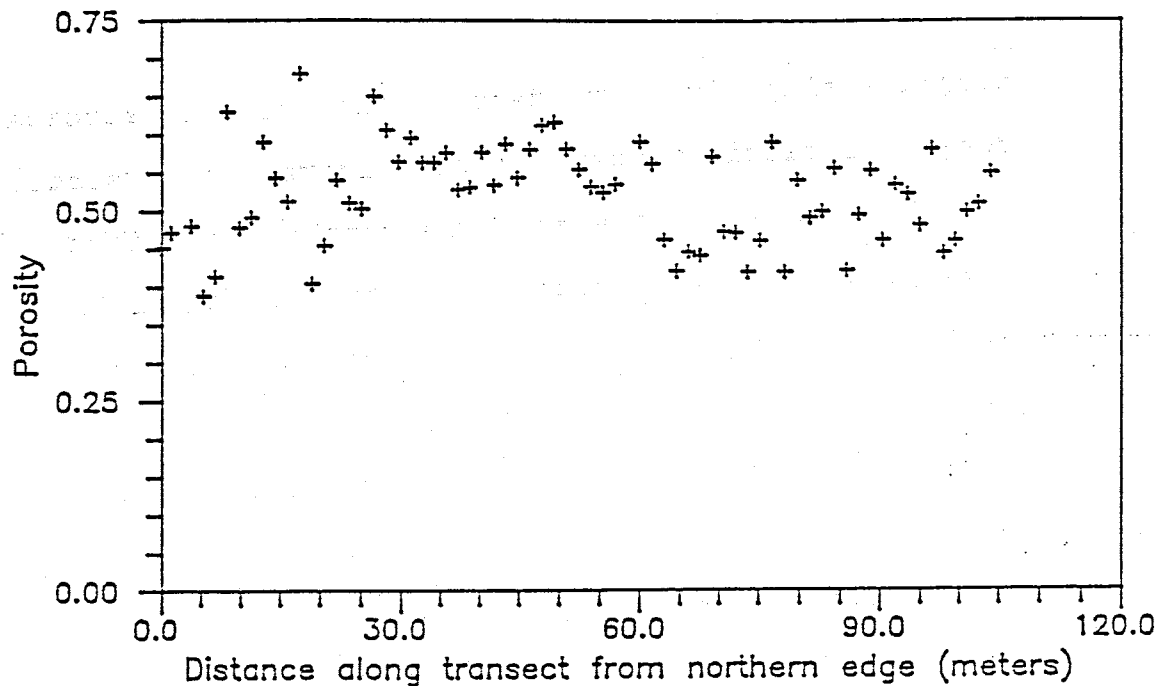


Figure 26a. Porosity distribution laterally at 205cm depth.

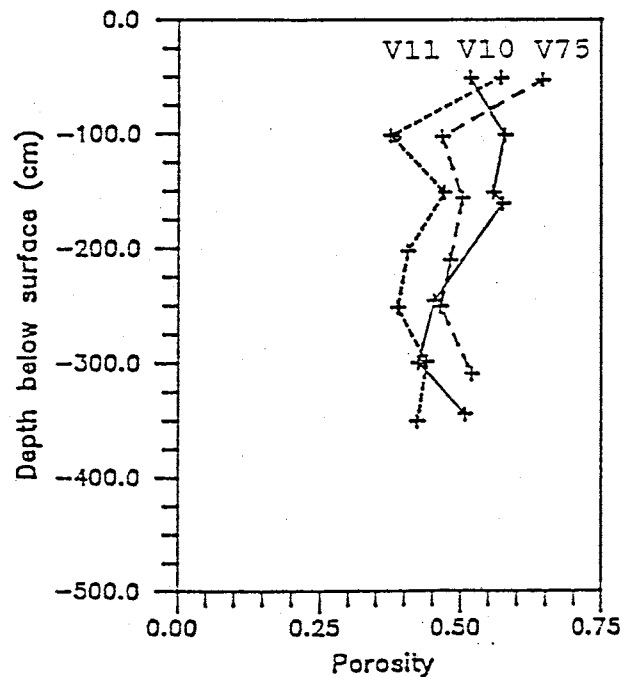


Figure 26b.

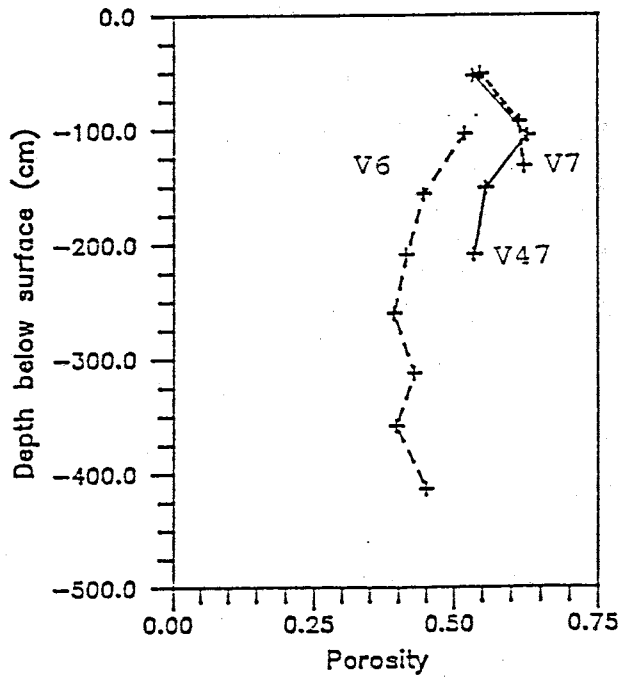


Figure 26c.

Porosity distribution with depth for each vertical transect.

decrease slightly with depth. This slight decrease could be the result of matrix compaction with increasing overburden.

Figure 27a is the moisture content distribution at 1.5 bars along the lower transect. The variability of the  $\theta_{1.5}$  distribution is much greater than that of the porosity distribution.  $\theta_{1.5}$  values range from 0.03 to 0.43. Once again, the fine-grained slimes (25-62 m) exhibit a rather uniform distribution. The sharp discontinuity that is present in the grain size distribution (figures 18a, 19a, & 20a) is found in the  $\theta_{1.5}$  distribution as well. The presence of this discontinuity was not evident from the porosity distribution plot. The sand-sized tails present from 62-73 m de-water easily in comparison to the adjacent slimes. The large fluctuation in the  $\theta_{1.5}$  data from 73-104 m is very similar to that observed in the porosity distribution.

The  $\theta_{1.5}$  distributions with depth (figures 27b & c) appear to be quite uniform in comparison to the horizontal transect. This is true for all the vertical transects except V75. The fluctuations along V75 are as great as the range of  $\theta_{1.5}$  in the horizontal direction. Once again, these fluctuations in  $\theta_{1.5}$  are caused by layering in this area.

The moisture content distribution at 15 bars ( $\theta_{15}$ ) is similar to that at 1.5 bars (figure 28a). The major difference between the two distributions is noted in the slime zone (25-62 m). The variability of  $\theta_{15}$  between samples in this area increased substantially (range 0.11-0.35) with the increased pressure. Wierenga (1984) also found this to be the case in fairly homogeneous soils. With increased tension, he discovered that the



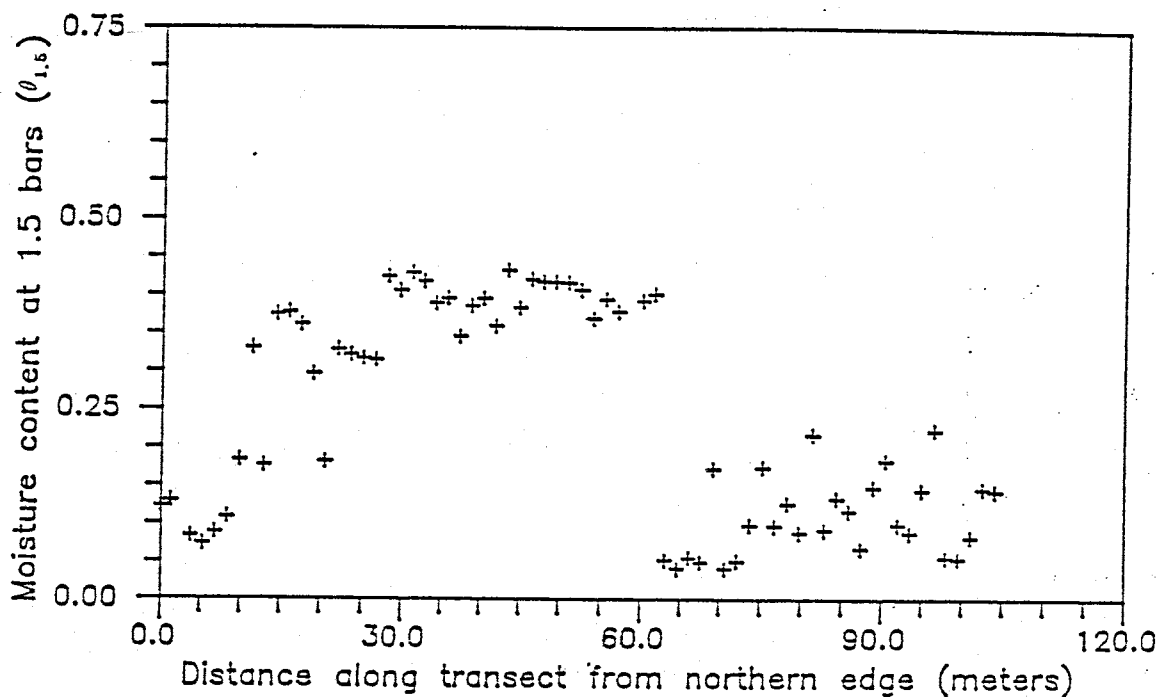


Figure 27a.  $\theta_{1.5}$  distribution laterally at 205cm depth.

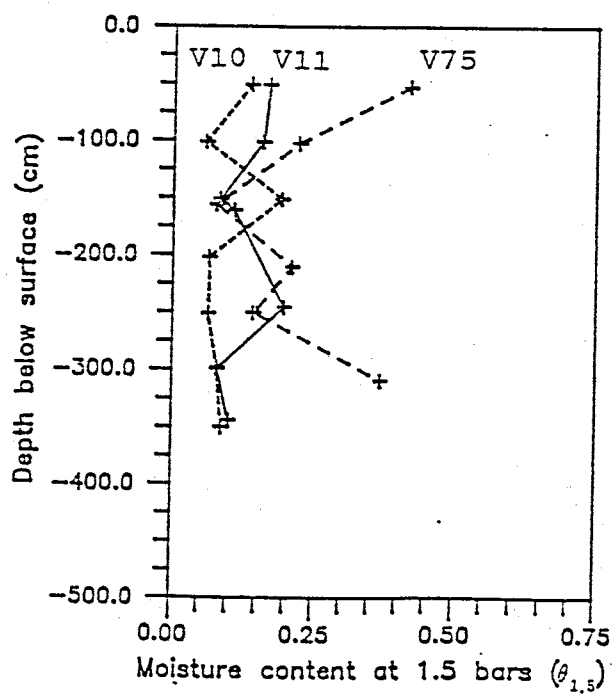


Figure 27b.

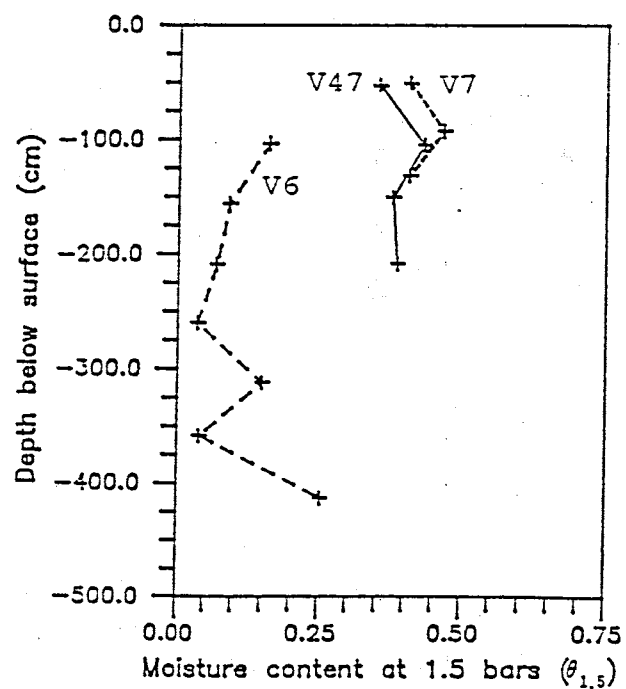


Figure 27c.

$\theta_{1.5}$  distribution with depth for each vertical transect.

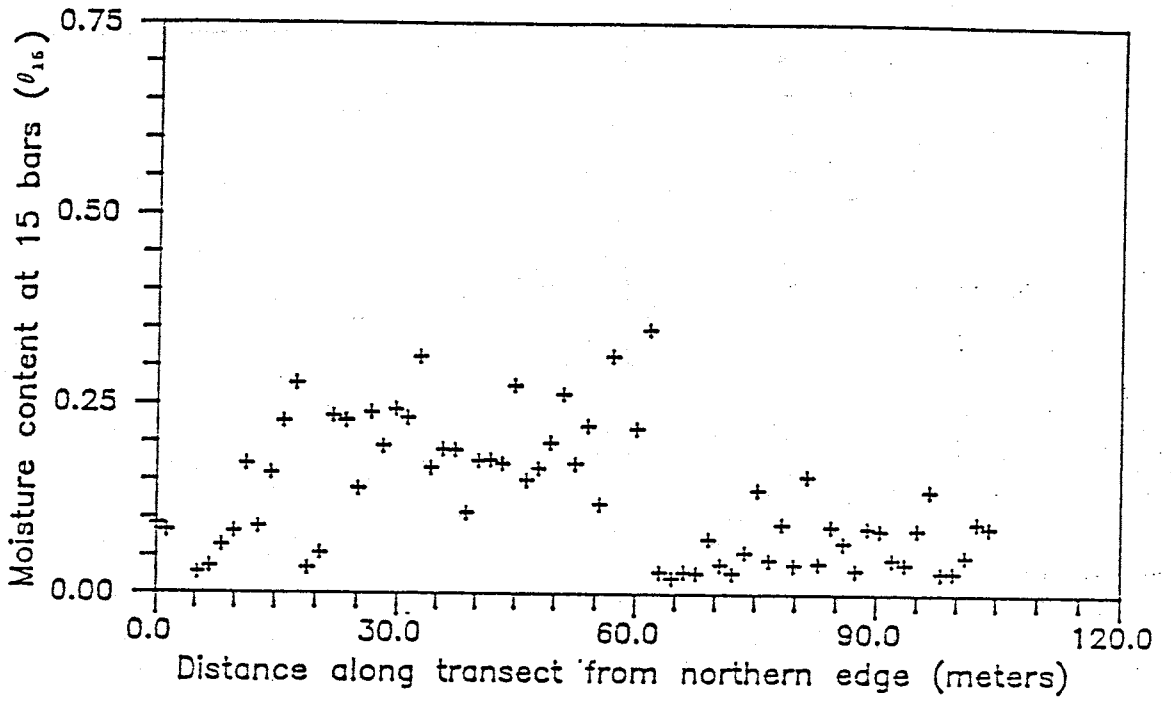


Figure 28a.  $\theta_{15}$  distribution laterally at 205cm depth.

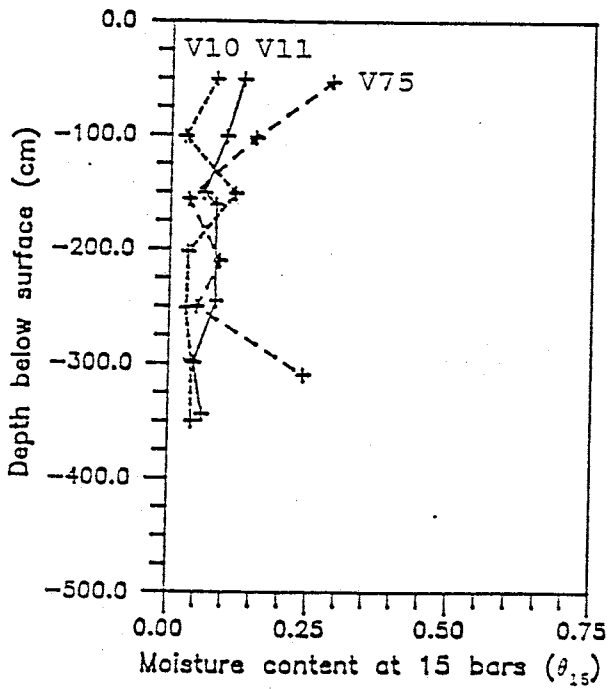


Figure 28b.

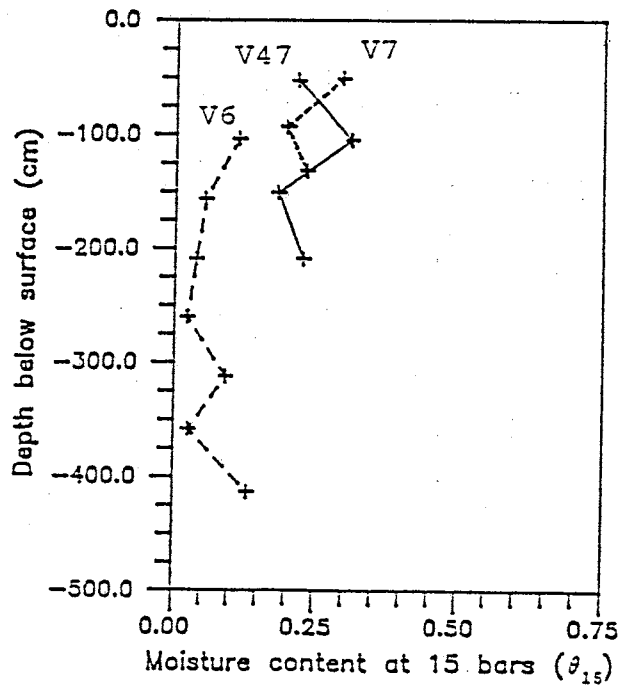


Figure 28c.

$\theta_{15}$  distribution with depth for each vertical transect.

variance in  $\theta$  between samples increased.

The  $\theta_{15}$  distribution with depth (figure 28b & c) is similar to the  $\theta_{1.5}$  distribution. Once again, the greatest variability is present along transect V75.

#### Hydraulic conductivity distribution

There is a problem of scale when sampling layered media with shelly tubes. Manometers are emplaced into the shelly tubes during conductivity reading to better delineate the presence of layering. Using these manometers, conductivity values can be determined at different places in the tubes every 13.3 cm. However, if the thickness of a layer is less than 13.3 cm, its conductivity will be affected by the overlying and/or underlying layers. Layers of 1 to 2 cm thickness are common throughout the cross section. Since all shelly tube samples were taken vertically, perpendicular to the layering, the K values determined are actually arithmetic averages for a given number of layers over 13.3 cm. This method does not measure the individual conductivity of each and every layer. This would not be practical on such a large scale. However, the presence of inter-layered fine and coarse-grained material should result in greater variable measurements of K when compared to uniform samples.

The size of the pore openings (intrinsic permeability) is, in part, a function of a sample's hydraulic conductivity (Fetter, 1980). As was described previously, the pore size distribution of the tailings varies greatly throughout the cross section. Therefore, it comes as no surprise that the conductivity distribution is also found to vary greatly as seen in figures 29-41.

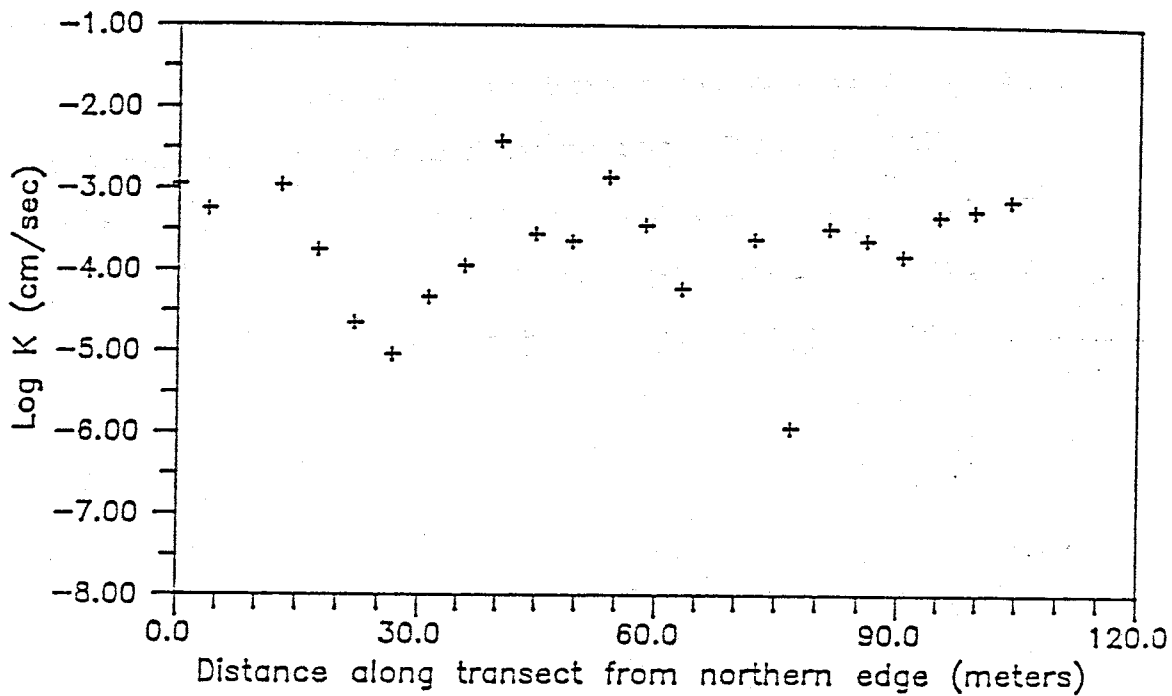


Figure 29. log K distribution laterally at 28cm depth.

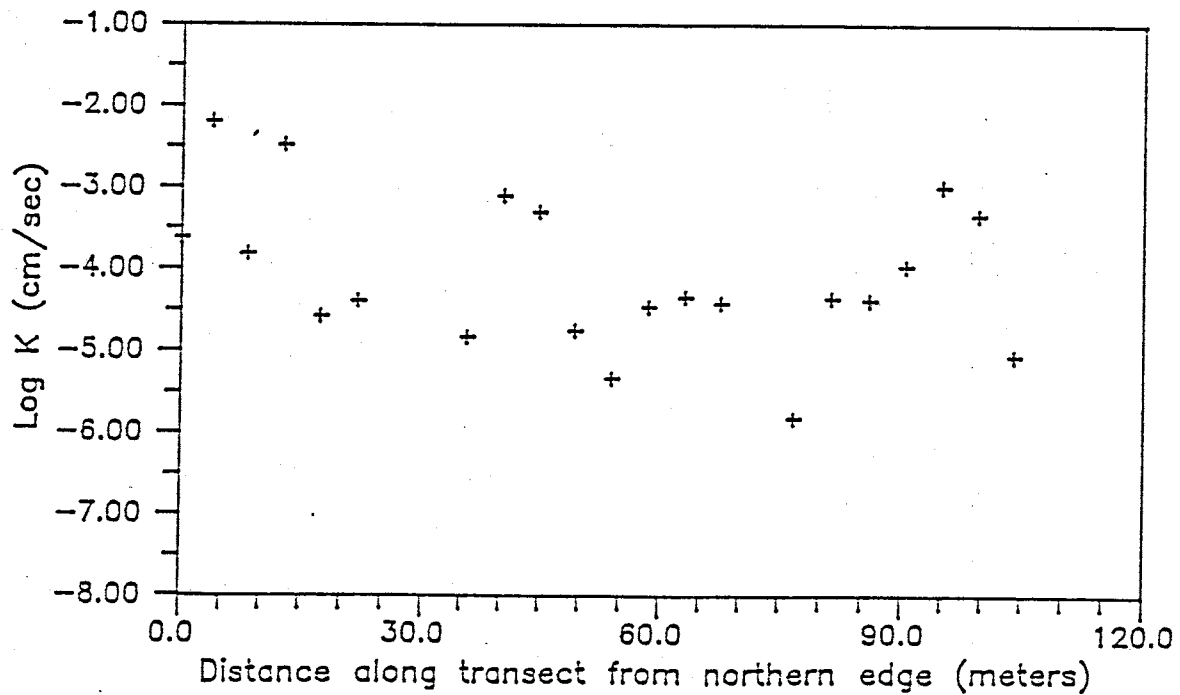


Figure 30. log K distribution laterally at 41cm depth.

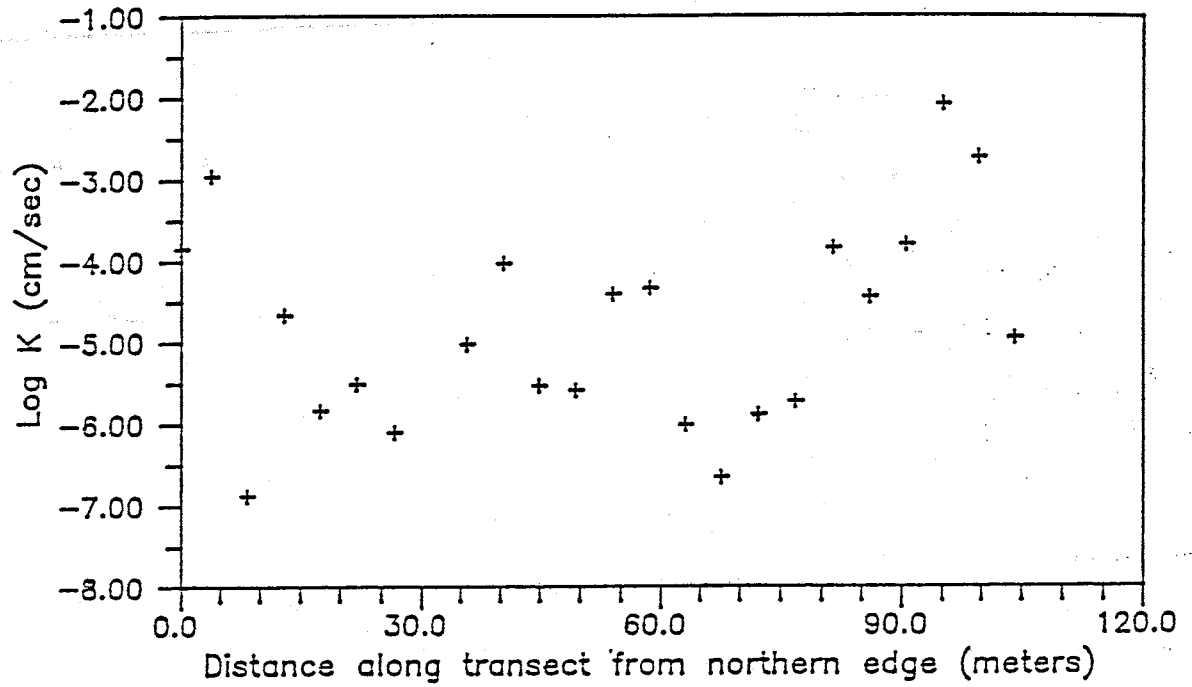


Figure 31. log K distribution laterally at 54cm depth.

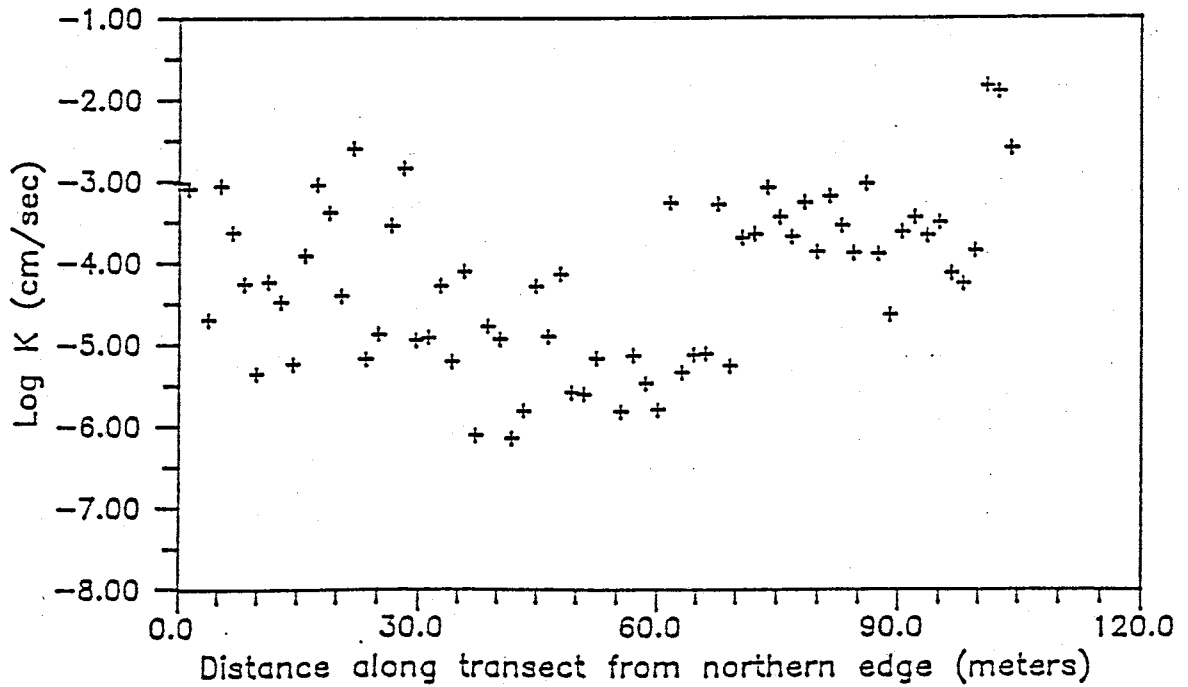


Figure 32. log K distribution laterally at 165cm depth.

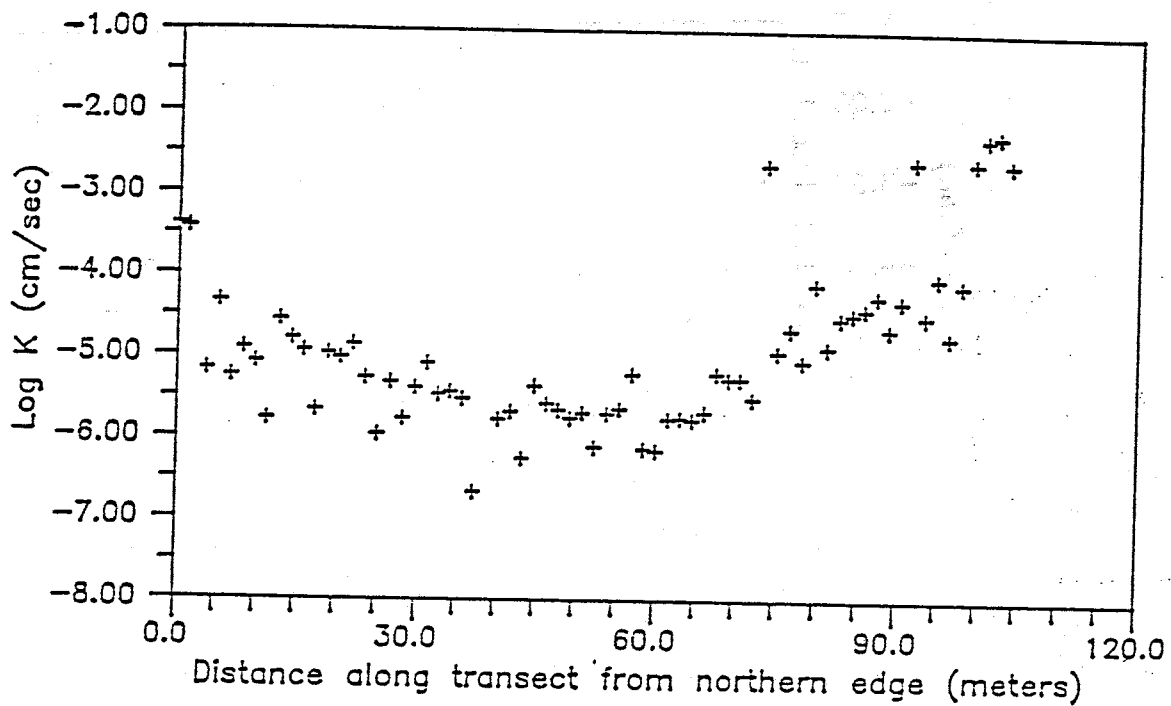


Figure 33. log K distribution laterally at 179cm depth.

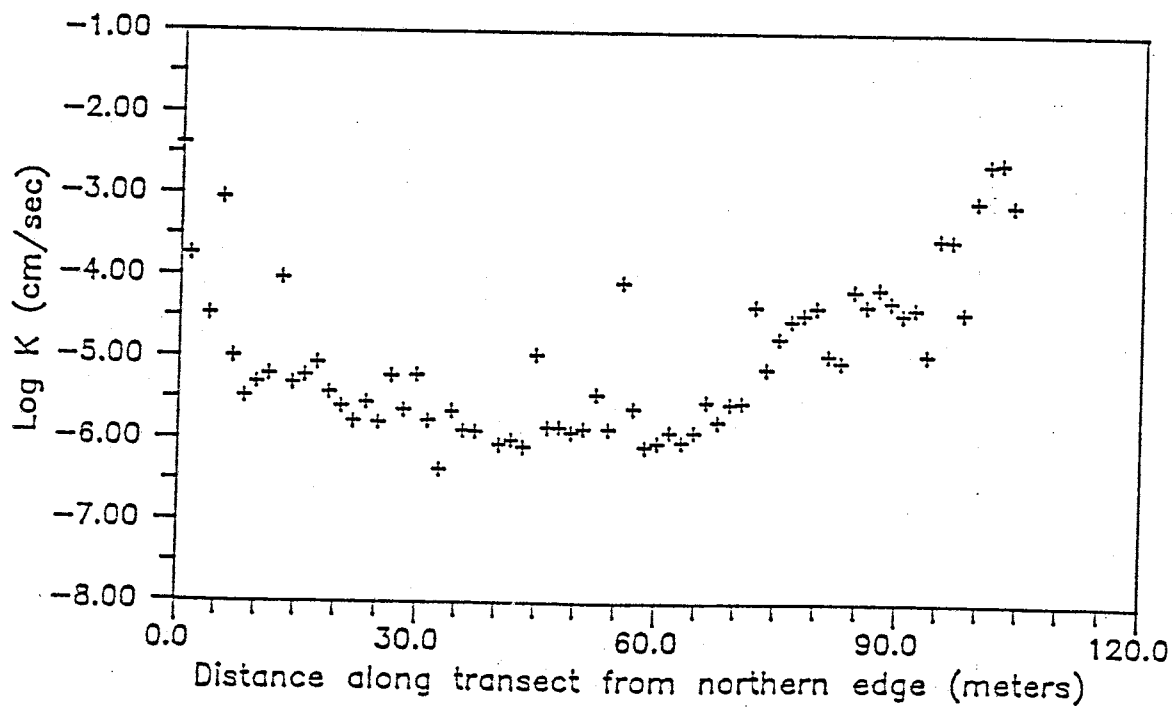


Figure 34. log K distribution laterally at 192cm depth.

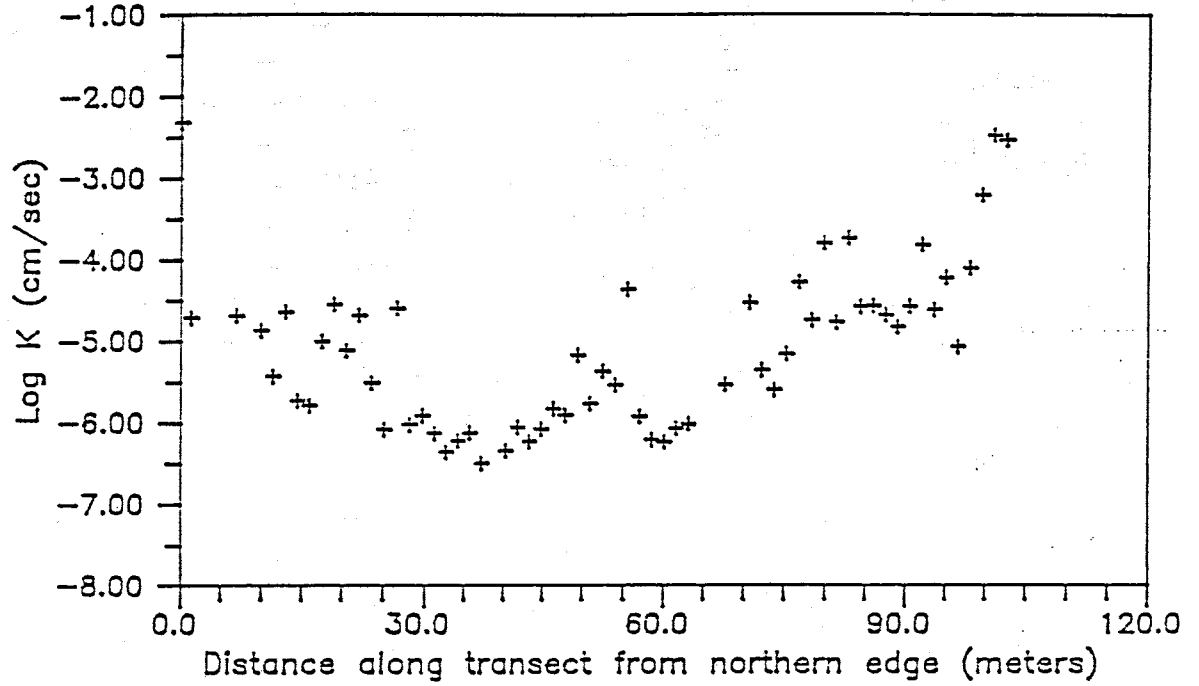


Figure 35. log K distribution laterally at 205cm depth.

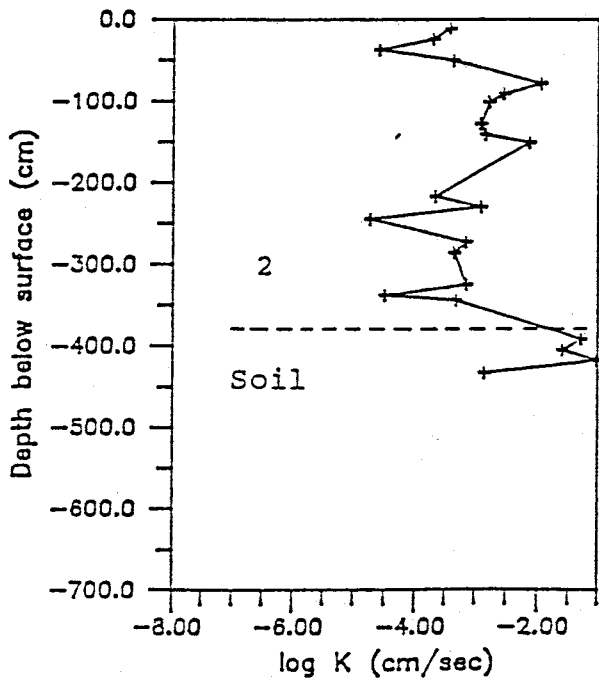


Figure 36. log K with depth, V11.

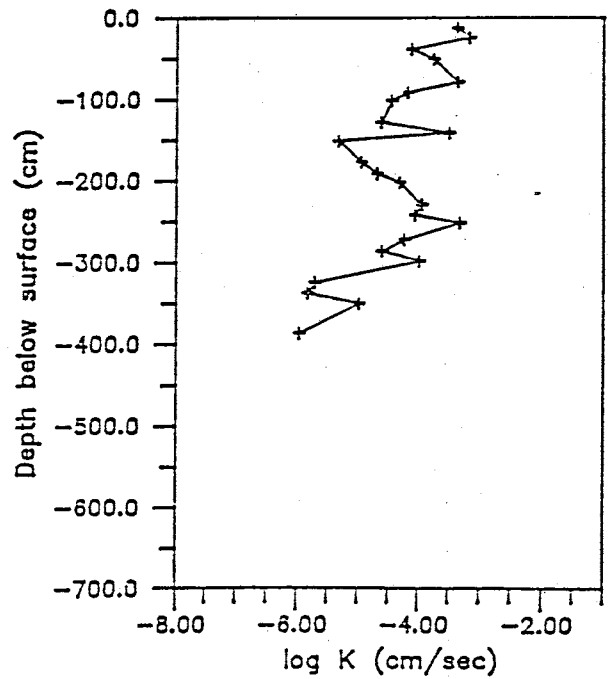


Figure 37. log K with depth, V10.

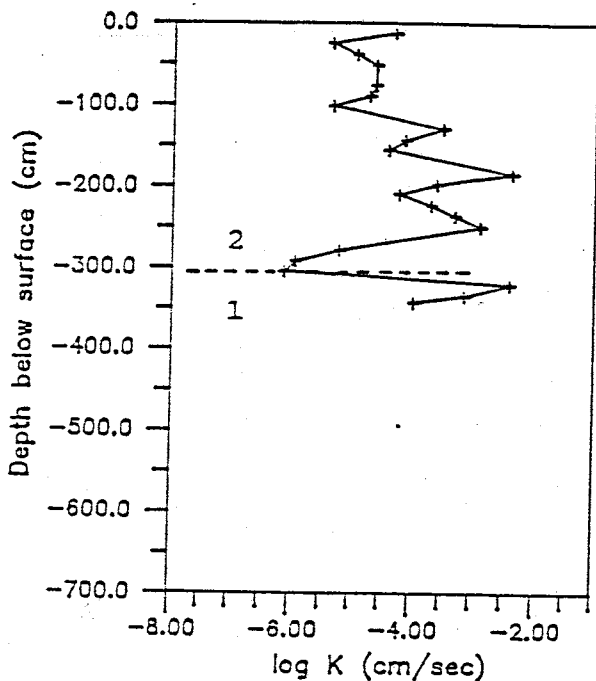


Figure 38. log K with depth, V75.

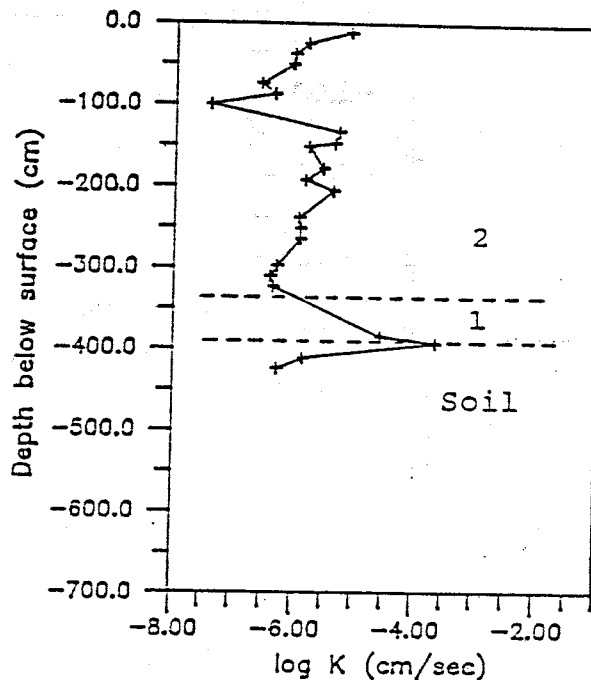


Figure 39. log K with depth, V47.

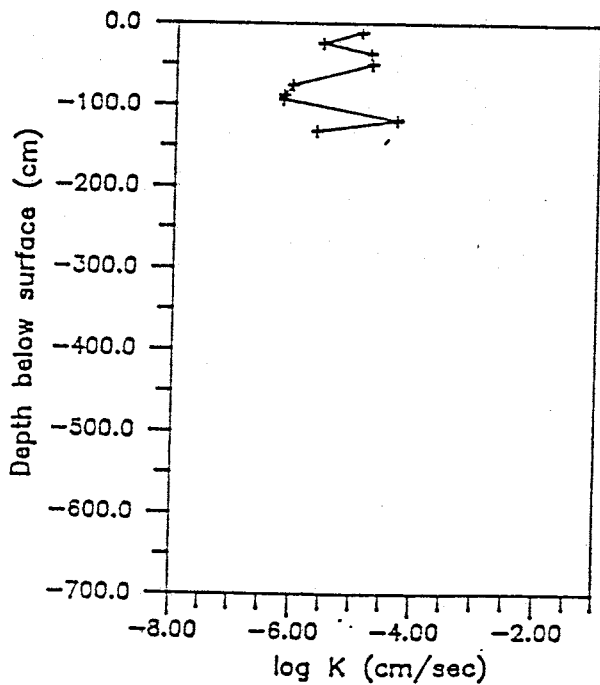


Figure 40. log K with depth, V7.

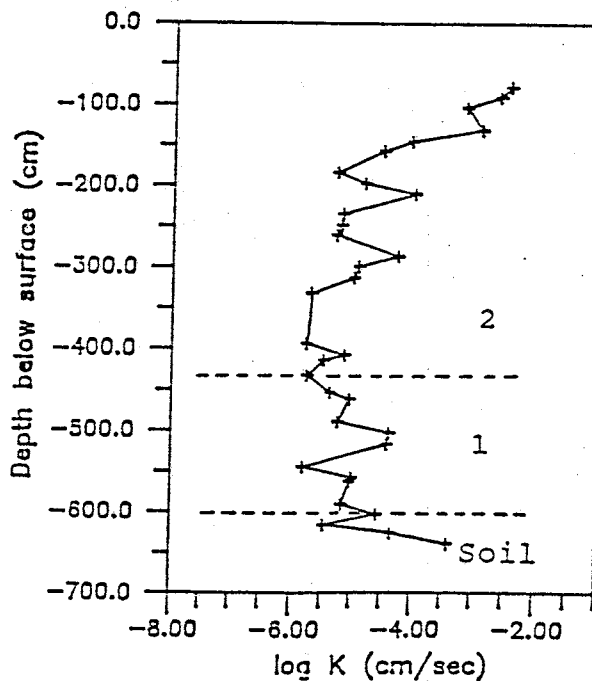


Figure 41. log K with depth, V6.



Plots 29-35 represent the logarithm (base 10) of K versus distance along the transect at depths from 54 to 205 cm with 0.00 m located at the northern edge. The possible range of conductivity values in naturally occurring sediments is presented in figure 42 (Freeze & Cherry, 1979). The 2 dashed lines delineate the range in K from the second layer of the impoundment.

The conductivity values from the shallow transects (28, 41, & 54 cm) are quite random. These values fluctuate greatly with no apparent trend to the data. This lack of trend for K along the upper transect could be caused by a number of secondary processes. The upper 50 to 75 cm of the second layer do not mimic the structure present at greater depths. This discrepancy is possibly due to surface wash, partial cementation, and/or precipitation of salts. Partial cementation has enabled extremely resistant layers (1-3 cm thick) to form near the surface (to depths of 1 m) in the coarser-grained zones of the second layer.

At greater depths (179, 192, & 205 cm), the K distribution is noted to have more of a trend rather than just a purely random distribution. The conductivity distribution at 205 cm somewhat mimics the particle size distribution. The variability in the particle size distribution, however, appears to be much greater.

The data from the 179, 192 and 205 cm depths are in close agreement with one another. This not the case, however, when comparing these 3 depths with K values from 165 cm. The mean value for 165 cm is almost an order of magnitude greater than the lower samples. This difference is believed to be the result of problems encountered during sampling. The diameter of the

### Range of Values of Hydraulic Conductivity

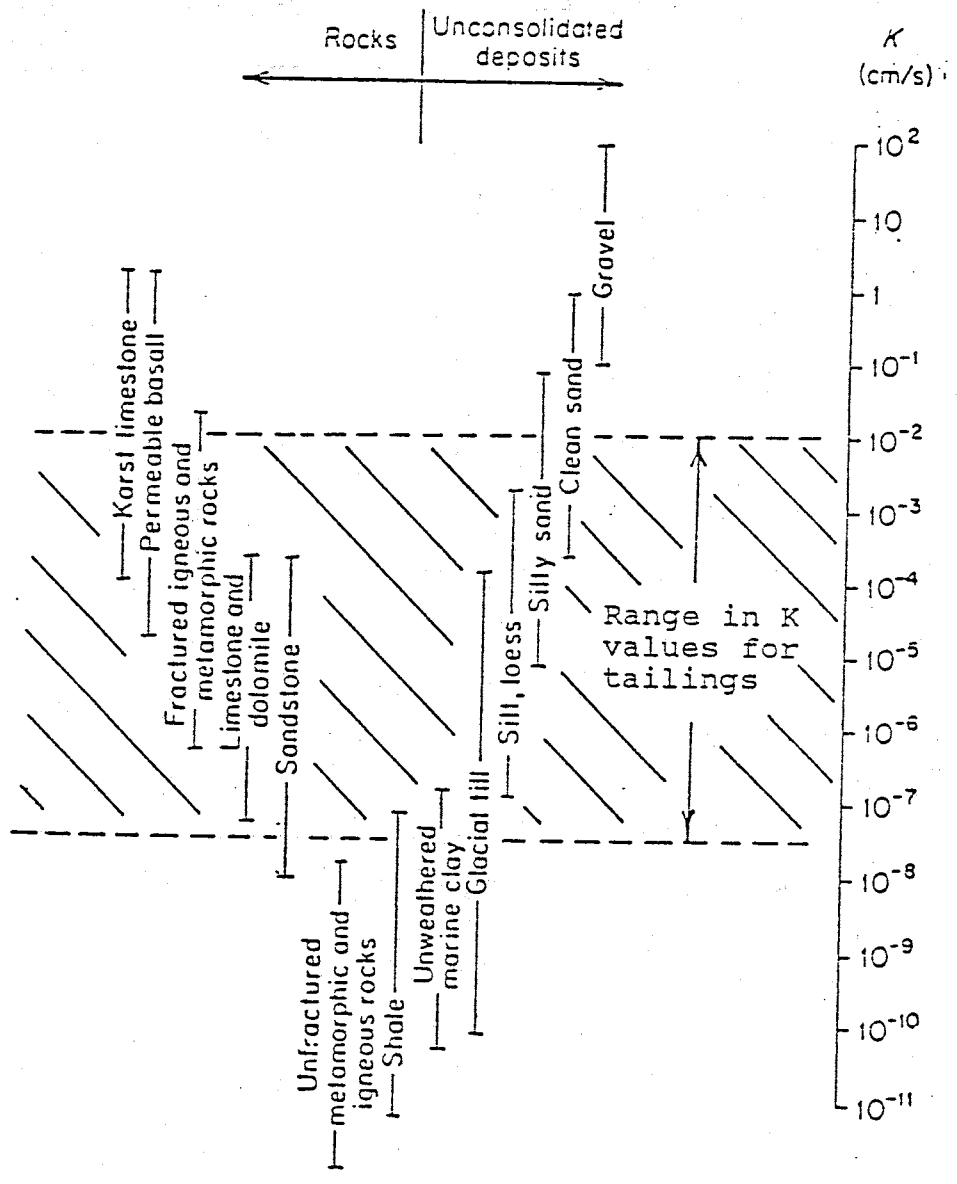


Figure 42. Range in hydraulic conductivity values for the cross section.

borehole drilled directly above the sample location was identical to that of the shelby diameter (7.62 cm). As a result, cuttings from the sides of the borehole were often mistakenly sampled and would thus end up on the top of the shelby tube sample. These cuttings (up to 6 cm in total thickness) tended to be very broken up and not at all reflective of the original matrix. Because of this, conductivity values measured in the upper portion of most shelby tubes were greater than one would expect. This 'false sample' was easily discernible by the presence of oxidized material (yellow to tan in color) in the upper portion of the shelby tube. Oxidized layers throughout the cross section are not common at depths greater than approximately one meter.

The conductivity values are found to vary greatly in the vertical direction as well (figures 36-41). The least amount of variation is seen in transects V7, V11, and V47. This was expected for the finer grained material. In both V6 and V10, K values vary greatly and appear to decrease slightly with depth. The K readings at V75 appear to fluctuate randomly with depth. Four orders of magnitude in conductivity values are present along the 3.5 meter depth of V75. The conductivity values, along with  $\theta$  and particle size data from V75, once again point out that layering must be present in this area.

#### In situ moisture content

In situ moisture content can be obtained with a neutron moisture probe. In order for the probe to operate accurately, it must be calibrated to each specific field site. The calibration is performed by comparing  $\theta$  values obtained from both the mois-

ture probe and destructive samples. A calibration curve is then produced from the data using a least squares regression fit.

Problems were encountered when using the moisture probe in tailings wetter than  $\theta_F=0.35$ . The model 503 Hydroprobe from Campbell Pacific Nuclear is limited in accuracy to moisture contents no greater than  $\theta_F=0.32$ . In situ moisture contents greater than 0.32 are common in the slimes. An accurate method for determining  $\theta_F$  values in tailings greater than 0.35 has yet to be developed.

The sphere of influence for a neutron moisture probe is approximately 30 cm. Therefore, if more than 1 soil type is present within the range of the probe, an averaged moisture content value will be reported. Fine layers (1-3 cm) are common in the tailings. Thus, by using this device, averaged values from the tailings layers are determined. This averaged process will have the greatest effect in the transition zones where interfingering slimes and sands are common.

Figures 43-46 represent the moisture content distributions with depth 5.2, 67.5, 78.6, and 102.3 meters from the northern edge along the cross section. The 5 lines on each figure signify moisture content readings obtained at various dates in 1986. The  $\theta_F$  distribution for each access tube is quite uniform over time. The plots 43-46 are included so that a general idea of the in situ moisture content with depth can be gained. Due to the problems encountered at high moisture contents, and because this device obtains  $\theta$  values over approximately 30 cm, this data will not be used in the following analysis sections.

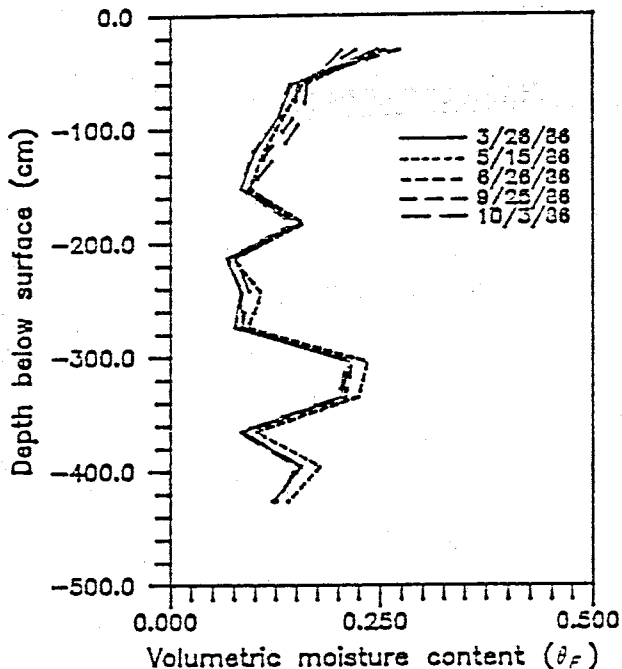


Figure 43.  $\theta_F$  distribution with depth, tube #6.

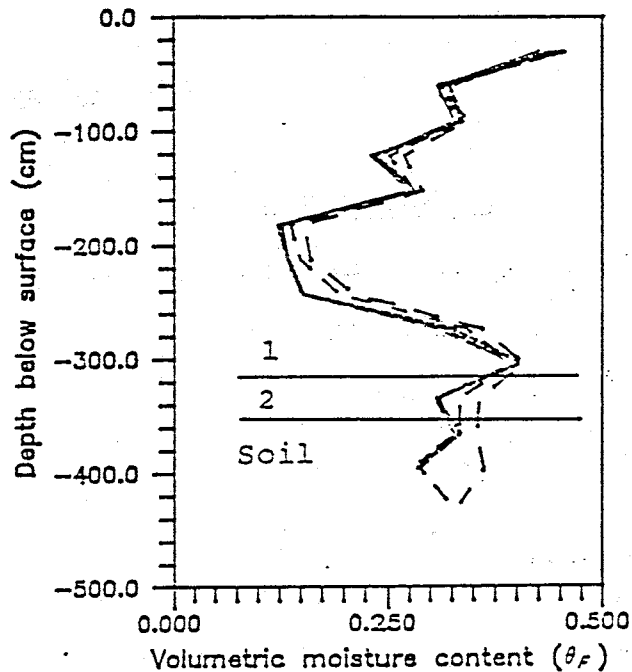


Figure 44.  $\theta_F$  distribution with depth, tube #9.

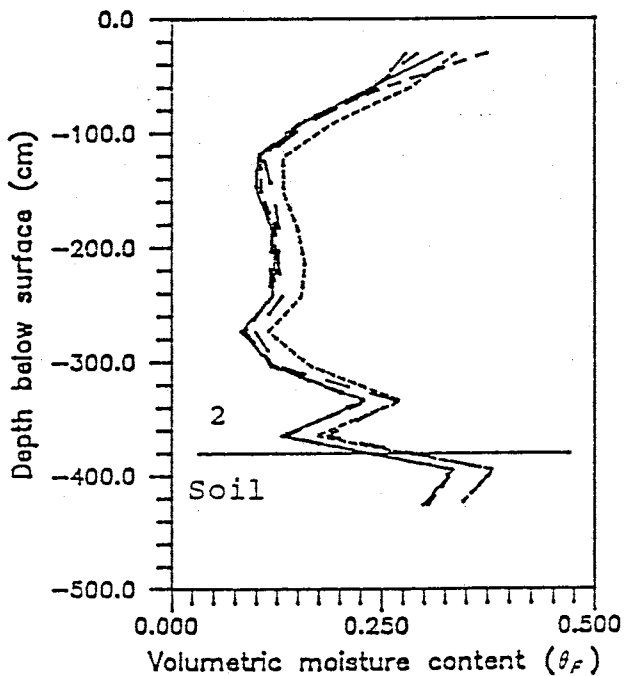


Figure 45.  $\theta_F$  distribution with depth, tube #10.

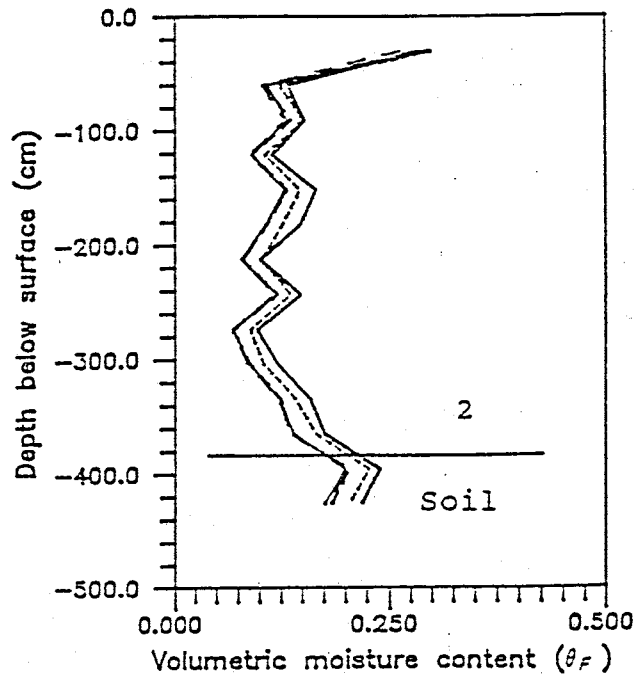


Figure 46.  $\theta_F$  distribution with depth, tube #11.

$n$ ,  $\theta_{1.5}$ ,  $\theta_{15}$  (unitless)  
 $d^*$ , GM (microns)  
 UC, CC, SORT, SKEW (unitless)

Variable, depth	# of samples	Mean	Std deviation	Range
log K, 28 cm	22	-3.700	0.787	3.521
" , 41 cm	21	-4.075	0.929	3.639
" , 54 cm	23	-4.823	1.259	4.804
" , 165 cm	68	-4.197	1.018	4.320
" , 179 cm	68	-4.944	1.000	4.422
" , 192 cm	68	-4.994	0.980	3.978
" , 205 cm	61	-5.101	0.992	4.180
n , 67 cm	20	0.525	0.075	0.330
n , 205 cm	68	0.520	0.065	0.293
$\theta_{1.5}$ , 67 cm	20	0.278	0.122	0.397
$\theta_{1.5}$ , 205 cm	68	0.234	0.142	0.392
$\theta_{15}$ , 67 cm	20	0.208	0.098	0.318
$\theta_{15}$ , 205 cm	67	0.128	0.086	0.327
$d_{10}$ , 205 cm	61	6.785	9.456	33.728
$d_{16}$ , "	61	13.258	16.881	58.132
$d_{30}$ , "	61	24.743	26.888	99.062
$d_{50}$ , "	61	43.218	42.116	144.869
$d_{60}$ , "	61	55.815	51.453	172.477
$d_{84}$ , "	61	102.225	81.405	292.578
GM , "	61	34.944	35.291	119.988
UC , "	61	14.527	7.691	36.489
CC , "	61	1.725	0.877	3.516
SORT , "	61	5.306	1.721	7.362
SKEW , "	61	0.660	0.464	2.688

TABLE 3

Vertical transects statistics: LAYER 2

units: see table 2

Variable, transect	# of samples	Mean	Std deviation	Range
log K, V6	20	-4.577	1.032	3.317
" , V7	9	-5.394	0.670	1.888
" , V47	19	-5.974	0.524	2.294
" , V75	19	-4.394	0.971	3.735
" , V10	23	-4.374	0.797	2.792
" , V11	18	-3.289	0.746	2.779
n , V6	7	0.434	0.041	0.129
" , V7	3	0.594	0.034	0.076

n	, V47	4	0.563	0.038	0.094
"	, V75	6	0.513	0.062	0.180
"	, V10	7	0.439	0.062	0.196
"	, V11	7	0.516	0.055	0.154
$\theta_{1.5}$	, V6	7	0.114	0.072	0.217
"	, V7	3	0.426	0.029	0.061
"	, V47	4	0.387	0.030	0.082
"	, V75	6	0.241	0.120	0.343
"	, V10	7	0.098	0.046	0.134
"	, V11	7	0.128	0.042	0.117
$\theta_{15}$	, V6	7	0.069	0.041	0.110
"	, V7	3	0.241	0.041	0.098
"	, V47	4	0.234	0.047	0.129
"	, V75	6	0.142	0.095	0.254
"	, V10	7	0.053	0.031	0.092
"	, V11	7	0.080	0.027	0.086
$d_{10}$	, V6	7	10.800	16.840	55.682
"	, V7	3	1.413	0.486	1.120
"	, V47	4	4.341	4.480	11.092
"	, V75	6	4.093	3.245	9.377
"	, V10	7	7.044	6.289	14.283
"	, V11	7	12.634	11.795	27.733
$d_{16}$	, V6	7	25.994	21.707	65.934
"	, V7	3	2.315	0.879	1.997
"	, V47	4	4.834	4.774	11.924
"	, V75	6	8.851	6.565	17.554
"	, V10	7	20.122	10.182	34.113
"	, V11	7	27.794	19.946	45.585
$d_{30}$	, V6	7	45.581	29.930	93.232
"	, V7	3	5.072	1.231	2.611
"	, V47	4	6.210	4.883	12.741
"	, V75	6	20.879	12.125	31.390
"	, V10	7	44.271	23.443	78.328
"	, V11	7	43.272	27.357	48.014
$d_{50}$	, V6	7	75.072	36.782	120.078
"	, V7	3	12.478	3.768	7.994
"	, V47	4	8.873	4.749	12.704
"	, V75	6	37.092	17.722	52.534
"	, V10	7	75.722	40.835	129.824
"	, V11	7	65.468	39.132	63.822
$d_{60}$	, V6	7	93.985	38.656	127.700
"	, V7	3	18.165	6.238	13.599
"	, V47	4	11.638	5.691	15.509
"	, V75	6	49.606	23.647	70.673
"	, V10	7	92.934	50.086	155.613
"	, V11	7	82.560	49.091	72.852

$d_{34}$	, V6	7	168.286	39.637	128.934
"	, V7	3	90.945	81.864	176.570
"	, V47	4	34.971	26.256	63.708
"	, V75	6	129.002	96.193	284.194
"	, V10	7	160.557	71.657	217.890
"	, V11	7	136.963	80.332	116.000
GM	, V6	7	53.106	37.507	106.114
"	, V7	3	14.022	9.243	20.243
"	, V47	4	12.531	11.353	7.939
"	, V75	6	28.335	24.717	70.778
"	, V10	7	49.225	31.054	87.291
"	, V11	7	54.498	41.451	80.754

The positions of the horizontal and vertical transects in cross section are presented in figures 47, 48, and 49. The mean and standard deviation values for  $d_{50}$ ,  $\theta_{1.5}$ , and log K (figures 47-49 respectively) are presented for each transect. Mean and standard deviation values for layer 1 and the soil are also included in figures 47-49 where data was available.

Statistical values calculated from the horizontal transects of the Waldo Mill impoundment compare favorably to work done on the Van Stone impoundment by Kealy (1970). Table 4 lists the statistical values calculated by Kealy. The mean values for the grain size parameters  $d_{10}$  and  $d_{50}$  are slightly higher for the Van Stone impoundment. This is no doubt due to the fact that Kealy collected the majority of his data near the edge of the impoundment where coarser tails predominate.

TABLE 4

Statistical values from the Van Stone lead/zinc tailings impoundment (Kealy, 1970)

<u>Variable</u>	<u>Mean</u>	<u>Range</u>	<u>Comment</u>
log K, (cm/sec)	-4.004	(-5.64)-(-3.48)	Intact,



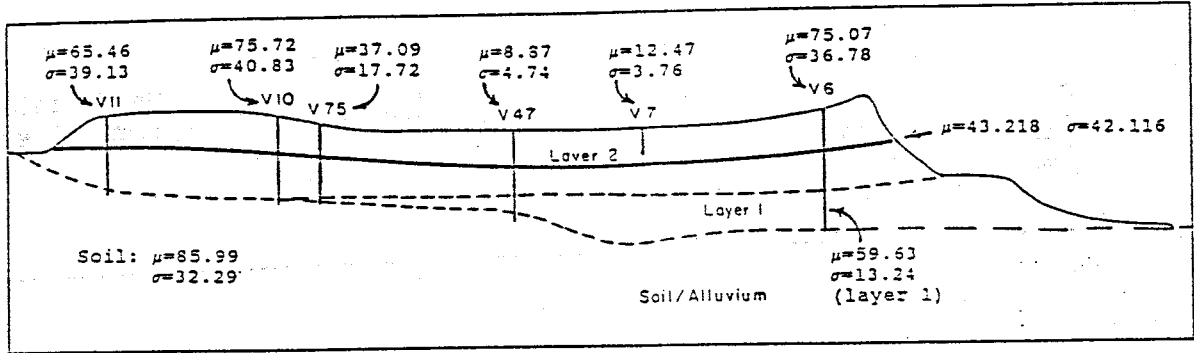


Figure 47. Mean and standard deviation values of  $d_{50}$  for each transect.

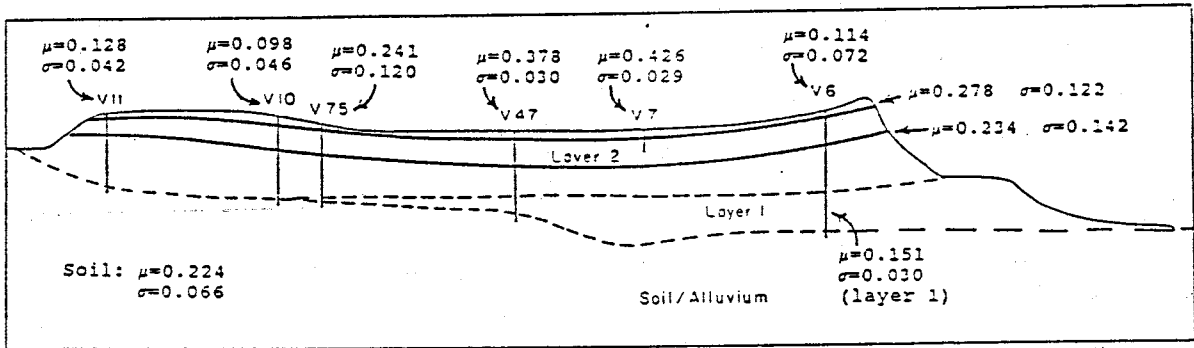


Figure 48. Mean and standard deviation values of  $\theta_{1.5}$  for each transect.

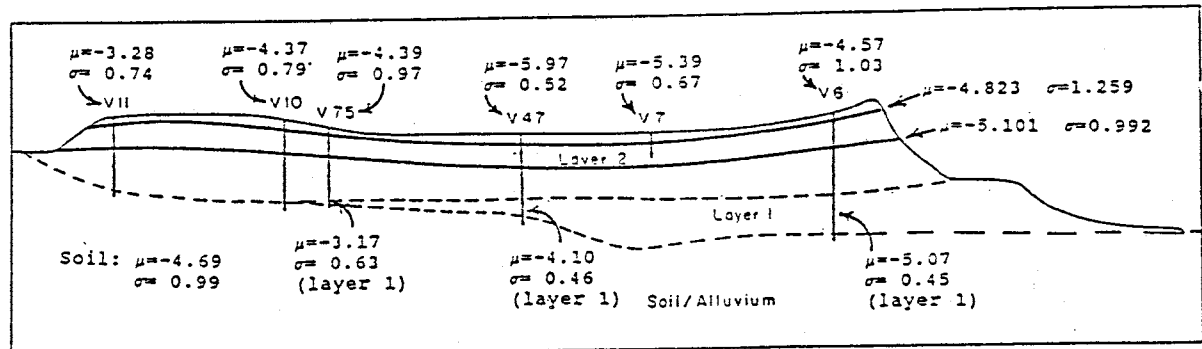


Figure 49. Mean and standard deviation values of  $\log K$  for each transect.

n	0.44	0.40-0.48	vertical cores
d <sub>10</sub> , (microns)	13.0		Repacked samples
d <sub>50</sub> , "	70.0		
UC, "	6.09		

### Conclusions

Characterization information gained using sample statistics is listed below.

- The grain size average from the cross section is interpreted as silt-sized. However, a great deal of variability is present in the parameters (d<sub>10</sub>, d<sub>16</sub>, d<sub>30</sub>, d<sub>50</sub>, d<sub>60</sub>, and d<sub>84</sub>) that make up this grain size curve.
- The trask skewness value for the horizontal transect (SKEW = 0.660) shows that the tailings, as a whole, are positively skewed with fines predominating.
- The grain size parameters (d<sub>10</sub>-d<sub>84</sub>) from table 3 exhibit a decrease towards the central portion of the cross section.
- The possibility of layering in grain size is indicated by high standard deviation and range values near the northern and southern edges of the cross section.
- The variability in grain size as measured by the standard deviation, is a function of the mean for the finer grain-size parameters d<sub>10</sub> and d<sub>50</sub> (figures 50 & 51). An increase in the mean value within the finer fractions of a sample results in an increase in the variability about this mean. This was not the case for the coarser-grained fraction (figure 52) within each sample. In the central portion of the cross section, the variability ( $\sigma$ ) in d<sub>84</sub> increases with increased mean values. As one nears both edges, however, the variability in d<sub>84</sub> decreases with an increasing mean value.
- Porosity decreases towards the central portion of the cross section (table 3).
- The greatest amount of variability in the  $\theta$  parameters (n,  $\theta_{1.5}$ , &  $\theta_{15}$ ) is present at 1.5 bars. This is because the shape of the individual  $\theta/\psi$  curves for fine and coarser-grained materials vary greatly at this intermediate pressure (figure 25).
- At increased pressure (15 bars), the variability ( $\sigma$ ) in  $\theta$  for the fine-grained samples (transects V7 & V47) increases (table 3). This is generally the case in a fairly homogeneous media.

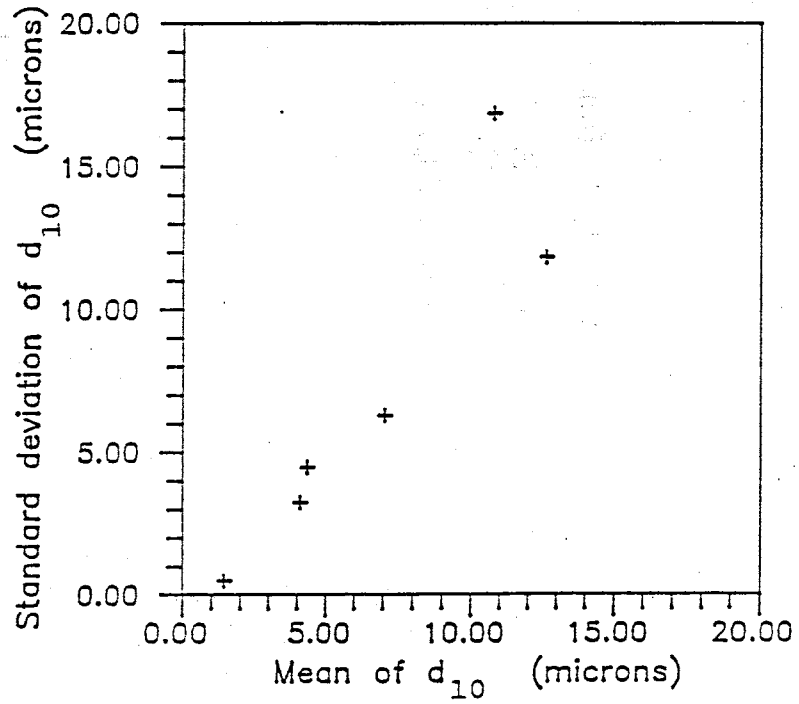


Figure 50. Mean vs. standard deviation values for  $d_{10}$  from the vertical transects.

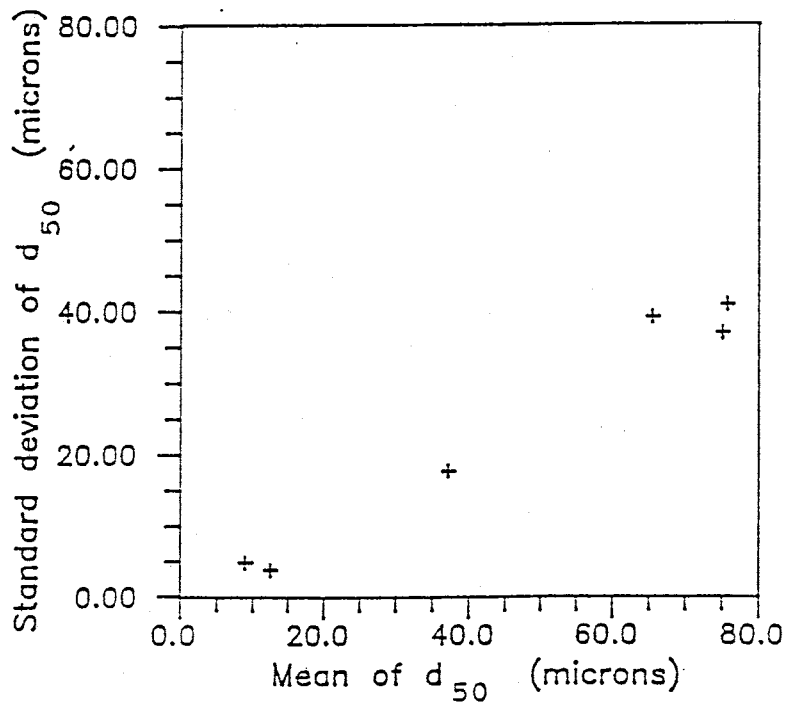


Figure 51. Mean vs. standard deviation values for  $d_{50}$  from the vertical transects.

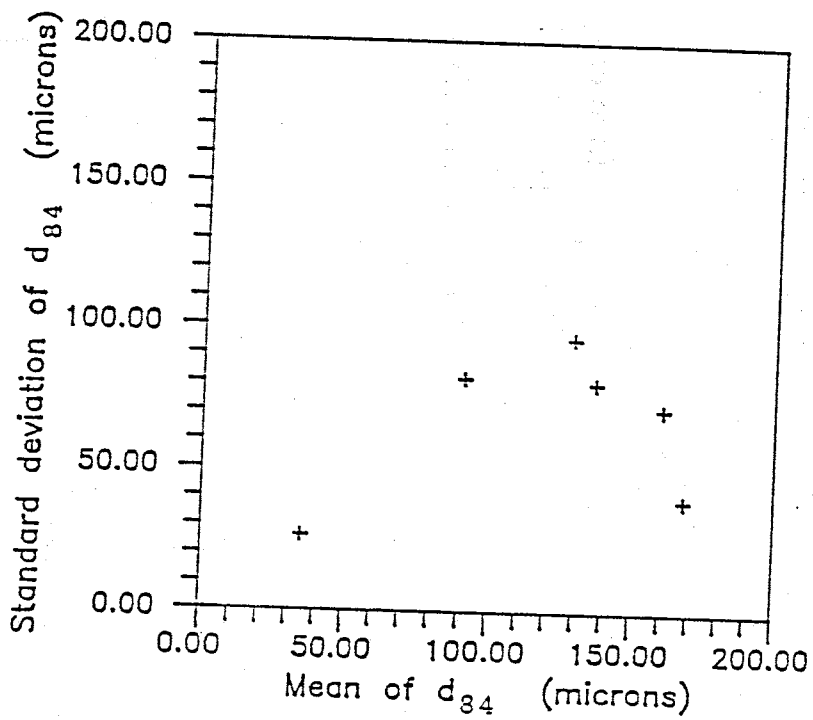


Figure 52. Mean vs. standard deviation values for  $d_{84}$  from the vertical transects.

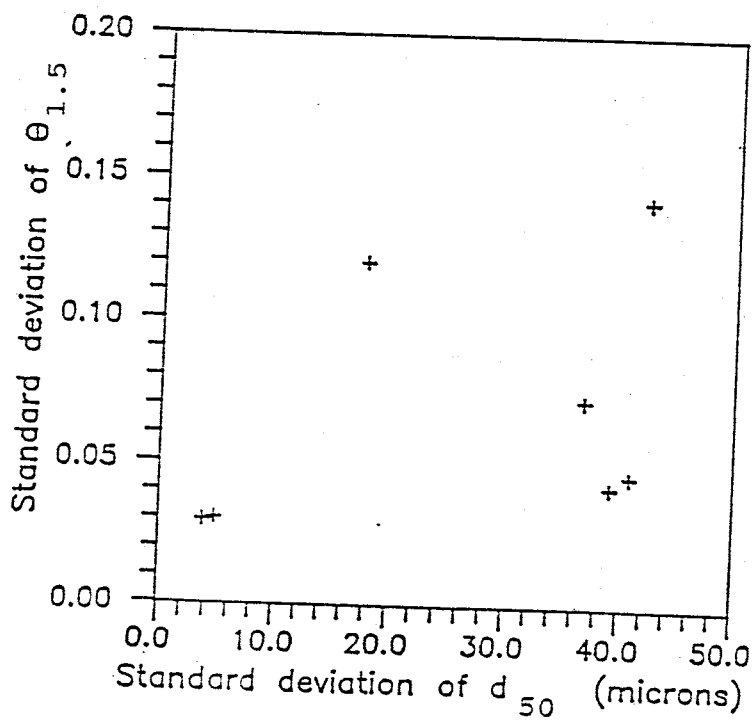


Figure 53. Standard deviation values of  $d_{50}$  vs.  $\theta_{1.5}$  from the vertical transects.

- The variability in theta decreases in the coarser-grained samples with increased pressure (15 bars). These samples are effectively de-watered at 1.5 bars in comparison to the finer-grained samples.
- The greatest variability in moisture contents with depth is located in the transition zone (V75). Large variability in the  $\theta$  values is also present, to a lesser extent, near the northern edge (V6).
- Log K decreases towards the center of the cross section (table 3).
- Log K decreases slightly with depth throughout the cross section as seen by the mean values from table 2. The variability in log K laterally with depth along the horizontal transects is relatively constant (table 2).
- The greatest variability in log K with depth is present along transects V6 and V75. These are also the areas where the greatest range in K values exist.
- The variability within the parameters  $d$ ,  $\theta$ , and K, as measured by their individual standard deviation values, are found to correlate slightly to each other. The standard deviation values of  $d_{50}$ ,  $\theta_{1.5}$ , and log K plotted against each other follow a crude linear trend (figures 53, 54, & 55). An increase in the variability in  $d_{50}$ , for example, results in an increase in the variability in both the  $\theta_{1.5}$  and log K distributions. The origin of this trend, however, does not appear to originate at the point (0,0). Hence, it appears that even if no variability in the  $d_{50}$  distribution exists ( $\sigma=0$ ), an appreciable variability in the log K distribution is still present (figure 54). This is also true in figure 55 and to a lesser extent in figure 53.

A shortcoming of solely using sample statistics for characterization is given below.

- This type of analysis neglects to interpret the presence of any trends in the data. Using this method, a possible trend in the data will show up as an increase in the standard deviation and range values. By making interpretations using solely the mean, standard deviation, and range values, one might postulate that layering or simply a random distribution of hydraulic properties is present when, in fact, a trend in the data may actually exist.

By observing the variability in the different hydraulic properties from the transects, it is apparent that assigning the entire cross section a single mean value for each parameter is

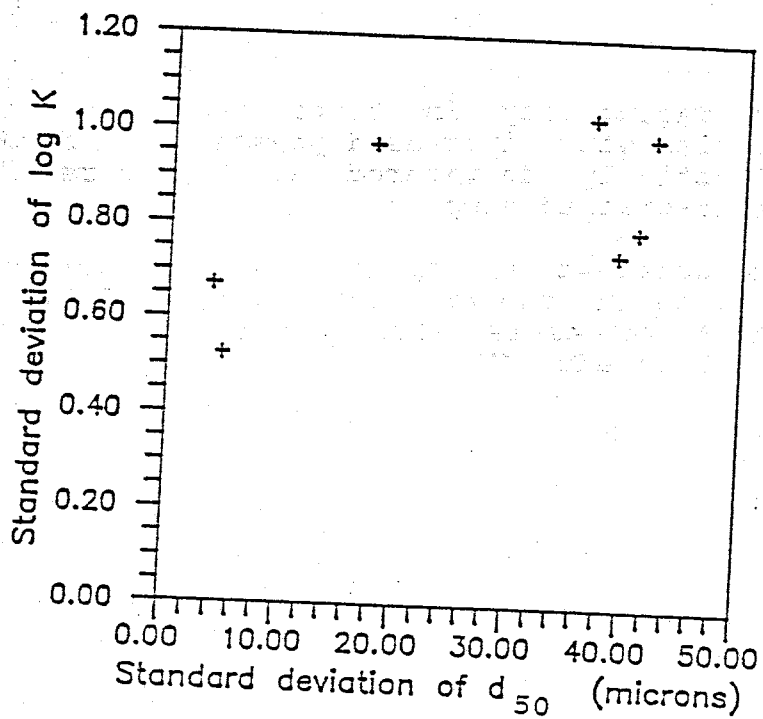


Figure 54. Standard deviation values of  $d_{50}$  vs.  $\log K$  from the vertical transects.

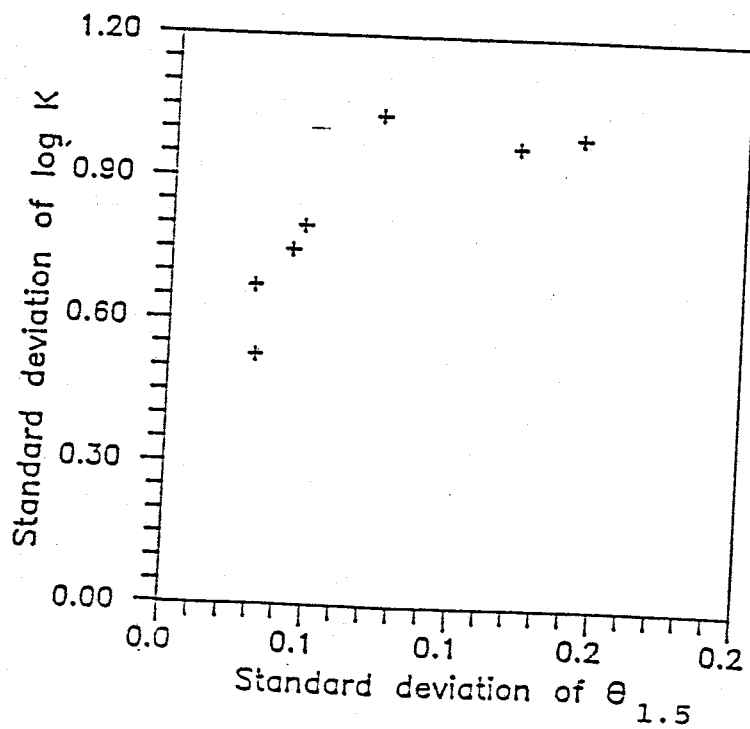


Figure 55. Standard deviation values of  $\theta_{1.5}$  vs.  $\log K$  from the vertical transects.

not an advantageous method of characterizing the tailings media.

### REGRESSION ANALYSES

One of the major shortcomings of solely using the sample statistics for characterization was the fact that this method does not address trends in the data. It appears from the data plots in the previous sections that trends do in fact exist in both the horizontal and vertical directions. In the following section, least squares regression analyses will be employed on the various parameter distributions throughout the cross section in an attempt to characterize the variability. This will include regression analyses in 1 dimension in both the horizontal and vertical directions. In addition, 2 dimensional regression analyses will be performed incorporating data from the entire cross section.

#### Theory

A regression analysis is formulated with the belief that a degree of relationship exists between 2 given variables (greater than 2 for a multiple-regression analysis). The relationship between these 2 variables can be described by a mathematical equation. The basic, linear equation for a 2 variable regression analysis is as follows:

$$(1) \quad Y_i = \beta_0 + \beta_1 X_{1i} + \mu_i \quad \begin{array}{l} i = 1, 2, \dots, n \\ n = \text{number of data points} \end{array}$$

$\beta_0$  and  $\beta_1$  are constants termed the model regression parameters (Chatterjee, 1977).  $\mu_i$  is the random disturbance which is the increment that any individual Y value may fall off the regression

line (Draper, 1966).

The method of least squares is then used to estimate the parameters  $\beta_0$  and  $\beta_1$ . This involves minimizing the sum of squares of the residuals  $S(\beta_0, \beta_1)$  where

$$(2) \quad S(\beta_0, \beta_1) = \sum_{i=1}^n (\mu_i)^2 = \sum_{i=1}^n (Y_i - \beta_0 - \beta_1 X_{1i})^2.$$

$b_0$  and  $b_1$  are used as estimates to minimize  $S(\beta_0, \beta_1)$  by the equations

$$(3) \quad b_1 = \frac{\sum (Y_i - \bar{Y})(X_{1i} - \bar{X}_1)}{\sum (X_{1i} - \bar{X}_1)^2}$$

$$(4) \quad b_0 = \bar{Y} - b_1 \bar{X}_1$$

where

$$(5) \quad \bar{Y} = (\sum Y_i)/n \quad \text{and} \quad (6) \quad \bar{X} = (\sum X_{1i})/n$$

In the case of a multiple regression analysis where more than 1 independent variable is present, the linear regression equation becomes.

$$(7) \quad Y_i = \beta_0 + \beta_1 X_{1i} + \beta_2 X_{2i} + \dots + \beta_p X_{pi} + \mu_i$$

$i = 1, 2, \dots, n$                        $p = \text{number of independent variables}$

This equation is solved in matrix form as follows

$$(8) \quad \sum_{i=1}^n [Y_i - \beta_0 - \beta_1 X_{1i} - \dots - \beta_p X_{pi}]^2 = (\underline{Y} - \underline{X}\underline{\beta})^t (\underline{Y} - \underline{X}\underline{\beta})$$

where

$$\underline{Y} = \begin{bmatrix} Y_1 \\ Y_2 \\ \vdots \\ Y_n \end{bmatrix} \quad \underline{X} = \begin{bmatrix} 1 & X_{11} & \dots & X_{p1} \\ 1 & X_{12} & \dots & X_{p2} \\ \vdots & \vdots & \ddots & \vdots \\ 1 & X_{1n} & \dots & X_{pn} \end{bmatrix} \quad \underline{\beta} = \begin{bmatrix} \beta_0 \\ \beta_1 \\ \vdots \\ \beta_p \end{bmatrix} \quad \underline{\mu} = \begin{bmatrix} \mu_1 \\ \mu_2 \\ \vdots \\ \mu_p \end{bmatrix}$$



Once again  $\underline{b}$  is used as an estimator for  $\underline{\beta}$

$$(9) \quad \underline{b} = (\underline{X}'\underline{X})^{-1}(\underline{X}'\underline{Y}) \quad \text{where} \quad \underline{b} = \begin{bmatrix} b_0 \\ b_1 \\ \vdots \\ b_p \end{bmatrix}$$

A regression analysis can be applied to any set of data no matter how randomly distributed the data points. However, the question, "What measure of precision can be associated with the newly produced regression line?", must be addressed. In order to use one of these equations as a predictive model, some degree of significance of fit should be known.

The first procedure in assessing the usefulness of a regression line is the ratio termed the multiple correlation coefficient ( $R^2$ ).

$$R^2 = \frac{\text{(sum of squares due to regression)}}{\text{(total sum of squares about the mean)}}$$

According to Draper & Smith (1966),  $R^2$  measures "the proportion of total variation about the mean  $\bar{Y}$  explained by the regression." If  $R^2$  is near unity, then  $X_1$  (the independent variable) explains a large part of the variation in the  $Y$  (the dependent variable). On the contrary, if little relationship exists between the independent and dependent variables, the  $R^2$  value will be nearer to zero. In this case, the best prediction for an observation  $Y_i$  is simply  $\bar{Y}$ , the sample mean.

A large value of  $R^2$  does not always guarantee an accurate fit of the model. The data must be observed closely to determine if the correct model is being fit (Chatterjee, 1977). For example, consider a set of data that exhibits a trend surface

parabolic in shape. Either a linear or a quadratic regression equation could be used to describe this trend. It is possible that the  $R^2$  values calculated for each model could be similar. Thus, the  $R^2$  values provide no additional information as to which model better describes the trend in the data. However, by the simple procedure of analysis of residuals in each case, the more advantageous model could be selected.

Examination of the residuals produced by a regression equation is an effective method for detecting model deficiencies (Chatterjee, 1977). Residual values can be analyzed to determine if they follow a normal distribution. An informal way to do this is to plot the residual values on probability paper. If this graph produces a straight line of points, the residual values are assumed to be approximately normally distributed, and the regression model is valid. When a normal distribution of residuals is not present, the model should be used with caution. This method of analyzing residuals is a very useful exercise for identifying hidden structures in the data (Chatterjee, 1977).

The F-test is another method available which helps to determine the significance of a 2 variable regression equation. This test is used to deduce the validity of the hypothesis  $\beta_1=0$ . The definition of the computed F value is "the mean square due to regression divided by the mean square due to residual variation."

$$(10) \quad F = MSr / s^2$$

This ratio is compared to the  $100(1-\alpha)\%$  point of the tabulated

F(1,n-2) distribution (n=number of data points) in order to determine whether  $\beta_1$  can be considered non-zero (Draper, 1966). If the calculated F is less than the tabulated F value, the hypothesis of  $\beta_1=0$  is accepted. Thus, the regression equation under analysis is actually collapsed to the simpler case with  $\beta_1=0$ . If the converse is true,  $\beta_1 \neq 0$ , the regression equation is considered significant, and the form is retained.

The addition of independent variables to a regression equation (multiple-regression analysis) will not always aid in the prediction of the dependent variable. An independent variable that is highly correlated with another independent variable within the same equation will not contribute greatly to the regression equation. To test the significance of a particular set of independent variables, a partial F-test can be performed to determine if deletion of this set ( $\beta_1=0, l=1, 2, \dots, p$ ) greatly affects the regression equation. The partial F value is calculated using the following equation

$$(11) \quad F = \frac{(SS1 - SS2) / (p - k)}{MSE1}$$

SS1 = sum of squares attributable to regression, full model  
 SS2 = sum of squares attributable to regression, reduced model  
 p = degrees of freedom attributable to regression, full model  
 k = degrees of freedom attributable to regression, reduced model  
 MSE1 = mean square deviation from regression, full model  
 m = degrees of freedom from deviation from regression, full model

This value is compared with the tabulated value  $F(p-k, m)$ . If the calculated value is less than the tabulated value, the hypothesis  $\beta_1=0, l=1, \dots, k$ , is accepted, and the reduced model is used. If

the converse is true, the hypothesis is not accepted and the independent variables are retained in the equation.

#### 1-D Horizontal

To begin with, regression analyses were applied to the data along the horizontal transects. Table 5 lists the various output parameters from these regression analyses. The independent value for each analysis is listed in the first column with the number in parenthesis representing the depth from the surface in which the samples were taken. The dependent value <dist>, listed in the second column, represents the distance along transect from the northern edge that the particular sample data was obtained. The regression equation employed for all horizontal analyses listed in table 5 is as follows:

$$(12) \quad \text{dep} = \beta_0 + \beta_1(\text{indep}) + \beta_2(\text{indep})^2.$$

Also included in table 5: number of samples employed in each regression analysis, and the multiple correlation coefficients and F values from each regression fit. The tabulated F values for the upper 5% and 1% points are also included in table 5 for comparison purposes.

The use of the quadratic regression equation (12) to describe the variability in the various particle size parameters proved only moderately successful. The coarsest particle size fraction ( $d_{84}$ ) was found to closest resemble the fit produced by the quadratic equation. The correlation coefficients from the regression analyses decreased with decreasing particle size

TABLE 5

Least squares regression statistics:

## 1-D Horizontal:

	Variables		number of samples	mult. correl. coeff	F stat	tabular	
	dep	indep				F(5%)	F(1%)
d <sub>10</sub>	(205 cm)	dist (12)	61	0.376	4.764*	3.15	5.00
d <sub>16</sub>	"	"	61	0.407	5.743**	3.15	5.00
d <sub>30</sub>	"	"	61	0.466	8.024**	3.15	5.00
d <sub>50</sub>	"	"	61	0.473	8.343**	3.15	5.00
d <sub>60</sub>	"	"	61	0.504	9.897**	3.15	5.00
d <sub>34</sub>	"	"	61	0.585	15.075**	3.15	5.00
GM	"	"	61	0.504	9.889**	3.15	5.00
UC	"	"	61	0.083	0.203	3.15	5.00
CC	"	"	61	0.389	5.165**	3.15	5.00
SORT	"	"	61	0.210	1.335	3.15	5.00
SKEW	"	"	61	0.368	4.549*	3.15	5.00
n	(67 cm)	dist (12)	20	0.675	7.117**	3.59	6.11
n	(205 cm)	"	68	0.317	3.628*	3.14	4.96
$\theta_{1.5}$	(67 cm)	"	20	0.681	7.351**	3.59	6.11
$\theta_{1.5}$	(205 cm)	"	68	0.666	25.850**	3.14	4.96
$\theta_{15}$	(67 cm)	"	20	0.624	5.429*	3.59	6.11
$\theta_{15}$	(205 cm)	"	67	0.536	12.873**	3.14	4.96
log K	(28 cm)	dist (12)	22	0.271	0.754	3.52	5.93
"	(41 cm)	"	21	0.507	3.117	3.55	6.01
"	(54 cm)	"	23	0.528	3.870*	3.49	5.85
"	(165 cm)	"	68	0.603	18.602**	3.14	4.96
"	(179 cm)	"	68	0.833	73.473**	3.14	4.96
"	(192 cm)	"	68	0.848	83.021**	3.14	4.96
"	(205 cm)	"	61	0.802	52.296**	3.15	5.00
(d <sub>30</sub> )	(205 cm)	dist (12)	55	0.725	28.764**	3.17	5.03
( $\theta_{1.5}$ )	"	"	61	0.813	56.382**	3.15	5.00

-----  
 dist = distance in meters from north edge (horizontal  
 transect)

(12): regression equation:  $dep = \beta_0 + \beta_1(ind) + \beta_2(ind)^2$

\* reject  $\beta_1 = \beta_2 = 0$  F (5%)

\*\* reject  $\beta_1 = \beta_2 = 0$  F (1%)

(d<sub>30</sub>) & ( $\theta_{1.5}$ ): regression equations determined excluding  
 data points from 62-73 meters

parameters. One reason for this decrease in correlation is the presence of the discontinuity in data at 62 meters along the transect. The magnitude of this discontinuity is greater for the finer particle size parameters (figures 18a-20a). Hence, a larger spread in the data results in a decrease in correlation using equation 12.

Figure 56a represents the  $d_{30}$  distribution along the horizontal transect at a depth of 205 cm. The solid line represents the regression fit using all of the data shown. The dashed line represents the fit produced excluding the data points from 62-73 meters. Improvements noted in the regression fit by excluding the data from 62-73 m include a higher correlation coefficient, an increased F value (table 5), and also a better normality plot (figures 56b & c). The fit produced excluding the data from 62-73 m also better characterizes the  $d_{30}$  distribution in the finer-grained fractions from 25-62 meters.

With exclusion of the outlying values from 62-73 m, it appears that the particle size distribution can be described effectively using the previously mentioned quadratic equation (12). Even though this analysis excludes 6 of the data values along the transect, the resulting regression fit represents 90 percent of the data. The nature of a regression analysis makes it difficult to effectively describe outlying points. Including the data from 62-73 m drastically effects the resultant quadratic fit. This fit does a poor job describing the trend in the data.

Other particle size coefficients that exhibit slight

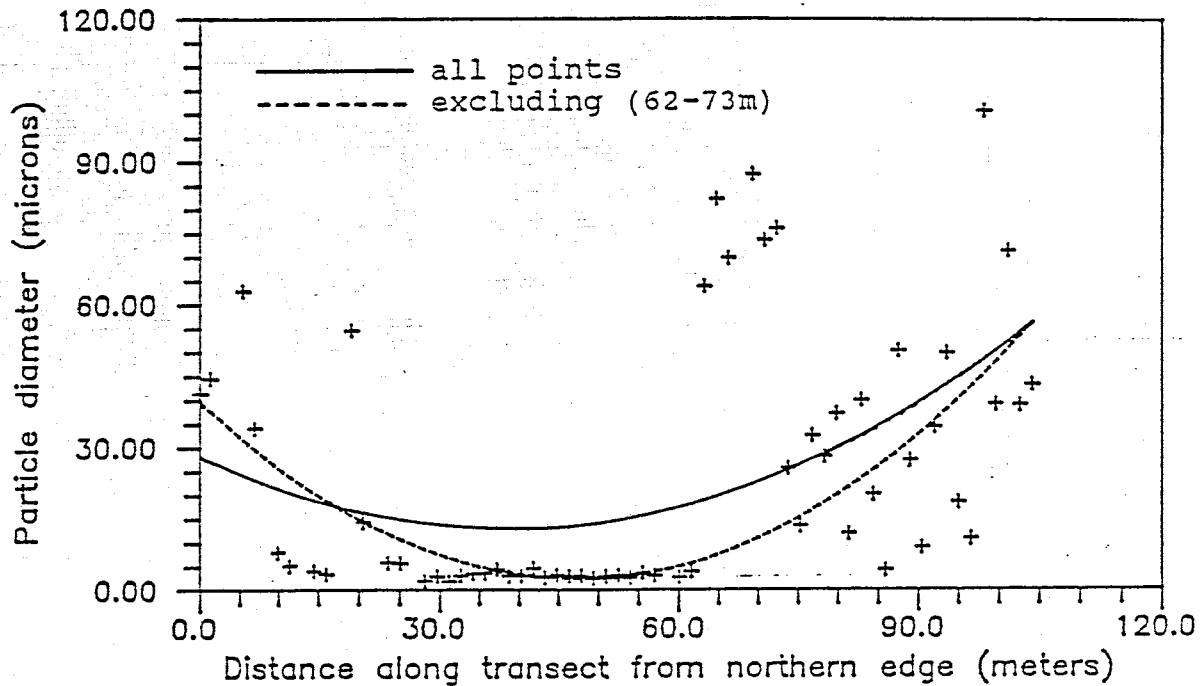


Figure 56a. Regression fit to the  $d_{30}$  data, 205cm depth.

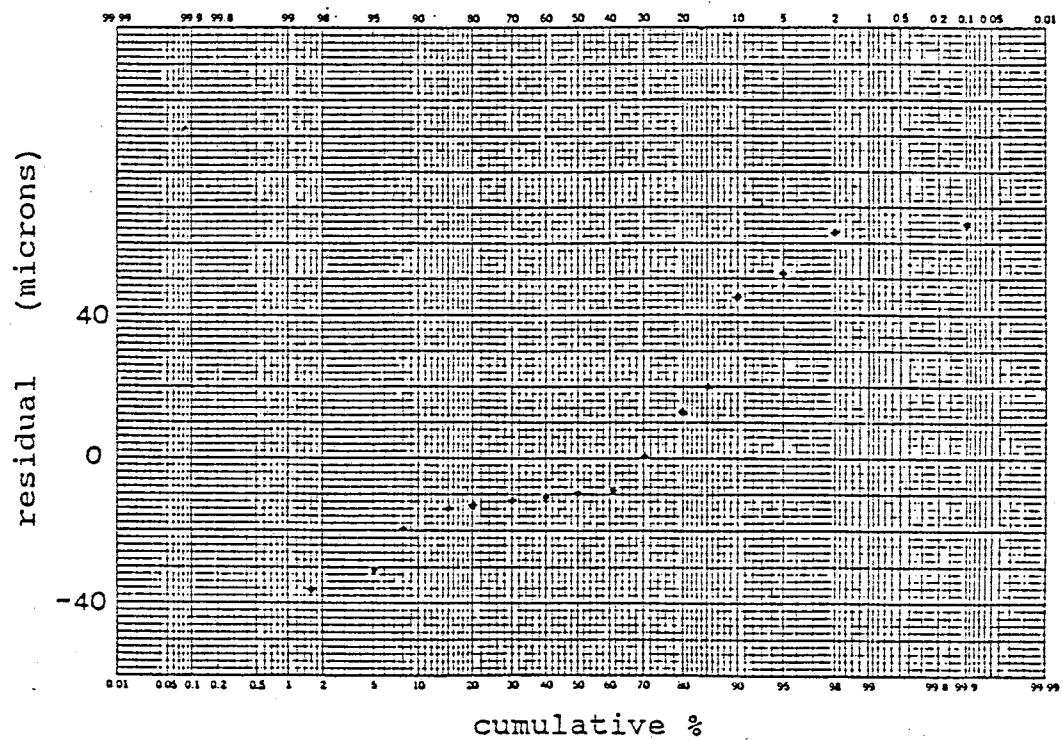


Figure 56b. Normality plot for figure 56a ( $d_{30}$ , all data, 205cm depth).

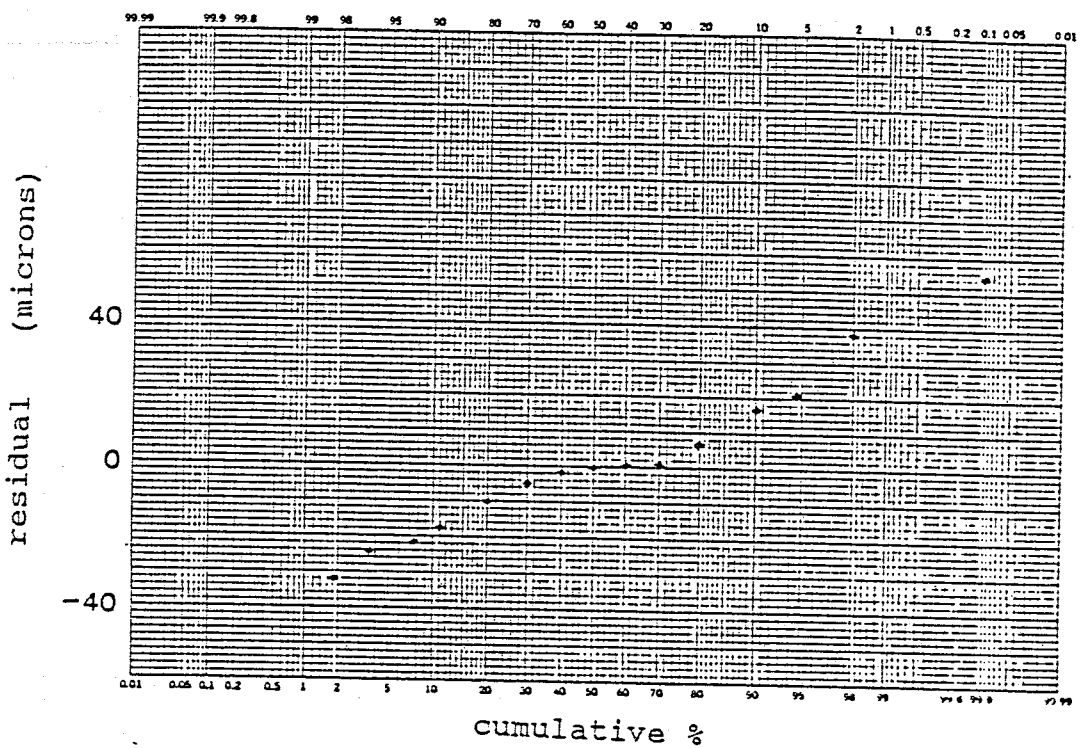


Figure 56c. Normality plot for figure 56a ( $d_{30}$ , data deleted, 205cm depth).

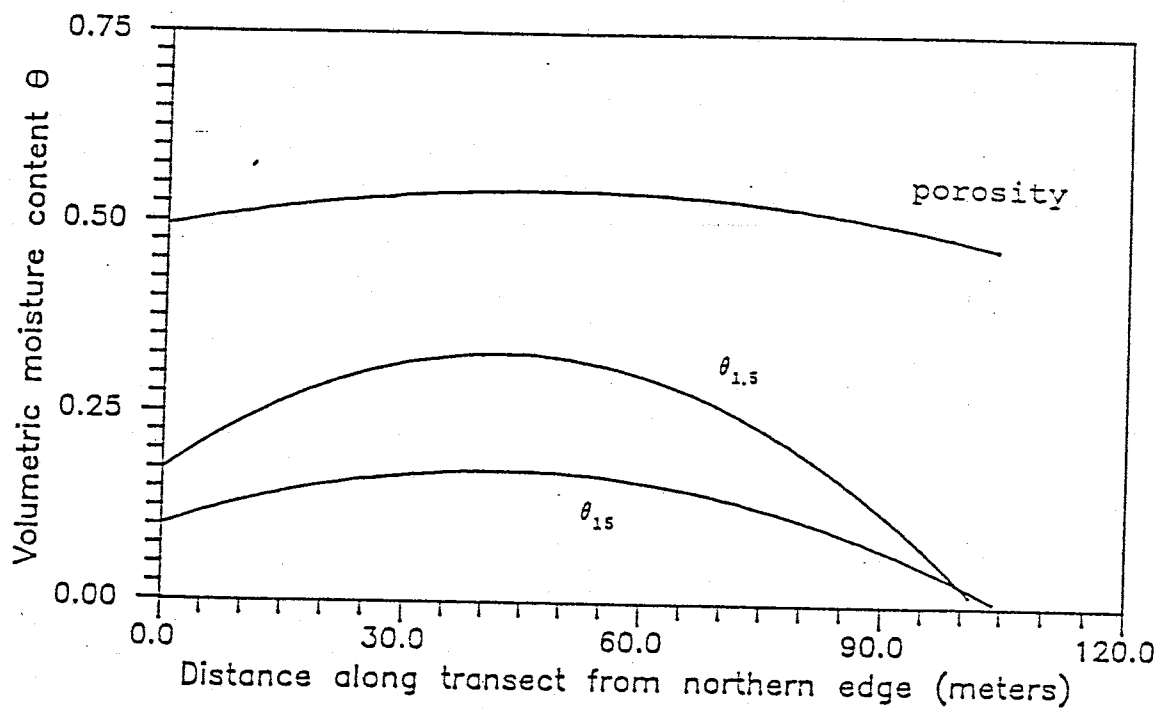


Figure 57a. Trends in  $\theta$  at the 205cm depth.



correlation with distance include coefficient of curvature and trunk skewness (table 5). Both exhibit a decrease in values towards the center of the transect similar to the previously mentioned particle size parameters. For the skewness parameter, this states that samples obtained in the central portion of the transect are more heavily skewed towards the fines in comparison to samples obtained near both edges.

There appears to be increased correlation with distance for the moisture content data in comparison to the particle size data. The plots of the porosity,  $\theta_{1.5}$ , and  $\theta_{15}$  regression fits for the same samples at 205 cm are present in figure 57a. It is evident that the greatest trend in the  $\theta$  data occurs in the values at 1.5 bars. At 100 m, the  $\theta_{1.5}$  plot crosses the  $\theta_{15}$  plot. This is caused by the regression equations and is not an actual occurrence in nature. The  $\theta_{15}$  regression plot is very similar in shape to the porosity regression plot.

The regression fit to the porosity values is quite similar to the mean value of the distribution. A low correlation coefficient and F value make the significance of the porosity regression fit questionable at best. The residual values for both  $n$  and  $\theta_{15}$ , however, appear quite normally distributed (figures 57b & c).

Of the 3 regression plots from figure 57a, the  $\theta_{1.5}$  plot best describes the trend in the data as noted by its high correlation coefficient and F value. Figure 58a represents the distribution of  $\theta_{1.5}$  along the horizontal transect at a depth of 205 cm. The solid line represents the regression fit incorporat-

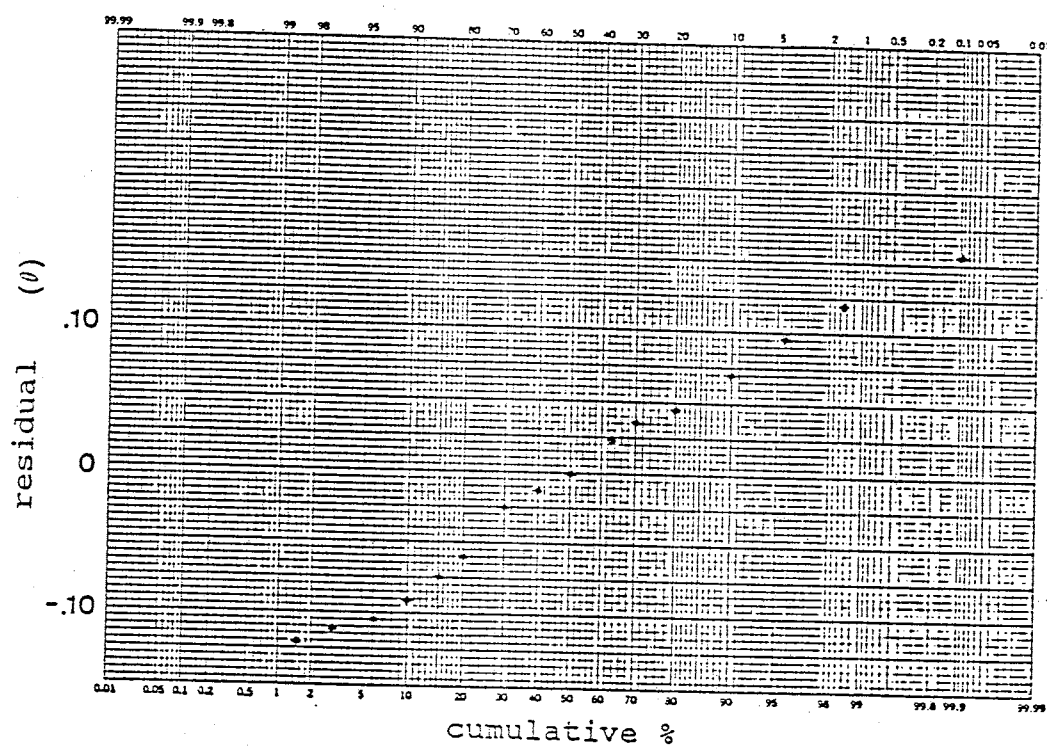


Figure 57b. Normality plot for figure 57a (porosity, 205cm depth).

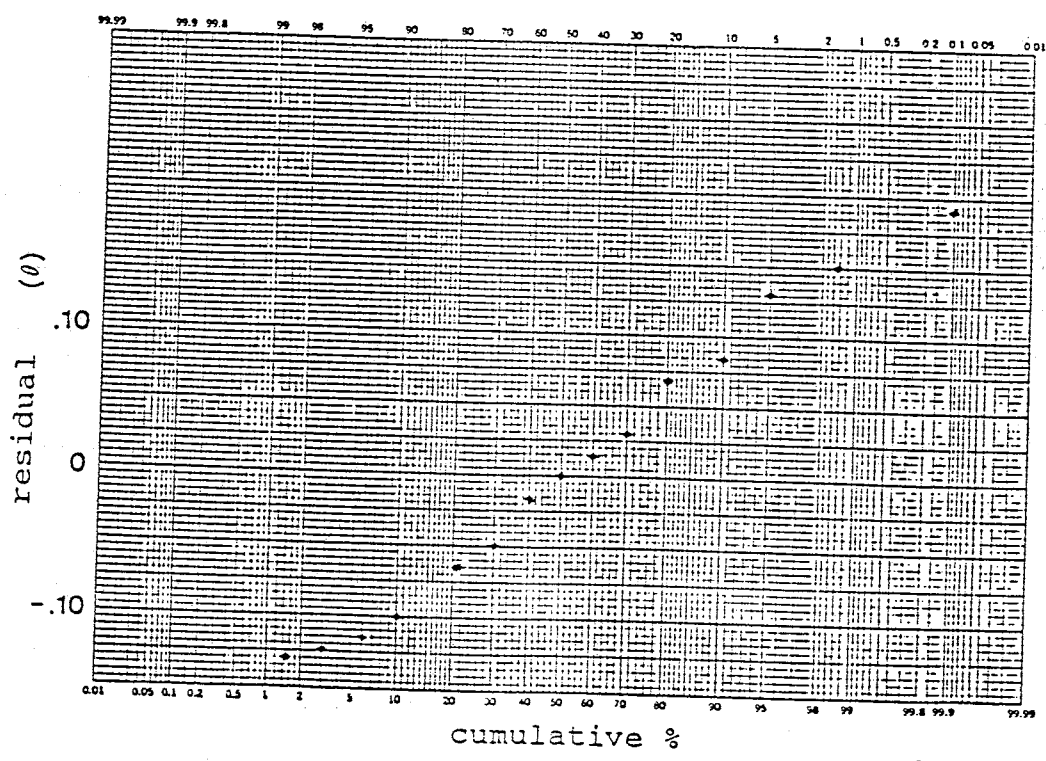


Figure 57c. Normality plot for figure 57a ( $\theta_{15}$ , 205cm depth).

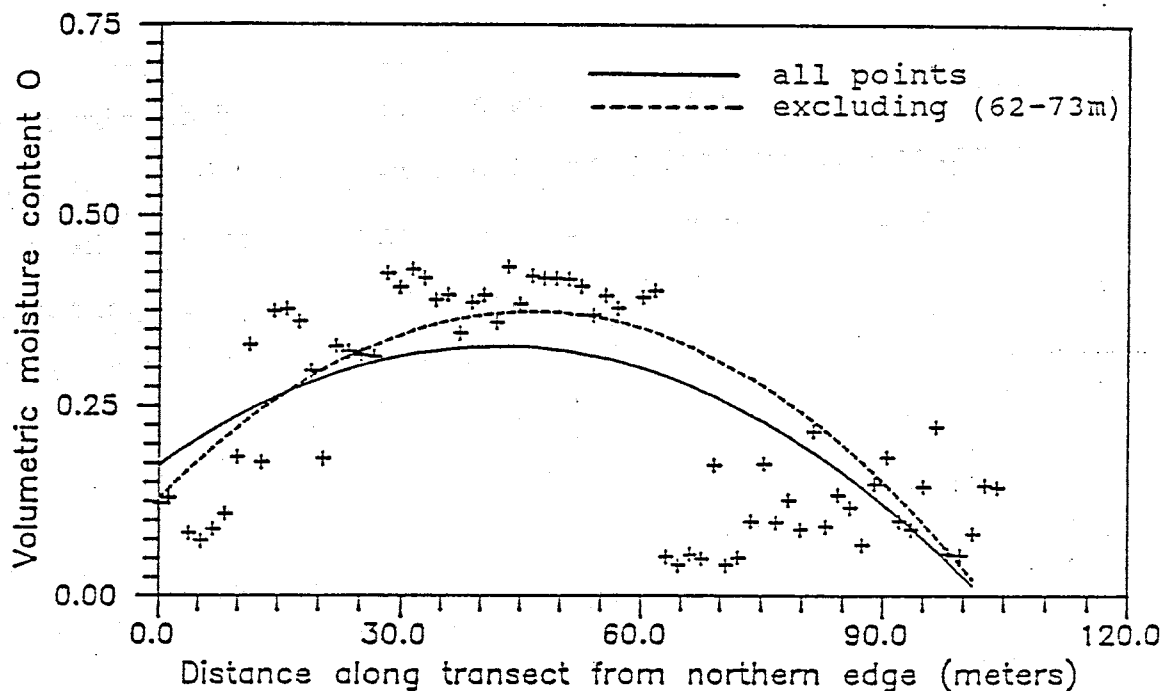


Figure 58a. Regression fits to the  $\theta_{1.5}$  data, 205cm depth.

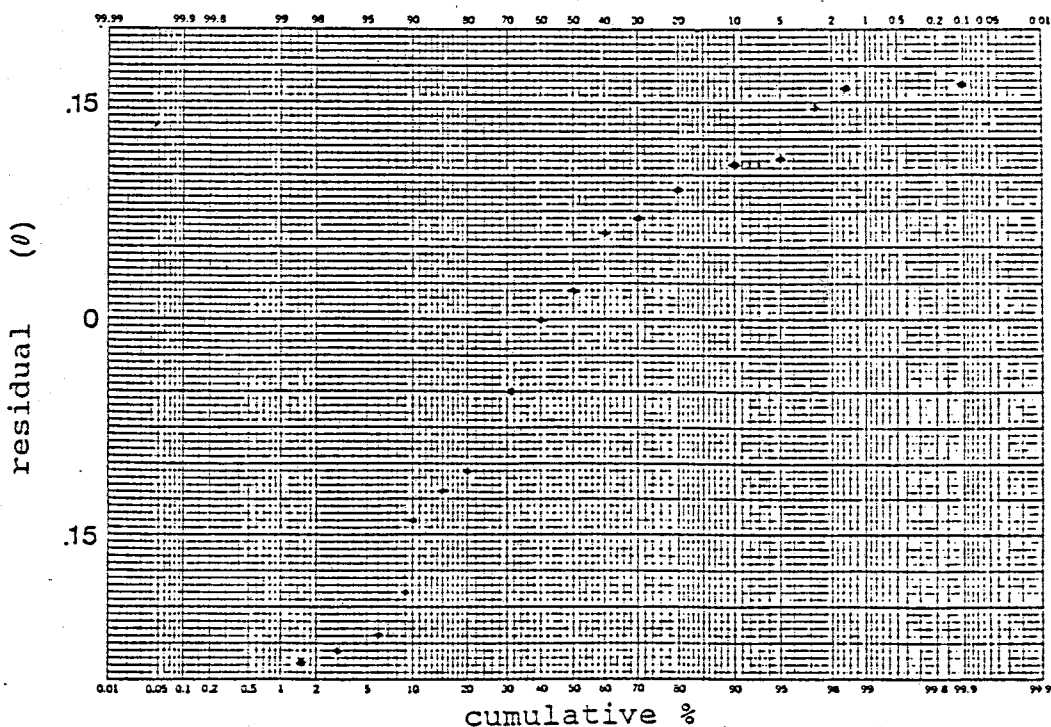


Figure 58b. Normality plot for figure 58a ( $\theta_{1.5}$ , all data, 205cm depth).

ing all of the available data. The data from figure 58a exhibits a sharp discontinuity at 62 meters similar to the discontinuity observed in the particle size distribution. The dashed line in figure 58a represents the regression analysis performed excluding the data values from 62-73 meters (table 5). As was the case for the particle size data, the regression analyses improved dramatically for  $\theta_{1.5}$  with the exclusion of these values. The normality plots 58b & c also echo this improved fit.

Once again, the regression equation is not able to effectively describe the outlying values from 62-73 m. The 6  $\theta_{1.5}$  values from 62-73 meters have a dramatic effect on the regression fit. As was the case for the  $d_{30}$  distribution, exclusion of these values results in a substantially improved regression fit to the remaining 90 percent of the  $\theta_{1.5}$  values.

The highest degree of correlation with distance is present in the conductivity distribution. This high degree of correlation, however, is not present at all depths. The regression analyses from the upper K samples (28 & 41 cm) are not significant due to the random nature of the tailings in the upper 50 cm. This can be seen in figure 59a. Observation of the normality plot for this regression fit (figure 59b) is also somewhat discouraging. On the opposite end of the scale, figure 60 exhibits the K distribution and regression fit for the depth 179 cm. The uniform trend in the data is quite evident at this depth.

The K regression plots for the various depths are presented in figure 61a. The regression fits for 28 and 41 cm were not

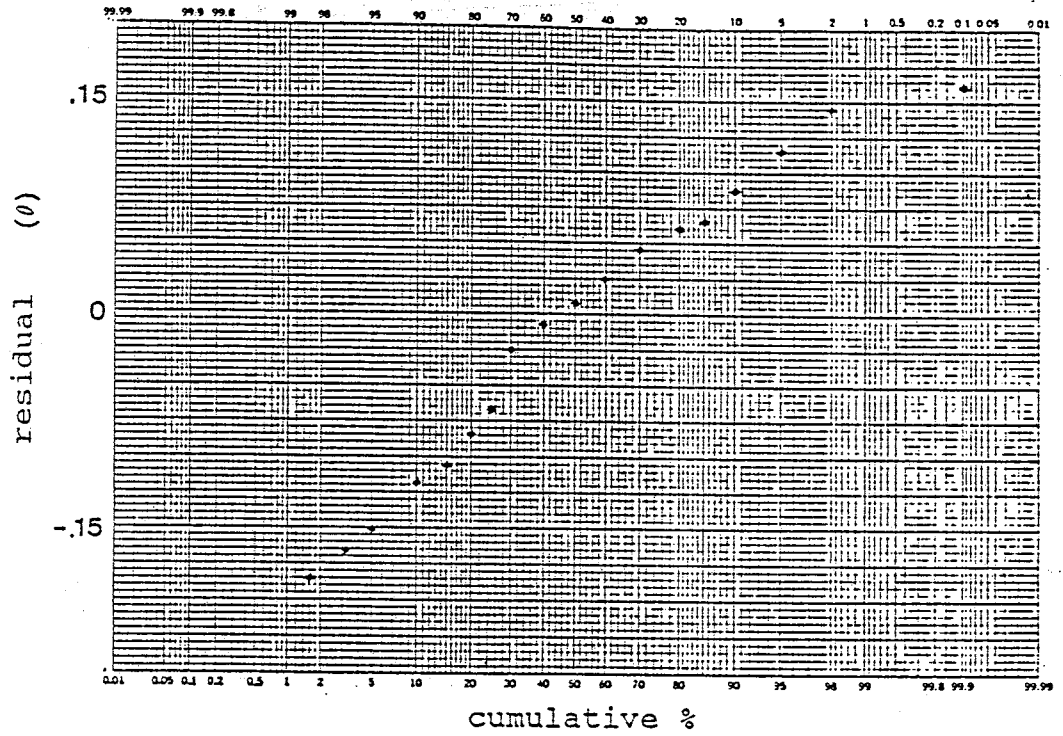


Figure 58c. Normality plot for figure 58a ( $\theta_{1.5}$ , data deleted, 205cm depth).

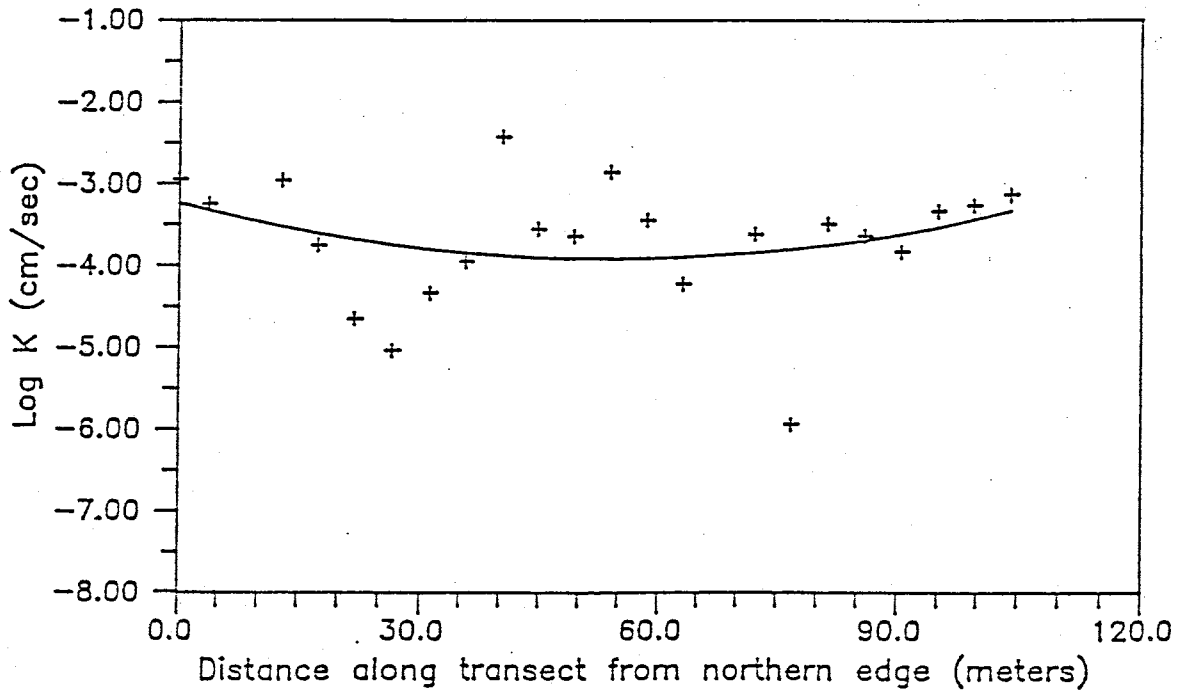


Figure 59a. Regression fit to the log K data, 28cm depth.

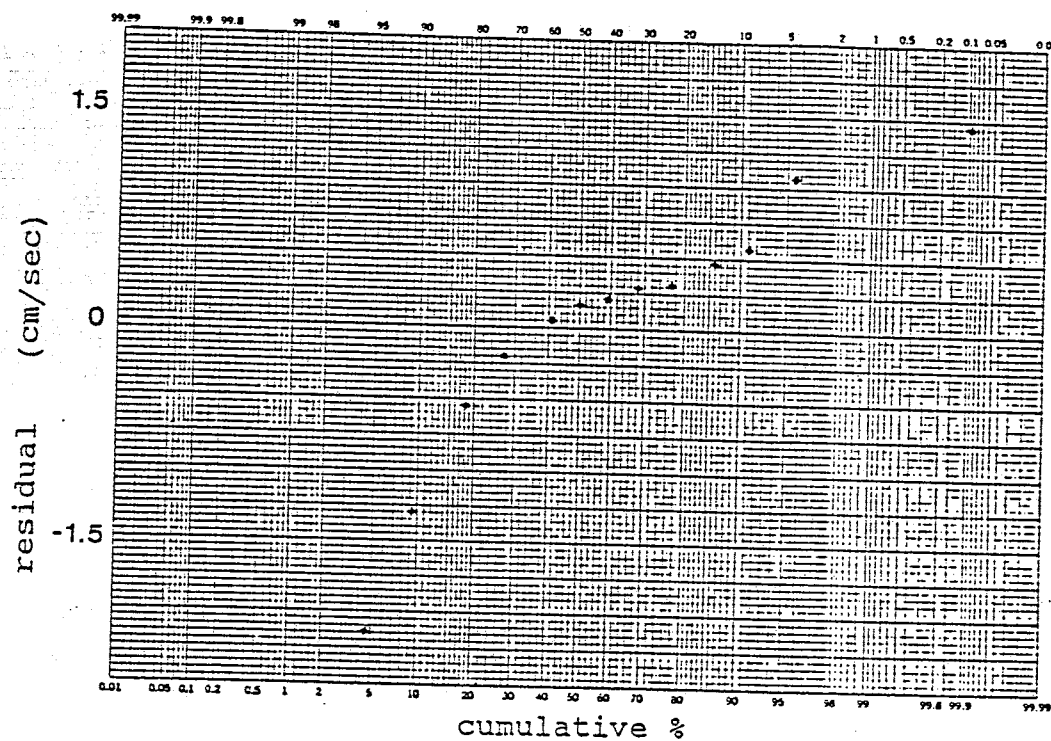


Figure 59b. Normality plot for figure 59a (log K, 28cm depth).

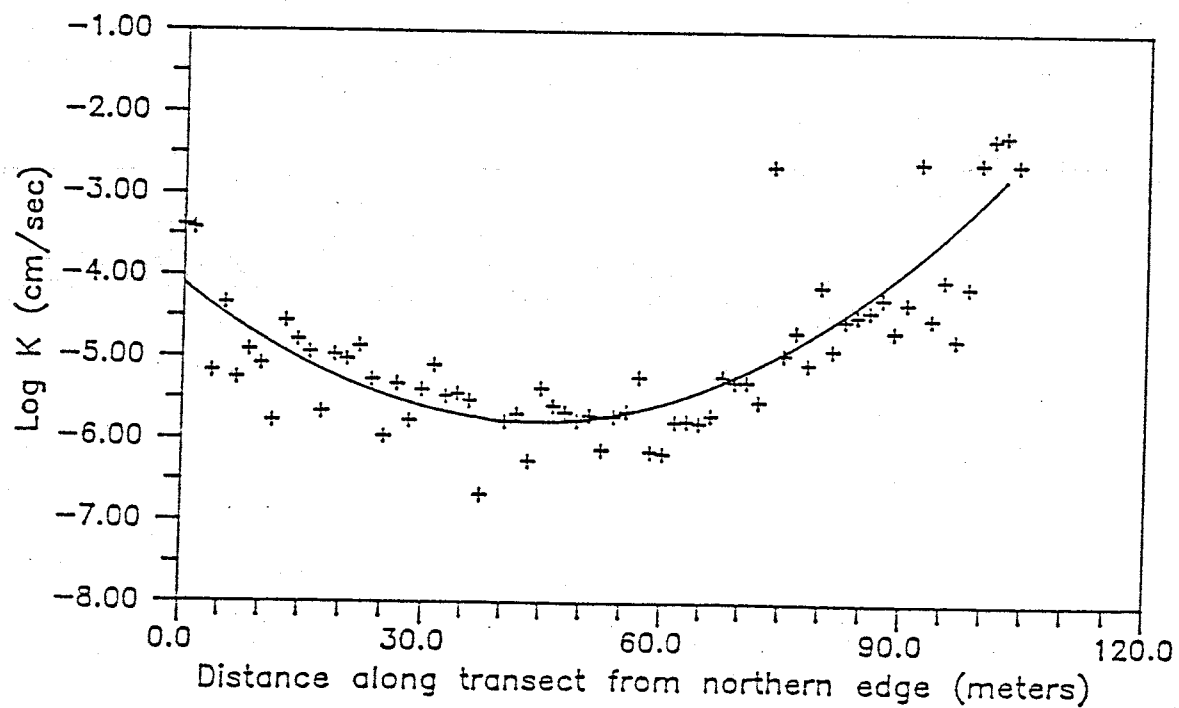


Figure 60. Regression fit to the log K data, 179cm depth.

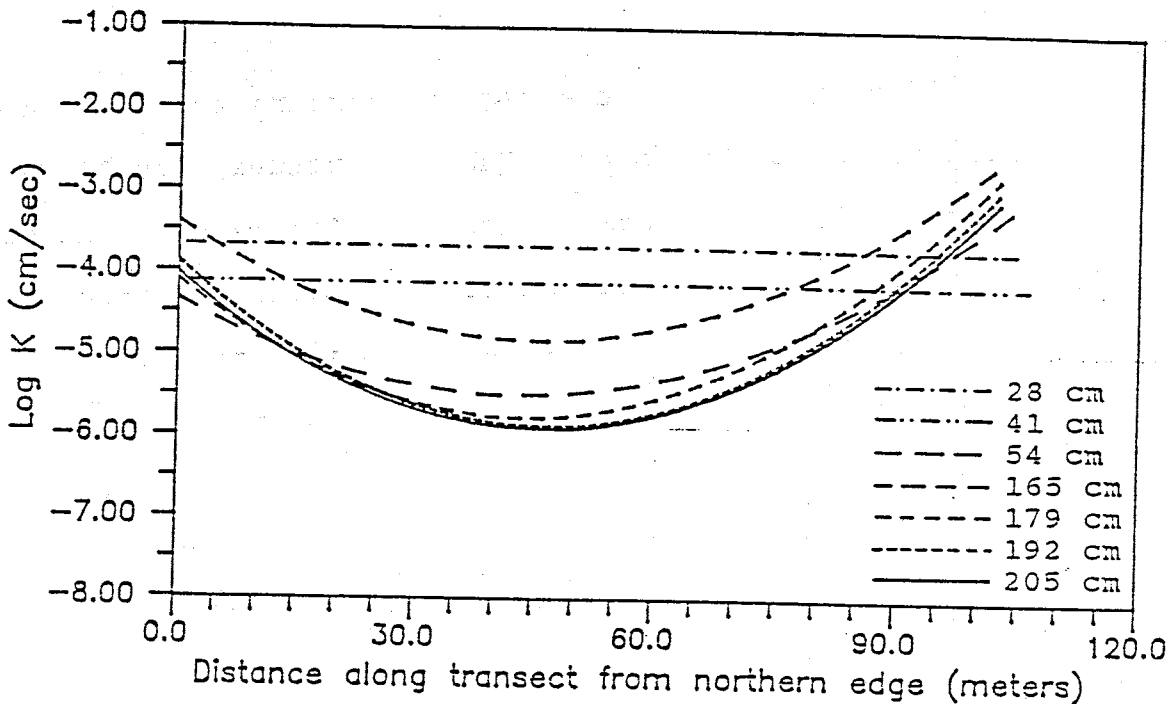


Figure 61a. Trends in hydraulic conductivity at various depths.

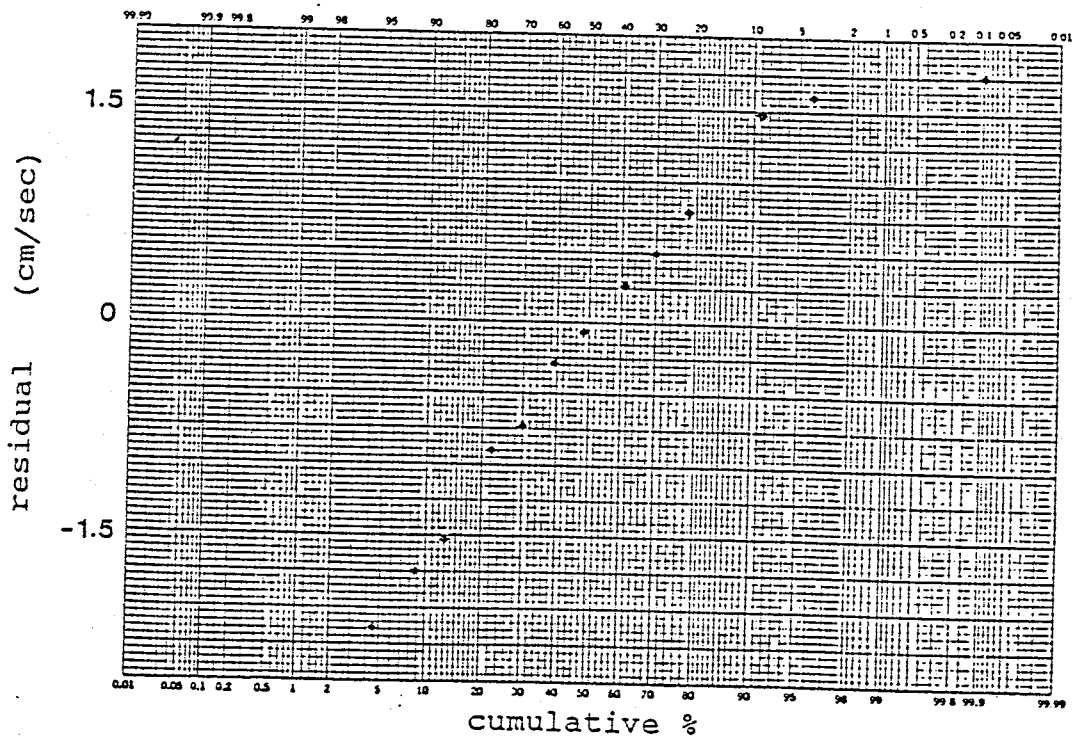


Figure 61b. Normality plot for figure 61a (log K, 54cm depth).

significant. Hence, the best representation for the data in each case is the sample mean. The mean values for 28 and 41 cm are plotted as horizontal lines in figure 61a. At depths greater than 50 cm, the horizontal trends in the various K distributions are all quite similar. An exception to this case is noted at the 165 cm depth. The reason for the discrepancy at 165 cm is due to the result of sampling error which in turn is reflected in the data. Reasons for the sampling error were discussed in the previous section on presentation of data. Aside from the 165 cm depth, the trends in K are noted to decrease slightly with depth. This decrease in K could be the result of compaction of the matrix with increasing overburden. The normality plots for the K regressions (figures 61b-61f) show that the residual values appear to be normally distributed.

The best results using the regression analyses were obtained for the hydraulic conductivity distribution. One reason for this could be the result of the sample scale. Layering on the order of 1-2 cm is common in the tailings. The K measurements were taken over 13.3 cm as opposed to 3 cm for the particle size and  $\theta$  measurements. This larger scale for the K measurement enables many layers to be incorporated into the conductivity measurement. This results in an averaged value across the 13.3 cm sample length. For  $\theta_{1.5}$  and  $d_{30}$ , the measurements were more like point measurements (3 cm) enabling the presence of discontinuities to be distinguished better. As was noted previously, the presence of large discontinuities in the data has an adverse effect on the regression analysis.



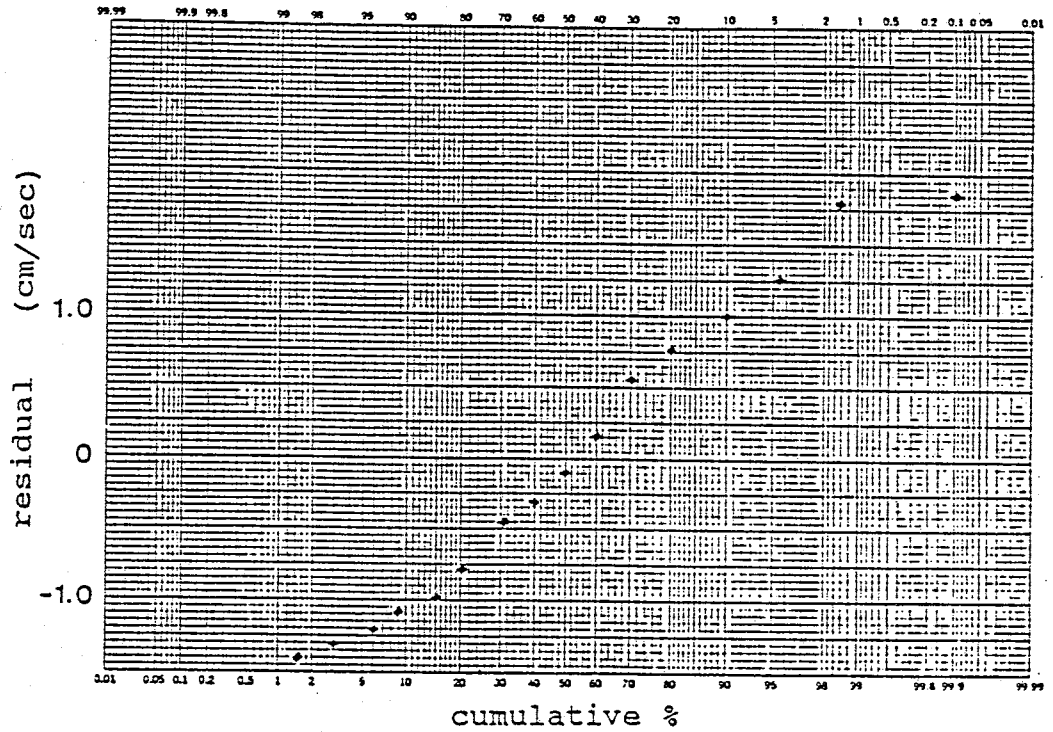


Figure 61c. Normality plot for figure 61a (log K, 165cm depth).

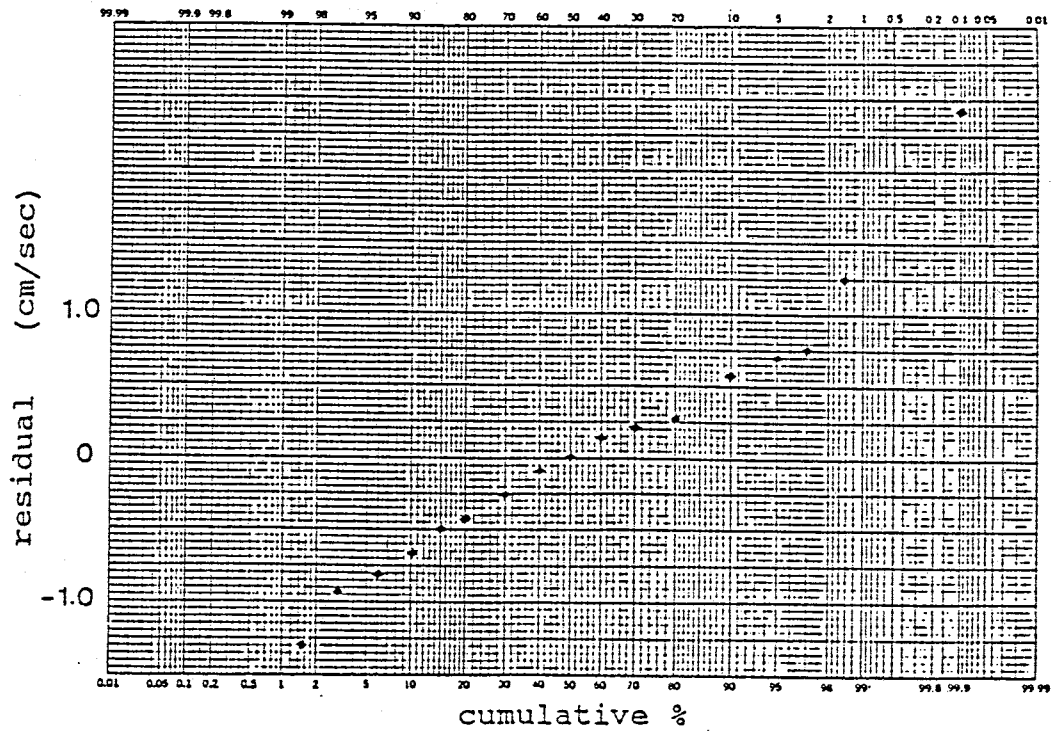


Figure 61d. Normality plot for figure 61a (log K, 179cm depth).

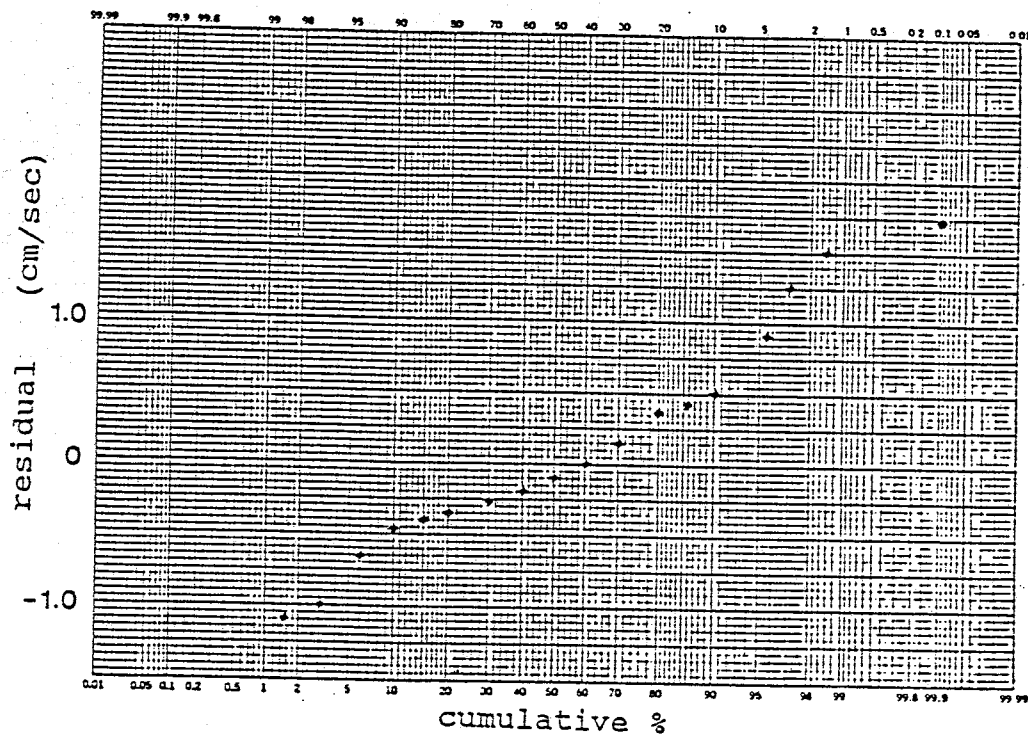


Figure 61e. Normality plot for figure 61a (log K, 192cm depth).

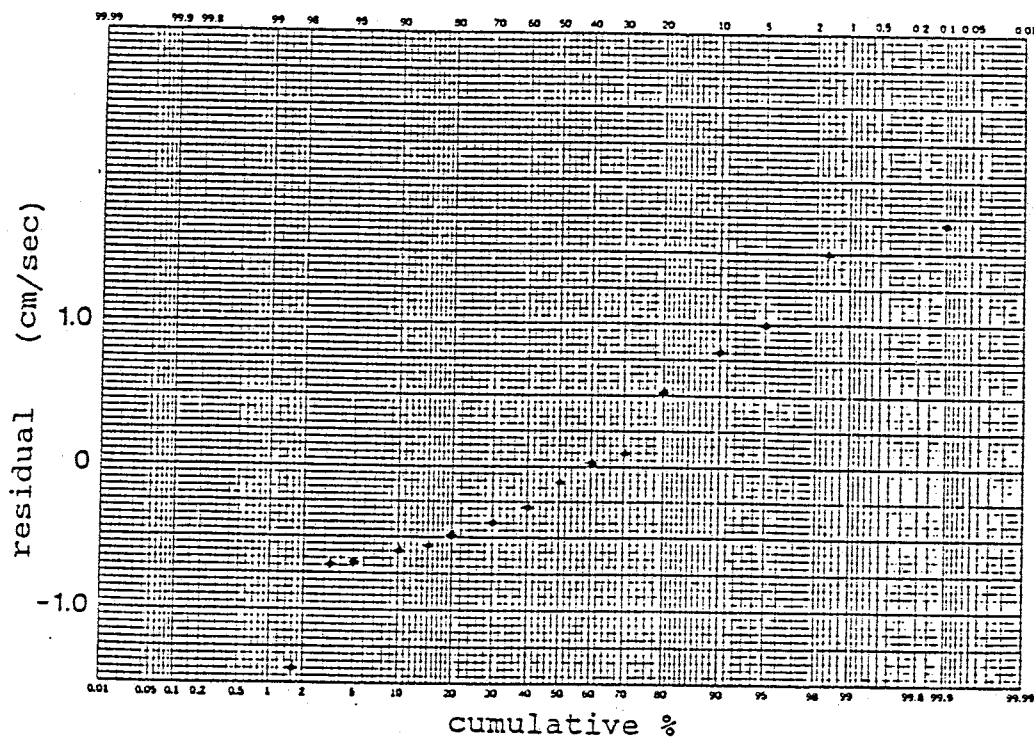


Figure 61f. Normality plot for figure 61a (log K, 205cm depth).

### 1-D Vertical

It is noted that trends in the data in the horizontal direction can be characterized with varying degrees of success. The next step is to determine if trends in the data exist in the vertical direction. This analysis was performed using data from the 6 vertical transects.

To determine if trends in the tailing's hydraulic properties exist vertically, each set of data (i.e.  $K$ ,  $n$ ,  $\theta_{1.5}$ , etc.) was grouped together from the 6 transects. In this way, an overall trend with depth throughout the entire cross section could be determined. As was noted in the sample statistics section, the mean values of the various vertical transects change according to location for each parameter. Therefore, the data was scaled prior to analysis so that it could be compared throughout the cross section. The following equation was used to scale the data for each hydraulic parameter:

$$(13) \quad z_n = (x_{ni} - \mu_n) / \sigma_n$$

$z$  = scaled value  
 $x$  = individual value  
 $n$  =  $K$ ,  $n$ ,  $\theta_{1.5}$ ,  $d_{10}$ , etc.  
 $i$  = sample number  
 $\mu$  = population  $x_n$  mean from each vertical transect  
 $\sigma$  = population  $x_n$  standard deviation from each vertical transect

Results of the regression analyses with depth are listed in table 6. Two equations were employed in these analyses in an attempt to describe the trends with depth. The regression equations included equation (12) and equation (14):

$$(14) \quad \text{dep} = \beta_0 + \beta_1(\text{indep}).$$

TABLE 6

Least squares regression statistics:

## 1-D Vertical

Variables		number of samples	mult. correl. coeff	F stat	tabular	
dep	indep				F(5%)	F(1%)
scaled log K (0-450 cm)	depth (12)	103	0.415	10.921**	3.93	6.89
scaled log K (0-375 cm)	depth (12)	103	0.365	7.704**	3.94	6.93
scaled log K (50-375 cm)	depth (12)	83	0.420	8.568**	3.97	7.00
scaled log K (0-50 cm)	depth (14)	20	0.232	1.020	4.35	8.10
scaled n (0-375 cm)	depth (14)	33	0.451	7.893**	4.16	7.53
scaled $\theta_{1.5}$ (0-375 cm)	depth (14)	33	0.266	2.364	4.16	7.53
scaled $d_{10}$ (0-375 cm)	depth (14)	33	0.020	0.012	4.16	7.53

---


$$\text{scaled } z_n = (x_{ni} - \mu_n) / \sigma_n$$

depth = depth in meters from the surface

(14): regression equation:  $\text{dep} = \beta_0 + \beta_1(\text{ind})$

(12): " :  $\text{dep} = \beta_0 + \beta_1(\text{ind}) + \beta_2(\text{ind})^2$

\* reject  $\beta_1 = \beta_2 = 0$  F (5%)

\*\* reject  $\beta_1 = \beta_2 = 0$  F (1%)

---

The conductivity distribution is noted to decrease slightly with depth as seen by figures 62a-64a. The differences between these figures are that the regressions were employed using varying amounts of data. Figure 62a is a plot using all of the available K data. The dashed line represents the quadratic fit with the solid line representing the linear fit. Observation

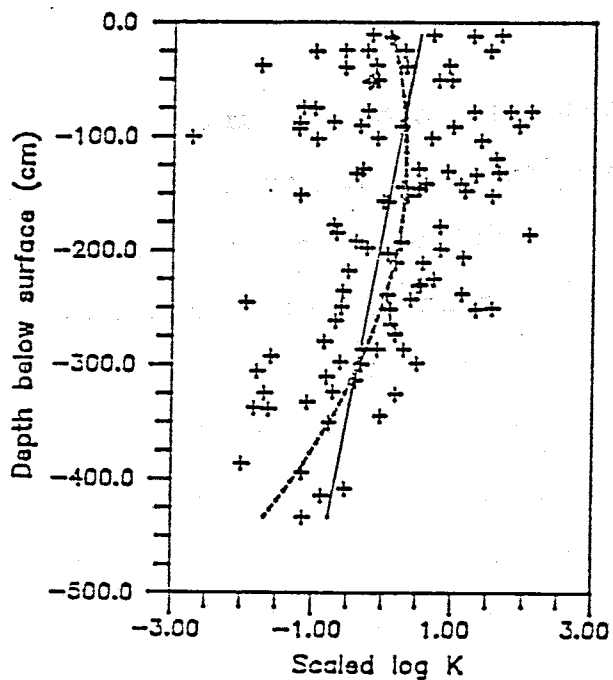


Figure 62a. Scaled log K  
vs. depth, 0-450cm.

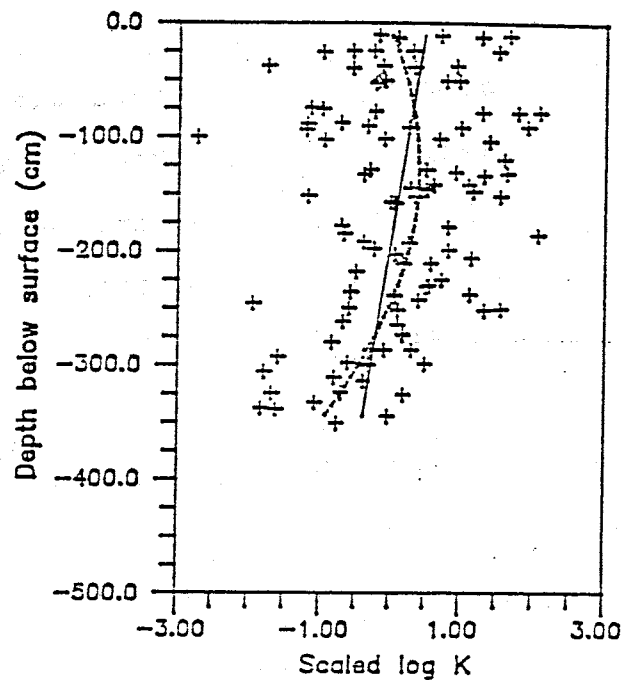


Figure 63a. Scaled log K  
vs. depth, 0-375cm.

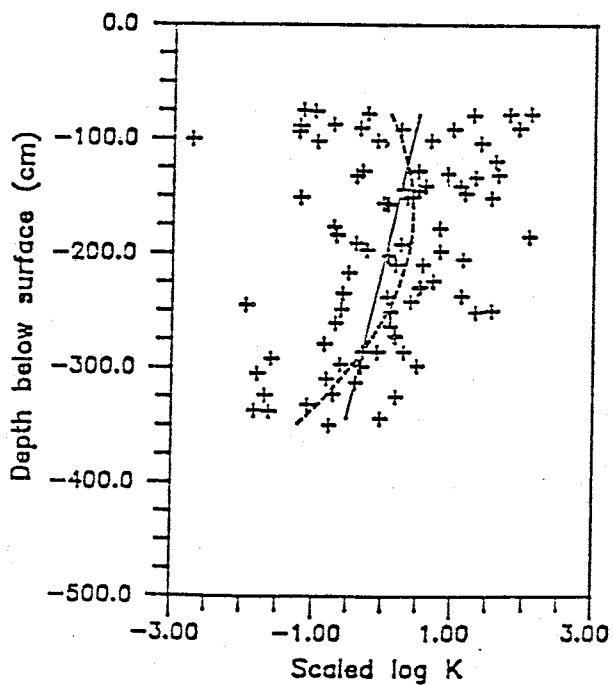


Figure 64a. Scaled log K  
vs. depth, 50-375cm.

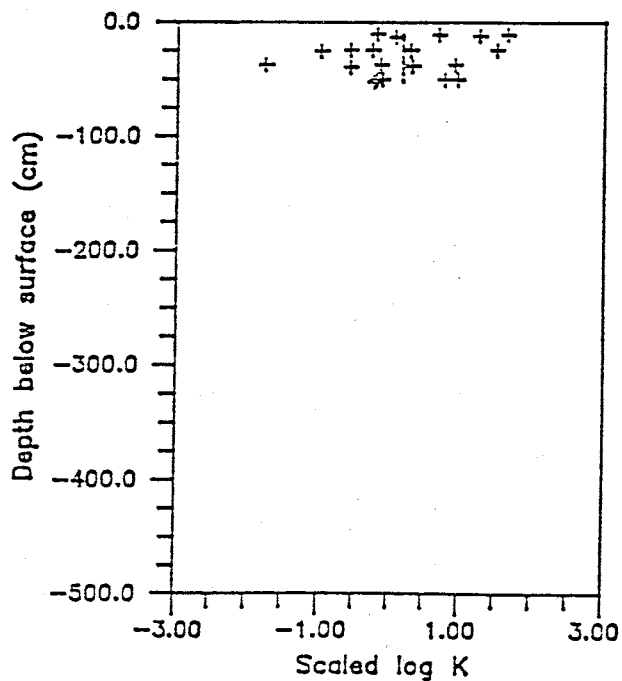


Figure 65. Scaled log K  
vs. depth, 0-50cm.

of table 6 shows that the best fit is given using this set of data. However, the K values from 375-450 cm in this plot were all obtained from transect V6. Thus, these values might tend to bias the data. Figure 63a shows that by removing the data from 375-450 cm a similar trend with depth is still observed. The correlation is decreased slightly, however, by removal of these data points (table 6).

The upper 50 cm of the cross section were previously described as being hydraulically altered by the processes of surface wash and partial cementation. It was discovered during the horizontal trend analyses that K samples from 28 and 41 cm depths do not mimic the trends present in K at greater depths. For this reason, a trend analysis with depth was performed excluding the data from 0-50 cm (figure 64a). The correlation of this analysis is found to increase over figure 63a. In all three cases (figures 62a-64a), K is seen to decrease slightly with depth with the quadratic fit being the preferable method of characterization. The residual values from these regression analyses all appear to follow a normal distribution (figures 62b-64b). The decrease in K with depth could be the result of matrix compaction. As the result of compaction, reorientation of particles and decreases in pore space can cause the K value of a sample to decrease.

A linear regression analysis was performed on the K data from the upper 50 cm (figure 65). The result of this analysis was not significant (table 6) and hence, the mean value becomes the best predictor in this case.

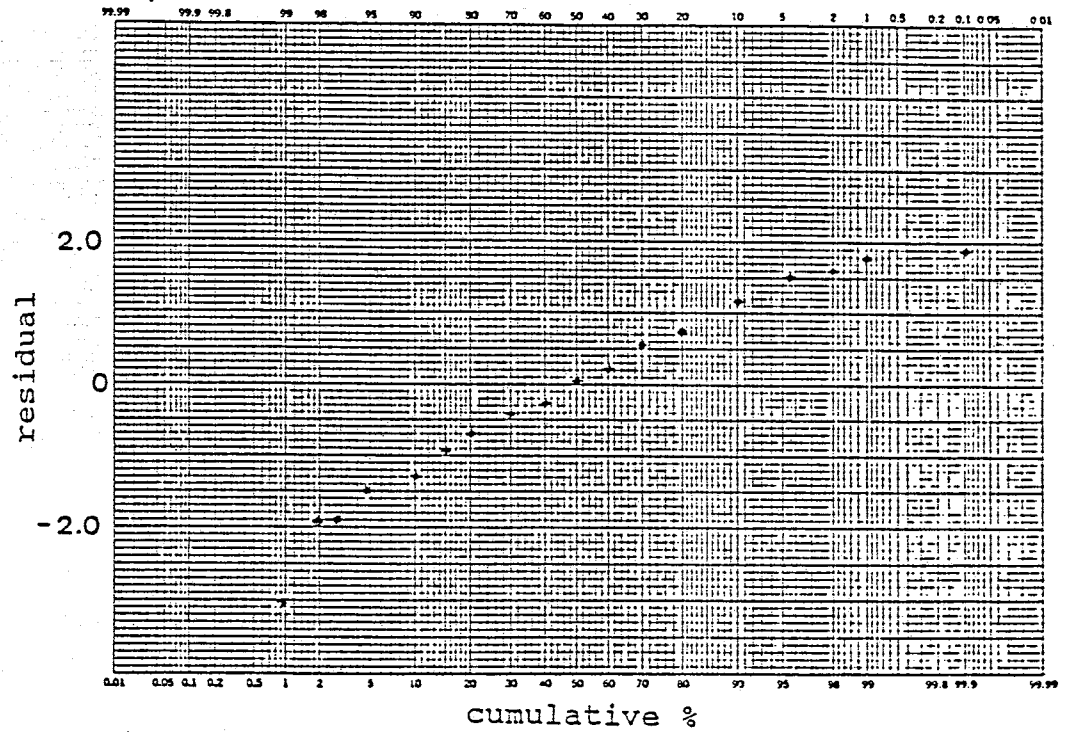


Figure 62b. Normality plot for figure 62a (scaled log K, 0-450cm).

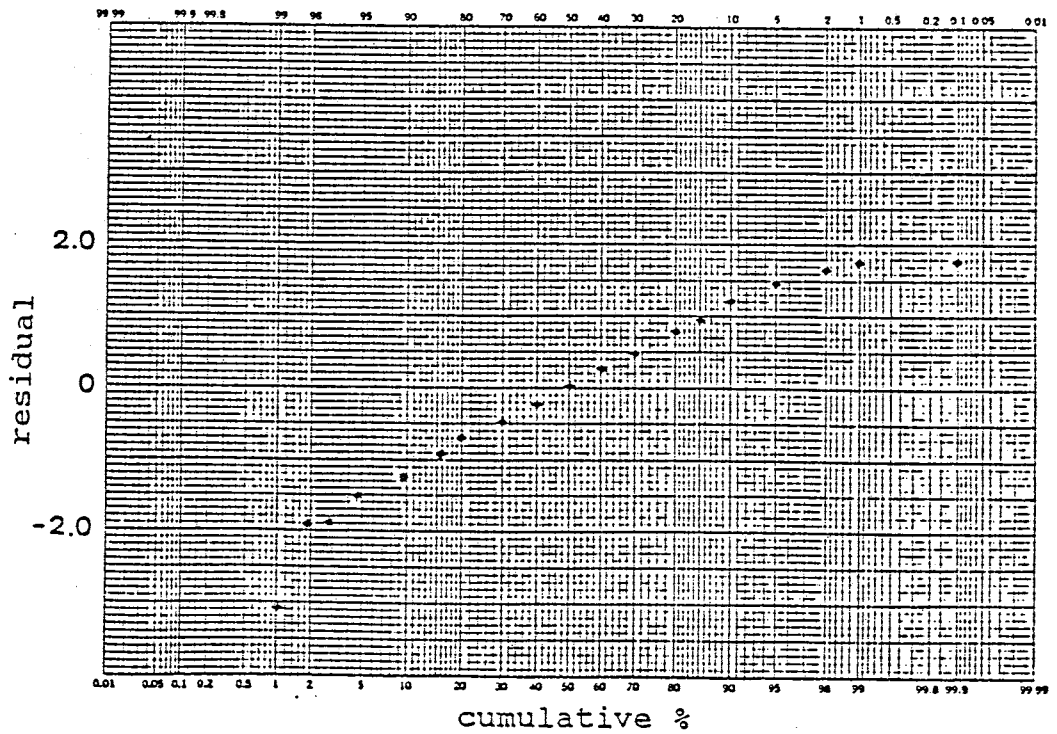


Figure 63b. Normality plot for figure 63a (scaled log K, 0-375cm).

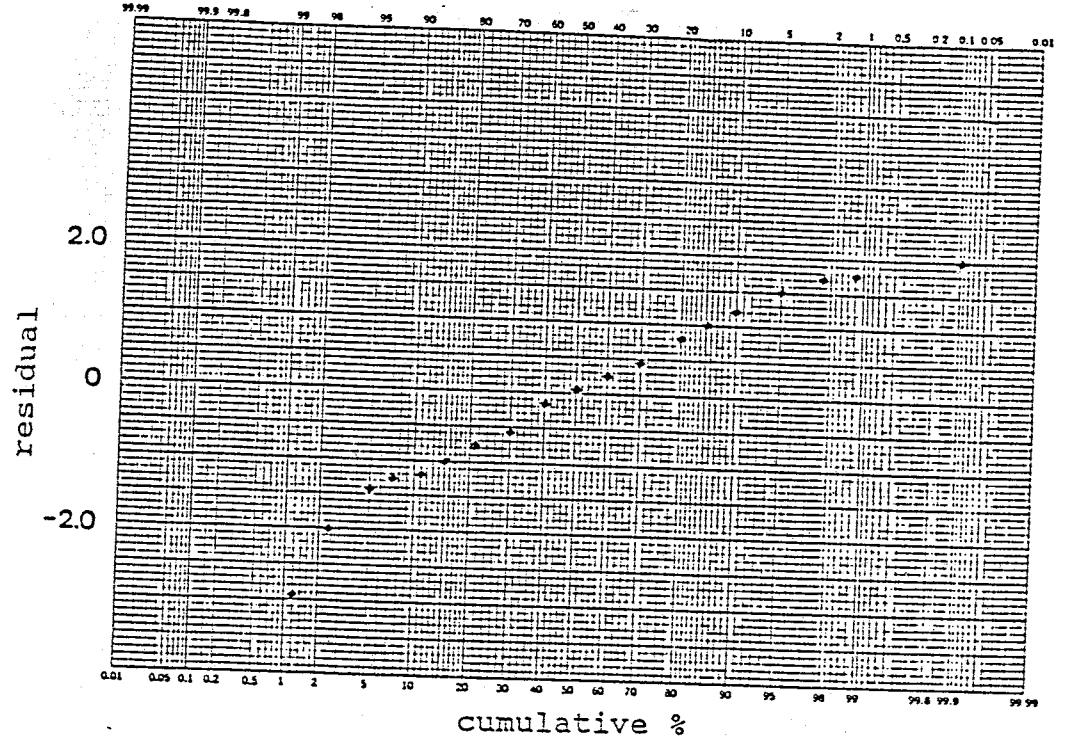


Figure 64b. Normality plot for figure 64a (scaled log K, 50-375cm).

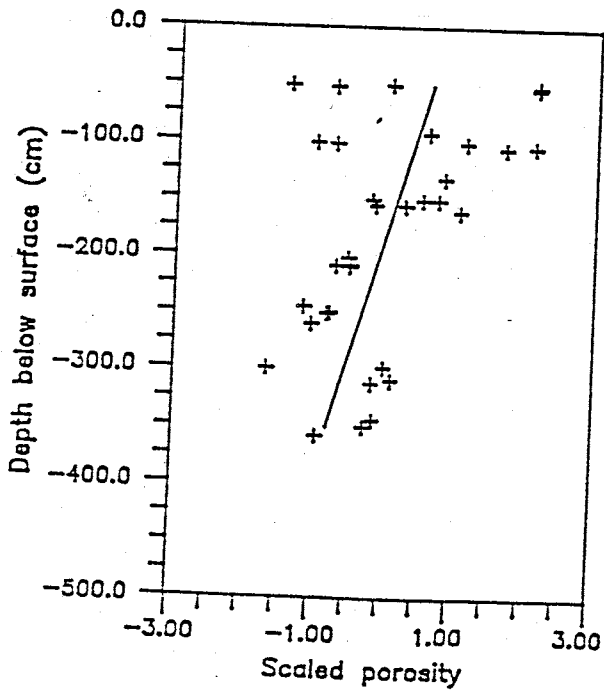


Figure 66a. Scaled n vs. depth, 0-375cm.

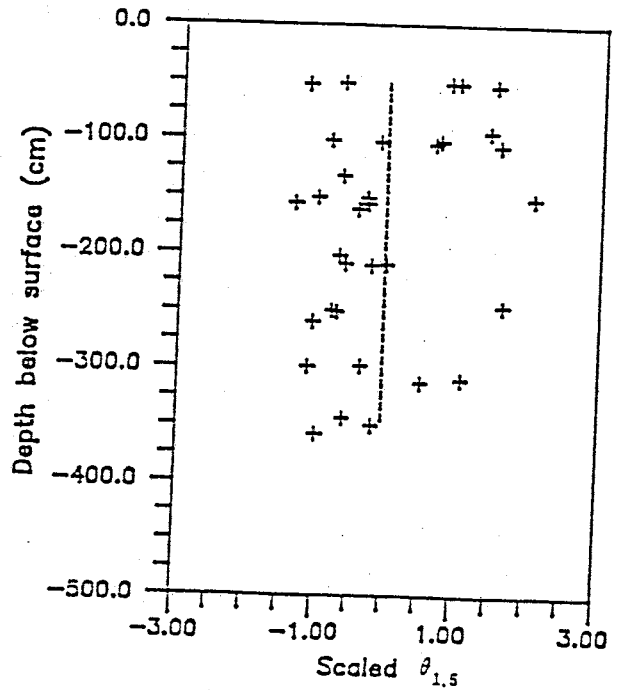


Figure 67. Scaled  $\theta_{1.5}$  vs. depth, 0-375cm.



Of the remaining data distributions for the cross section, the only other discernible trend with depth was discovered for the porosity distribution. Once again, all data was scaled using equation (13) prior to analysis. For  $n$ , a general decrease with depth is noted in figure 66a. Compaction of the matrix with depth will also result in a decrease in porosity. The residual values from this linear regression appear normally distributed (figure 66b).

If compaction with depth has actually occurred throughout the cross section, it will not have as direct an effect on  $\theta_{1.5}$  as it does on  $K$  and  $n$ . Compaction will cause a reorientation of grains which will tend to increase the number of the finer pores present within a sample. Hence, it is possible that compaction could cause an increase in the  $\theta_{1.5}$  distribution with depth. The regression fit to the  $\theta_{1.5}$  data was not significant (table 6), and hence, the mean value is the best predictor (figure 67). Thus,  $\theta_{1.5}$  appears to remain constant with depth even though porosity decreases.

The particle size distribution at 10% finer by weight was also discovered to be constant with depth (figure 68). The regression analysis for  $d_{10}$  with depth was not significant (table 6). Therefore, the mean value of  $d_{10}$  is the best predictor. It was foreseen that the overall trend in particle size should be fairly constant with depth. The large fluctuations in the scaled data of figure 68 are due to layering of particle sizes in the media.

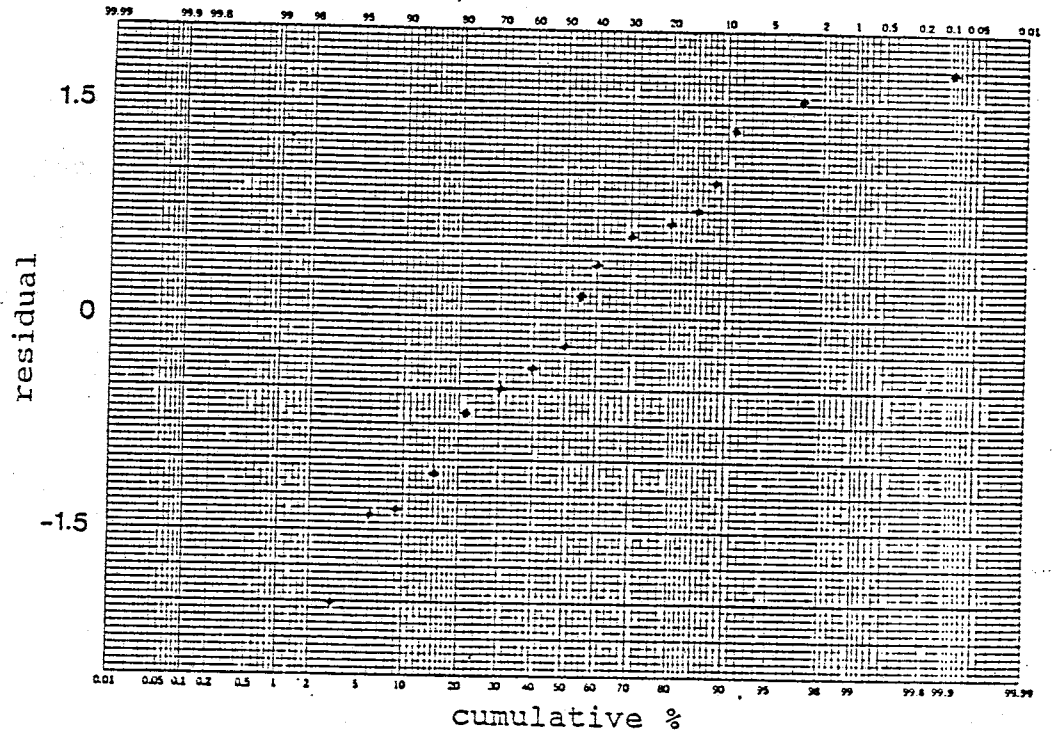


Figure 66b. Normality plot for figure 66a (scaled n, 0-375cm).

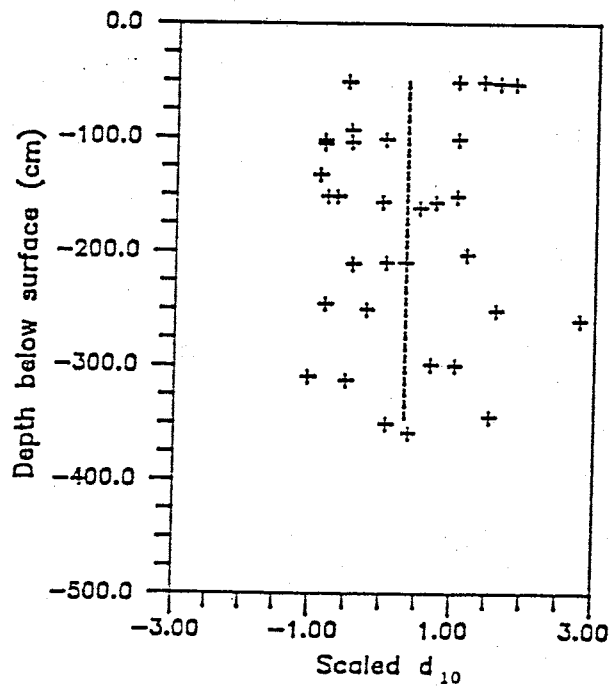


Figure 68. Scaled  $d_{10}$  vs. depth, 0-375cm.

### 2-D Cross Section

Trends in the data are found to exist in both the horizontal and, to a lesser extent, the vertical directions. The following section is included to determine if the various data distributions (K, n, d<sub>10</sub>, etc.) can be characterized in cross section using 2 dimensional regression equations.

For each of the data distributions, the following regression equation was used for each of the initial analyses

$$(15) \quad \text{dep} = \beta_0 + \beta_1(Y) + \beta_2(x) + \beta_3(Y)(x) + \beta_4(Y)^2 + \beta_5(x)^2 + \beta_6(x)(Y)^2 + \beta_7(Y)(x)^2.$$

The best equation for each data distribution was then formulated using partial F-tests to determine the significant variables. The following 2 equations were eventually decided upon

$$(16) \quad \text{dep} = \beta_0 + \beta_1(Y) + \beta_2(x) + \beta_3(x)^2$$

$$(17) \quad \text{dep} = \beta_0 + \beta_1(Y) + \beta_2(x) + \beta_3(x)^2 + \beta_4(Y)(x)^2.$$

The equation employed on each data distribution is listed in table 7. The coordinate position in cross section is given by x and y, measured in meters. The origin of this coordinate system is at the surface along the northern edge of the cross section.

---

TABLE 7

Least squares regression statistics:

		2-D Cross section				
Variables		number	mult.	F	tabular	
dep	indep	of	correl.	stat	F(5%)	F(1%)
		samples	coeff			

log K (0-50 cm)	position (x,y)	(16)	63	0.447	4.907**	2.76	4.13
log K (50-400 cm)	position (x,y)	(16)	303	0.760	136.023**	2.60	3.78
log K (0-400 cm)	position (x,y)	(17)	366	0.725	100.069**	2.37	3.32
n (0-400 cm)	position (x,y)	(16)	122	0.427	8.752**	2.68	3.95
$\theta_{1.5}$ (0-400 cm)	position (x,y)	(16)	122	0.636	26.672**	2.68	3.95
$d_{10}$ (0-400 cm)	position (x,y)	(16)	95	0.454	7.882**	2.72	4.04

-----  
 position = (x,y) coordinates in cross section in meters

$$(16): \text{dep} = \beta_0 + \beta_1(y) + \beta_2(x) + \beta_3(x)^2$$

$$(17): \text{dep} = \beta_0 + \beta_1(y) + \beta_2(x) + \beta_3(x)^2 + \beta_4(y)(x)^2$$

\* reject  $\beta_1 = \dots = \beta_4 = 0$  F (5%)

\*\* reject  $\beta_1 = \dots = \beta_4 = 0$  F (1%)

It was discovered in both the horizontal and vertical 1-D regressions that the K values from the upper 50 cm do not reflect the values from the rest of the cross section. Therefore, 3 separate regression analyses for K were performed. The first analysis incorporated K data to a depth of 50 cm, the second used the values from 50-400 cm, and the third analysis employed all the K data from the entire cross section.

Results from the K regression analyses are listed in table 7. Regression equation (16) does a marginal job of describing the trend in the K data from 0-50 cm as seen by its low correlation coefficient and F value. The 2 dimensional regression equation, however, does a better job of characterizing K in this upper zone than did either of the regression equations in one

dimension. The plots of the K regression fits from 0-50 cm and 50-400 cm for the cross section are shown in figure 69a. Good correlation is noted using equation (16) for the K values at the lower depth. A very marked difference is present (figure 69a) in the trends from the upper and lower data distributions. For both analyses, the residual values appear to be normally distributed (figures 69b & c).

The plot of the K distribution for the entire cross section using equation (17) is exhibited in figure 70a. The results of this analysis appear quite favorable (table 7). The residual values from this analysis appear to be normally distributed (figure 70b).

The regression plot incorporating all of the data (figure 70a) gives the impression that K decreases greatly with depth. Observation of the lower plot (below 50 cm) in figure 69a shows that this is not the case. The discrepancy between figures 69a and 70a is due to the discontinuity in K values between the upper (0-50 cm) and lower (below 50 cm) samples.

The following regression equations were found to best describe the K distribution throughout the cross section:

$$(18) \quad 0-50 \text{ cm} \quad K = -2.770 + 1.090(y) - 0.0508(x) + 0.000458(x)^2$$

$$(19) \quad 50-400 \text{ cm} \quad K = -3.705 + 0.224(y) - 0.0741(x) + 0.000834(x)^2$$

$$(20) \quad 0-400 \text{ cm} \quad K = -2.969 + 0.634(y) - 0.0693(x) + 0.000665(x)^2 - 0.0000617(y)(x)^2$$

Once again, the (x,y) coordinates are in meters.

Results from the 2 dimensional regression analyses for the

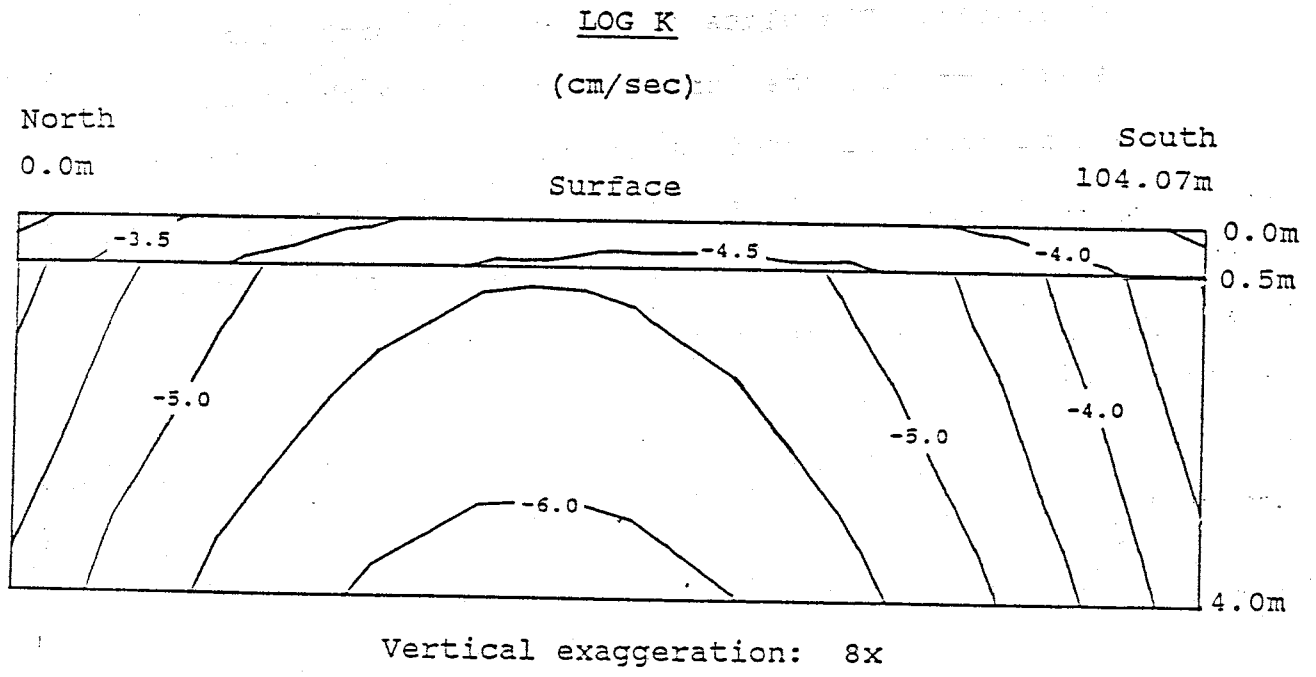


Figure 69a. Contoured cross section of the 2-D regression fits to the log K data (0-50cm and 50-400cm).

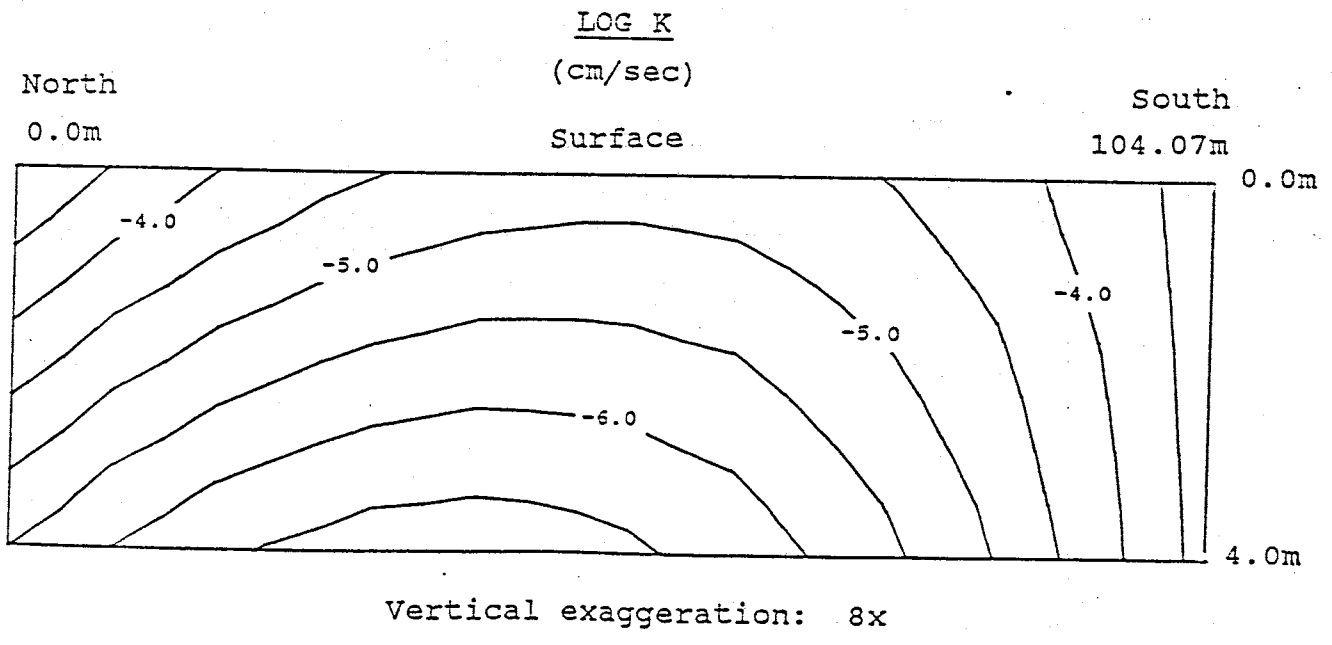


Figure 70a. Contoured cross section of the 2-D regression fit to the log K data (0-400cm).

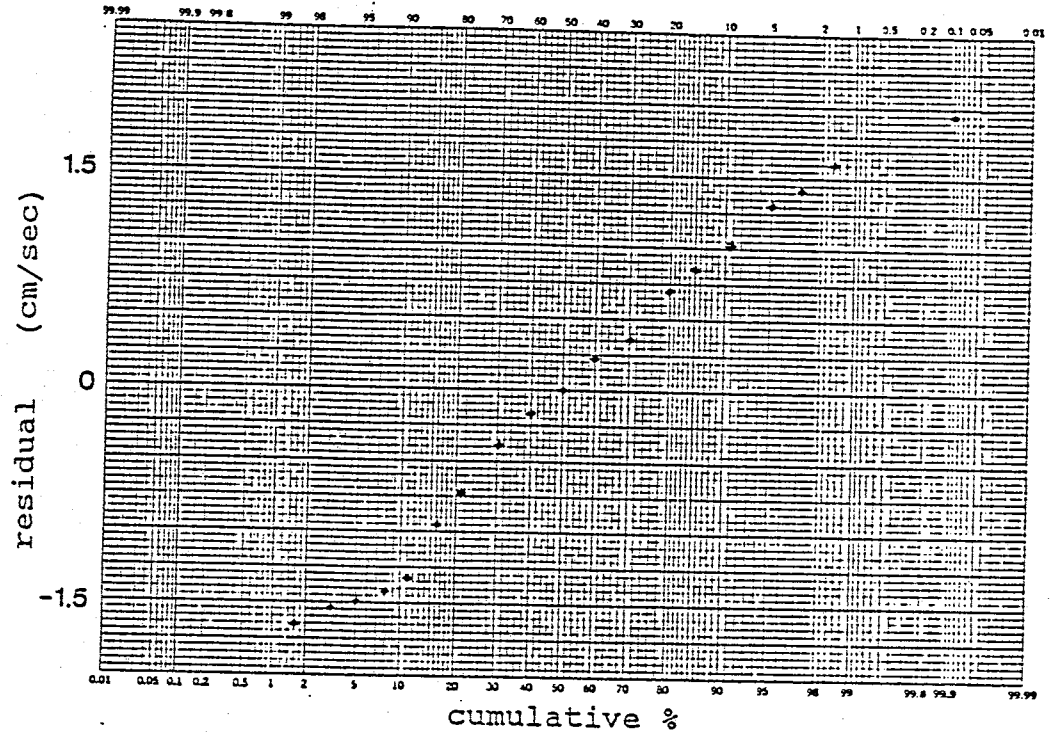


Figure 69b. Normality plot for figure 69a (2-D, log K, 0-50cm).

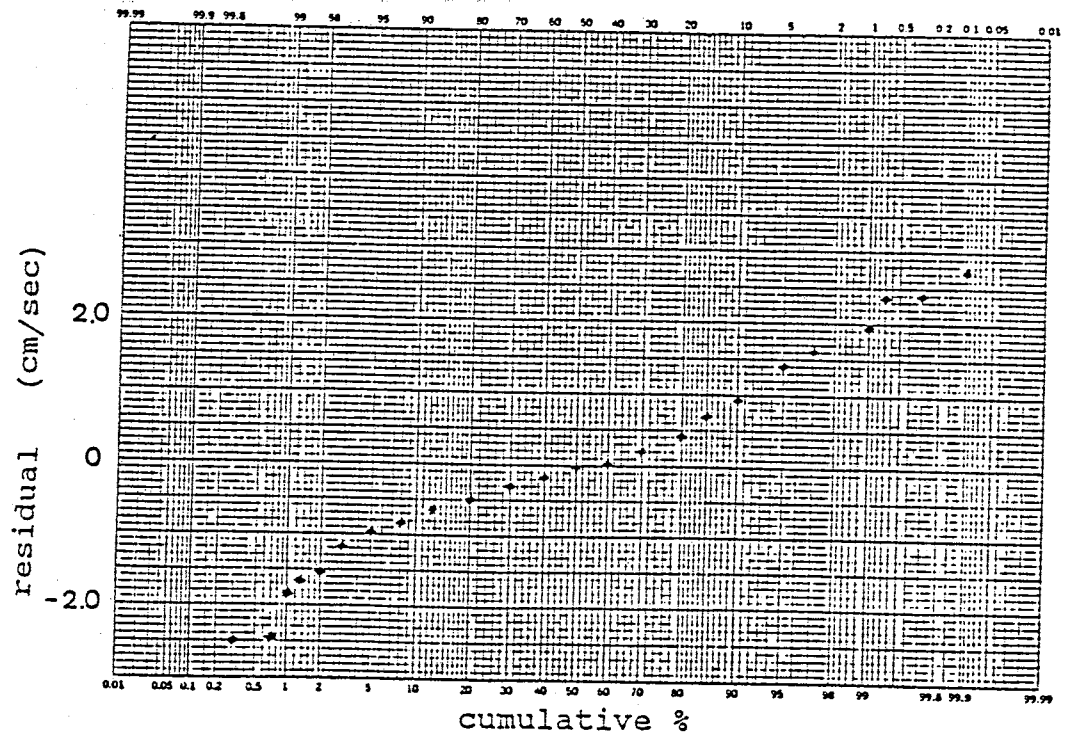


Figure 69c. Normality plot for figure 69a (2-D, log K, 50-400cm).

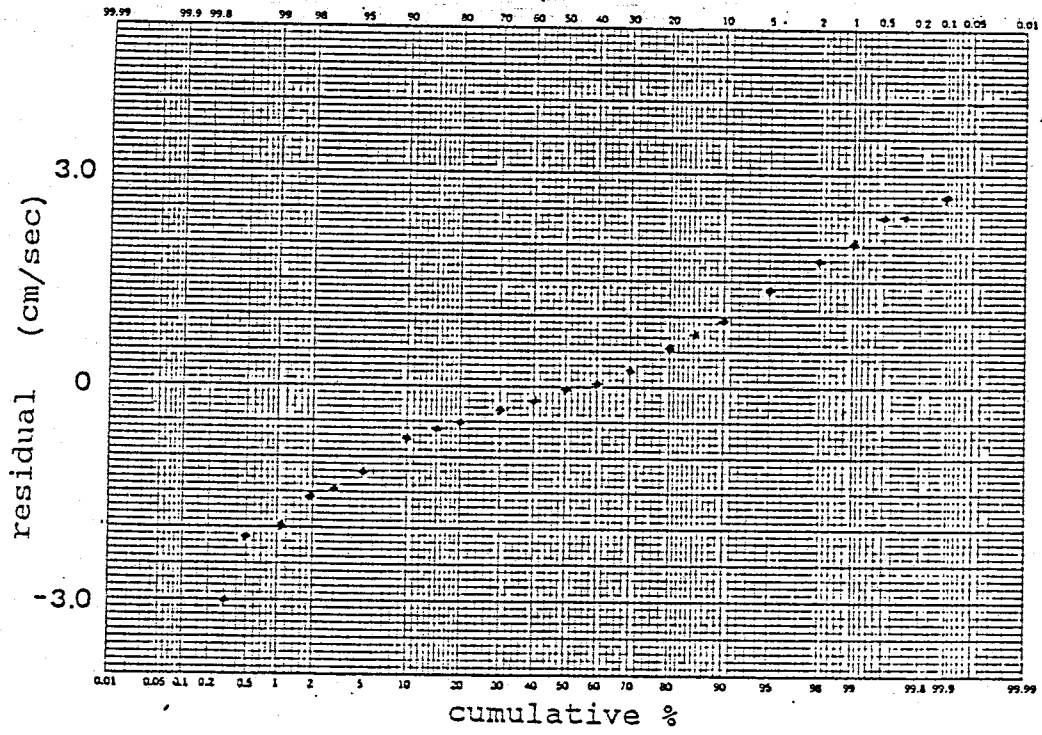


Figure 70b. Normality plot for figure 70a (2-D, log K, 0-400cm).



$\theta$  and  $d$  distributions were not as encouraging (table 7). Even so, the regression analyses for  $n$ ,  $\theta_{1.5}$ , and  $d_{10}$  were all significant as seen by their F values. The plots of the regression fits are presented in figures 71a-73a. Separate regression analyses for the upper 50 cm were not performed due to the absence of data in this area. The greatest correlation among these analyses is present for the  $\theta_{1.5}$  data values. This high degree of correlation for  $\theta_{1.5}$  was previously noted in the 1-D horizontal regression. The 2 dimensional regression equations were found to better characterize both the porosity and  $d_{10}$  distributions in comparison to the 1-D regression equations previously mentioned. The following regression equations were found to best describe the  $n$ ,  $\theta_{1.5}$ , and  $d_{10}$  distributions throughout the cross section:

$$(21) \quad 0-400 \text{ cm} \quad n = 0.508 + 0.0219(y) + 0.00273(x) - 0.0000261(x)^2$$

$$(22) \quad 0-400 \text{ cm} \quad \theta_{1.5} = 0.197 + 0.0285(y) + 0.00772(x) - 0.0000848(x)^2$$

$$(23) \quad 0-400 \text{ cm} \quad d_{10} = 11.326 - 0.776(y) - 0.428(x) + 0.00464(x)^2$$

The residual values from the porosity regression analysis appear to be normally distributed (figure 71b). Figures 72b and 73b show that the normality test for the  $\theta_{1.5}$  and  $d_{10}$  distributions are questionable. The absence of straight line plots in figures 72b and 73b discount the validity of the F-value tests.

The highest correlation values for the 2-D regression analyses are present for the K distribution. Once again, this is no doubt partially the result of sample scale.

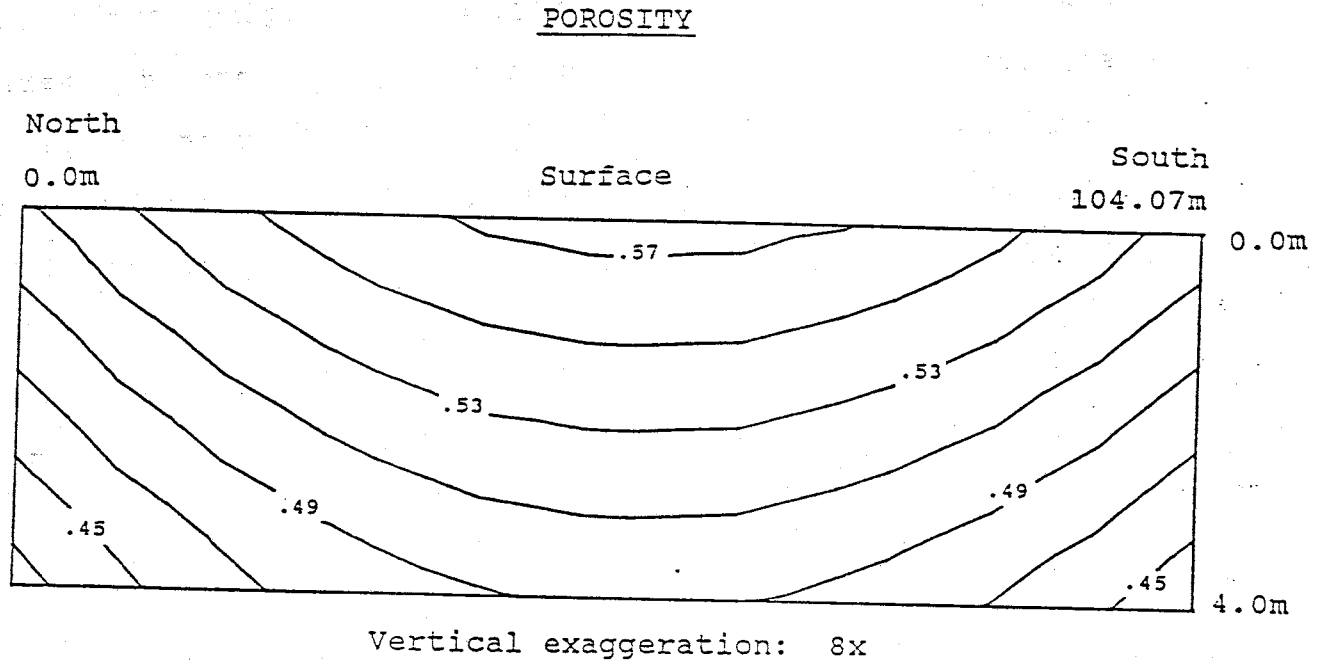


Figure 71a. Contoured cross section of the 2-D regression fit to the porosity data.

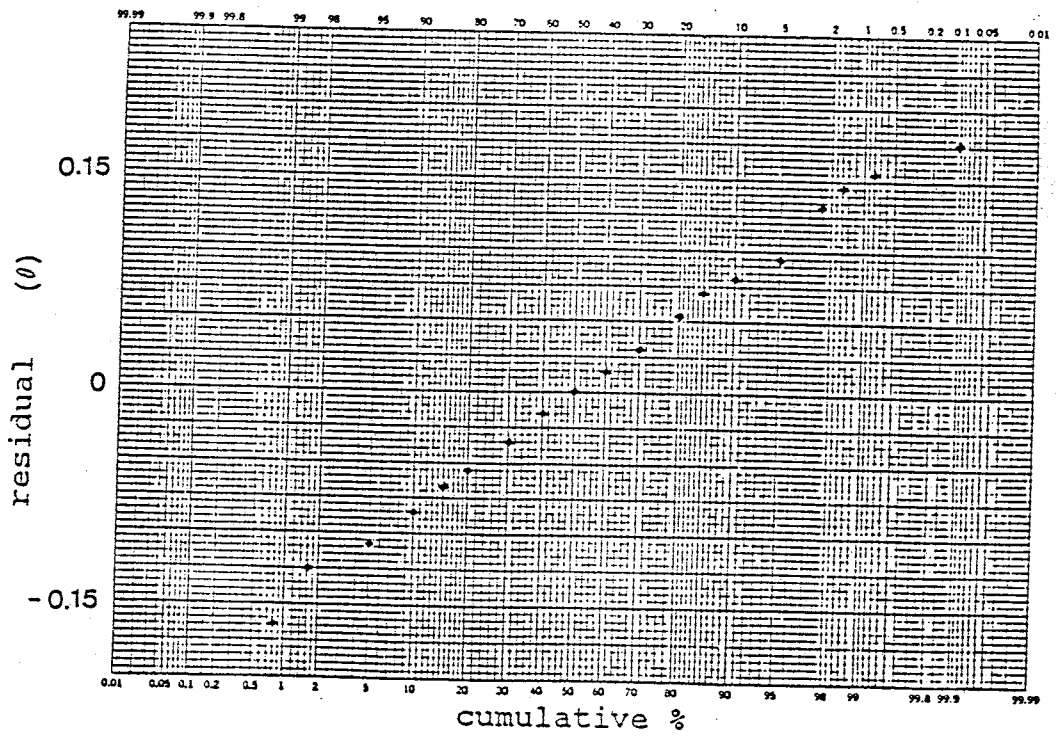
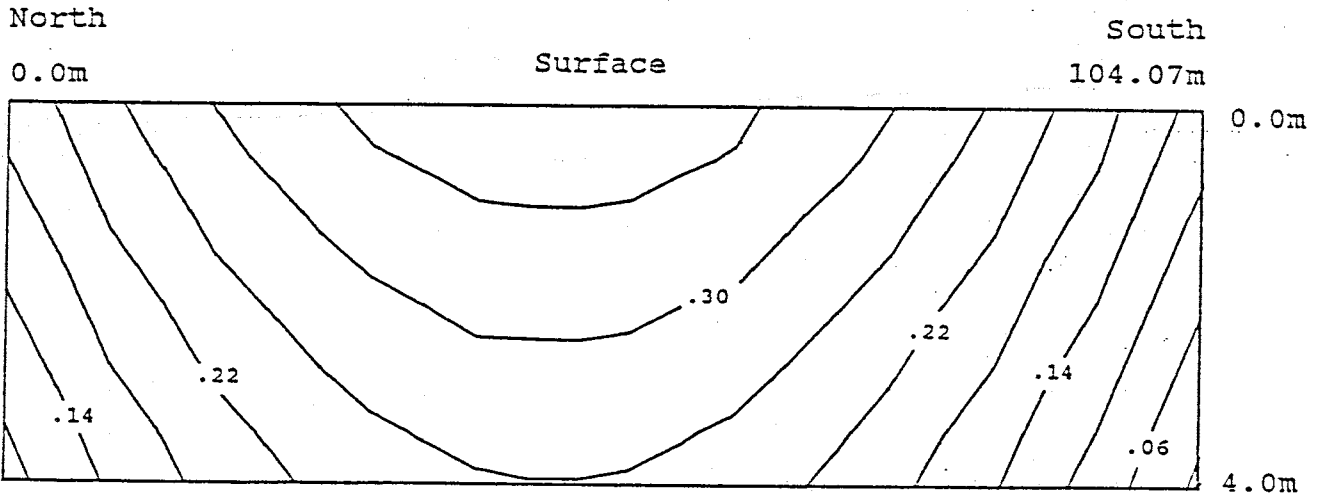


Figure 71b. Normality plot for figure 71a (2-D, n).

$\theta$  @ 1.5 bars



Vertical exaggeration: 8x

Figure 72a. Contoured cross section of the 2-D regression fit to the  $\theta_{1.5}$  data.

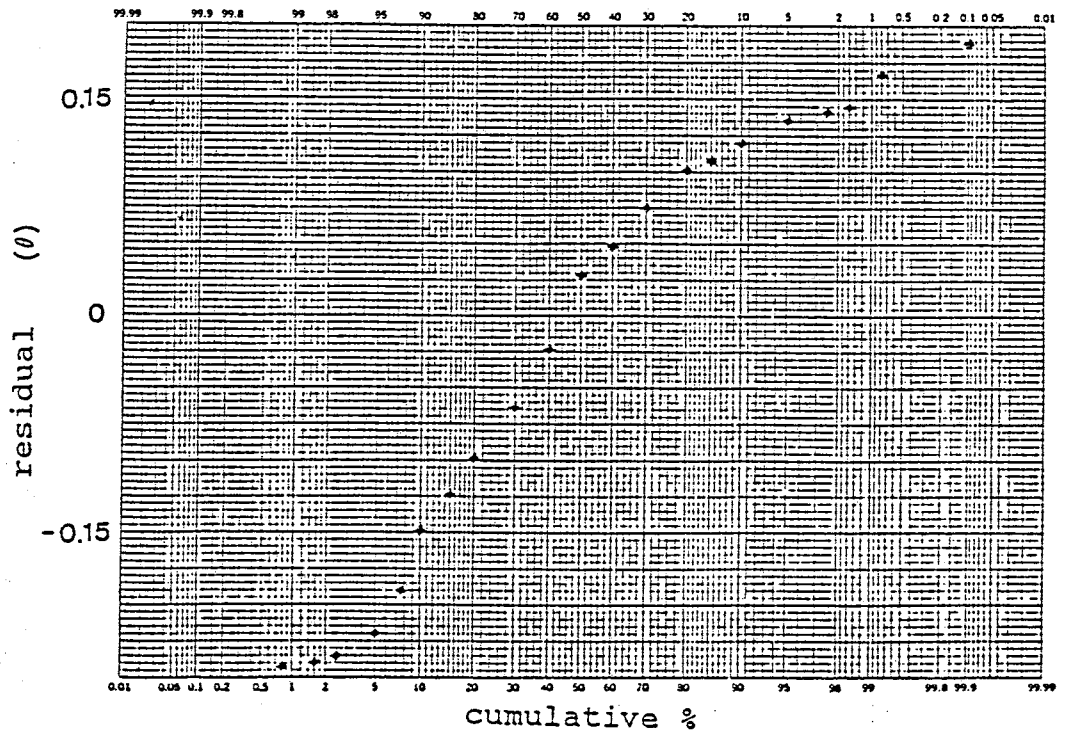


Figure 72b. Normality plot for figure 72a (2-D,  $\theta_{1.5}$ ).

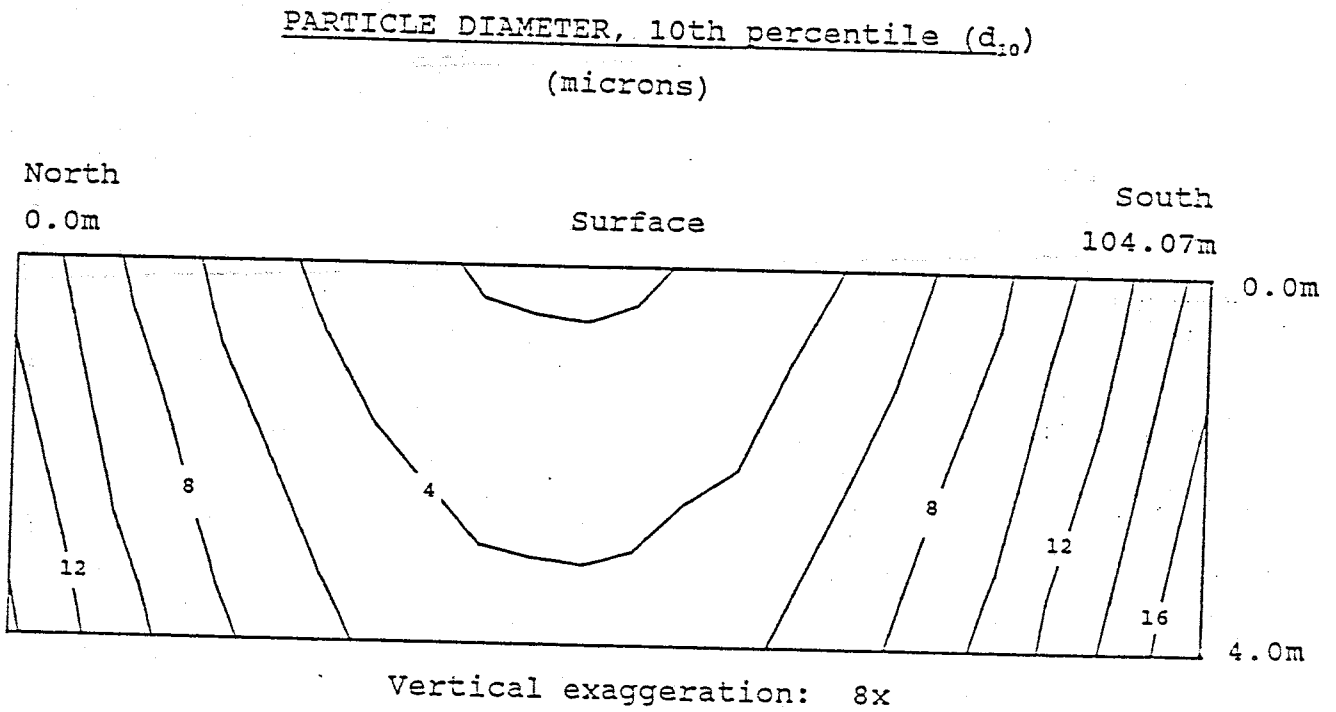


Figure 73a. Contoured cross section of the 2-D regression fit to the  $d_{10}$  data.

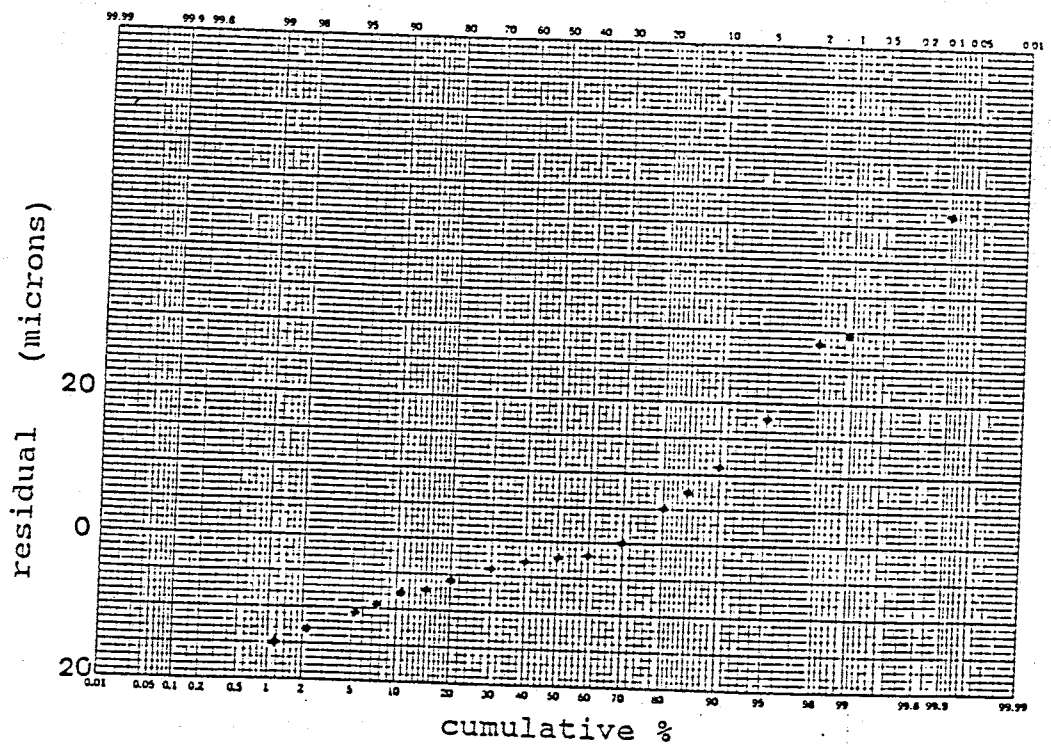


Figure 73b. Normality plot for figure 73a (2-D,  $d_{10}$ ).

### Conclusions

Characterization information gained using regression analyses is listed below.

- Regression analyses were able to describe trends in the data which could not be accounted for using sample statistics.
- Regression analyses were able to describe the variability in data both horizontally and, in a general sense, vertically.
- Regression analyses led to development of equations to describe each data distribution for the entire cross section. These equations give good general representations of the tailings properties depending on location.
- Using regression analyses, the magnitude of a trend could be determined. The regression analysis output parameters and normality plot test the validity of the regression fit.
- The regression equations describe the data distributions in cross section in more detail than works in the past such as Mittal and Morgenstern (1976), and Isaacs and Hunt (1981). The Waldo Mill tailings impoundment is not simply made up of a homogeneous slime zone restrained by a homogeneous sand embankment. Mixing between these 2 'zones' is quite evident.
- Regression analyses uncovered the possibility of secondary processes (compaction) occurring in the tailings. This is noted in figures 63a, 66a, and 68 by the fact that the K and n distributions decrease with depth while the  $d_{10}$  distribution remains relatively constant.

The shortcomings of regression analyses are listed below.

- Success of a regression analysis in this study was dependent, in part, on sample scale. K measurements were taken over 13.3 cm compared to 3 cm for  $\theta_{1.5}$  and  $d_{10}$ . Thus, the K values from the cross section were more of an 'averaged' value in comparison and, as a result, were more conducive to regression analyses.
- Regression analyses are not able to describe the magnitude or location of discontinuities such as layering in an environment like tailings impoundments.
- Regression analyses are sensitive to exclusion of data values. This was noted in figures 56a, 58a, 69a, and 70a. Including the K values from the upper 50 cm greatly affected the regressions' characterization of the K data below 50 cm in figure 70a.

## GEOSTATISTICAL ANALYSES

The Waldo Mill impoundment is an extremely heterogeneous environment in the hydrologic sense. We saw in the previous section that discernible trends exist in each of the data distributions. Regression equations were used to aid in the interpretation of these trends. These equations were able to describe the data trends with varying degrees of success.

The next question to address is, "Now that the overall trends have been removed from the individual sample populations, does any structure remain?" The scope of this section is to attempt to interpret any remaining structure in the individual data distributions using variograms. If this analysis proves successful, kriging equations can be employed to aid in the prediction of sample values throughout the cross section.

### Previous Work

A great deal of work has been done in the past in an attempt to characterize the spatial variability of various soil properties. Autocorrelation functions and variogram analyses have been used extensively in the soil science field to uncover structures in soil. Various authors have discovered the correlation length for many soil properties to be significant. For a Typic Torri-fluvent soil, Gajem et.al. (1981) reported correlation lengths of up to 20 times the sample spacing for the soil properties  $\theta_{0.1}$ ,  $\theta_{15}$ , pH, EC, and bulk density. Byers and Stephens (1983) discovered that both  $d_{10}$  and  $K(\text{sat})$  were correlated up to 1 meter in the horizontal direction at a medium grained sand site. Russo and Bresler (1981) found similar results for  $K(\text{sat})$  along with

porosity and sorptivity for a Hamra Red Mediterranean soil (Rhodorexalf). Even more recently, Saddiq et. al. (1985) and Yeh et. al. (1986) tested the correlation of soil-water tension along separate agricultural plots. Both studies reported that  $\psi$  values were correlated up to and beyond 6 meters. Thus, it is evident that many soil properties are not independent of surrounding values. Interpreting the underlying structure of these properties is an important factor for understanding the system as a whole.

To the author's knowledge, no studies similar to those mentioned above have been performed on mill tailings. The scope of this section is to determine if any spatial structure exists for various tailings properties like permeability or moisture content. The analysis performed in this section will employ geostatistical techniques common in the study of soil spatial variability. These analyses include construction of variograms and the use of kriging equations.

### Variogram analysis

#### Theory

To aid in the interpretation of the structure of a random field, variograms can be constructed. For a random field that meets the requirements of an intrinsic random function of order zero, the following properties are true (Gutjahr, 1985):

$$(24) \quad E(V(\underline{x})) = m$$

$$(25) \quad \gamma(\xi) = E[(V(\underline{x}+\underline{\xi}) - V(\underline{x}))^2]$$

$m$  = mean value of the sample population  
 $V(\underline{x})$  = experimental data value at point  $\underline{x}$

$V(\underline{x}+\xi)$  = experimental data value at a point  $\xi$  distance from  $\underline{x}$   
 $\xi$  = lag or separation distance (distance between measurement points).

To determine the variogram value  $\gamma(\xi)$  at a given lag distance  $\xi$ , all pairs of data values  $\xi$  distance apart in the random field  $V(\underline{x})$  are compared. This is done using the following equation (Delhomme, 1978):

$$(26) \quad \hat{\gamma}(\xi) = \frac{N(\xi)}{\sum_{i=1}^{N(\xi)} [(V(\underline{x}_i+\xi) - V(\underline{x}_i))^2]} / 2N(\xi)$$

where  $N(\xi)$  is the number of data pairs separated by the lag distance  $\xi$ .

Variograms are always greater than or equal to zero ( $\gamma(\xi) \geq 0$ ). In addition, variograms are symmetric about the origin ( $\gamma(\xi) = \gamma(-\xi)$ ). The variogram value  $\gamma(\xi)$  tends to increase with increasing lag distances  $\xi$ . If the population  $V(\underline{x})$  is statistically homogeneous as well ( $\gamma(\xi) = C(0) - C(\xi)$ ), the variogram  $\gamma(\xi)$  will reach a sill value as  $\xi$  increases. This sill value is equal to the variance of the data field  $V(\underline{x})$  (Delhomme, 1978). The average distance over which points are significantly correlated is termed the 'scale'. For the statistically homogeneous case, this distance is also termed the 'range' (Gutjahr, 1985).

Variograms can take on many forms depending on the structure of the random field. For this study, exponential and pure nugget effect variograms dominated. The first form represents a variogram that follows the exponential function  $\sigma^2[1 - e^{-\xi/L}]$  (figure 74). This type of variogram originates at the origin



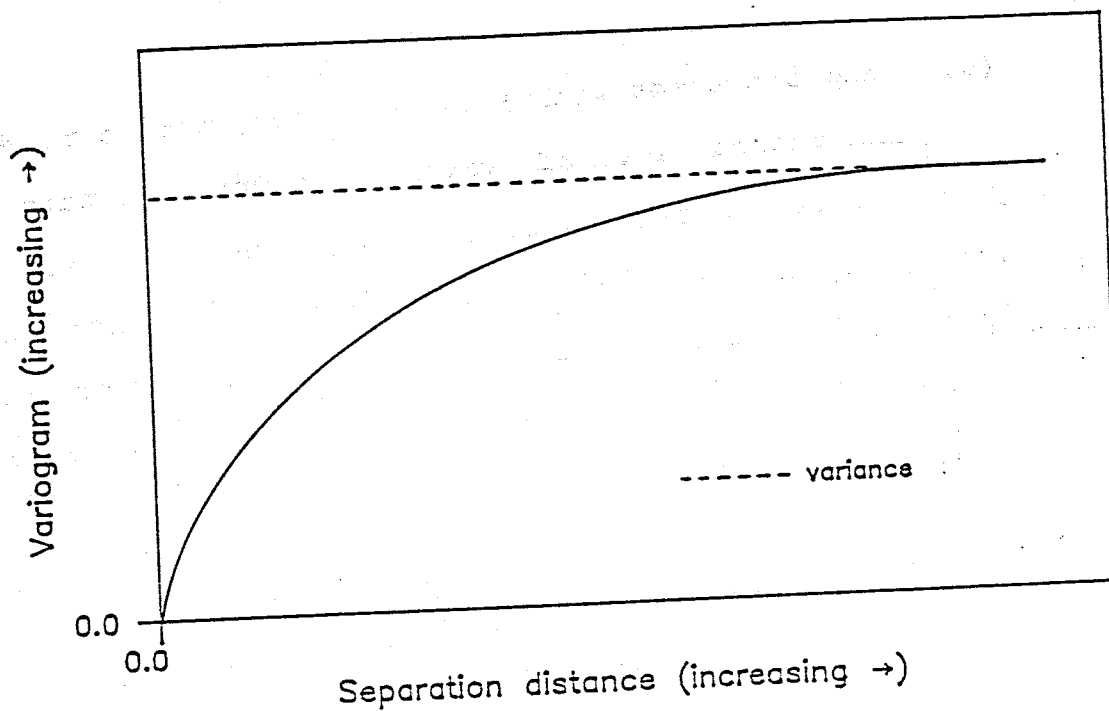


Figure 74. Example of an exponential variogram.

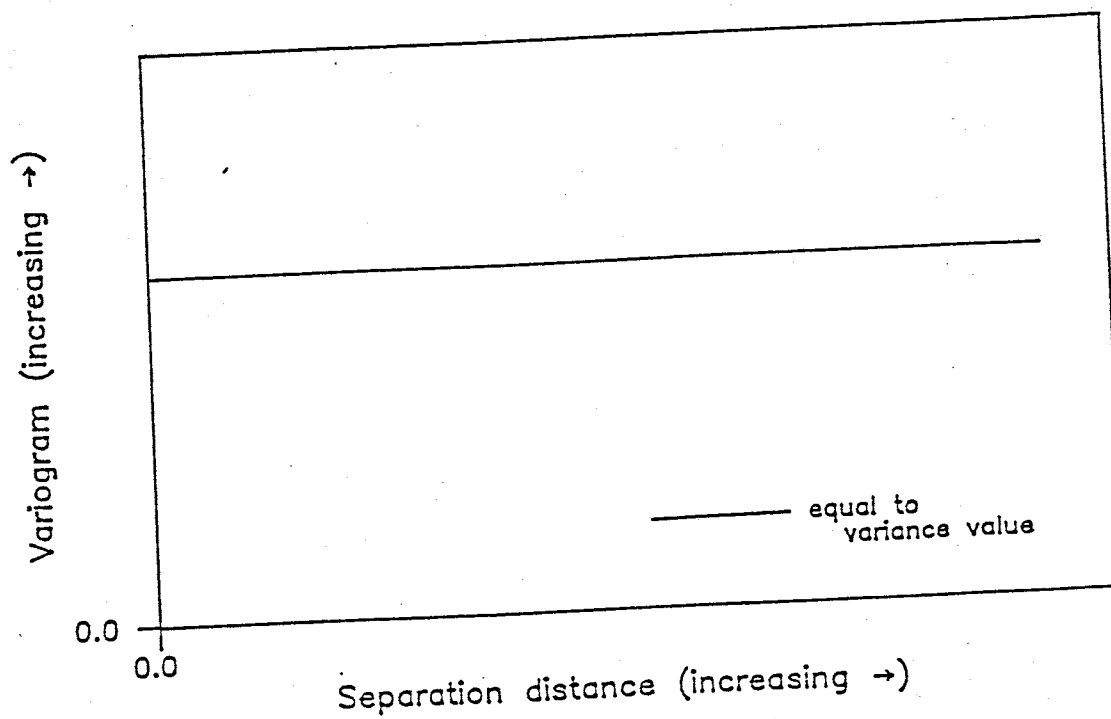


Figure 75. Example of a pure nugget effect variogram.

(0,0) and increases with  $\xi$  becoming asymptotic to  $\sigma^2$ .

The second form of variogram common to this study is the pure nugget effect variogram (figure 75). With this type of variogram, no correlation exists between the data points and  $\gamma(\xi)$  is equal to the population variance. The lack of correlation can be due to measurement error in the sampling process or simply independence between experimental values. Thus, with a pure nugget effect variogram, knowing a data value at one point yields no additional information about the surrounding points.

#### Analysis

Variograms of the mill tailings hydraulic data were constructed using the program VGRAM written by Allan Gutjahr (appendix K). From the cross section, the detrended data distributions of  $\log K$ ,  $n$ ,  $\theta_{1.5}$ , and  $d_{10}$  were analyzed. Three individual variograms were produced for each data set. First, a variogram was constructed assuming the distribution to be homogeneous in cross section. This was followed by the formulation of anisotropic variograms in the horizontal and vertical directions.

The poorest correlation was noted in the conductivity distribution (figure 76). The solid line in figure 76 represents the homogeneous variogram while the dashed lines represent the horizontal and vertical variograms. All 3 variograms represent pure nugget effect. Therefore, by previously removing the trend using the regression model, all of the structure from the  $\log K$  system was removed. It is noted in figure 76 that a greater variance in values is present in the vertical direction.

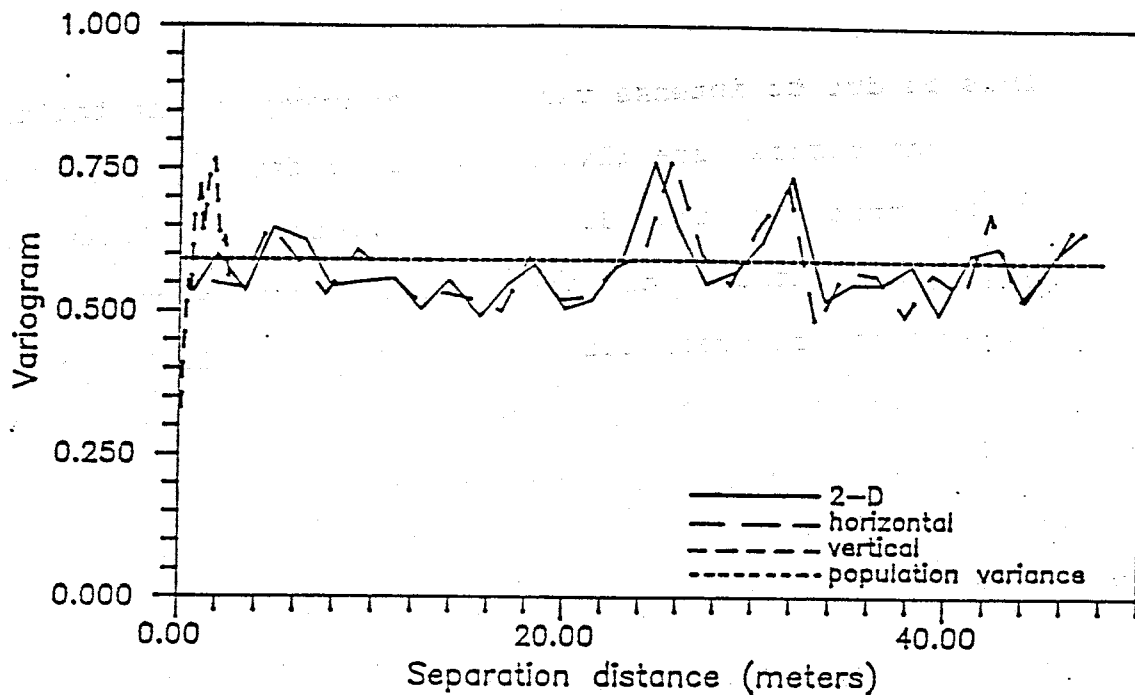


Figure 76. Variograms of detrended log K values from the cross section.

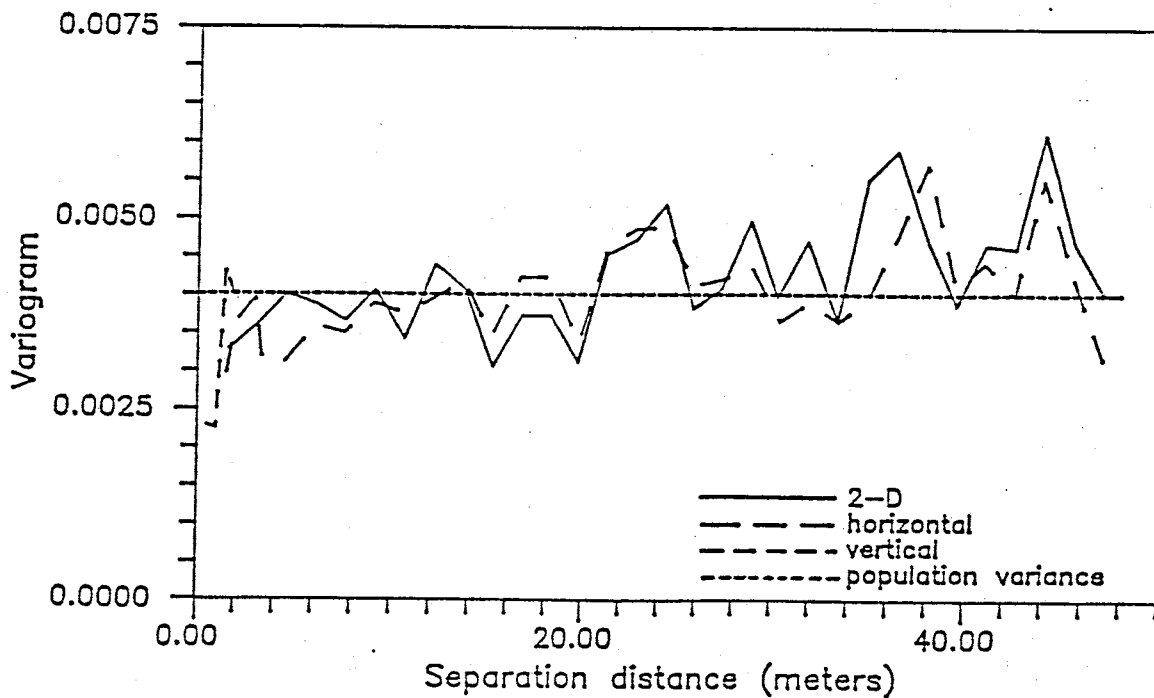


Figure 77. Variograms of detrended porosity values from the cross section.

This is due to intense vertical layering in the tailings.

Variograms were also constructed for log K exclusively using values from the upper 50 cm and values from below 50 cm. This was done similar to the log K regression analyses. These variograms are presented in appendix L. Both of these variograms exhibited pure nugget effect similar to that in figure 76. Log K values from the upper 50 cm have a higher variance than the lower samples.

A large amount of nugget effect is also present in the variogram of the porosity distribution (figure 77). Only a slight degree of correlation is noted. As was the case for log K, the porosity distribution exhibits greater variance in the vertical direction.

In comparison, significant correlation is present in the  $\theta_{1.5}$  distribution (figure 78). This variogram shows little nugget effect. Once again, the variability is greatest in the vertical direction. However, a minor degree of correlation exists vertically due to the fact that the vertical variogram is at all times less than the overall population variance. The homogeneous case variogram (solid line) does not intersect the variance value until a lag distance of approximately 16 meters. In addition, it appears that a degree of correlation continues at lag distances greater than 16 meters.

The variograms for the  $d_{10}$  distribution are similar to those of the porosity distribution (figure 79). Increased variability in  $d_{10}$  vertically is quite evident. Furthermore,  $d_{10}$  appears to be slightly correlated in the horizontal direction. A pure

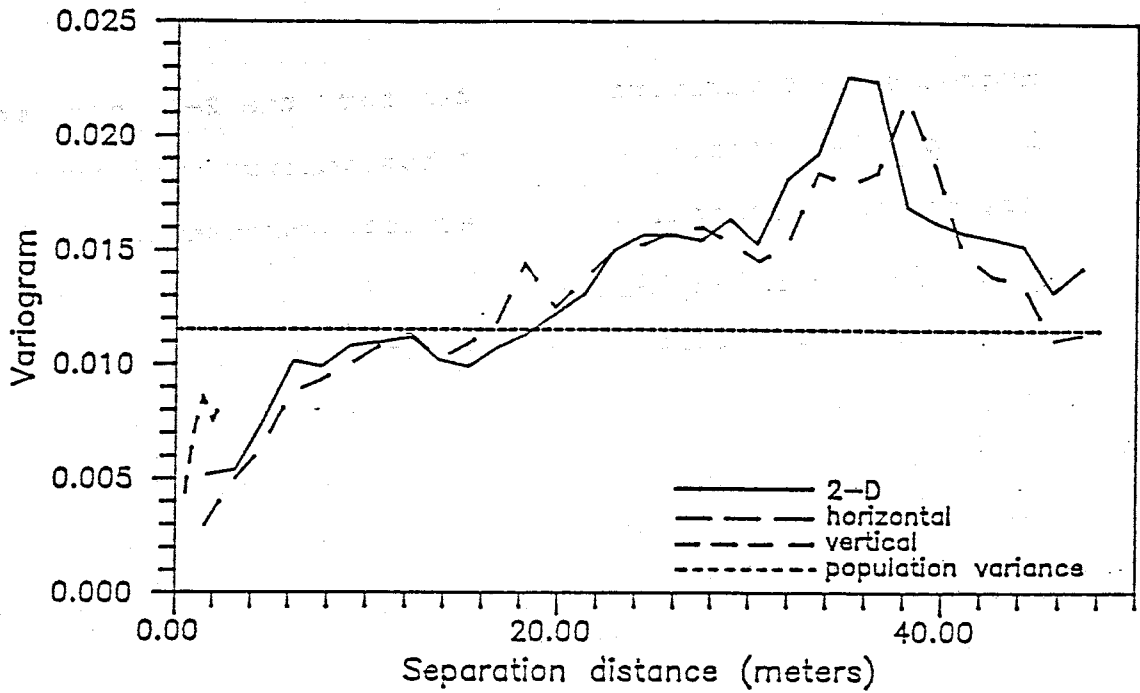


Figure 78. Variograms of detrended  $\theta_{1.5}$  values from the cross section.

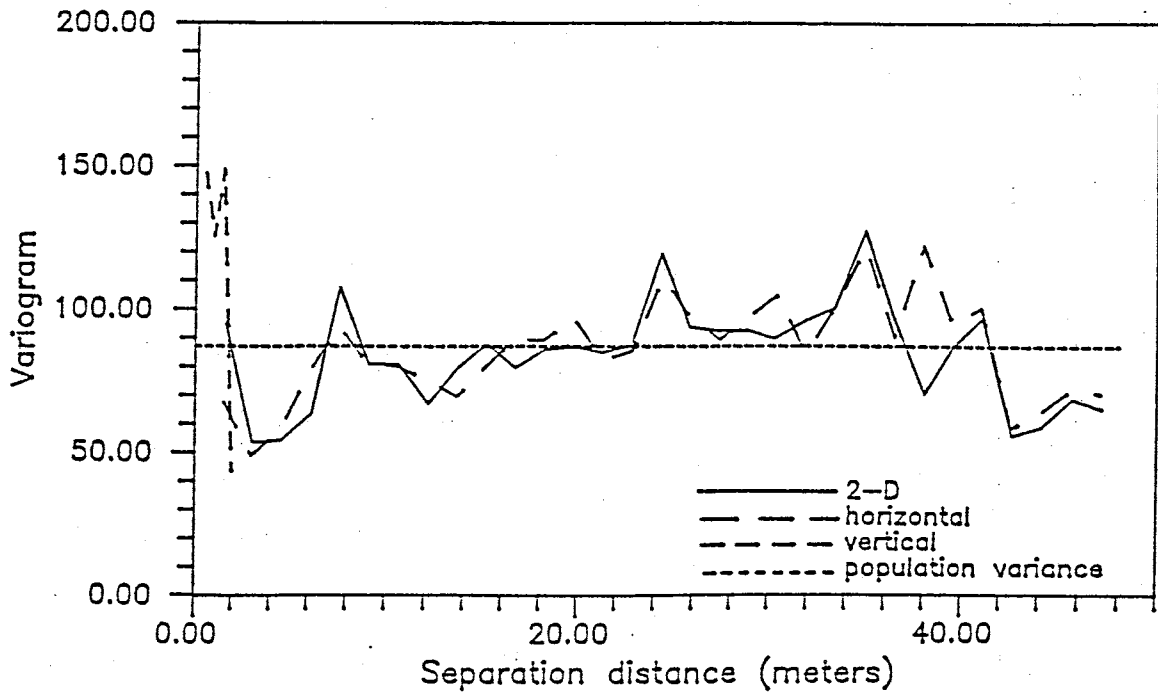


Figure 79. Variograms of detrended  $d_{10}$  values from the cross section.

nugget effect variogram is noted for the 2-D homogeneous case. At short lag distances for the homogeneous variogram,  $\gamma(\xi)$  values are greatly affected by the vertical component.

#### Fitting variogram models

Before a variogram can be used in a kriging equation, a model must be fit to the experimental variogram. For this process, various equations can be used. Some of these equations include linear, logarithmic, exponential, and spherical, to name a few. For an in-depth discussion on these theoretical models, refer to Delhomme (1978).

For this study, the variogram of  $\theta_{1.5}$  was chosen because it was the only variable that exhibited significant correlation. The  $\theta_{1.5}$  variogram was found to closest resemble that of an exponential function. The equation for the exponential fit is as follows:

$$(27) \quad \gamma(\xi) = B[1 - \exp(-|\xi|/A)]$$

Using equation 27 and the experimental variogram, the constants A and B can be determined. B is equal to the  $\gamma(\xi)$  value where the experimental variogram reaches a sill. For the statistically homogeneous case, B is equal to the population variance,  $\text{Var}[V(\underline{x})]$ . The A value (scale) is equal to the lag distance at which 1 e-fold drop occurs. The A value is considered the average distance over which points are significantly correlated (Gutjahr, 1985). Figure 80 is an example of an exponential fit to a variogram.

To compare the effects that differing variogram fits have on

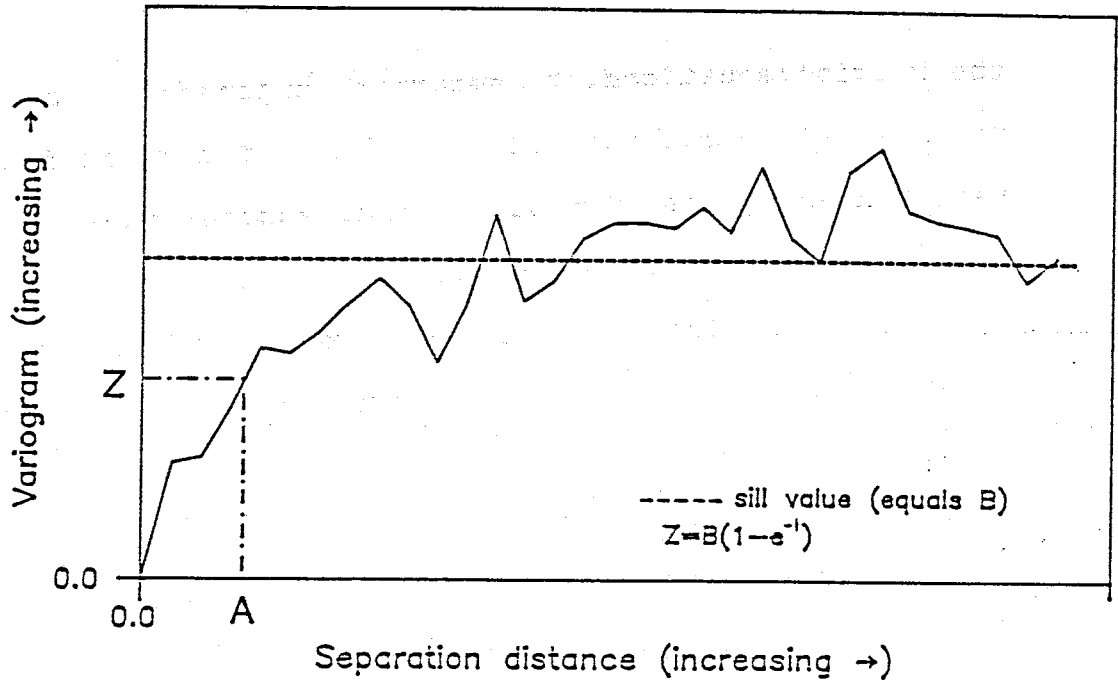


Figure 80. Example of fitting an exponential variogram.

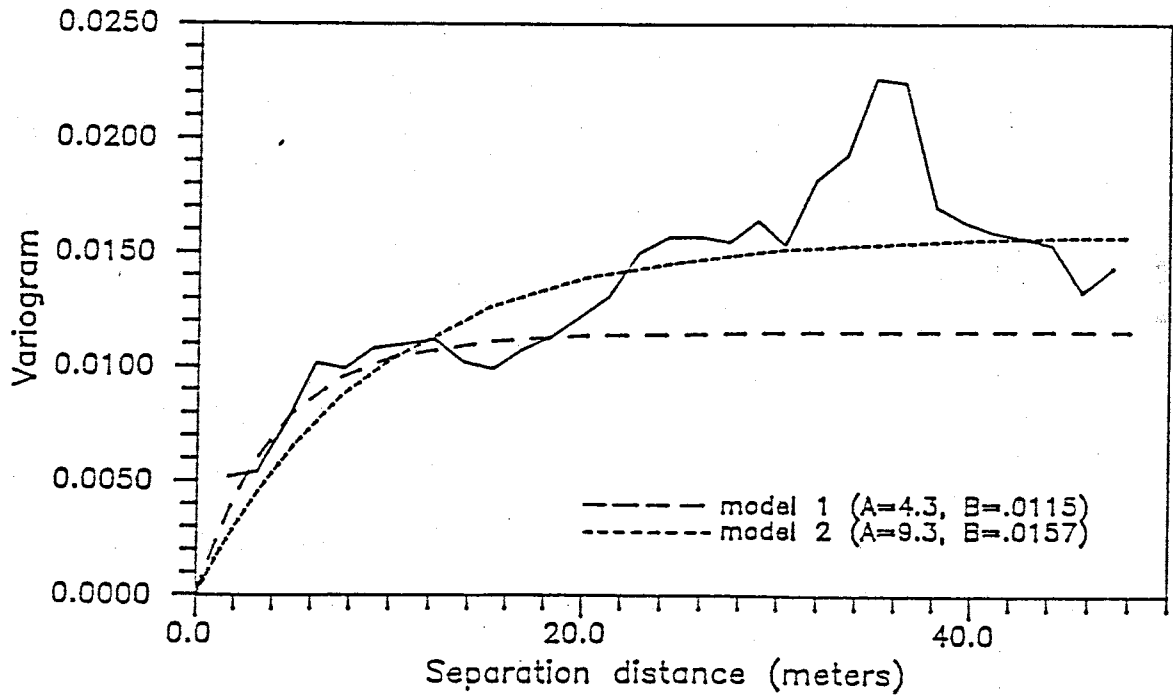


Figure 81. Variogram models for  $\theta_{1.5}$ .

the kriging equations, 2 separate exponential models were fit to the  $\theta_{1.5}$  variogram (figure 81). The first fit (model 1), represented by the bold solid line, assumes the sill value, B, to be equal to the variance 0.0115. With this assumption, the A value is calculated to be 4.3 m. However, the correlation appears to exist at  $\gamma(\xi)$  values greater than 0.0115. For model 2, the sill value is set equal to 0.0157. Hence, the A value becomes 9.3 m. Model 2 interprets the scale value of the  $\theta_{1.5}$  variogram to be over twice the length of model 1. Fitting variogram models by eye is a very subjective process and thus, neither model for the  $\theta_{1.5}$  distribution is necessarily correct.

It was noted in figure 78 that anisotropy exists between the horizontal and vertical variograms for  $\theta_{1.5}$ . However, the exponential models above were fit to the 2-D, homogeneous variograms (solid line). The homogeneous case was employed because the kriging program used in the next section is not able to account for anisotropic conditions.

### Kriging analysis

The next step is to apply the information gained in the variogram analysis to kriging equations. Given known data values in a random field, and information about the structure of this field (variogram), one should be able to describe values at non-observed locations with some certainty.

### Theory

In kriging, a prediction at a location  $\underline{x}_0$  can be made using the linear estimator

$$(28) \quad \hat{V}(\underline{x}_0) = \sum_{i=1}^n \lambda_i V(\underline{x}_i).$$



The  $\lambda_i$  values in this equation are weights. The values are solved for equation 28 such that the prediction  $V(\underline{x}_0)$  is unbiased

$$(29) \quad E[V(\underline{x}_0)] = E(\hat{V}),$$

and the mean squared error of the predicted minus actual value is minimum (Gutjahr, 1985)

$$(30) \quad \text{MSE} = E([\hat{V} - V(\underline{x}_0)]^2).$$

The kriging equations are derived from the MSE equation (30) above. These equations can be based upon either covariance functions (statistically homogeneous case) or variograms (intrinsic random function of order 0). From this, the following equations are developed (Gutjahr, 1985)

$$(31) \quad \sum_{j=1}^n \lambda_j \gamma(\underline{x}_i - \underline{x}_j) + u = \gamma(\underline{x}_0 - \underline{x}_i) \quad , \quad i=1, 2, \dots, n$$

$$(32) \quad \sum_{j=1}^n \lambda_j = 1$$

$$(33) \quad \sigma_k^2 = \sum_{j=1}^n \lambda_j \gamma(\underline{x}_j - \underline{x}_0) + u$$

$\lambda_i$  = kriging weights

$\gamma(\underline{x}_i - \underline{x}_j)$  = variogram function separated by a lag of  $(\underline{x}_i - \underline{x}_j)$

$u$  = Lagrange multiplier

$\sigma_k^2$  = kriging variance

$\underline{x}_0$  = prediction location.

These equations can be solved in matrix form from  $n+1$  equations in  $n+1$  unknowns. Thus, a set of weights are produced for every prediction location  $\underline{x}_0$ . These values are then used in the linear estimation equation (28) to determine the  $V(\underline{x}_0)$  value.

For a thorough derivation of kriging equations, refer to Delhomme (1978).

One property of kriging estimates is that  $V(\underline{x})$  is an exact interpolator. By this it is meant that  $\hat{V}(\underline{x}_0) = V(\underline{x}_0)$  at a known observation point. The kriging weights  $\lambda_i$  and  $u$  depend on the variogram and sample locations but not on the actual data values involved. Thus, the weights are dependent on the structure and not on the observation points. The mean value of the sample population ( $m$ ) is not needed to estimate  $V(\underline{x})$ . Knowing the population mean, however, will reduce the kriging variance. The kriging variance ( $\sigma_k^2$ ) gives a measure of the reliability of a prediction at a given location.  $\sigma_k^2$  depends only on  $\lambda$ ,  $u$ , and the variogram function (Gutjahr, 1985).

#### Analysis

Kriging analyses were performed on the  $\theta_{1.5}$  detrended data distribution using the variogram models previously discussed. The kriging equations were solved using the program KRIG written by Allan Gutjahr. The computer code is listed in appendix M. The 122 known  $\theta_{1.5}$  values were used in the program to predict an additional 508 points throughout the cross section. From the northern edge of the cross section, the first 4 prediction locations were spaced horizontally 1.25 meters apart. At a distance 3.75 m from the northern edge, the remaining prediction locations in the horizontal direction were equally spaced at 1.52 meters. In the vertical direction, the prediction locations were spaced 0.5 meters apart throughout the entire cross section. The reason for the difference in the spacing horizontally was due to

the difference in the original sample spacing from 0-3.75 m and 3.75-104.07 m.

Kriging analyses were performed using both of the variogram models from the previous section. Figures 82 and 83 are the 2-D contour plots of the  $\theta_{1.5}$  kriged distribution. It is evident from the 2 figures that no significant change in the  $\theta_{1.5}$  distribution is predicted depending on the variogram. Simple calculations were made to determine the net change in  $\theta_{1.5}$  values at the prediction locations. The difference equation is as follows

$$(34) \quad |Z(x_{1i}) - Z(x_{2i})| / n, \quad i = 1, 2, \dots, n$$

$Z(x_{1i})$  = kriged prediction at location  $i$  using  
variogram model 1 (A=4.3, B=0.0115)

$Z(x_{2i})$  = kriged prediction at location  $i$  using  
variogram model 2 (A=9.3, B=0.0157)

$n$  = number of kriged prediction locations.

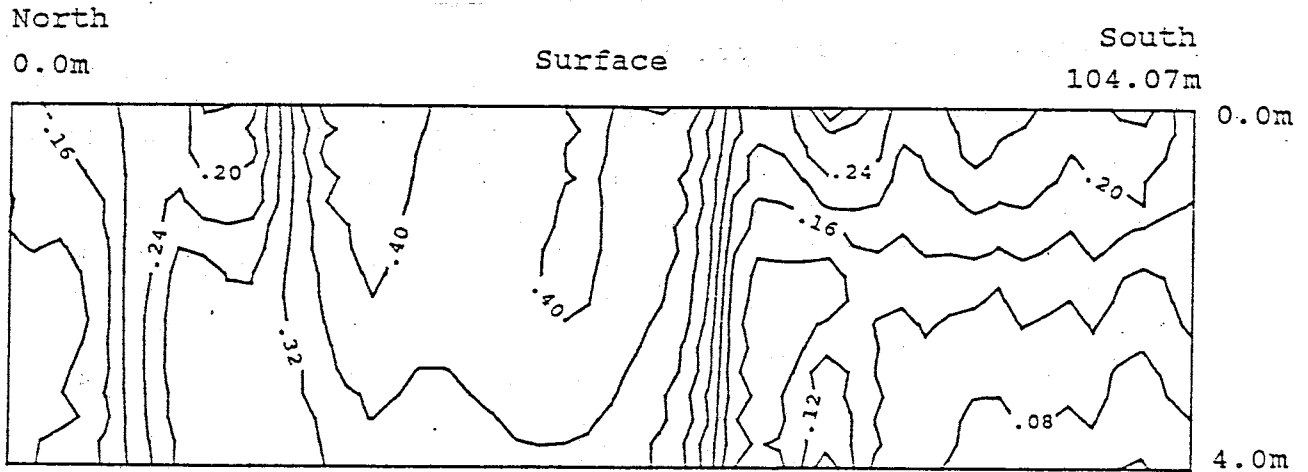
Using equation (34), the net change in  $\theta_{1.5}$  values was equal to 0.010 for the 508 kriged values. This relates to a 1% change in the volumetric moisture content.

The remaining detrended data distributions from the cross section ( $\log K, n, d_{10}$ ) all exhibited pure nugget effect variograms. Therefore, nothing would be gained using kriging equations on this data due to the lack of correlation between sample points.

#### Kriging variance

A kriging standard deviation value ( $\sigma_k$ ) was determined at each prediction location along with the estimated value. This is a measure of how precise the kriging estimate is at a given

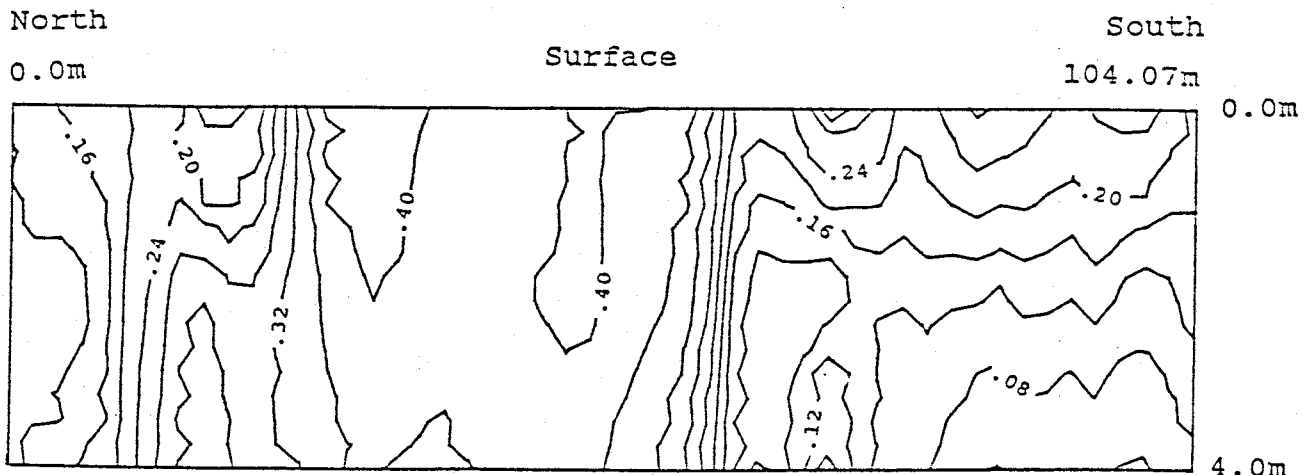
KRIGED DISTRIBUTION of  $\theta$  @ 1.5 bars



Vertical exaggeration: 8x

Figure 82. Contoured cross section of the  $\theta_{1.5}$  kriged distribution (variogram model 1).

KRIGED DISTRIBUTION of  $\theta$  @ 1.5 bars



Vertical exaggeration: 8x

Figure 83. Contoured cross section of the  $\theta_{1.5}$  kriged distribution (variogram model 2).

location. The kriging standard deviation is equal to 0 at a sample location and will increase as the distance between a prediction point and experimental value increases. Figures 84 and 85 are the 2-D contour plots of the kriging standard deviation distributions for the 2 kriged estimates of  $\theta_{1,3}$  (figures 82 and 83). Lower  $\sigma_k$  values are noted in figure 85 due to the longer correlation length (scale) interpreted for variogram model 2. Equation (34) was also used to calculate the average difference in kriging standard deviations for the two variogram models. The value determined is equal to 0.0117. The difference in  $\sigma_k$  between the 2 figures is especially evident near the bottom edge of the cross section. Here, the standard deviation decreases by as much as 0.0150.

#### Validation

Even after the variogram model has been fit and the kriging analysis employed, kriging tests must be performed to ensure the validity of the adopted structural parameters (Delhomme, 1978). Validation is a process that enables one to determine how accurately the kriged model fits the data. The validation process for this analysis was performed using the program VALID written by Allan Gutjahr (appendix N). In principal, it is a succession of kriging runs that delete a known value each time and use the remaining data to predict the value at the deleted location. This is done for each data point. The estimated versus the actual value are then compared along with the kriging standard deviation at each sample location. From this, a constant referred to as the normalized difference is determined

KRIGING STANDARD DEVIATION DISTRIBUTION for  $\theta$  @ 1.5 bars

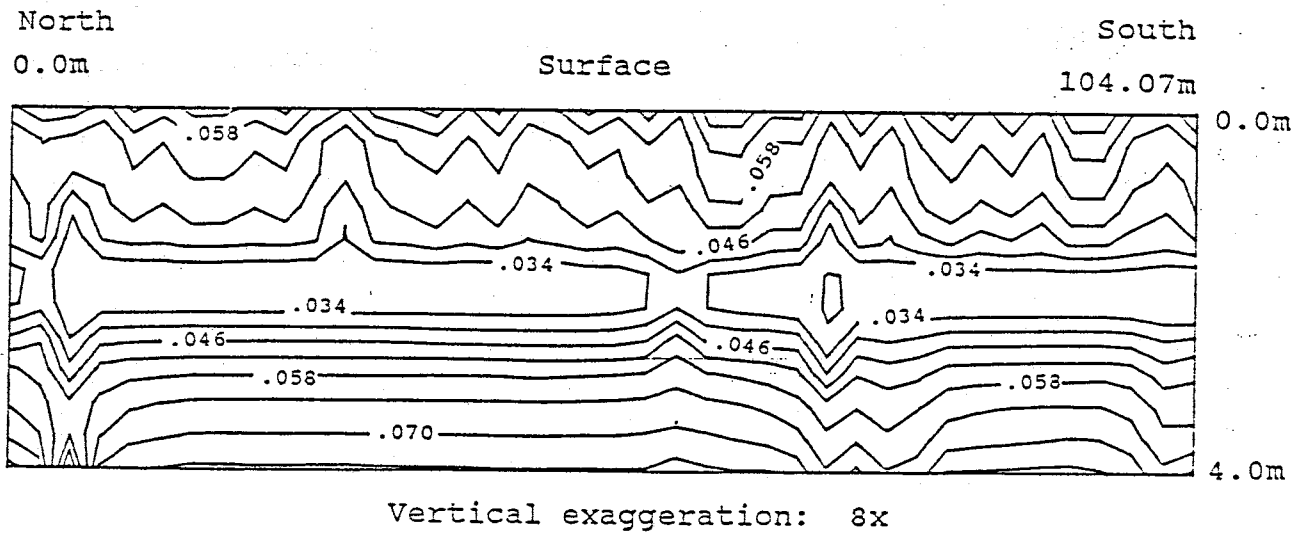


Figure 84. Contoured cross section of the kriging standard deviation distribution for  $\theta_{1.5}$  (variogram model 1).

KRIGING STANDARD DEVIATION DISTRIBUTION for  $\theta$  @ 1.5 bars

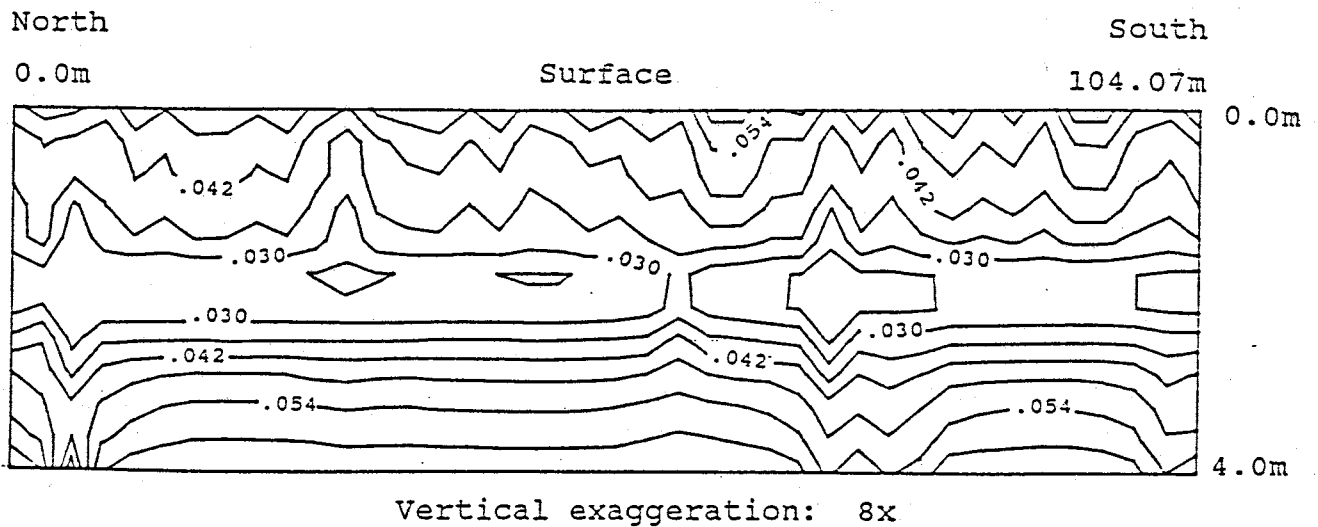


Figure 85. Contoured cross section of the kriging standard deviation distribution for  $\theta_{1.5}$  (variogram model 2).

by the following equation where  $i$  denotes the deleted point and  $V_0(\underline{x}_i)$  is the kriged value based on the other data.

$$(35) \quad N_i = [\hat{V}_0(\underline{x}_i) - V(\underline{x}_i)] / \sigma_{ki}$$

A mean value of the differences  $\sum[\hat{V}_0(\underline{x}_i) - V(\underline{x}_i)]$  and  $N_i^2$  are then summed over the entire population. Mean values near 0 and average squared normalized difference values ( $\sum(N_i^2)$ ) near 1 are ideal.  $\sum(N_i^2)$  values up to 2.5 are considered quite good.

Validation tests were performed on both of the kriged estimates of  $\theta_{1,5}$ . High normalized difference values resulted for both analyses.

	<u>Variogram model 1</u>	<u>Variogram model 2</u>
$\sum(N_i^2)$	3.2595	5.0384
Mean of difference	-0.0002	-0.0005

The high  $\sum(N_i^2)$  values would indicate that there are problems with the variogram and kriging models used. However, after observing the input data, it was discovered that 2 of the 122 points produced very high normalized difference values. The  $\theta_{1,5}$  values in question are located at the points A:(72.15,-2.05) and B:(72.20,-2.11) in cross section. At these locations, the  $\theta_{1,5}$  values are equal to 0.051 and 0.211 respectively. This is quite a large difference in  $\theta$  values over such a short distance and is no doubt due to layering in this area. Because points A and B are relatively close, deletion of point A during the validation process will result in the predicted value at point A to be near the actual value given at point B and vice versa. Thus, large differences between the actual and predicted values result at

both locations.

To determine the extent that points A and B exerted on N, the two points were deleted from the data. Validation was then performed on the reduced data set (120 pts). Output from the analysis is listed below.

	<u>Variogram model 1</u>	<u>Variogram model 2</u>
$\sum(N_i^2)$	2.3355	3.5713
Mean of difference	-0.0001	-0.0004

Deletion of only 2 of the data points results in a substantial reduction of  $\sum(N_i^2)$  for both cases. The  $\sum(N_i^2)$  values for the smaller data set appear quite reasonable. Thus, the variogram and kriging models employed appear to provide reasonable estimations of the  $\theta_{1.5}$  distribution.

It is noted for both data sets (120 & 122 pts) that the normalized difference values are less when variogram model 1 is employed. In the case of variogram model 2, the longer correlation length results in lower  $\sigma_k$  values but does not appear to significantly improve the accuracy of the kriged estimates. Therefore, according to the normalized difference equation (35), a decrease in the denominator with little or no change in the numerator will result in a higher normalized difference value.

### Conclusions

- Each of the data distributions were discovered to be anisotropic as noted by their variograms. Greater variability exists in the vertical direction for each parameter. This is especially true for the parameters  $d_{1.0}$  and  $\log K$ .
- Of the detrended data values, only  $\theta_{1.5}$  presents significant correlation. Thus,  $\theta_{1.5}$  is the only variable from the cross section where additional information can be gained using variogram and kriging analyses.




- The porosity data lacked any significant underlying structure that could be characterized. A portion of the variability noted in the porosity data might have been the result of measurement error due to the method used to determine porosity. Whether saturated conditions are obtained within a soil sample is always a matter of debate.
- $d_{10}$  is noted to exhibit slight correlation in the horizontal direction. A greater degree of correlation horizontally was envisioned prior to the variogram analysis. Variability of  $d_{10}$  in the 'transition zones' no doubt reduced the correlation horizontally. Extreme variability is noted vertically which is due to fine layering of coarse and fine grained tails.
- No additional information could be gained about the detrended conductivity distribution due to its lack of structure throughout the cross section.
- One possible reason for the lack of structure in the detrended log K data could be due to sample scale. One of the reasons why the log K regression analysis was so successful is that the K values were averaged over a larger scale than the other parameters. This resulted in a more gradual trend to the log K data. Once this trend was removed, no structure remained. The  $\theta$  and  $d$  measurements were more like point measurements and thus, could better describe areas of discontinuity.
- Using different exponential variogram models in the kriging equations had little effect on the kriged estimates of  $\theta_{1.5}$  (average change in  $\theta_{1.5} = 0.010$ ).
- A reduction in  $\sigma_k$  was noted for the variogram model with the longer correlation length (model 2). However, more favorable results were obtained using variogram model 1 during the validation process. In either case, the results obtained using either model were not substantially different.
- Attention must be paid to the original sample values and locations when using predictive models such as kriging in such a heterogeneous environment. This was especially evident in the kriging validation process where 2 values had quite a large effect on the final  $\sum(N_i^2)$  value.
- The kriging analysis experiences difficulties when describing the variability in finely layered areas. This was noted in the validation process. However, as long as a degree of correlation exists, kriging enables improved characterization of variability in comparison to the previously discussed methods.

V) SUMMARY

The following section contains the concluding remarks of this study. General conclusions were drawn not only on the validity of the statistical and geostatistical methods, but also on the effectiveness of the data generation techniques. For a thorough discussion of the conclusions drawn from each characterization analysis, refer back to the concluding remarks at the end of each analysis section.

General conclusions drawn from the mill tailings characterization study are listed below.

- Prior to sampling a field site, as much information as possible should be obtained about the methods of deposition. With information on the depositional history, the structure of the impoundment can be hypothesized. This process will allow for more effective positioning of sample sites.
- The use of galvanized shelby tubes obtained with the aid of a drilling rig was the most satisfactory method for sampling in such a corrosive, heterogeneous environment. A feasible, 'non-destructive' method for obtaining undisturbed samples in tailings slimes has yet to be developed.
- Problems were encountered when attempting to determine in situ  $\theta$  using the model 503 neutron probe from Campbell Pacific Nuclear. The metering device reports an averaged  $\theta$  value over a sphere approximately 30 cm in diameter. The thickness of the tailings layers are commonly on the order of 1 cm. The moisture meter does not operate accurately at field conditions of  $\theta \geq 0.35$ . In situ  $\theta$  values greater than 0.35 are common in the slimes. The presence of the elements Fe, Ti, Ca, and Cd in the tailings will adversely effect the attenuation of neutrons resulting in incorrect moisture readings. The magnitude of this effect as it relates to this study is not known.
- All of the laboratory procedures employed in this study worked well. One recommendation is to reverse the direction of flow in the shelby tube permeameter from vertically downward to vertically upward. This would assure that saturated conditions could be better obtained.

- Areas of layering or similar discontinuity in the tailings can be detected quite well by comparison of sample uniformity coefficients. High UC values were common in areas where layering between coarse and fine grained tails predominated.
- Describing the variability in the pore size distribution between samples using only a single pressure value ( $\theta/\psi$ ) can be best done between the pressure range 0.5 and 1.5 bars. The fluctuation in  $\theta$  values between fine and coarse grained tailings samples is the greatest within this pressure range.
- The use of a single set of data values ( $K$ ,  $n$ ,  $\theta/\psi$ ,  $d_{10}$ , etc.) to characterize the hydraulic properties of the entire cross section is not an advantageous method of characterization. The amount of variability in the hydraulic parameters at the Waldo site no doubt exceeded what was characterized by this study. However, this study shows that the use of a single, averaged set of data values is not representative. If it is only possible to collect a minor amount of data for a field site (financial or time constraints, etc.), data should be collected in the most permeable tails (sands near the emitters) and also in the least permeable tails (slimes). With this data, at least a best case/worst case analysis can be performed, which would allow for the range in seepage predictions to be established.
-  The tailings from the upper 50 cm were not representative of the impoundment as a whole. Secondary processes such as oxidation and partial cementation have occurred throughout this upper zone altering the tailings composition. This points out the necessity of obtaining data from a site both horizontally and vertically.
- The calculation of sample statistics was helpful as it provided information on the areas where the greatest variability in data occurs. The mean values of the various hydraulic properties calculated from the vertical borehole transects also provided general information on the change in data values horizontally through the cross section. Unfortunately, this type of analysis neglects to interpret any structure that may be present in the variability.
- Trends in the data which could not be described by the sample statistics were effectively characterized using regression analyses. This method worked well for each data distribution but especially for hydraulic conductivity. Characterizing the variability using regression analyses is somewhat similar to the model employed by Kealy (1971, figure 7). However, Kealy only described 3 zones of variability with each zone being homogeneous. The regression equations allow a data value to be calculated at any point in the cross section. The main disadvantage of this type of analysis is that it is unable to describe the location or magnitude of discontinuities in the

data. Even so, this method appears quite reasonable in the general sense and is definitely an improvement over using a single set of data values to describe the entire cross section.

- The geostatistical analyses employing both variogram and kriging equations is the most advantageous characterization method. It is not only an exact interpolator, but also places a measure of significance on the predictions. For this type of analysis to be effective, a degree of structure must remain in the detrended data distribution. This was only the case for the  $\theta_{1.5}$  data. The tailings pile is a very heterogeneous environment which for most hydraulic parameters lacks correlation structure. This method experienced difficulty when attempting to describe discontinuities in  $\theta_{1.5}$  on a fine scale, but this is not surprising in such a heterogeneous environment. The benefit of employing geostatistical analyses, however, is that, if structure exists, the variability can be characterized to a greater extent than was possible using the previous methods.

Characterizing the spatial variability in an extremely heterogeneous environment such as a tailings impoundment is a very time consuming process. If the final goal of a project is to incorporate the variability into a numerical model, realistic limits (financially, etc.) must be set on the degree of variability that should be incorporated. The amount of variability present in a field site is always going to be greater than the degree to which it can be characterized. Finer sample spacing for increased characterization is always a possibility. However, discretizing a numerical model grid into finer and finer elements to incorporate a greater amount of spatial variability can be a very costly proposition in the long run.

The degree of characterization done for this study appears to be quite adequate. The sampling spacing was fine enough to ensure that the 2-D regression equations produced were reliable. The sample spacing employed was also able to distin-

guish that the correlation length for each of the variables (except  $\theta_{1.5}$ ) was at least less than 1.52 m, if correlated at all. Using a correlation structure less than 1.52 m in a computer model grid over a cross section 104.07 x 4.00 meters would require an immense amount of computer time during seepage computations. Thus, decreasing the sample spacing to incorporate a greater degree of spatial variability would not have been practical.

Therefore, in the general sense of the overall study (this and Ken Harris' research), the most advantageous method for characterizing the variability in the tailings hydraulic properties was the use of regression analyses. Due to the lack of structure in each of the hydraulic parameters (except  $\theta_{1.5}$ ), the geostatistical analyses of variogram and kriging were unable to provide additional characterization information.

## VI) RECOMMENDATIONS FOR FUTURE WORK

This statistical and geostatistical analysis was performed in an attempt to characterize the spatial variability of hydraulic properties in mill tailings. One of the main purposes of this characterization process was to develop accurate estimates of the hydraulic properties throughout the cross section to supplement the known data. Once again, this study was performed concurrently with similar research by Ken Harris. Harris' research should shed light on the sensitivity of a seepage prediction to increased variability within the input variables (hydraulic property data). In addition, information should be gained on the degree of characterization necessary for accurate seepage predictions. For results of his study, the reader is referred to the Hydrology Independent Study by Ken Harris.

Pertinent analyses beyond the scope of this and Ken Harris' study could include:

- analyses similar to Harris' using a different numerical code. This would concentrate not only on the sensitivity of seepage predictions to the input data, but also on the sensitivity of the prediction to the model chosen. In addition, the sensitivity of the model chosen could be tested by performing conditional simulations with the input data.
- separation of the cross section into zones (sand, transition, and slime) prior to characterization using the geostatistical methods employed in this analysis. It is possible that improved characterization within an individual zone will occur due to a decrease in variability within that zone in comparison to the entire cross section.
- addressing the presence of anisotropy in hydraulic conductivity. It is possible that anisotropy is partially dependent on a sample's location in cross section.

### Predictive Equations

Due to the heterogeneous nature of the Waldo impoundment, a great deal of data was needed for accurate characterization of the tailings hydraulic properties. Generating accurate values for parameters such as hydraulic conductivity and  $\theta/\psi$  relationships was a very time consuming process. Both hydraulic conductivity and  $\theta/\psi$  relationships are necessary input variables for numerical models that predict seepage. It would be beneficial if accurate predictions of  $K(\text{sat})$  and other variables could be made using other more easily measured sample parameters such as particle size.

As an introductory step to such an analysis, correlation coefficients were determined between each data distribution (table 8). The best correlation for each dependent variable as it relates to both particle size and pore distribution is represented by the underlined value. In all cases but one, the best correlation with each dependent variable is noted for  $\theta_{1.5}$  and  $d_{3.4}$ . The most significant correlation is present between the intermediate pore size distribution  $\theta_{1.5}$  and particle size. Marginal results are noted between  $\log K$  and the other parameters.

Next, multiple regression analyses were employed on the data distributions. The best predictive equation for each data distribution was formulated using partial F-tests to determine the significant independent variables (table 9). Three equations were developed for each distribution excluding porosity. For each distribution, the first equation relates solely to

TABLE 8

Correlation coefficients between the various data distributions\*

$$\rho = \text{Cov}(X_{\text{indep}}, X_{\text{dep}}) / (\sigma_{\text{indep}} \sigma_{\text{dep}}) \quad (\text{Scheaffer and Mendenhall, 1975})$$

Variables		# of correlating points	Correlation coefficient ( $\rho$ )
Dependent	Independent		
log K	n	60	-0.338
"	$\theta_{1.5}$	"	-0.664
"	$\theta_{15}$	"	-0.580
"	$d_{10}$	55	0.610
"	$d_{16}$	"	0.556
"	$d_{30}$	"	0.586
"	$d_{50}$	"	0.549
"	$d_{60}$	"	0.532
"	$d_{84}$	"	0.653
"	GM	"	0.642
"	UC	"	-0.262
"	CC	"	0.347
"	SORT	"	-0.356
"	SKEW	"	0.453
n	$\theta_{1.5}$	68	0.604
"	$\theta_{15}$	67	0.595
"	$d_{10}$	61	-0.414
"	$d_{16}$	"	-0.443
"	$d_{30}$	"	-0.513
"	$d_{50}$	"	-0.547
"	$d_{60}$	"	-0.538
"	$d_{84}$	"	-0.530
"	GM	"	-0.486
"	UC	"	-0.035
"	CC	"	-0.400
"	SORT	"	0.093
"	SKEW	"	-0.006
$\theta_{1.5}$	$\theta_{15}$	67	0.855
"	$d_{10}$	61	-0.650
"	$d_{16}$	"	-0.730
"	$d_{30}$	"	-0.789
"	$d_{50}$	"	-0.813
"	$d_{60}$	"	-0.826
"	$d_{84}$	"	-0.858
"	GM	"	-0.814
"	UC	"	0.128
"	CC	"	-0.511
"	SORT	"	0.319
"	SKEW	"	-0.258



$\theta_{15}$	$d_{10}$	61	-0.557
"	$d_{16}$	"	-0.648
"	$d_{30}$	"	-0.730
"	$d_{50}$	"	-0.751
"	$d_{60}$	"	-0.761
"	$d_{84}$	"	-0.774
"	GM	"	-0.730
"	UC	"	0.078
"	CC	"	-0.505
"	SORT	"	0.264
"	SKEW	"	-0.154

\* all data derived from 205cm depth

particle size, the second was derived using moisture content data, and the third by employing a combination of both. Results from the regression analyses for prediction of log K (equation 38),  $\theta_{15}$  (equation 42), and  $\theta_{15}$  (equation 45) are positive.

This was the extent of research done on the predictive equation for this analysis. The goal of this section was to determine if predictive equations could be developed for such a heterogeneous environment. Results appear favorable for the prediction of both K and  $\theta$  values. Future work related to the analysis discussed above could involve:

- comparison of the equations (36-45) to the work done by Bates and Wayment (1967). Determine if the predictive equation for K developed by Bates and Wayment is applicable to the Waldo impoundment. Also, determine if the predictive equations developed from the Waldo tailings can be used on similar tailings sites.
- analysis to determine if entire soil moisture characteristics ( $\theta/\psi$  curves) can be predicted accurately by solely using tailings grain-size data.
- employing regression and kriging analyses on the predicted data distributions to determine the magnitude of change in comparison to the original data set. Also, the differences in seepage predictions depending on the data set used (actual vs. predicted) could be determined with the use of a conducive numerical model. A study similar to this would once again check the sensitivity of a seepage prediction as it relates to the input data.

TABLE 9

Final predictive equations using multiple regression\*

<u>To Predict log K</u>	<u>multiple correlation coefficient</u>
(36) $\log K = -6.113 - (0.0318*d_{50}) + (0.0273*d_{34})$	0.758
(37) $\log K = -3.914 - (4.708*\theta_{1.5})$	0.668
(38) $\log K = -4.668 - (0.0298*d_{50}) + (0.0204*d_{34}) - (3.600*\theta_{1.5})$	0.798
<u>To Predict Porosity</u>	
(39) $n = 0.539 - (0.000223*d_{10}) - (0.00205*d_{30}) + (0.000772*GM)$	0.519
<u>To Predict <math>\theta_{1.5}</math></u>	
(40) $\theta_{1.5} = 0.393 - (0.00151*d_{34})$	0.858
(41) $\theta_{1.5} = -0.460 + (1.336*n)$	0.609
(42) $\theta_{1.5} = -0.00542 + (0.719*n) - (0.00124*d_{34})$	0.894
<u>To Predict <math>\theta_{15}</math></u>	
(43) $\theta_{15} = 0.208 - (0.000805*d_{34})$	0.774
(44) $\theta_{15} = 0.00490 + (0.522*\theta_{1.5})$	0.855
(45) $\theta_{15} = 0.0405 + (0.427*\theta_{1.5}) - (0.000159*d_{34})$	0.859

\* all data derived from 205cm depth

All of the equations listed above reject the hypothesis:  
 $\beta_1 = \beta_2 = \dots = \beta_n = 0$ ,  $F(1\%)$ ,  $n =$  number of independent variables

REFERENCES

- Austin, C.F. 1960. Some Scheelite Occurrences in the Magdalena Mining District of New Mexico. New Mexico State Bureau of Mines and Mineral Resources. Circular 55, p. 5.
- Bartlett, C.L. 1983. Unsaturated seepage and evaporation from a deposited mine tailings profile. Univ. of Arizona Thesis.
- Bates, R.C. and W.R. Wayment. 1967. Laboratory study of factors influencing waterflow in mine backfill. U.S. Dept. of Interior, Bureau of Mines. report no. 7034. 45 pp.
- Blake, G.R. 1965. Bulk density. Methods of Soil Analysis, Part 1. ed. C. A. Black. American Society of Agronomy, Inc. pp. 374-390.
- Bouma, J. and others. 1974. Measurement of water movement in soil pedons above the water table. Univ. of Wisc. Ext. Geol. and Nat. Hist. Survey. Inf. Circ. no. 27.
- Byer, E., and D.B. Stephens. 1983. Statistical and stochastic analysis of hydraulic conductivity and particle size in a fluvial sand. Soil Sci. Soc. Am. J., vol. 47, pp. 1072-1081.
- Chatterjee, Samprit and Bertram Price. 1977. Regression Analysis by Example. John Wiley & Sons, Inc. 228 pp.
- Compton, R.R. 1962. Manual of Field Geology. John Wiley & Sons, Inc. 378 pp.
- Dabney, T.E. 1946. Kelly-and our lady of Magdalena. New Mexico Bureau of Mines and Mineral Resources. December 1946, pp. 31-32.
- Davis, L.A. and S.P. Neuman. 1983. Documentation and User's Guide: UNSAT2 - Variably Saturated Flow Model. U.S. Nuclear Regulatory Commission, NUREG/CR-3390.
- Day, P.R. 1965. Particle fractionation and particle size analysis. Methods of Soil Analysis, Part 1. ed. C. A. Black. American Society of Agronomy, Inc. pp. 545-567.
- Delhomme, J.P. 1978. Kriging in the hydrosciences. Advances in Water Resources. vol. 1, no. 5, pp. 251-266.
- Draper, N.R., and H. Smith. 1966. Applied Regression Analysis. John Wiley & Sons, Inc. 407 pp.
- Fetter, C.W. Jr. 1980. Applied Hydrogeology. C.E. Merrill Publishing Co. 488 pp.

- Freeze, R.A. and J.A. Cherry. 1979. Groundwater. Prentice-Hall, Inc. 604 pp.
- Gajem, Y.M., A.W. Warrick, and D.E. Myers. 1981. Spatial dependence of physical properties of a Typic Torrifluvent soil. Soil Sci. Soc. Am. J., vol. 45, pp. 709-715.
- Gutjahr, A.L. 1985. Spatial variability: geostatistical methods. Soil Spatial Variability (proceedings of a workshop of the ISSS and the SSSA, Las Vegas, USA, 11/30/84 - 12/1/84). Pudoc Wageningen publishers. pp. 9-34.
- Gray, Steve. 1985. Personal conversation 3/85. Driller, Fox Consulting, Denver, Colorado.
- Highter, W.H. and R.P. Vallee. 1980. The liquefaction of different mine tailings under stress controlled loading. Engineering Geology. vol. 16, pp. 147-150.
- Hillel, Daniel. 1980. Fundamentals of Soil Physics. Academic Press. 413 pp.
- Isaacs, L.T. and Bruce Hunt. 1981. Seepage from free water above impermeable tailings. ASCE. vol. 107, no. GT11. pp. 1563-1577.
- Kealy, C.D. 1970. Seepage patterns in mill-tailings dams as determined by finite-element models. Univ. of Idaho Masters Thesis, 89 pp.
- ✓ Kealy, C.D. and Richard Busch. 1979. Evaluation of mine tailings disposal. ASCE, Current Geotechnical Practice in Mine Waste Disposal. pp. 181-201.
- ✓ Lusk, Don. 1947. The Magdalena unit of the American Smelting & Refining Company. New Mexico Miner and Prospector. August 1947, vol. 9, no. 50, pp. 1-5.
- ✓ Lusk, Don. 1948. Magdalena number. New Mexico Miner & Prospector. August 1948, vol. 10, no. 8, pp. 1-11.
- McWhorter, D.B. and J.D. Nelson. 1980. Seepage in the partially saturated zone beneath tailing impoundments. Mining Engineering. April 1980, pp. 432-439.
- Martin, A.J., and F.J. Kelly. 1953. Minerals Yearbook Area Reports, Volume III, U.S. Dept. of the Interior, Bureau of Mines. pp. 689-714.
- Minerals Yearbook. 1917. U.S. Dept. of the Interior, Bureau of Mines.
- Minerals Yearbook. 1942. C. E. Needham, editor. U.S. Dept. of the Interior, Bureau of Mines. 1574 pp.

- Minerals Yearbook. 1944. C. E. Needham, editor. U.S. Dept. of the Interior, Bureau of Mines. 1636 pp.
- Minerals Yearbook. 1949. A. F. Matthews, editor. U.S. Dept. of the Interior, Bureau of Mines. 1662 pp.
- Mittal, H.K. and N.R. Morgenstern. 1976. Seepage control in tailings dams. Canadian Geotech. J., vol. 13, pp. 277-293.
- Morgan, Clarence. 1986. Personal conversation 10/22/86. Range Conservationist, U.S. Forest Service, Magdalena District, New Mexico.
- New Mexico Water Quality Standards. 1981. State Water Laws, S-607, 856:1001-1011.
- Russo, David and Eshel Bresler. 1981. Soil hydraulic properties as stochastic processes: I. An analysis of field spatial variability. Soil Sci. Soc. Am. J., vol. 45, pp. 682-687.
- Saddiq, M.H., P.J. Wierenga, J.M.H. Hendrickx, and M.Y. Hussain. 1985. Spatial variability of soil water tension in an irrigated soil. Soil Science. vol. 140, no. 2, pp. 126-132.
- Scheaffer, R.L. and W. Mendenhall. 1975. Introduction to Probability: Theory and Applications. Duxbury Press, North Scituate, Massachusetts. 289 pp.
- Soderberg, R.L. and R.A. Busch. 1975. Design guide for metal and nonmetal tailings disposal. U.S. Dept. of Interior, Bureau of Mines. Information Circular 8755, 29 pp.
- van Genuchten, Rien. 1978. Calculating the unsaturated hydraulic conductivity with a new closed-form analytical model. Research Report No. 78-WR-08. Water Resources Program, Princeton University. 65 pp.
- Wierenga, P.J. 1984. Spatial variability of soil-water properties in irrigated soils. Soil Spatial Variability (proceedings of a workshop of the ISSS and the SSSA, Las Vegas, USA, 11/30/84). pp 112-129.
- Yeh, T.C. Jim, L.W. Gelhar, and P.J. Wierenga. 1986. Observation of spatial variability of soil-water pressure in a field soil. Soil Science, vol. 142, no. 1, pp. 7-12.

APPENDIX

LIST OF APPENDICES

- A. Laboratory procedure: shelby tube permeameter .... A-1
- B. Computer code for program MANOMET ..... A-6
- C. Laboratory procedure: sample extrusion ..... A-8
- D. Vertical transect sample core photographs ..... A-10
- E. Laboratory procedure:  $\theta/\psi$  relationships ..... A-12
- F. Laboratory procedure: particle size analysis ..... A-15
- G. Computer code for program GRAIN ..... A-16
- H. Computer code for program GS ..... A-19
- I. Data values described in this study in tabular form A-21
- J. Sample statistics from layer 1 and underlying soil . A-63
- K. Computer code for program VGRAM ..... A-65
- L. Variograms of detrended log K values ..... A-71
- M. Computer code for program KRIG ..... A-72
- N. Computer code for program VALID ..... A-80

APPENDIX ALaboratory procedure: shelby tube permeameter

The shelby tube permeameter uses Darcy's law  $[Q=K(dh/dl)A]$  to determine saturated hydraulic conductivity (figure A1). The apparatus that was used enables 12 shelby tubes to be tested simultaneously.

Three manometer tubes were installed into each shelby tube sample. The distance separating these manometers equaled 13.3 cm. These tubes, along with the constant head source, enabled 4 distinct conductivity readings to be made along each sample. The manometers remained closed (using a Hoffman tubing clamp) during carbon dioxide flooding and initial wet-up.

Prior to wetting, 20 pore volumes of carbon dioxide ( $CO_2$ ) were forced through each sample.  $CO_2$  is readily soluble in water and thus, reduces the occurrence of entrapped air during wetting. The field moisture contents in many of the fine-grained 'slimes' were close to saturation. Thus, the air phase in such a sample was discontinuous and  $CO_2$  flooding was of no use.

Next, the samples were allowed to wet up slowly using distilled water. Distilled water was chosen because its chemical composition is similar to the rainwater that falls on the impoundment. The constant head source was then raised until all the shelby tubes exhibited recordable outflow (at least 1 ml/hour). At this time, the manometers were opened, allowing them to interact with the sample.

Permeability readings were then taken daily for up to 9



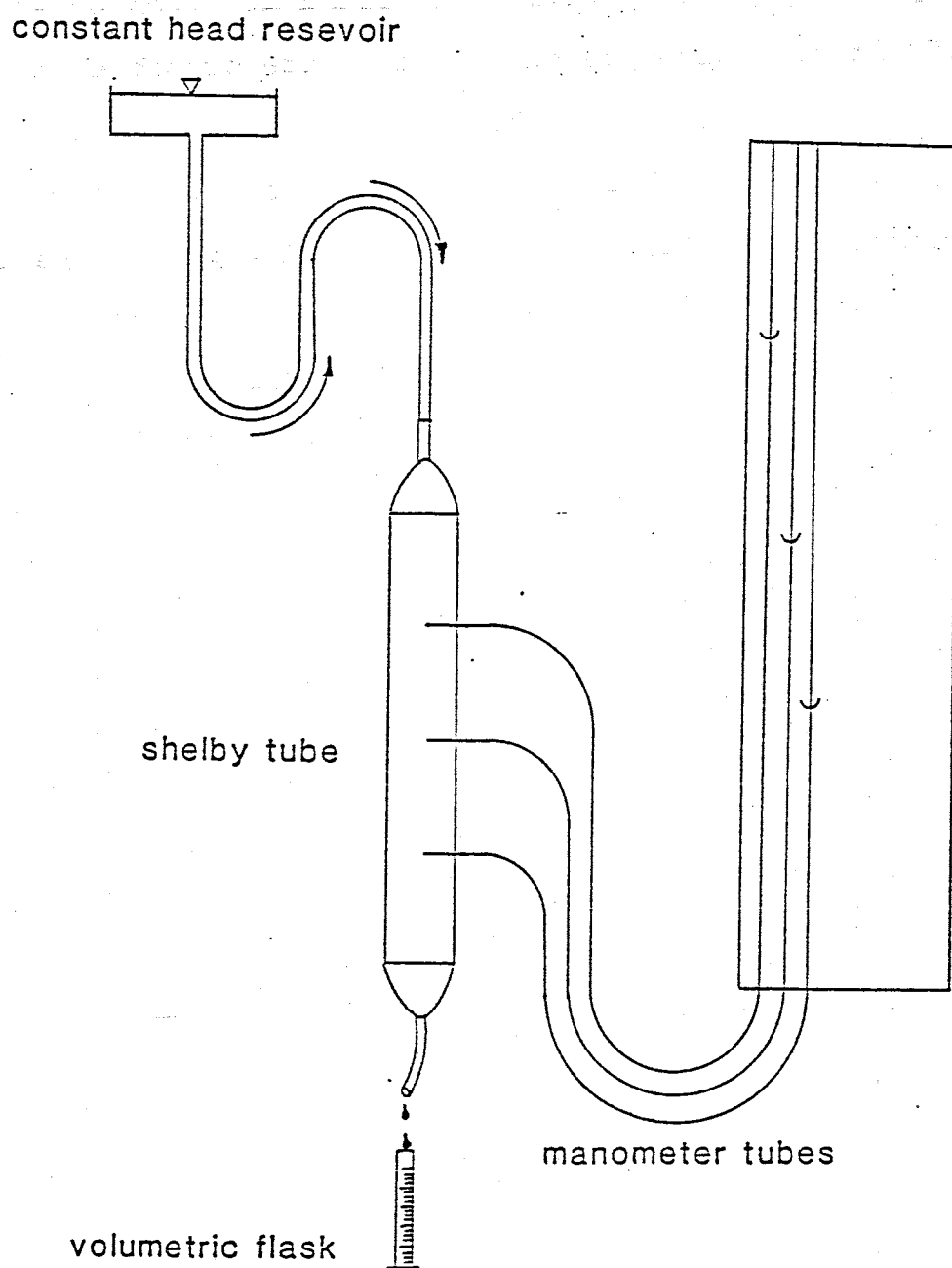


Figure A1. Diagram of the shelby tube permeameter.

days. All the samples were found to reach an equilibrium value within this time period. It is quite probable that conductivity measurements for a particular location will fluctuate over time (figure A2). Fluctuations in K can be caused by bacterial growth, dissolution of entrapped air, piping, sealing of cracks, and redistribution of fines, to name a few. To be consistent, the last recorded conductivity measurement at each location is considered the representative K for that particular area.

The conductivity values were calculated using the BASIC program MANOMET (appendix B). Table A1 is an example of the program's output. All conductivity values were calibrated to 20°C.

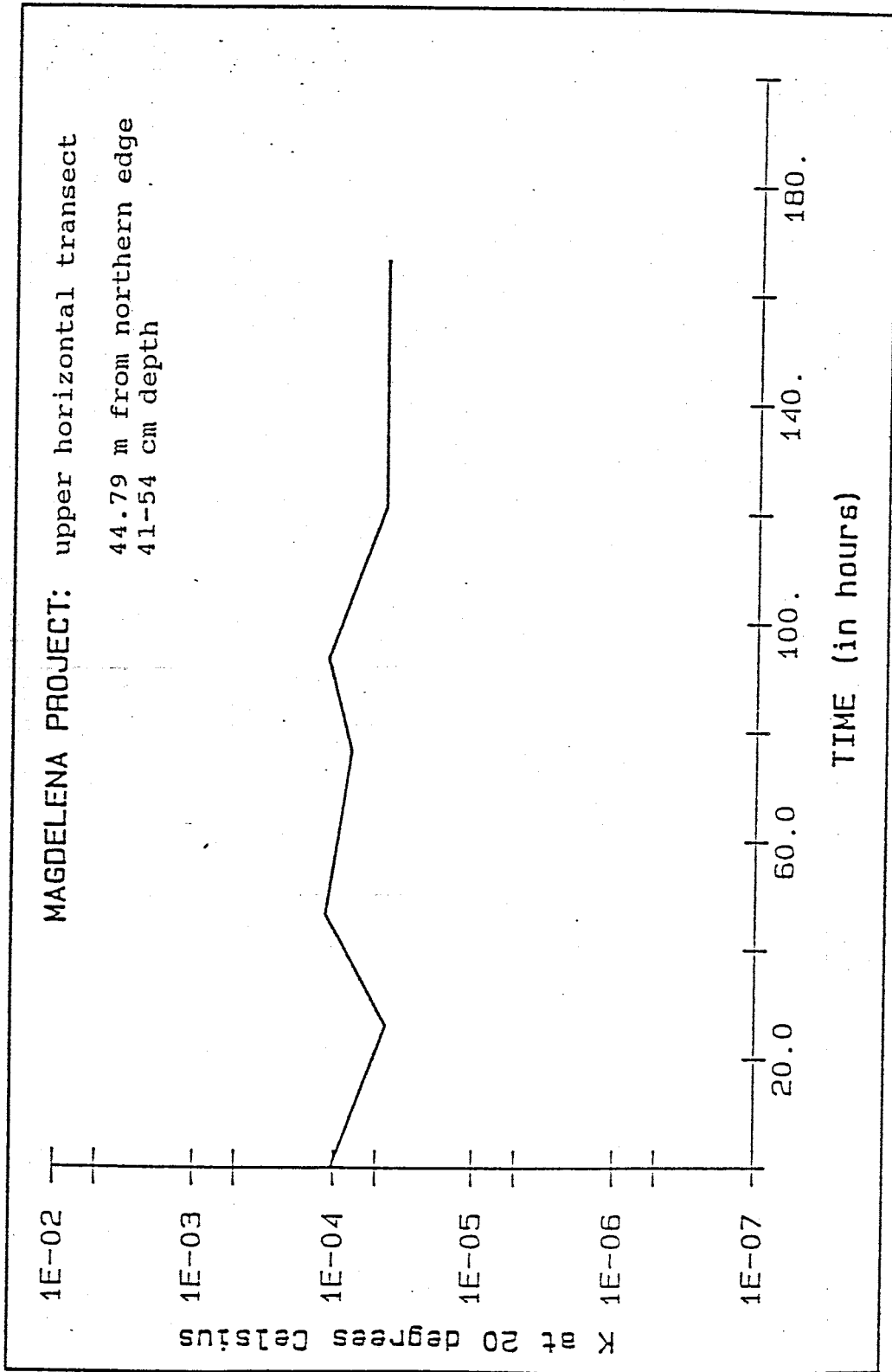


Figure A2. Fluctuation in K for a given sample over time.

Table A1

SHELBY TUBE PERMEAMETER

PAGE NO. 1  
TUBE NO. 4

TRANSECT BEARING: N 6 W      POSITION: 90.52 m from northern edge  
SAMPLE DEPTH (cm): 7.8      TUBE DEPTH (cm): 152

\*\*\*\*\*  
UNITS: Q=cc/sec    q=cm/sec    HEAD=cm    DH=cm    DL=cm    vol=cc    K=cm/sec  
\*\*\*\*\*

DATE	TIME	TEMP	MANOMETER	HEAD	DH	DL	FLOW DATA	K at 20C
9/2	2130	22	resevoir	207.5			secs= 780	
			165 cm	188.7	18.8	13.2	vol= 5.60	1.053E-04
			DEPTH BELOW SURFACE( 179 cm	143.5	45.2	13.3	Q= 7.18E-03	4.424E-05
			192 cm	88.4	55.1	13.3	q= 1.57E-04	3.630E-05
9/3	2130	21	resevoir	207.5			secs= 600	
			165 cm	194.0	13.5	13.2	vol= 4.20	1.465E-04
			DEPTH BELOW SURFACE( 179 cm	151.7	42.3	13.3	Q= 7.00E-03	4.721E-05
			192 cm	100.4	51.3	13.3	q= 1.54E-04	3.893E-05
9/4	1400	22	resevoir	207.5			secs= 540	
			165 cm	188.3	19.2	13.2	vol= 3.60	9.578E-05
			DEPTH BELOW SURFACE( 179 cm	135.7	52.6	13.3	Q= 6.67E-03	3.530E-05
			192 cm	85.8	49.9	13.3	q= 1.46E-04	3.721E-05
9/5	1700	21	resevoir	207.5			secs= 600	
			165 cm	191.3	16.2	13.2	vol= 4.20	1.221E-04
			DEPTH BELOW SURFACE( 179 cm	146.6	44.7	13.3	Q= 7.00E-03	4.468E-05
			192 cm	96.0	50.6	13.3	q= 1.54E-04	3.947E-05
9/6	1620	20	resevoir	207.5			secs= 660	
			165 cm	197.5	10.0	13.2	vol= 6.00	2.632E-04
			DEPTH BELOW SURFACE( 179 cm	150.0	47.5	13.3	Q= 9.09E-03	5.595E-05
			192 cm	92.0	58.0	13.3	q= 1.99E-04	4.582E-05
9/7	1400	21	resevoir	207.5			secs= 600	
			165 cm	196.8	10.7	13.2	vol= 5.50	2.420E-04
			DEPTH BELOW SURFACE( 179 cm	157.8	39.0	13.3	Q= 9.17E-03	6.706E-05
			192 cm	101.5	56.3	13.3	q= 2.01E-04	4.645E-05

## APPENDIX B

Computer code for program: MANOMET

```

10 CLS
20 DIM KA(100),R1(100),R2(100),R3(100),DH1(100),DH2(100),DH3(100),Q(100),LQ(100),
TP(100),TIS(100),T(100),H(100),V(100),K1(100),DS(100),DY(100),TH(100),HD(100),K
2(100),K3(100),C(35)
25 FOR W=5 TO 30:READ C(W):NEXT W
27 DATA 1.519,1.472,1.428,1.386,1.346,1.307,1.271,1.235,1.202,1.16667,1.13673,1.
10679,1.07884,1.05090,1.02495,1.97595,.95289,.93064,.90928,.88862,.86876,.84960
,.83104,.81317,.79591
30 KEY OFF
40 INPUT"ENTER TRANSECT NUMBER";TNS
45 INPUT"ENTER TUBE NUMBER";TBS
50 INPUT"ENTER DEPTH OF SAMPLE FROM TOP OF SHELBY TUBE";D
55 PN=1
60 INPUT"ENTER DISTANCE FROM EDGE OF PILE (10N' FOR 10 METERS FROM NORTH EDGE)";D
$
62 INPUT"ENTER BEARING";BRS
65 INPUT"ENTER TUBE DEPTH";TD
67 D3=61-D+TD-13.33:DL3=13.33
69 D2=D3-13.34:DL2=13.33
71 D1=D2-13.33:DL1=21-D
73 SS=RIGHT$(DS,1):JS=LEFT$(DS,LEN(DS)-1)
75 IF SS="N" THEN P$=JS+" FROM NORTH EDGE"
77 IF SS="W" THEN P$=JS+" FROM WEST EDGE"
100 N=N+1
110 PRINT
120 INPUT"ENTER DATE OF SAMPLE OR -999 TO STOP";DS(N)
125 IF DS(N)="-999" THEN N=N-1:GOTO 500
130 INPUT"ENTER TIME OF SAMPLE (MILITARY ie. 13:00 FOR 1 pm)";TIS(N)
140 INPUT"ENTER TEMPERATURE";TP(N)
150 INPUT"ENTER RESEVOIR HEAD READING";HD(N)
160 INPUT"ENTER MANOMETER 1 READING";R1(N)
170 INPUT"ENTER MANOMETER 2 READING";R2(N)
180 INPUT"ENTER MANOMETER 3 READING";R3(N)
190 PRINT
200 PRINT"*****ENTER FLOW DATA*****"
210 PRINT
220 INPUT"ENTER TIME (MIN.SEC)";TM
230 TI=INT(TM):TT=TM-TI:SC=TT*100
240 T(N)=SC+TI*60
250 INPUT"ENTER VOLUME IN CUBIC CENTIMETERS";V(N)
260 IF MID$(DS(N),2,1)="/" THEN DY(N)=VAL(MID$(DS(N),3,LEN(DS(N)))) ELSE DY(N)=V
AL(MID$(DS(N),4,LEN(DS(N))))
265 IF DY(N)<DY(N-1) THEN DY(N)=DY(N-1)+DY(N)
270 H(N)=VAL(TIS(N))
280 M=VAL(RIGHT$(TIS(N),2))
290 H=M/60
300 H(N)=H(N)+H
310 TH(N)=(DY(N)-DY(1))*24-H(1)+H(N)
320 Q(N)=V(N)/T(N)
330 LQ(N)=Q(N)/45.6
340 DH1(N)=HD(N)-R1(N)
350 DH2(N)=R1(N)-R2(N)
360 DH3(N)=R2(N)-R3(N)
370 K1(N)=LQ(N)*DL1/DH1(N)*C(TP(N))
380 K2(N)=LQ(N)*DL2/DH2(N)*C(TP(N))
390 K3(N)=LQ(N)*DL3/DH3(N)*C(TP(N))
400 GOTO 100
500 D1$=STR$(INT(D1)):D2$=STR$(INT(D2)):D3$=STR$(INT(D3))
540 F$="TR"+TNS+"T"+TBS+"TAB"
550 OPEN F$ FOR OUTPUT AS #1

```

```

555 FOR G=1 TO 5:PRINT #1,"":NEXT G
560 PRINT #1,"
NO. ";PN
570 PRINT #1,"
NO. ";TBS
575 PRINT #1,""
577 PRINT #1,"TRANSECT BEARING: ";BRS;"          POSITION: ";PS
580 PRINT #1,"SAMPLE DEPTH (cm):";D;"          TUBE DEPTH (cm):";TD
585 PRINT #1,""
590 PRINT #1,"*****"
592 PRINT #1,"UNITS: Q=cc/sec   q=cm/sec   HEAD=cm   DH=cm   DL=cm   vol=cc   K=
cm/sec"
594 PRINT #1,"*****"
596 PRINT #1,""
600 AS="DATE   TIME   TEMP   MANOMETER   HEAD   DH   DL   FLOW DATA   K at
20C"
610 BS="\   \   \   \   ##   Reservoir   ###.#
620 CS="          ###.##   ###.##   ###.##   secs=####"
^^^          vol=###.##   ##.###^
630 DS=" DEPTH BELOW SURFACE(   ##.##   ###.##   ###.##   Q=##.##^
^^^          ^
640 ES="          ##.##   ###.##   ###.##   q=##.##^
^^^          ^
650 FS="-----   -----   -----   -----   -----   -----
-----"
660 X=X+1
664 IF INT(X/7)=X/7 AND PN=1 THEN X=X-1:PN=PN+1:PRINT #1,CHR$(12):GOTO 555
670 PRINT #1,AS
680 PRINT #1,FS
690 PRINT #1,USING BS;DS(X);T1$(X);TP(X);HD(X);T(X)
700 PRINT #1,USING CS;D1;R1(X);DH1(X);DL1;V(X);K1(X)
710 PRINT #1,USING DS;D2;R2(X);DH2(X);DL2;Q(X);K2(X)
720 PRINT #1,USING ES;D3;R3(X);DH3(X);DL3;LQ(X);K3(X)
730 PRINT #1,""
735 IF X=N THEN GOTO 990
740 GOTO 660
990 CLOSE
992 F3$=TN$+"T"+TBS+"D"+RIGHT$(D3$,LEN(D3$)-1)+".DAT"
994 F2$=TN$+"T"+TBS+"D"+RIGHT$(D2$,LEN(D2$)-1)+".DAT"
996 F1$=TN$+"T"+TBS+"D"+RIGHT$(D1$,LEN(D1$)-1)+".DAT"
1000 OPEN F2$ FOR OUTPUT AS #2
1010 OPEN F1$ FOR OUTPUT AS #1
1020 OPEN F3$ FOR OUTPUT AS #3
1030 FOR X=1 TO N
1040 WRITE #1,K1(X)
1050 WRITE #2,K2(X)
1060 WRITE #3,K3(X)
1070 NEXT X
1080 CLOSE
1090 F4$="TR"+TN$+"T"+TBS+"H"+".DAT"
1100 OPEN F4$ FOR OUTPUT AS #1
1110 FOR X=1 TO N
1120 WRITE #1,TH(X)
1130 NEXT X
1140 CLOSE
1150 END
555 FOR G=1 TO 5:PRINT #1,"":NEXT G
10 CLS

```

APPENDIX CLaboratory procedure: sample extrusion

The samples were extruded from the shelby tubes using the Vertiject device from Soiltest Inc. (figure C1). This device works on the same principle as a hydraulic jack. A piston, operated by a foot pedal, is slowly forced from the bottom of the shelby tube upward. Extruding the samples in this method enabled intact sample cores to be preserved (sample photos, appendix D).

This device only worked successfully when extruding samples that were near saturation. The Vertiject was not able to extrude samples which had been allowed to air dry. The friction between the dry sample and the tube wall was greater than the maximum hydraulic force that could be supplied by the piston.

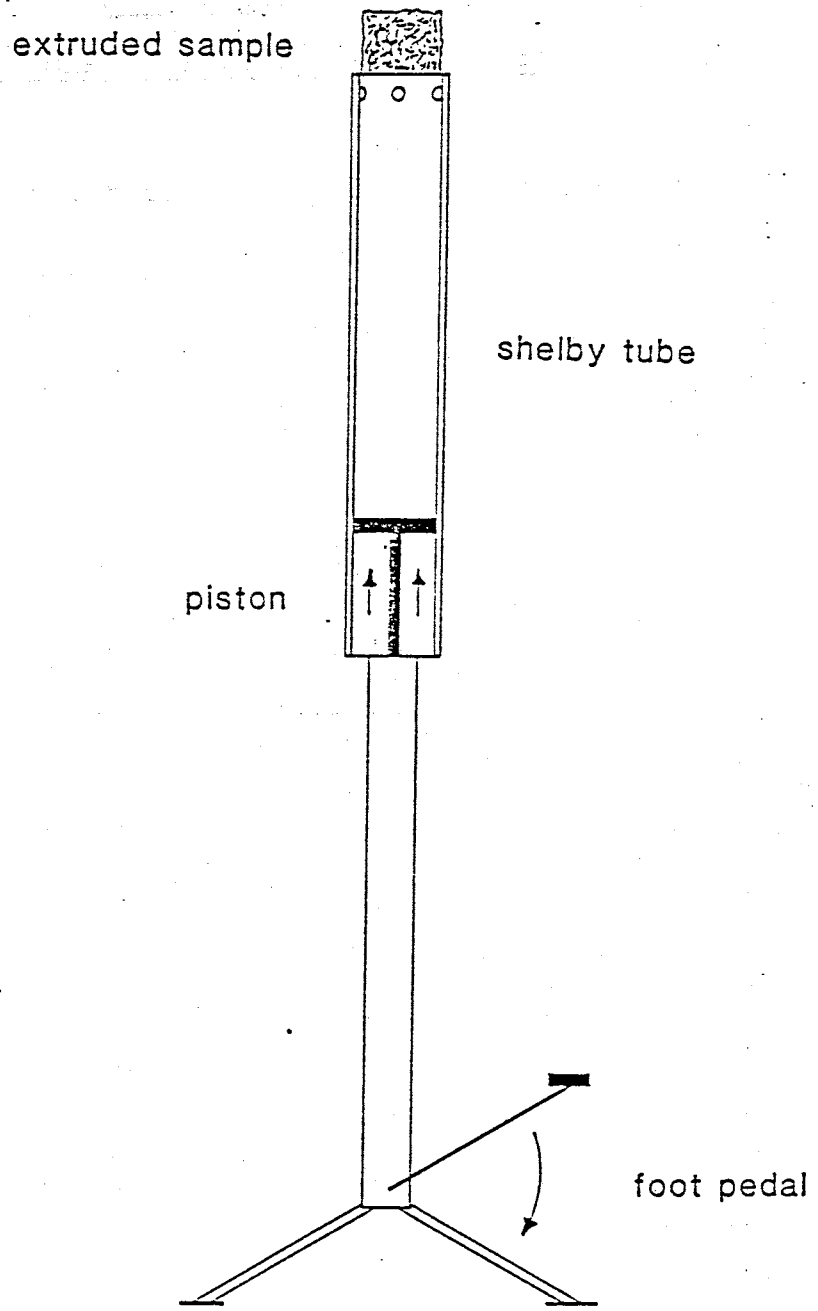


Figure C1. Diagram of the Vertiject sample extrusion device.



APPENDIX DVertical transect sample core photographsPhotograph D-1, (V47, photo # 3)

This sample was obtained from the slimes along transect V47. Layering is evident, however, the composition of the layers is quite uniform. The sample has pulled away from the sides of the trough upon drying and yet, has remained cohesive. This is common in the very fine grained, slime samples. The matrix in such samples that were air dried was often able to withstand the force of a hammer blow. Very thin sand layers are present in this sample similar to the sample in figure 14.

Photograph D-2, (V11, photo # 5)

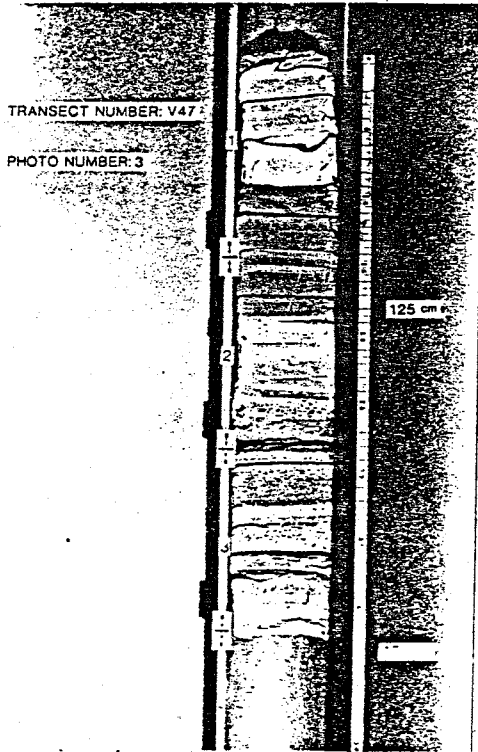
This sample was obtained from the sand zone near the southern edge of the cross section. The sample is quite uniform and coarser grained than the sample from V47. Samples taken from this area of the cross section were relatively cohesionless and broke apart easily upon drying.

Photograph D-3, (V75, photo # 6)

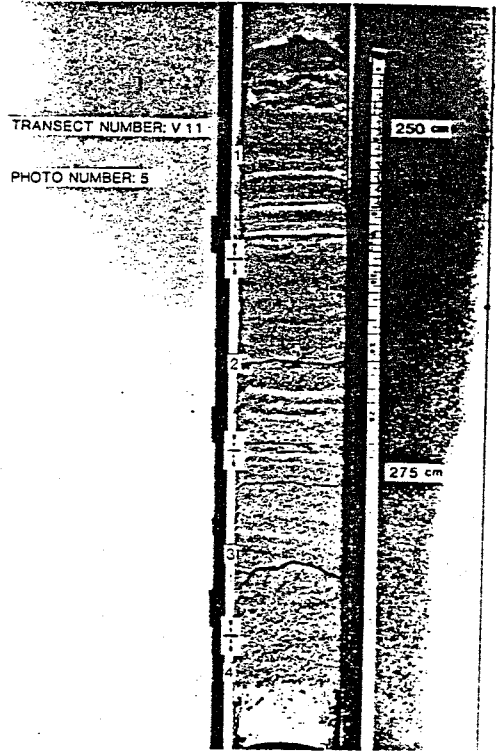
This sample was obtained from transect V75 in an area where interfingering of slimes and sands is common. This sample core is essentially made up of two parts. The upper part, 0-28 cm, is composed primarily of coarse grained tails with very thin interlayered slimes (18, 21, and 27 cm). The fine grained slime layers appear lighter in color in the photograph. Below 28 cm, slime layers predominate. In this area, thin layers of coarser-grained tails cause the sample to separate upon drying. The curved shaped of the sample edges below 30 cm is due to core deformation during sample extrusion.

Photograph D-4, (V75, photo # 7)

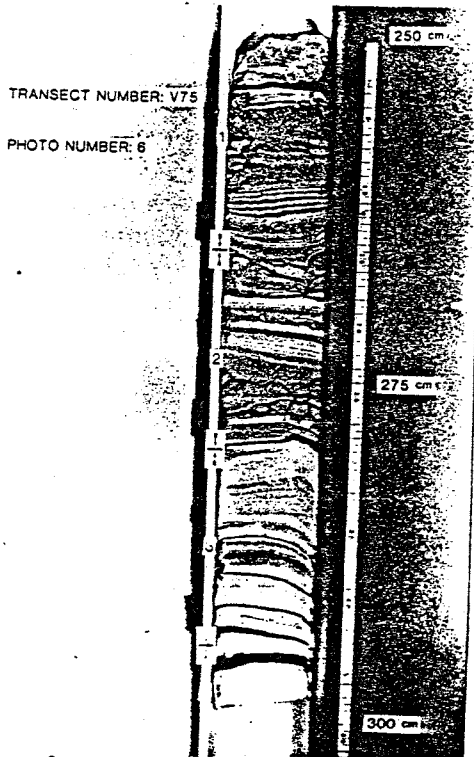
This photograph shows the contact between layer 1 and the underlying soil at the transect location V75. Interlayering of coarse and finer-grained tails is evident in layer 1. A fairly large stone is noted in the soil at 43 cm along the tape measure. The rocky nature of the underlying soil made sampling in this media very difficult.



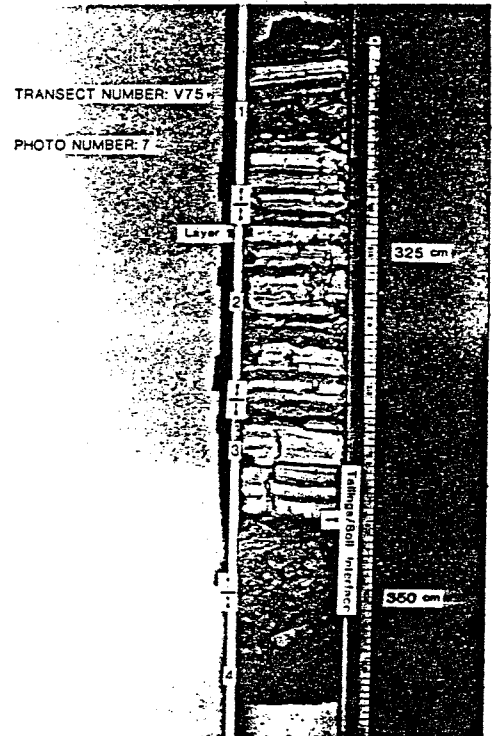
Photograph D-1



Photograph D-2



Photograph D-3



Photograph D-4

APPENDIX ELaboratory procedure:  $\theta/\psi$  relationshipsHanging column method

$\theta/\psi$  relationships at low suction values can be determined using a hanging column apparatus (figure E1). The cup (C) in the figure is a 350 ml buchner funnel with a fine-fritted ceramic plate (P). The funnel is connected to a 50 ml burette (B) by fine tubing (1/16" ID). A large rubber stopper (RS) is placed over the buchner funnel. A tube connects this stopper to the burette. This setup is used to prevent evaporation of water from the sample. De-aired, distilled water is used in the hanging column system.

Prior to placing a ring sample in the buchner funnel, it was set in a pan of distilled water for at least 24 hours to ensure saturation. The saturated sample is then weighed and placed in the buchner funnel. Care must be taken to ensure that good hydraulic connection is obtained between the sample and the porous plate. A suction is applied to the sample by lowering the water level in the burette. This suction will cause water to drain from the sample until an equilibrium  $\theta$  is reached at the given pressure. Equilibrium is usually attained within 24 hours.  $\psi$  is measured from the center of the sample length to the water meniscus in the burette. To obtain a representative amount of data for a  $\theta/\psi$  curve, the burette is lowered in 10 to 15 cm increments daily. Suctions up to 180 cm can be applied to a sample using this method. Both wetting and drying curves can be

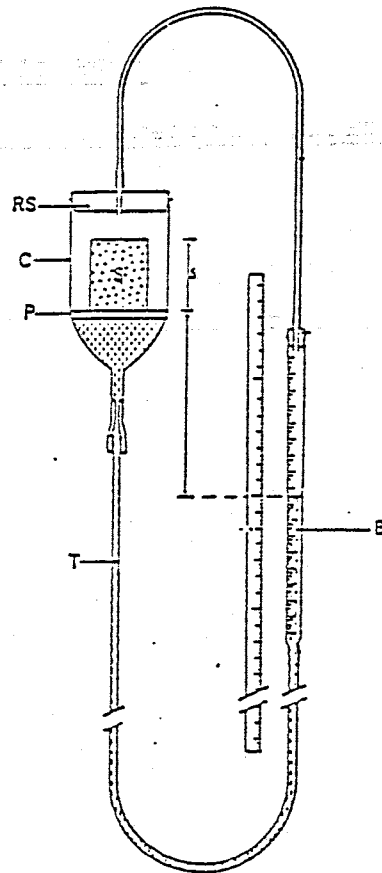


Figure E1. Diagram of the hanging column used to measure theta/psi relationships (Bouma, 1974).

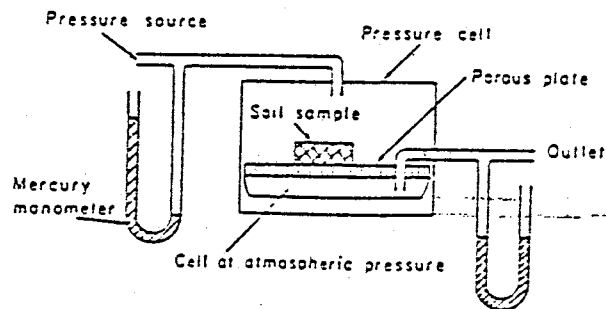


Figure E2. Diagram of a volumetric pressure plate extractor (Hillel, 1980).

obtained using this apparatus.

#### Volumetric pressure plate method

The volumetric pressure plate serves the same function as the hanging column apparatus (figure E2). The pressure plate, however, enables  $\theta/\psi$  drying relationships to be determined up to 15 bars (15255 cm).

The apparatus is prepared for use by saturating the porous plate under pressure with de-aired, distilled water. Up to 12 samples at a given time can be placed on the porous plate. Once again, care must be taken to ensure that good hydraulic connection is obtained between the sample and the porous plate. With the samples in place, the chamber is sealed and positive pressure is applied using bottled nitrogen gas. Pressure can be applied at various increments up to 15 bars. When the samples have reached equilibrium, the chamber is opened and the samples are weighed to determine the loss in moisture at the given pressure.

The last step in the  $\theta/\psi$  procedure is to oven dry and weigh the samples. With this weight,  $n$ ,  $\theta_{1.5}$ ,  $\theta_{15}$ , and  $\theta/\psi$  curves can be calculated.

THE HISTORY OF THE  
CITY OF BOSTON

The history of the city of Boston is a subject of great interest and importance. It is a city that has played a significant role in the development of the United States. From its early days as a small settlement to its current status as a major metropolitan area, Boston has a rich and varied history. The city's location on a peninsula in the harbor of Massachusetts has made it a natural center of trade and commerce. Its strategic position has also made it a key location in many of the nation's most important events. The city's history is a testament to the resilience and ingenuity of its people. It is a city that has shaped the course of American history and continues to do so today.

obtained using this apparatus.

#### Volumetric pressure plate method

The volumetric pressure plate serves the same function as the hanging column apparatus (figure E2). The pressure plate, however, enables  $\theta/\psi$  drying relationships to be determined up to 15 bars (15255 cm).

The apparatus is prepared for use by saturating the porous plate under pressure with de-aired, distilled water. Up to 12 samples at a given time can be placed on the porous plate. Once again, care must be taken to ensure that good hydraulic connection is obtained between the sample and the porous plate. With the samples in place, the chamber is sealed and positive pressure is applied using bottled nitrogen gas. Pressure can be applied at various increments up to 15 bars. When the samples have reached equilibrium, the chamber is opened and the samples are weighed to determine the loss in moisture at the given pressure.

The last step in the  $\theta/\psi$  procedure is to oven dry and weigh the samples. With this weight,  $n$ ,  $\theta_{1.5}$ ,  $\theta_{15}$ , and  $\theta/\psi$  curves can be calculated.

APPENDIX FLaboratory procedure: particle size analysisHydrometer analysis

Hydrometer analyses were performed following the procedure of Day (1965). Sodium pyrophosphate ( $\text{Na}_2\text{P}_2\text{O}_7 \cdot 10\text{H}_2\text{O}$ ) was used as the dispersing agent for this analysis.

Particle density is one of the input variables in Stoke's equation (equation used to determine particle size in a hydrometer analysis). The particle densities of 10 tailings samples were determined following the procedures of Blake (1965). The average particle density of the ten samples was found to equal 3.12 g/cm.

Sieve analysis

At the conclusion of each hydrometer analysis, the sample was wet sieved using a 200 mesh (75  $\mu$ ,  $\mu$ =microns) sieve. The sample retained in this sieve was then oven dried and dry sieved following the methods of Day (1965). Sieve sizes 30 (600 $\mu$ ), 40 (425 $\mu$ ), 60 (250 $\mu$ ), 100 (150 $\mu$ ), 140 (106 $\mu$ ), and 200 (75 $\mu$ ) were sufficient to characterize the particle fractionation of the tailings. Additional sieve sizes 1/4" (6300 $\mu$ ), 10 (2000 $\mu$ ), and 20 (850 $\mu$ ) were needed to characterize the soil samples.

Grain size parameters (% finer by weight) were calculated using the fortran program GRAIN (appendix G). The particle diameters at the 10th, 16th, 30th, 50th, 60th, and 84th percentile were linearly interpolated from the GRAIN output using the fortran program GS (appendix H).



APPENDIX G

Computer code for program: GRAIN

```

C *****
C *
C * PROGRAM TO COMPUTE GRAIN SIZE VS. PERCENTAGE OF WEIGHT PASSING. *
C * DATA TAKEN FROM BOTH SIEVE AND HYDROMETER TESTS. *
C *
C * WRITTEN BY: GARY JOHNSON, 4/2/86 *
C *
C *****
C
C VARIABLE DEFINITIONS:
C
C TWT-TOTAL SAMPLE WEIGHT
C PD-PARTICLE DIAMETER
C WTR-WEIGHT RETAINED PER SIEVE
C PERC-PERCENTAGE OF WEIGHT PASSING
C DEN-PARTICLE DENSITY
C TIME-TIME OF READING (HYDROMETER TEST)
C RC-CORRECTED R VALUE (HYDROMETER TEST)
C R-UNCORRECTED R VALUE (HYDROMETER TEST)
C TEMP-WATER TEMPERATURE
C LEN-LENGTH OF HYDROMETER BULB BELOW WATER SURFACE
C DIA-PARTICLE DIAMETER
C DIAC-CORRECTED PARTICLE DIAMETER
C TVIS-WATER VISCOSITY AT GIVEN TEMPERATURE
C VISC-VISCOSITY CORRECTION
C THETA-INTERMEDIATE VALUE
C L-LENGTH OF HYDROMETER BULB BELOW WATER SURFACE
C T-WATER TEMPERATURE
C V-WATER VISCOSITY AT GIVEN TEMPERATURE
C
C *****
C REAL TWT,N,PD,WTR,PERC,DEN,TIME,RC,TEMP,LEN,THETA,DIA,TVIS,VISC,DIAC,I
C REAL R(100),L(100),T(100),V(100),TTW
C
C *****
C
C OPEN(UNIT=22)
C OPEN(UNIT=23,FILE='LENGTH.DAT')
C OPEN(UNIT=24,FILE='VISCOS.DAT')
C
C *****
C
C WRITE(5,*)'INPUT TOTAL SAMPLE WEIGHT IN GRAMS:'
C READ(5,*) TWT
C
C WRITE(5,*)'INPUT NUMBER OF SIEVE READINGS: '
C READ(5,*) N
C
C *****
C
C TTW=TWT
C
C WRITE(5,*)'INPUT PARTICLE DIAMETER (MICRONS) & WEIGHT RETAINED:'
C
C DO 10 I=1,N
C READ(5,*) PD,WTR
C PERC=(TTW-WTR)/TWT
C WRITE(22,*)PD,PERC
C TTW=TTW-WTR

```

```

10      CONTINUE
C
C
C      *****
DO 30 I=1,61
      READ(23,*) R(I),L(I)
30      CONTINUE
C
DO 40 I=1,18
      READ(24,*) T(I),V(I)
40      CONTINUE
C
C
C      *****
WRITE(5,*) 'INPUT NUMBER OF HYDROMETER READINGS: '
READ(5,*)N
C
WRITE(5,*) 'INPUT PARTICLE DENSITY (GM/CM**3): '
READ(5,*)DEN
C
C
C      *****
WRITE(5,*) 'INPUT TIME OF READING (MINUTES), CORRECTED R VALUE, TEMP
* (DEGREES C): '
C
DO 20 I=1,N
      READ(5,*) TIME,RC,TEMP
C
      J=1
102     IF(RC.EQ.R(J))THEN
          LEN=L(J)
          GOTO 101
      ELSE
          J=J+1
          GOTO 102
      END IF
C
101     THETA=1000*(((30*.008007*LEN)/(980.7*(DEN-.99949)))**.5)
      DIA=THETA/(TIME**.5)
C
      J=1
202     IF(TEMP.EQ.T(J))THEN
          TVIS=V(J)
          GOTO 201
      ELSE
          J=J+1
          GOTO 202
      ENDIF
C
201     VISC=((TVIS/.008007)**.5)
      DIAC=DIA*VISC
      PERC=RC/TWT
      WRITE(22,*) DIAC,PERC
20      CONTINUE
C
C
C      *****
CLOSE(UNIT=22)
CLOSE(UNIT=23)
CLOSE(UNIT=24)

```

C  
C  
C

\*\*\*\*\*

WRITE(5,\*)'\*\*\*\*\*'  
WRITE(5,\*)'COPY FILE <FOR22.DAT> TO APPROPRIATE FILE NAME: '  
WRITE(5,\*)'\*\*\*\*\*'

C  
C  
C

\*\*\*\*\*

STOP  
END

C  
C

\*\*\*\*\*

## APPENDIX H

Computer code for program: GS

```

C *****
C THIS PROGRAM INTERPOLATES BETWEEN POINTS ON A GRAIN
C SIZE ANALYSIS CURVE IN ORDER TO DETERMINE PARAMETERS
C SUCH AS D50, AND UNIFORMITY COEFF.
C *****
C L=NO OF PTS IN ORIGINAL X,Y FILE
C MD=NO OF DEPENDENT VARIABLES
C M=NO OF POINTS TO BE INTERPOLATED
C BETWEEN 2 KNOWN POINTS
C N=((L-1)*M)+1
C *****
C TO RUN: EX GS.FOR,SYS:PLTLIB/LIB
C *****

REAL X(100),Y(100),U(1210),V(1210)
INTEGER Md,L,M,N
OPEN (UNIT=99,DIALOG)
OPEN (UNIT=98,DIALOG)

C *****
C WRITE(5,*) 'INPUT NUMBER OF READINGS: '
C READ(5,*) L
C Md=1
C M=30
C N=((L-1)*M)+1
C *****

DO 10 I=1,L
  READ(99,*)X(I),Y(I)
CONTINUE

C *****
C CALL CRVFIT(Md,L,X,Y,M,N,U,V)
C *****

DO 20 I=1,N
  IF((V(I).LT..15).AND.(V(I).GT..085))THEN
    WRITE(98,*)U(I),V(I)
  END IF
CONTINUE
20 DO 25 I=1,N
  IF((V(I).LT..21).AND.(V(I).GT..145))THEN
    WRITE(98,*)U(I),V(I)
  END IF
CONTINUE
25 DO 30 I=1,N
  IF((V(I).LT..35).AND.(V(I).GT..285))THEN
    WRITE(98,*)U(I),V(I)
  END IF
CONTINUE
30 DO 40 I=1,N
  IF((V(I).LT..55).AND.(V(I).GT..485))THEN
    WRITE(98,*)U(I),V(I)
  END IF
CONTINUE
40 DO 50 I=1,N

```

```
IF((V(I).LT..65).AND.(V(I).GT..585))THEN  
WRITE(98,*)U(I),V(I)  
END IF  
50 CONTINUE  
DO 60 I=1,N  
IF((V(I).LT..89).AND.(V(I).GT..825))THEN  
WRITE(98,*)U(I),V(I)  
END IF  
60 CONTINUE  
STOP  
END
```

APPENDIX IData values described in this study in tabular form

- Upper Horizontal Transect Data  
(K, n,  $\theta_{1.5}$ ,  $\theta_{15}$ ) ..... A-22
- Lower Horizontal Transect Data  
(K, n,  $\theta_{1.5}$ ,  $\theta_{15}$ ,  $d_*$ ) ..... A-25
- Vertical Transects Data  
(K, n,  $\theta_{1.5}$ ,  $\theta_{15}$ ,  $d_*$ ) ..... A-41
- Vertical Transect Theta/Psi Data  
( $\theta/\psi$ , Rel K, Abs K, Diffus) ..... A-55
- Neutron Probe Data  
( $\theta_F$ , tubes 6, 9-11) ..... A-59

HORIZONTAL TRANSECT  
HYDRAULIC PROPERTIES

Transect bearing & distance from central drain (m):

N 6 W ,  
3.4m west

dist north edge (m)	depth (cm)	K(sat) (cm/sec)	porosity	theta (cm <sup>3</sup> /cm <sup>3</sup> )		theta/psi
				1.5 bar	15 bar	
0.00	15-28	1.13E-03				
	28-42	2.36E-04				
	42-56	1.39E-04				
	56-69	3.03E-05	0.460	0.101	0.070	
3.75	15-28	5.52E-04				
	28-42	6.40E-03				
	42-56	1.11E-03				
	56-69	4.26E-03	0.470	0.142	0.108	
8.31	15-28	1.52E-04				
	28-42	1.30E-05				
	42-56	2.28E-05	0.390	0.155	0.110	
	56-69					
12.87	15-28	1.10E-03				
	28-42	3.33E-03				
	42-56	2.18E-05				
	56-69	1.26E-04	0.460	0.214	0.184	
17.43	15-56	4.93E-06				
	56-69	1.33E-05	0.510	0.047	0.032	
21.99	15-28	2.18E-05				
	28-42	4.12E-05				
	42-56	3.08E-05				
	56-69	9.33E-06	0.460	0.123	0.079	
26.55	15-28	8.84E-06				
	28-56	3.46E-06				
	56-69	7.41E-07	0.530	0.444	0.324	
31.11	15-28	4.52E-05				
	28-69	2.82E-06				
	56-69		0.570	0.425	0.262	
35.67	15-28	2.10E-05				
	28-42	1.46E-05				
	42-56	9.27E-06				
	56-69		0.560	0.393	0.309	

HORIZONTAL TRANSECT  
HYDRAULIC PROPERTIES

Transect bearing & distance from central drain (m):

N 6 W ,  
3.4m west

dist north edge (m)	depth (cm)	K(sat) (cm/sec)	porosity	theta (cm <sup>3</sup> /cm <sup>3</sup> )		theta/psi
				1.5 bar	15 bar	
40.23	15-28	3.75E-03				
	28-42	7.95E-04				
	42-56	9.31E-05				
	56-69	1.19E-04	0.520	0.362	0.331	
44.79	15-28	6.80E-05				
	28-42	4.53E-05				
	42-56	2.83E-06				
	56-69		0.530	0.335	0.280	
49.35	15-28	2.24E-04				
	28-42	1.76E-05				
	42-56	2.55E-06				
	56-69		0.720	0.416	0.251	
53.91	15-28	1.50E-04				
	28-42	4.49E-06				
	42-56	3.86E-05				
	56-69		0.620	0.365	0.350	
58.47	15-28	3.59E-04				
	28-42	3.42E-05				
	42-56	4.63E-05				
	56-69	1.50E-05	0.590	0.407	0.243	
63.03	15-28	5.83E-05				
	28-42	4.59E-05				
	42-56	9.70E-07				
	56-69	4.10E-06				
67.59	15-56	6.68E-07				
	56-69	1.44E-06	0.450	0.168	0.075	
72.15	15-56	4.08E-06				
	56-69	1.42E-06	0.630	0.334	0.215	
76.71	15-28					
	28-42	1.48E-06				
	42-56	1.87E-06				
	56-69		0.540	0.265	0.241	



HORIZONTAL TRANSECT  
HYDRAULIC PROPERTIES

Transect bearing & distance from central drain (m):

N 6 W ,  
3.4m west

dist north edge (m)	depth (cm)	K(sat) (cm/sec)	porosity	theta (cm <sup>3</sup> /cm <sup>3</sup> )		theta/psi
				1.5 bar	15 bar	
81.27	15-28	3.23E-04				
	28-42	4.43E-05				
	42-56	1.49E-04				
	56-69	5.11E-05				
85.83	15-28	2.33E-04				
	28-42	4.14E-05				
	42-56	3.56E-05				
	56-69	5.35E-06	0.500	0.325	0.282	
90.39	15-28	1.48E-04				
	28-42	1.08E-04				
	42-56	1.57E-04				
	56-69	6.10E-05	0.510	0.244	0.205	
94.95	15-28	5.04E-04				
	28-42	1.06E-03				
	42-56	3.62E-03				
	56-69					
99.51	15-28	5.32E-04				
	28-42	4.56E-04				
	42-56	1.88E-03				
	56-69	2.57E-03	0.480	0.295	0.217	
104.07	15-28	7.15E-04				
	28-42	8.47E-06				
	42-56	1.13E-05				
	56-69	4.63E-05				

HORIZONTAL TRANSECT  
HYDRAULIC PROPERTIES

Transect bearing & distance from central drain (m):

N 6 W ,  
3.4m west

dist north edge (m)	depth (cm)	K(sat) (cm/sec)	porosity	theta (cm <sup>3</sup> /cm <sup>3</sup> )		theta/psi
				1.5 bar	15 bar	
0.00	152-165	9.32E-04				
	165-179	4.02E-04				
	179-192	4.03E-03				
	192-205	4.69E-03	0.450	0.121	0.091	
1.25	152-165	7.90E-04				
	165-179	3.70E-04				
	179-192	1.76E-04				
	192-205	1.91E-05	0.471	0.129	0.082	
3.75	152-165	1.96E-05				
	165-179	6.55E-06				
	179-192	3.23E-05	0.480	0.082		
	192-205					
5.27	152-165	8.74E-04				
	165-179	4.59E-05				
	179-192	8.83E-04				
	192-205		0.387	0.072	0.027	
6.79	152-165	2.32E-04				
	165-179	5.47E-06				
	179-192	9.74E-06				
	192-205	2.05E-05	0.413	0.088	0.036	
8.31	152-165	5.42E-05				
	165-179	1.22E-05				
	179-192	3.20E-06				
	192-205		0.630	0.108	0.064	
9.83	152-165	4.30E-06				
	165-179	8.08E-06				
	179-192	4.80E-06				
	192-205	1.33E-05	0.477	0.183	0.082	
11.35	152-165	5.89E-05				
	165-179	1.62E-06				
	179-192	6.09E-06				
	192-205	3.68E-06	0.491	0.330	0.171	
12.87	152-165	3.30E-05				
	165-179	2.74E-05				
	179-192	9.21E-05				
	192-205	2.29E-05	0.590	0.175	0.088	

HORIZONTAL TRANSECT  
GRAIN SIZE ANALYSIS

Transect bearing & distance from central drain (m): N 6 W ,  
3.4m west

dist north edge (m)	depth (cm)	(microns)					
		d 10	d 16	d 30	d 50	d 60	d 84
0.00	152-165						
	165-179						
	179-192						
	192-205	30.749	34.510	41.175	49.008	52.460	142.667
1.25	152-165						
	165-179						
	179-192						
	192-205	10.670	20.110	44.432	74.070	96.700	156.667
3.75	152-165						
	165-179						
	179-192						
	192-205						
5.27	152-165						
	165-179						
	179-192						
	192-205	10.674	27.611	62.892	96.700	117.733	180.000
6.79	152-165						
	165-179						
	179-192						
	192-205	6.066	14.647	33.941	53.176	65.559	117.733
8.31	152-165						
	165-179						
	179-192						
	192-205						
9.83	152-165						
	165-179						
	179-192						
	192-205	1.766	4.532	7.849	33.496	44.502	122.133
11.35	152-165						
	165-179						
	179-192						
	192-205	0.931	1.715	5.053	15.771	22.875	84.300
12.87	152-165						
	165-179						
	179-192						
	192-205						

HORIZONTAL TRANSECT  
HYDRAULIC PROPERTIES

Transect bearing & distance from central drain (m): N 6 W ,  
3.4m west

dist north edge (m)	depth (cm)	K(sat) (cm/sec)	porosity	theta (cm <sup>3</sup> /cm <sup>3</sup> )		theta/psi
				1.5 bar	15 bar	
14.39	152-165	5.69E-06				
	165-179	1.59E-05				
	179-192	4.69E-06				
	192-205	1.83E-06	0.542	0.374	0.159	
15.91	152-165	1.24E-04				
	165-179	1.12E-05				
	179-192	5.96E-06				
	192-205	1.61E-06	0.511	0.377	0.227	
17.43	152-165	9.08E-04				
	165-179	2.10E-06				
	179-192	8.50E-06				
	192-205	9.91E-06	0.680	0.360	0.277	
18.95	152-165	4.09E-04				
	165-179	1.06E-05				
	179-192	3.64E-06				
	192-205	2.81E-05	0.403	0.295	0.033	
20.47	152-165	3.93E-05				
	165-179	9.33E-06				
	179-192	2.48E-06				
	192-205	7.53E-06	0.454	0.180	0.054	
21.99	152-165	2.52E-03				
	165-179	1.36E-05				
	179-192	1.64E-06				
	192-205	2.06E-05	0.540	0.328	0.234	
23.51	152-165	6.67E-06				
	165-179	5.24E-06				
	179-192	2.83E-06				
	192-205	3.01E-06	0.509	0.321	0.228	
25.03	152-165	1.35E-05				
	165-179	1.06E-06				
	179-192	1.58E-06				
	192-205	8.07E-07	0.502	0.316	0.138	
26.55	152-165	2.89E-04				
	165-179	4.70E-06				
	179-192	6.00E-06				
	192-205	2.52E-05	0.650	0.314	0.239	

HORIZONTAL TRANSECT  
GRAIN SIZE ANALYSIS

Transect bearing & distance from central drain (m): N 6 W ,  
3.4m west

dist north edge (m)	depth (cm)	(microns)					
		d 10	d 16	d 30	d 50	d 60	d 84
14.39	152-165 165-179 179-192 192-205	0.746	1.237	4.057	10.456	14.663	37.510
15.91	152-165 165-179 179-192 192-205	0.653	1.249	3.380	9.351	13.133	31.920
17.43	152-165 165-179 179-192 192-205						
18.95	152-165 165-179 179-192 192-205	7.797	18.452	54.581	80.167	97.733	153.333
20.47	152-165 165-179 179-192 192-205	1.536	5.029	14.200	36.337	48.295	92.567
21.99	152-165 165-179 179-192 192-205						
23.51	152-165 165-179 179-192 192-205	1.102	2.254	5.662	14.621	20.380	44.830
25.03	152-165 165-179 179-192 192-205	0.940	1.655	5.662	15.406	22.293	52.083
26.55	152-165 165-179 179-192 192-205						

HORIZONTAL TRANSECT  
HYDRAULIC PROPERTIES

Transect bearing & distance from central drain (m):

N 6 W ,  
3.4m wes

dist north edge (m)	depth (cm)	K(sat) (cm/sec)	porosity	theta (cm <sup>3</sup> /cm <sup>3</sup> )		theta/psi
				1.5 bar	15 bar	
28.07	152-165	1.45E-03				
	165-179	1.65E-06				
	179-192	2.27E-06				
	192-205	9.20E-07	0.605	0.424	0.194	
29.59	152-165	1.13E-05				
	165-179	4.01E-06				
	179-192	6.16E-06				
	192-205	1.20E-06	0.563	0.405	0.243	
31.11	152-165	1.23E-05				
	165-179	7.98E-06				
	179-192	1.68E-06				
	192-205	7.30E-07	0.595	0.429	0.231	
32.63	152-165	5.30E-05				
	165-179	3.29E-06				
	179-192	4.24E-07				
	192-205	4.27E-07	0.562	0.417	0.312	
34.15	152-165	6.17E-06				
	165-179	3.58E-06				
	179-192	2.22E-06				
	192-205	5.92E-07	0.562	0.388	0.165	
35.67	152-165	7.94E-05				
	165-179	2.91E-06				
	179-192	1.27E-06				
	192-205	7.47E-07	0.575	0.395	0.190	
37.19	152-165	7.62E-07				
	165-179	2.08E-07				
	179-192	1.26E-06				
	192-205	3.10E-07	0.526	0.344	0.189	
38.71	152-165	1.67E-05				
	165-179					
	179-192					
	192-205		0.530	0.385	0.106	
40.23	152-165	1.15E-05				
	165-179	1.67E-06				
	179-192	8.56E-07				
	192-205	4.51E-07	0.576	0.395	0.175	

HORIZONTAL TRANSECT  
GRAIN SIZE ANALYSIS

Transect bearing & distance from central drain (m): N 6 W ,  
3.4m west

dist north edge (m)	depth (cm)	(microns)					
		d 10	d 16	d 30	d 50	d 60	d 84
28.07	152-165 165-179 179-192 192-205	0.559	0.860	1.838	5.131	7.523	15.755
29.59	152-165 165-179 179-192 192-205	0.746	1.235	2.973	7.921	11.287	24.933
31.11	152-165 165-179 179-192 192-205	0.621	0.959	1.895	5.463	7.882	17.030
32.63	152-165 165-179 179-192 192-205	0.708	1.153	3.087	6.902	10.279	21.014
34.15	152-165 165-179 179-192 192-205	0.708	1.400	3.537	9.462	13.289	32.299
35.67	152-165 165-179 179-192 192-205	0.708	1.397	3.581	8.645	12.516	29.719
37.19	152-165 165-179 179-192 192-205	0.916	1.435	4.408	12.439	17.818	38.300
38.71	152-165 165-179 179-192 192-205	0.621	1.147	2.889	6.902	10.297	26.713
40.23	152-165 165-179 179-192 192-205	0.708	1.505	3.037	7.702	11.022	23.177

HORIZONTAL TRANSECT  
HYDRAULIC PROPERTIES

Transect bearing & distance from central drain (m):

N 6 W ,  
3.4m west

dist north edge (m)	depth (cm)	K(sat) (cm/sec)	porosity	theta (cm <sup>3</sup> /cm <sup>3</sup> )		theta/psi
				1.5 bar	15 bar	
41.75	152-165	6.98E-07				
	165-179	2.06E-06				
	179-192	9.82E-07				
	192-205	8.67E-07	0.532	0.358	0.176	
43.27	152-165	1.53E-06				
	165-179	5.43E-07				
	179-192	8.01E-07				
	192-205	5.82E-07	0.587	0.432	0.171	
44.79	152-165	5.17E-05				
	165-179	4.26E-06				
	179-192	1.09E-05				
	192-205	8.33E-07	0.542	0.382	0.274	
46.31	152-165	1.24E-05				
	165-179	2.58E-06				
	179-192	1.39E-06				
	192-205	1.48E-06	0.580	0.420	0.149	
47.83	152-165	7.26E-05				
	165-179	2.14E-06				
	179-192	1.40E-06				
	192-205	1.22E-06	0.612	0.417	0.165	
49.35	152-165	2.52E-06				
	165-179	1.71E-06				
	179-192	1.20E-06				
	192-205	6.74E-06	0.616	0.417	0.199	
50.87	152-165	2.44E-06				
	165-179	2.00E-06				
	179-192	1.35E-06				
	192-205	1.69E-06	0.580	0.416	0.263	
52.39	152-165	6.71E-06				
	165-179	7.54E-07				
	179-192	3.51E-06				
	192-205	4.24E-06	0.553	0.406	0.171	
53.91	152-165					
	165-179	1.95E-06				
	179-192	1.31E-06				
	192-205	2.86E-06	0.530	0.368	0.221	



HORIZONTAL TRANSECT  
GRAIN SIZE ANALYSIS

Transect bearing & distance from central drain (m): N 6 W ,  
3.4m west

dist north edge (m)	depth (cm)	(microns)					
		d 10	d 16	d 30	d 50	d 60	d 84
41.75	152-165 165-179 179-192 192-205	0.914	1.426	4.695	12.041	16.276	38.791
43.27	152-165 165-179 179-192 192-205	0.848	1.163	2.646	7.485	10.144	18.926
44.79	152-165 165-179 179-192 192-205	0.912	1.150	3.142	7.485	11.083	26.519
46.31	152-165 165-179 179-192 192-205	0.916	1.326	2.910	6.044	9.441	18.598
47.83	152-165 165-179 179-192 192-205	0.849	1.155	2.985	6.800	9.441	19.168
49.35	152-165 165-179 179-192 192-205	0.847	1.157	2.496	6.156	8.575	17.494
50.87	152-165 165-179 179-192 192-205	0.846	1.149	2.913	6.678	9.114	18.598
52.39	152-165 165-179 179-192 192-205	0.912	1.151	3.145	7.213	10.176	22.094
53.91	152-165 165-179 179-192 192-205	0.850	1.136	2.582	6.141	8.155	15.755

HORIZONTAL TRANSECT  
HYDRAULIC PROPERTIES

Transect bearing & distance from central drain (m):

N 6 W ,  
3.4m west

dist north edge (m)	depth (cm)	K(sat) (cm/sec)	porosity	theta (cm <sup>3</sup> /cm <sup>3</sup> )		theta/psi
				1.5 bar	15 bar	
55.43	152-165	1.47E-06	0.523	0.394	0.118	
	165-179	2.25E-06				
	179-192	8.33E-05				
	192-205	4.32E-05				
56.95	152-165	7.24E-06	0.534	0.377	0.313	
	165-179	5.98E-06				
	179-192	2.34E-06				
	192-205	1.16E-06				
58.47	152-165	3.26E-06				
	165-179	7.15E-07				
	179-192	7.91E-07				
	192-205	6.05E-07				
59.99	152-165	1.56E-06	0.590	0.392	0.217	
	165-179	6.88E-07				
	179-192	8.87E-07				
	192-205	5.71E-07				
61.51	152-165	5.35E-04	0.560	0.401	0.348	
	165-179	1.69E-06				
	179-192	1.22E-06				
	192-205	8.44E-07				
63.03	152-165	4.45E-06	0.460	0.051	0.029	
	165-179	1.73E-06				
	179-192	9.13E-07				
	192-205	9.45E-07				
64.55	152-165	7.47E-06	0.419	0.040	0.021	
	165-179	1.64E-06				
	179-192	1.22E-06				
	192-205					
66.07	152-165	7.67E-06	0.445	0.055	0.030	
	165-179	2.05E-06				
	179-192	2.87E-06				
	192-205					
67.59	152-165	5.14E-04	0.440	0.049	0.028	
	165-179	6.16E-06				
	179-192	1.63E-06				
	192-205	2.89E-06				

HORIZONTAL TRANSECT  
HYDRAULIC PROPERTIES

Transect bearing & distance from central drain (m):

N 6 W ,  
3.4m west

dist north edge (m)	depth (cm)	K(sat) (cm/sec)	porosity	theta (cm <sup>3</sup> /cm <sup>3</sup> )		theta/psi
				1.5 bar	15 bar	
55.43	152-165	1.47E-06	0.523	0.394	0.118	
	165-179	2.25E-06				
	179-192	8.33E-05				
	192-205	4.32E-05				
56.95	152-165	7.24E-06	0.534	0.377	0.313	
	165-179	5.98E-06				
	179-192	2.34E-06				
	192-205	1.16E-06				
58.47	152-165	3.26E-06				
	165-179	7.15E-07				
	179-192	7.91E-07				
	192-205	6.05E-07				
59.99	152-165	1.56E-06	0.590	0.392	0.217	
	165-179	6.88E-07				
	179-192	8.87E-07				
	192-205	5.71E-07				
61.51	152-165	5.35E-04	0.560	0.401	0.348	
	165-179	1.69E-06				
	179-192	1.22E-06				
	192-205	8.44E-07				
63.03	152-165	4.45E-06	0.460	0.051	0.029	
	165-179	1.73E-06				
	179-192	9.13E-07				
	192-205	9.45E-07				
64.55	152-165	7.47E-06	0.419	0.040	0.021	
	165-179	1.64E-06				
	179-192	1.22E-06				
	192-205					
66.07	152-165	7.67E-06	0.445	0.055	0.030	
	165-179	2.05E-06				
	179-192	2.87E-06				
	192-205					
67.59	152-165	5.14E-04	0.440	0.049	0.028	
	165-179	6.16E-06				
	179-192	1.63E-06				
	192-205	2.89E-06				

HORIZONTAL TRANSECT  
GRAIN SIZE ANALYSIS

Transect bearing & distance from central drain (m): N 6 W ,  
3.4m west

dist north edge (m)	depth (cm)	(microns)					
		d 10	d 16	d 30	d 50	d 60	d 84
55.43	152-165 165-179 179-192 192-205	0.740	1.095	3.627	7.316	11.335	22.9
56.95	152-165 165-179 179-192 192-205	0.738	1.094	3.073	6.407	8.906	19.552
58.47	152-165 165-179 179-192 192-205						
59.99	152-165 165-179 179-192 192-205	0.778	1.093	2.740	6.526	8.906	20.055
61.51	152-165 165-179 179-192 192-205	1.057	1.933	3.920	7.301	9.943	25.52
63.03	152-165 165-179 179-192 192-205	16.192	34.258	63.826	75.000	117.733	186.667
64.55	152-165 165-179 179-192 192-205	34.287	54.453	82.233	120.667	139.733	196.66
66.07	152-165 165-179 179-192 192-205	22.722	47.797	69.664	122.133	144.133	210.000
67.59	152-165 165-179 179-192 192-205						

HORIZONTAL TRANSECT  
HYDRAULIC PROPERTIES

Transect bearing & distance from central drain (m):

N 6 W ,  
3.4m west

dist north edge (m)	depth (cm)	K(sat) (cm/sec)	porosity	theta (cm <sup>3</sup> /cm <sup>3</sup> )		theta/psi
				1.5 bar	15 bar	
69.11	152-165	5.40E-06				
	165-179	5.23E-06				
	179-192	2.71E-06				
	192-205		0.570	0.172	0.073	
70.63	152-165	2.01E-04				
	165-179	5.29E-06				
	179-192	2.83E-06				
	192-205	2.95E-05	0.471	0.040	0.039	
72.15	152-165	2.24E-04				
	165-179	3.01E-06				
	179-192	4.35E-05				
	192-205	4.33E-06	0.470	0.051	0.028	
73.67	152-165	8.25E-04				
	165-179	2.28E-03				
	179-192	7.28E-06				
	192-205	2.47E-06	0.418	0.098	0.056	
75.19	152-165	3.54E-04				
	165-179	1.12E-05				
	179-192	1.76E-05				
	192-205	6.97E-06	0.460	0.174	0.138	
76.71	152-165	2.04E-04				
	165-179	2.15E-05				
	179-192	2.91E-05				
	192-205	5.30E-05	0.590	0.096	0.045	
78.23	152-165	5.37E-04				
	165-179	8.61E-06				
	179-192	3.47E-05				
	192-205	1.78E-05	0.418	0.126	0.093	
79.75	152-165	1.32E-04				
	165-179	7.80E-05				
	179-192	4.28E-05				
	192-205	1.60E-04	0.540	0.087	0.039	
81.27	152-165	6.43E-04				
	165-179	1.28E-05				
	179-192	1.08E-05				
	192-205	1.67E-05	0.490	0.217	0.156	

HORIZONTAL TRANSECT  
GRAIN SIZE ANALYSIS

Transect bearing & distance from central drain (m): N 6 W ,  
3.4m west

dist north edge (m)	depth (cm)	(microns)					
		d 10	d 16	d 30	d 50	d 60	d 84
69.11	152-165						
	165-179						
	179-192						
	192-205	22.722	48.448	87.400	138.267	163.333	267.50
70.63	152-165						
	165-179						
	179-192						
	192-205	34.088	57.765	73.457	108.933	126.533	190.000
72.15	152-165						
	165-179						
	179-192						
	192-205	24.427	58.992	76.033	119.200	141.200	210.00
73.67	152-165						
	165-179						
	179-192						
	192-205	4.189	8.579	25.537	120.667	160.000	250.000
75.19	152-165						
	165-179						
	179-192						
	192-205	1.394	3.719	13.341	27.781	36.585	99.80
76.71	152-165						
	165-179						
	179-192						
	192-205	8.176	15.183	32.557	62.218	81.291	176.667
78.23	152-165						
	165-179						
	179-192						
	192-205	5.120	9.013	28.041	62.218	86.652	160.00
79.75	152-165						
	165-179						
	179-192						
	192-205	6.379	16.730	37.105	67.529	81.801	170.000
81.27	152-165						
	165-179						
	179-192						
	192-205	1.952	4.692	11.795	27.909	37.179	101.867

HORIZONTAL TRANSECT  
HYDRAULIC PROPERTIES

Transect bearing & distance from central drain (m):

N 6 W ,  
3.4m west

dist north edge (m)	depth (cm)	K(sat) (cm/sec)	porosity	theta (cm <sup>3</sup> /cm <sup>3</sup> )		theta/psi
				1.5 bar	15 bar	
82.79	152-165	2.79E-04				
	165-179	2.96E-05				
	179-192	8.99E-06				
	192-205	1.83E-04	0.499	0.091	0.041	
84.31	152-165	1.29E-04				
	165-179	3.37E-05				
	179-192	6.94E-05				
	192-205	2.61E-05	0.556	0.133	0.090	
85.83	152-165	9.20E-04				
	165-179	3.85E-05				
	179-192	4.52E-05				
	192-205	2.68E-05	0.420	0.116	0.068	
87.35	152-165	1.25E-04				
	165-179	5.56E-05				
	179-192	7.37E-05				
	192-205	2.05E-05	0.494	0.067	0.032	
88.87	152-165	2.24E-05				
	165-179	2.15E-05				
	179-192	5.04E-05				
	192-205	1.47E-05	0.553	0.148	0.088	
90.39	152-165	2.36E-04				
	165-179	4.86E-05				
	179-192	3.53E-05				
	192-205	2.66E-05	0.460	0.183	0.085	
91.99	152-165	3.55E-04				
	165-179	2.55E-03				
	179-192	4.21E-05				
	192-205	1.53E-04	0.534	0.098	0.046	
93.43	152-165	2.12E-04				
	165-179	3.08E-05				
	179-192	1.12E-05				
	192-205	2.39E-05	0.521	0.087	0.041	
94.95	152-165	3.07E-04				
	165-179	9.35E-05				
	179-192	3.02E-04				
	192-205	6.02E-05	0.480	0.144	0.086	

HORIZONTAL TRANSECT  
GRAIN SIZE ANALYSIS

Transect bearing & distance from central drain (m): N 6 W ,  
3.4m west

dist north edge (m)	depth (cm)	(microns)					
		d 10	d 16	d 30	d 50	d 60	d 84
82.79	152-165 165-179 179-192 192-205	6.733	17.336	40.007	76.001	96.906	163.303
84.31	152-165 165-179 179-192 192-205	2.301	8.602	20.065	38.926	50.256	126.533
85.83	152-165 165-179 179-192 192-205	0.748	1.442	4.144	8.561	12.226	26.207
87.35	152-165 165-179 179-192 192-205	5.832	19.739	50.413	80.077	102.526	170.000
88.87	152-165 165-179 179-192 192-205	14.675	23.426	27.190	34.889	68.107	139.703
90.39	152-165 165-179 179-192 192-205	1.729	2.895	8.874	25.722	42.899	111.867
91.91	152-165 165-179 179-192 192-205	4.033	14.941	34.357	50.412	76.196	135.301
93.43	152-165 165-179 179-192 192-205	5.996	19.053	49.892	110.400	141.200	250.000
94.95	152-165 165-179 179-192 192-205	3.210	9.593	18.403	29.395	35.052	50.870



HORIZONTAL TRANSECT  
HYDRAULIC PROPERTIES

Transect bearing & distance from central drain (m):

N 6 W ,  
3.4m west

dist north edge (m)	depth (cm)	K(sat) (cm/sec)	porosity	theta (cm <sup>3</sup> /cm <sup>3</sup> )		theta/psi
				1.5 bar	15 bar	
96.47	152-165	7.23E-05				
	165-179	1.74E-05				
	179-192	2.92E-04				
	192-205	8.40E-06	0.581	0.223	0.137	
97.99	152-165	5.40E-05				
	165-179	7.79E-05				
	179-192	3.77E-05				
	192-205	7.91E-05	0.443	0.055	0.029	
99.51	152-165	1.39E-04				
	165-179	2.55E-03				
	179-192	8.78E-04				
	192-205	6.25E-04	0.460	0.054	0.030	
101.03	152-165	1.46E-02				
	165-179	4.99E-03				
	179-192	2.49E-03				
	192-205	3.36E-03	0.498	0.082	0.051	
102.55	152-165	1.23E-02				
	165-179	5.50E-03				
	179-192	2.63E-03				
	192-205	2.90E-03	0.509	0.146	0.095	
104.07	152-165	1.36E-02				
	165-179	2.47E-03				
	179-192	7.83E-04	0.550	0.143	0.089	
	192-205					

HORIZONTAL TRANSECT  
GRAIN SIZE ANALYSIS

Transect bearing & distance from central drain (m): N 6 W ,  
3.4m west

dist north edge (m)	depth (cm)	(microns)					
		d 10	d 16	d 30	d 50	d 60	d 84
96.47	152-165						
	165-179						
	179-192						
	192-205	1.680	4.229	10.762	23.796	31.626	116.27
97.99	152-165						
	165-179						
	179-192						
	192-205	26.033	55.954	100.900	150.000	180.000	273.333
99.51	152-165						
	165-179						
	179-192						
	192-205	11.008	18.122	39.009	67.487	77.911	147.07
101.03	152-165						
	165-179						
	179-192						
	192-205	17.153	36.776	71.389	123.600	166.667	308.333
102.55	152-165						
	165-179						
	179-192						
	192-205	30.758	34.588	38.805	45.986	52.743	173.33
104.07	152-165						
	165-179						
	179-192						
	192-205	9.206	22.286	43.122	66.386	74.479	95.67

VERTICAL TRANSECT  
HYDRAULIC PROPERTIES

Transect bearing & distance from central drain (m):

N 7.5 W  
7.5m west

Distance from north edge (m): 5.2m (V 6)

Correlate with neutron probe tube #: 6

depth (cm)	photo #	sample #	K(sat) (cm/sec)	porosity	theta (cm <sup>3</sup> /cm <sup>3</sup> )	
					1.5 bar	15 bar
51-65	1	1	6.72E-03			
65-78	1	2	3.61E-03			
78-91	1	3	2.44E-03			
91-104	1	4	7.02E-04	0.520	0.160	0.113
104-119	2	1	5.64E-04			
119-132	2	2	1.26E-03			
132-146	2	3	8.57E-05			
146-158	2	4	2.95E-05	0.445	0.091	0.054
158-171	3	1	4.88E-05			
171-185	3	2	5.19E-06			
185-198	3	3	1.48E-05			
198-211			1.00E-04	0.413	0.069	0.038
211-223	4	1	4.03E-06			
223-236	4	2	6.48E-06			
236-250	4	3	6.19E-06			
250-262	4	4	5.11E-06	0.391	0.036	0.023
262-273	5	1	8.26E-05			
273-287	5	2	5.31E-05			
287-300	5	3	1.23E-05			
300-314			1.02E-05	0.427	0.150	0.093
314-319	6	1	1.97E-05			
319-333	6	2	1.99E-06			
333-346	6	3				
346-359	6	4		0.395	0.041	0.026
369-382	7	1	7.35E-04			
382-395	7	2	1.69E-06			
395-409	7	3	7.33E-06			
409-415			3.26E-06	0.450	0.253	0.133
415-428	8	1				
428-434	Layer 2	2	1.74E-06			
434-441	Layer 1	2	1.74E-06			
441-455	8	3	4.26E-06			
455-463	8	4	9.10E-06	0.489	0.117	0.075
463-478	9	1	3.29E-04			
478-491	9	2	5.83E-06			
491-504	9	3	4.13E-05			
504-518	9	4	3.73E-05	0.484	0.146	0.089
518-533	10	1	2.28E-05			
533-546	10	2	1.57E-06			
546-559	10	3	1.02E-05			
559-564	10	4	9.40E-06	0.482	0.191	0.148

VERTICAL TRANSECT  
GRAIN SIZE ANALYSIS

Transect bearing & distance from central drain (m):

N 7.5 W  
7.5m west

Distance from north edge (m): 5.2m (V 6)

Correlate with neutron probe tube #: 6

depth (cm)	(microns)					
	d 10	d 16	d 30	d 50	d 60	d 84
51-65						
65-78						
78-91						
91-104	2.811	7.684	22.190	53.375	83.267	166.66
104-119						
119-132						
132-146						
146-158	10.314	23.883	43.353	67.286	77.067	123.60
158-171						
171-185						
185-198						
198-211	15.966	33.332	50.464	68.647	76.033	117.73
211-223						
223-236						
236-250						
250-262	57.745	69.788	101.867	150.000	173.333	246.667
262-273						
273-287						
287-300						
300-314	2.063	6.544	22.190	53.375	78.959	180.000
314-319						
319-333						
333-346						
346-359	17.025	36.875	70.370	102.900	123.600	180.00
359-382						
382-395						
395-409						
409-415	2.072	3.854	8.635	29.922	45.633	163.33
415-428						
428-434						
434-441						
441-455						
455-463	10.141	16.891	26.111	41.336	54.081	69.489
463-478						
478-491						
491-504						
504-518	4.835	12.091	27.258	72.221	97.733	186.667
518-533						
533-546						
546-559						
559-564	5.070	9.533	27.575	65.361	104.967	261.667

VERTICAL TRANSECT  
HYDRAULIC PROPERTIES

Transect bearing & distance from central drain (m):

N 7.5 W  
7.5m west

Distance from north edge (m): 5.2m (V 6)

Correlate with neutron probe tube #: 6

depth (cm)	photo #	sample #	K(sat) (cm/sec)	porosity	theta (cm <sup>3</sup> /cm <sup>3</sup> )	
					1.5 bar	15 bar
564-573	11	1	6.54E-05			
578-592	11	2	6.88E-06			
592-604	Layer 1 11	3	2.67E-05			
604-605	Soil 11	3	2.67E-05			
605-617	11	4	3.48E-06	0.616	0.387	0.343
617-627	12	3	4.54E-05			
627-640	12	4	4.00E-04	0.490	0.187	0.156

VERTICAL TRANSECT  
GRAIN SIZE ANALYSIS

Transect bearing & distance from central drain (m):

---

N 7.5 W  
7.5m west

Distance from north edge (m): 5.2m (V 6)

---

Correlate with neutron probe tube #: 6

---

depth (cm)	(microns)					
	d 10	d 16	d 30	d 50	d 60	d 84
564-578						
578-592						
592-604						
604-605						
605-617	5.084	7.229	10.942	34.418	142.667	646.667
617-627						
627-640	0.868	2.257	10.329	84.631	147.067	465.833

VERTICAL TRANSECT  
HYDRAULIC PROPERTIES

Transect bearing & distance from central drain (m):

---

N 7.5 W  
7.5m west

Distance from north edge (m): 29.6m (V 7)

---

Correlate with neutron probe tube #: 7

---

depth (cm)	photo #	sample #	K(sat) (cm/sec)	porosity	theta (cm <sup>3</sup> /cm <sup>3</sup> )	
					1.5 bar	15 bar
0-11	1	1	1.16E-05			
11-25	1	2	2.66E-06			
25-38	1	3	1.65E-05			
38-51	1	4	1.76E-05	0.546	0.406	0.295
51-62	2	1	2.39E-06			
62-76	2	2	8.51E-07			
76-89	2	3	6.13E-07			
89-94	2	4	6.05E-07	0.614	0.467	0.197
94-106	3	2	1.10E-04			
106-120	3	3	4.68E-05			
120-133	3	4	2.16E-06	0.622	0.406	0.232

VERTICAL TRANSECT  
GRAIN SIZE ANALYSIS

Transect bearing & distance from central drain (m):

N 7.5 W  
7.5m wes

Distance from north edge (m): 29.6m (V 7)

Correlate with neutron probe tube #: 7

depth (cm)	(microns)					
	d 10	d 16	d 30	d 50	d 60	d 84
0-11						
11-25						
25-38						
38-51	2.090	3.546	6.813	17.807	26.976	206.667
51-62						
62-76						
76-89						
89-94	1.178	1.849	4.202	9.813	13.377	36.071
94-106						
106-120						
120-133	0.970	1.549	4.202	9.813	14.143	30.097



VERTICAL TRANSECT  
HYDRAULIC PROPERTIES

Transect bearing & distance from central drain (m):

N 7.5 W  
7.5m west

Distance from north edge (m): 46.9m (V 47)

Correlate with neutron probe tube #: 8

depth (cm)	photo #	sample #	K(sat) (cm/sec)	porosity	theta (cm <sup>3</sup> /cm <sup>3</sup> )	
					1.5 bar	15 bar
0-11	1	1	7.75E-06			
11-25	1	2	1.49E-06			
25-38	1	3	8.92E-07			
38-51	1	4	8.33E-07	0.534	0.351	0.216
53-62	2	1	3.29E-07			
62-75	2	2	2.60E-07			
75-88	2	3	4.34E-07			
88-101	2		3.93E-08	0.628	0.433	0.311
107-121	3	1	1.40E-06			
121-134	3	2	5.13E-06			
134-148	3	3	4.31E-06			
148-152			1.59E-06	0.555	0.377	0.182
152-166	4	1	1.63E-04			
166-179	4	2	2.79E-06			
179-193	4	3	1.42E-06			
193-206			4.21E-06	0.536	0.386	0.228
211-225	5	1	3.21E-05			
225-239	5	2	1.12E-06			
239-252	5	3	1.19E-06			
252-265			1.19E-06			
269-285	6	1	3.37E-06			
285-298	6	2	5.04E-07			
298-311	6	3	3.97E-07			
311-324			4.46E-07			
324-339	Layer 2	7				
339-371	Layer 1	7				
371-385		8	1	2.69E-05		
385-393	Layer 1	8	2	2.31E-04		
393-398	Soil	8	2	2.31E-04		
398-412		8	3	1.37E-06		
412-425		8	4	5.27E-07	0.491	0.205
429-442		9				0.147
442-455		9				
455-468		9				
468-480		9		0.443	0.183	0.129

VERTICAL TRANSECT  
GRAIN SIZE ANALYSIS

Transect bearing & distance from central drain (m):

N 7.5 W  
7.5m wes

Distance from north edge (m): 46.9m (V 47)

Correlate with neutron probe tube #: 8

depth (cm)	(microns)					
	d 10	d 16	d 30	d 50	d 60	d 84
0-11						
11-25						
25-38						
38-51	11.606	12.632	14.349	16.769	20.514	80.167
53-62						
62-75						
75-88						
88-101	0.514	0.708	1.608	4.065	5.005	16.459
107-121						
121-134						
134-148						
148-152	0.759	1.181	3.519	7.363	11.974	24.464
152-166						
166-179						
179-193						
193-206	4.483	4.814	5.364	7.296	9.059	18.792
211-225						
225-239						
239-252						
252-265						
269-285						
285-298						
298-311						
311-324						
324-339						
339-371						
371-385						
385-393						
393-398						
398-412						
412-425	0.470	1.658	15.187	136.800	196.667	967.333
429-442						
442-455						
455-468						
468-480	1.384	5.103	23.965	92.567	142.667	547.500

VERTICAL TRANSECT  
HYDRAULIC PROPERTIES

Transect bearing & distance from central drain (m):

N 7.5 W  
7.5m west

Distance from north edge (m): 72.2m (V 75)

Correlate with neutron probe tube #: 9

depth (cm)	photo #	sample #	K(sat) (cm/sec)	porosity	theta (cm <sup>3</sup> /cm <sup>3</sup> )	
					1.5 bar	15 bar
0-13	1	1	4.75E-05			
13-26	1	2	4.33E-06			
26-40	1	3	1.11E-05			
40-53	1	4	2.37E-05	0.644	0.420	0.287
53-64	2	1	2.09E-05			
64-78	2	2	2.30E-05			
78-91	2	3	1.81E-05			
91-103			4.55E-06	0.467	0.222	0.151
103-118	3	1	1.18E-03			
118-131	3	2	3.05E-04			
131-145	3	3	7.31E-05			
145-157			3.88E-05	0.503	0.077	0.033
157-172	4	1	2.57E-04			
172-186	4	2	4.03E-03			
186-199	4	3	2.45E-04			
199-211			5.86E-05	0.481	0.211	0.091
211-212	5	1	2.20E-03			
212-225	5	2	1.99E-04			
225-238	5	3	4.94E-04			
238-251			1.29E-03	0.464	0.143	0.049
251-265	6	1	2.03E-05			
265-280	6	2	6.02E-06			
280-293	6	3	1.13E-06			
293-306 Layer 2	6	4	7.42E-07	0.520	0.370	0.240
309-322 Layer 1	7	1	3.86E-03			
322-336	7	2	7.16E-04			
336-344 Layer 1	7	3	1.05E-04			
344-349 Soil	7	3	1.05E-04			
349-362	7	4		0.437	0.167	0.125
362-409	8					
409-412	8			0.456	0.223	0.164

VERTICAL TRANSECT  
GRAIN SIZE ANALYSIS

Transect bearing & distance from central drain (m):

---

N 7.5 W  
7.5m west

Distance from north edge (m): 72.2m (V 75)

---

Correlate with neutron probe tube #: 9

---

depth (cm)	(microns)					
	d 10	d 16	d 30	d 50	d 60	d 84
0-13						
13-26						
26-40						
40-53	✓ 10.083	19.003	32.756	45.809	63.323	320.000
53-64						
64-78						
78-91						
91-103	1.323	3.729	9.268	22.693	31.174	49.705
103-118						
118-131						
131-145						
145-157	6.443	16.492	34.733	51.082	65.076	116.26
157-172						
172-186						
186-199						
199-211	2.660	5.152	15.485	33.062	40.133	82.23
211-212						
212-225						
225-238						
238-251	3.344	7.279	29.690	61.219	84.300	170.00
251-265						
265-280						
280-293						
293-306	0.706	1.449	3.343	8.685	13.627	35.806
309-322						
322-336						
336-344						
344-349						
349-362	1.326	4.387	42.550	122.133	220.000	600.00
362-409						
409-412	0.675	1.052	9.639	56.523	71.814	203.333

VERTICAL TRANSECT  
HYDRAULIC PROPERTIES

Transect bearing & distance from central drain (m):

---

N 7.5 W  
7.5m west

Distance from north edge (m): 78.6m (V 10)

---

Correlate with neutron probe tube #: 10

---

depth (cm)	photo #	sample #	K(sat) (cm/sec)	porosity	theta (cm <sup>3</sup> /cm <sup>3</sup> )	
					1.5 bar	15 bar
0-12	1	1	4.31E-04			
12-25	1	2	6.64E-04			
25-39	1	3	7.45E-05			
39-51	1	4	1.73E-04	0.571	0.137	0.081
51-65	2	1	9.18E-05			
65-79	2	2	4.37E-04			
79-92	2	3	6.44E-05			
92-102	2	4	3.43E-05	0.375	0.058	0.025
102-116	3	1	1.53E-05			
116-129	3	2	2.34E-05			
129-142	3	3	3.16E-04			
142-152	3	4	4.66E-06	0.471	0.192	0.117
152-165	4	1	2.60E-05			
165-178	4	2	1.11E-05			
178-192	4	3	2.01E-05			
192-203	4	4	4.70E-05	0.405	0.065	0.032
203-216	5	1	1.74E-04			
216-230	5	2	1.12E-04			
230-243	5	3	8.56E-05			
243-252	5	4	4.77E-04	0.387	0.064	0.030
252-260	6	1	5.94E-05			
260-273	6	2	5.59E-05			
273-287	6	3	2.43E-05			
287-299	6	4	1.02E-04	0.439	0.081	0.041
299-312	7	1	4.86E-06			
312-325	7	2	1.92E-06			
325-338	7	3	1.47E-06			
338-351	7	4	1.02E-05	0.422	0.089	0.042
363-376	8	1	5.24E-06			
376-387 Layer 2	8	2	1.07E-06			
Soil	8					
413-416				0.412	0.263	0.201

VERTICAL TRANSECT  
GRAIN SIZE ANALYSIS

Transect bearing & distance from central drain (m):

---

N 7.5 W  
7.5m wes

Distance from north edge (m): 78.6m (V 10)

---

Correlate with neutron probe tube #: 10

---

depth (cm)	(microns)					
	d 10	d 16	d 30	d 50	d 60	d 84
0-12						
12-25						
25-39						
39-51	3.679	12.544	30.908	53.107	68.092	138.267
51-65						
65-79						
79-92						
92-102	13.529	19.537	35.146	49.063	56.779	77.722
102-116						
116-129						
129-142						
142-152	2.882	5.530	14.239	26.843	34.387	72.94
152-165						
165-178						
178-192						
192-203	14.461	28.032	60.729	111.867	141.200	216.66
203-216						
216-230						
230-243						
243-252	17.165	39.643	92.567	156.667	190.000	290.83
252-260						
260-273						
273-287						
287-299	11.333	18.227	39.737	69.664	87.918	183.333
299-312						
312-325						
325-338						
338-351	7.388	17.339	36.568	62.845	72.164	144.133
363-376						
376-387						
Soil						
413-416	1.337	4.138	13.963	74.111	132.400	646.667

VERTICAL TRANSECT  
HYDRAULIC PROPERTIES

Transect bearing & distance from central drain (m):

N 7.5 W  
7.5m west

Distance from north edge (m): 102.3m (V 11)

Correlate with neutron probe tube #: 11

depth (cm)	photo #	sample #	K(sat) (cm/sec)	porosity	theta (cm <sup>3</sup> /cm <sup>3</sup> )	
					1.5 bar	15 bar
0-11	1	1	3.66E-04			
11-25	1	2	1.89E-04			
25-38	1	3	2.50E-05			
38-51	1	4	4.25E-04	0.518	0.169	0.130
51-66	2	1	4.23E-02			
66-79	2	2	1.09E-02			
79-92	2	3	2.77E-03			
92-102	2	4	1.61E-03	0.578	0.158	0.100
102-116	3	1	3.41E-03			
116-129	3	2	1.18E-03			
129-142	3	3	1.42E-03			
142-152	3	4	7.18E-03	0.557	0.084	0.060
152-162				0.574	0.109	0.083
hardpan						
191-205	4	1	1.90E-03			
205-218	4	2	2.13E-04			
218-231	4	3	1.21E-03			
231-246			1.81E-05	0.452	0.197	0.084
246-260	5	1	1.67E-04			
260-274	5	2	6.89E-04			
274-287	5	3	4.38E-04			
287-300	5	4		0.424	0.080	0.044
300-313	6	1	4.84E-04			
313-326	6	2	7.01E-04			
326-339	6	3	3.15E-05			
339-345			4.76E-04	0.508	0.102	0.061
hardpan						
379-386 Layer 2	7	1	5.14E-02			
386-393 Soil	7	1	5.14E-02			
393-406	7	2	2.45E-02			
406-419	7	3	9.38E-02			
419-434			1.40E-03	0.441	0.231	0.176
450-453				0.414	0.164	0.126

VERTICAL TRANSECT  
GRAIN SIZE ANALYSIS

Transect bearing & distance from central drain (m):

N 7.5 W  
7.5m west

Distance from north edge (m): 102.3m (V 11)

Correlate with neutron probe tube #: 11

depth (cm)	(microns)					
	d 10	d 16	d 30	d 50	d 60	d 84
0-11						
11-25						
25-38						
38-51	24.710	43.874	69.753	92.567	119.200	210.000
51-66						
66-79						
79-92						
92-102	12.663	25.338	42.894	65.565	73.428	120.667
102-116						
116-129						
129-142						
142-152	24.710	52.607	69.703	76.033	103.933	163.333
152-162	18.495	31.024	61.936	97.733	120.667	180.000
hardpan						
191-205						
205-218						
218-231						
231-246	2.979	7.022	23.014	50.978	69.815	135.333
246-260						
260-274						
274-287						
287-300	24.710	52.607	71.028	114.800	142.667	236.667
300-313						
313-326						
326-339						
339-345	30.71	37.68	51.12	91.53	113.33	186.67
hardpan						
379-386						
386-393						
393-406						
406-419						
419-434	0.749	1.248	7.746	56.511	104.967	325.833
450-453	0.971	3.564	23.638	116.267	196.667	1253.333



VERTICAL TRANSECT  
THETA/PSI DATA

Transect bearing & distance from central drain (m): N 7.5 W  
7.5m west

Distance from north edge (m): 5.2m (V 6)

Correlate with neutron probe tube #: 6

sample depth (cm): 258-261

Lab data		Output from van Genuchten model				Diffus
theta	psi	psi	theta	Rel K	Abs K	
0.391	0.00E+00	0.00E+00	0.391	1.00E+00	5.11E-06	
0.394	1.25E+01	1.41E+00	0.391	9.98E-01	5.10E-06	4.94E-01
0.393	2.60E+01	1.68E+00	0.391	9.97E-01	5.10E-06	3.64E-01
0.386	4.05E+01	2.00E+00	0.391	9.96E-01	5.09E-06	2.69E-01
0.300	5.40E+01	2.37E+00	0.391	9.94E-01	5.09E-06	1.98E-01
0.263	6.35E+01	2.82E+00	0.391	9.92E-01	5.08E-06	1.46E-01
0.225	7.70E+01	3.35E+00	0.391	9.90E-01	5.06E-06	1.07E-01
0.191	9.10E+01	3.98E+00	0.391	9.86E-01	5.04E-06	7.90E-02
0.160	1.07E+02	4.73E+00	0.391	9.81E-01	5.02E-06	5.80E-02
0.151	1.24E+02	5.62E+00	0.391	9.74E-01	4.98E-05	4.26E-02
0.141	1.39E+02	6.68E+00	0.391	9.65E-01	4.94E-06	3.11E-02
0.134	1.54E+02	7.94E+00	0.390	9.53E-01	4.87E-06	2.27E-02
0.053	5.09E+02	9.44E+00	0.390	9.37E-01	4.79E-06	1.65E-02
0.045	1.02E+03	1.12E+01	0.389	9.15E-01	4.68E-06	1.20E-02
0.036	1.53E+03	1.33E+01	0.388	8.85E-01	4.53E-06	8.61E-03
0.031	3.05E+03	1.58E+01	0.387	8.46E-01	4.33E-06	6.14E-03
0.023	1.53E+04	1.88E+01	0.384	7.95E-01	4.06E-06	4.33E-03
		2.24E+01	0.381	7.29E-01	3.73E-06	3.02E-03
		2.66E+01	0.375	6.47E-01	3.31E-06	2.07E-03
		3.16E+01	0.366	5.49E-01	2.81E-06	1.39E-03
		3.76E+01	0.352	4.38E-01	2.24E-06	9.10E-04
		4.47E+01	0.333	3.22E-01	1.65E-06	5.80E-04
		5.31E+01	0.308	2.15E-01	1.10E-06	3.58E-04
		6.31E+01	0.277	1.28E-01	6.56E-07	2.15E-04
		7.50E+01	0.243	6.79E-02	3.47E-07	1.25E-04
		8.91E+01	0.207	3.20E-02	1.64E-07	7.13E-05
		1.06E+02	0.173	1.37E-02	6.99E-08	3.98E-05
		1.26E+02	0.143	5.39E-03	2.76E-08	2.19E-05
		1.50E+02	0.118	2.01E-03	1.03E-08	1.19E-05
		1.78E+02	0.098	7.16E-04	3.66E-09	6.43E-06
		2.11E+02	0.083	2.49E-04	1.27E-09	3.46E-06
		2.51E+02	0.071	8.51E-05	4.35E-10	1.85E-06
		2.99E+02	0.062	2.87E-05	1.47E-10	9.92E-07
		3.55E+02	0.056	9.60E-06	4.91E-11	5.28E-07
		4.22E+02	0.051	3.21E-06	1.64E-11	2.83E-07
		5.01E+02	0.047	1.07E-06	5.46E-12	1.51E-07
		5.96E+02	0.044	3.55E-07	1.82E-12	8.06E-08
		7.08E+02	0.042	1.18E-07	6.03E-13	4.30E-08
		8.41E+02	0.041	3.91E-08	2.00E-13	2.30E-08

Lab data		Output from van Genuchten model				
theta	psi	psi	theta	Rel K	Abs K	Diffus
		1.00E+03	0.040	1.30E-08	6.63E-14	1.23E-08
		1.19E+03	0.039	4.30E-09	2.20E-14	6.54E-09
		1.41E+03	0.038	1.42E-09	7.28E-15	3.49E-09
		1.68E+03	0.038	4.72E-10	2.41E-15	1.86E-09
		2.00E+03	0.038	1.56E-10	8.00E-16	9.93E-10
		2.37E+03	0.037	5.18E-11	2.65E-16	5.30E-10
		2.82E+03	0.037	1.72E-11	8.77E-17	2.83E-10
		3.35E+03	0.037	5.68E-12	2.91E-17	1.51E-10
		3.98E+03	0.037	1.88E-12	9.63E-18	8.04E-11
		4.73E+03	0.037	6.24E-13	3.19E-18	4.29E-11
		5.62E+03	0.037	2.07E-13	1.06E-18	2.29E-11
		6.68E+03	0.037	6.85E-14	3.50E-19	1.22E-11
		7.94E+03	0.037	2.27E-14	1.16E-19	6.51E-12
		9.44E+03	0.037	7.51E-15	3.84E-20	3.47E-12
		1.12E+04	0.037	2.49E-15	1.27E-20	1.85E-12
		1.33E+04	0.037	8.24E-16	4.22E-21	9.89E-13
		1.58E+04	0.037	2.73E-16	1.40E-21	5.27E-13

VERTICAL TRANSECT  
THETA/PSI DATA

Transect bearing & distance from central drain (m): N 7.5 W  
 Distance from north edge (m): 46.9m (V 47) 7.5m west  
 Correlate with neutron probe tube #: 8  
 sample depth (cm): 103-106

Lab data		Output from van Genuchten model				
theta	psi	psi	theta	Rel K	Abs K	Diffus
0.628	0.00E+00	0.00E+00	0.628	1.00E+00	3.93E-08	
0.625	1.00E+01	1.41E+00	0.628	3.01E-01	1.19E-08	4.31E-05
0.619	1.90E+01	1.68E+00	0.628	2.87E-01	1.13E-08	4.00E-05
0.616	2.65E+01	2.00E+00	0.628	2.73E-01	1.07E-08	3.69E-05
0.612	4.00E+01	2.37E+00	0.627	2.58E-01	1.02E-08	3.40E-05
0.605	5.90E+01	2.82E+00	0.627	2.44E-01	9.59E-09	3.13E-05
0.599	8.70E+01	3.35E+00	0.627	2.30E-01	9.03E-09	2.87E-05
0.590	1.12E+02	3.98E+00	0.627	2.15E-01	8.47E-09	2.62E-05
0.580	1.32E+02	4.73E+00	0.627	2.01E-01	7.91E-09	2.38E-05
0.571	1.61E+02	5.62E+00	0.626	1.87E-01	7.36E-09	2.16E-05
0.506	5.08E+02	6.68E+00	0.626	1.73E-01	6.81E-09	1.95E-05
0.468	1.02E+03	7.94E+00	0.626	1.60E-01	6.27E-09	1.76E-05
0.433	1.53E+03	9.44E+00	0.625	1.46E-01	5.75E-09	1.58E-05
0.399	3.05E+03	1.12E+01	0.624	1.33E-01	5.23E-09	1.41E-05
0.348	7.12E+03	1.33E+01	0.624	1.20E-01	4.73E-09	1.25E-05
0.311	1.53E+04	1.58E+01	0.623	1.08E-01	4.25E-09	1.10E-05
		1.88E+01	0.621	9.63E-02	3.79E-09	9.71E-06
		2.24E+01	0.620	8.50E-02	3.34E-09	8.49E-06
		2.66E+01	0.618	7.44E-02	2.93E-09	7.38E-06
		3.16E+01	0.616	6.44E-02	2.53E-09	6.38E-06
		3.76E+01	0.614	5.52E-02	2.17E-09	5.49E-06
		4.47E+01	0.611	4.67E-02	1.84E-09	4.69E-06
		5.31E+01	0.608	3.90E-02	1.54E-09	3.98E-06
		6.31E+01	0.604	3.22E-02	1.27E-09	3.36E-06
		7.50E+01	0.600	2.62E-02	1.03E-09	2.82E-06
		8.91E+01	0.595	2.09E-02	8.23E-10	2.36E-06
		1.06E+02	0.589	1.65E-02	6.49E-10	1.96E-06
		1.26E+02	0.583	1.28E-02	5.04E-10	1.62E-06
		1.50E+02	0.576	9.80E-03	3.85E-10	1.34E-06
		1.78E+02	0.568	7.37E-03	2.90E-10	1.10E-06
		2.11E+02	0.559	5.47E-03	2.15E-10	8.97E-07
		2.51E+02	0.550	4.00E-03	1.57E-10	7.31E-07
		2.99E+02	0.541	2.89E-03	1.13E-10	5.95E-07
		3.55E+02	0.531	2.06E-03	8.09E-11	4.84E-07
		4.22E+02	0.520	1.45E-03	5.70E-11	3.92E-07
		5.01E+02	0.509	1.01E-03	3.98E-11	3.18E-07
		5.96E+02	0.498	7.01E-04	2.75E-11	2.57E-07
		7.08E+02	0.487	4.81E-04	1.89E-11	2.08E-07
		8.41E+02	0.476	3.28E-04	1.29E-11	1.68E-07

Lab data		Output from van Genuchten model				
theta	psi	psi	theta	Rel K	Abs K	Diffus
		1.00E+03	0.465	2.22E-04	8.75E-12	1.35E-07
		1.19E+03	0.454	1.50E-04	5.90E-12	1.09E-07
		1.41E+03	0.443	1.01E-04	3.97E-12	8.82E-08
		1.68E+03	0.432	6.75E-05	2.66E-12	7.12E-08
		2.00E+03	0.421	4.51E-05	1.77E-12	5.74E-08
		2.37E+03	0.411	3.00E-05	1.18E-12	4.63E-08
		2.82E+03	0.400	2.00E-05	7.85E-13	3.73E-08
		3.35E+03	0.390	1.33E-05	5.21E-13	3.01E-08
		3.98E+03	0.380	8.78E-06	3.45E-13	2.42E-08
		4.73E+03	0.371	5.81E-06	2.29E-13	1.95E-08
		5.62E+03	0.361	3.84E-06	1.51E-13	1.57E-08
		6.68E+03	0.352	2.54E-06	9.99E-14	1.27E-08
		7.94E+03	0.343	1.68E-06	6.60E-14	1.02E-08
		9.44E+03	0.334	1.11E-06	4.35E-14	8.23E-09
		1.12E+04	0.326	7.31E-07	2.87E-14	6.63E-09
		1.33E+04	0.318	4.82E-07	1.89E-14	5.34E-09
		1.58E+04	0.309	3.18E-07	1.25E-14	4.31E-09

NEUTRON PROBE DATA  
(MOISTURE CONTENT CM3/CM3)

Tube #: 6

Bearing & Distance from central drain : N 340, 38.7 (m)

Depth (cm)	Julian date (reference 1/1/86)				
	85	135	177	268	276
30.48	0.278	0.290	0.312	0.247	0.226
60.96	0.152	0.168	0.149	0.161	0.174
91.44	0.131	0.138	0.132	0.152	0.167
121.92	0.099	0.111	0.096	0.116	0.133
152.40	0.082	0.093	0.082	0.092	0.092
182.88	0.159	0.169	0.154	0.158	0.162
213.36	0.064	0.078	0.064	0.065	0.075
243.84	0.082	0.109	0.084	0.083	0.094
274.32	0.072	0.090	0.074	0.086	0.082
304.80	0.237	0.263	0.241	0.082	0.236
335.28	0.223	0.250	0.231	0.238	0.225
365.76	0.080	0.102	0.083	0.219	0.083
396.24	0.167	0.193	0.164	0.080	0.166
426.72	0.125	0.146	0.127	0.160	0.127
457.20	0.316	0.345	0.327	0.127	0.320
487.68	0.172	0.177	0.172	0.327	0.169
518.16	0.166	0.183	0.174	0.181	0.171
548.64	0.304	0.328	0.306	0.181	0.313
579.12	0.269	0.287	0.270	0.315	0.276
609.60	0.223	0.244	0.319	0.272	0.230
640.08	0.333	0.343	0.335	0.218	0.340
670.56	0.305	0.322	0.312	0.333	0.309
701.04	0.204	0.213	0.202	0.200	0.209
731.52	0.229	0.242	0.227	0.240	0.231
762.00	0.292	0.313	0.297	0.303	
792.48					
822.96					
853.45					
883.42					

NEUTRON PROBE DATA  
(MOISTURE CONTENT CM3/CM3)

Tube #: 9

Bearing & Distance from central drain : N 198, 26.2 (m)

Depth (cm)	Julian date (reference 1/1/86)				
	85	135	177	268	276
30.48	0.511	0.530	0.553	0.541	0.550
60.96	0.356	0.375	0.364	0.351	0.362
91.44	0.383	0.396	0.392	0.393	0.408
121.92	0.258	0.264	0.260	0.283	0.304
152.40	0.310	0.320	0.320	0.320	0.333
182.88	0.133	0.126	0.127	0.145	0.163
213.36	0.143	0.143	0.142	0.160	0.174
243.84	0.164	0.163	0.161	0.214	0.235
274.32	0.368	0.381	0.357	0.401	0.424
304.80	0.470	0.485	0.474	0.470	0.490
335.28	0.359	0.354	0.354	0.390	0.421
365.76	0.383	0.392	0.382	0.392	0.416
396.24	0.326	0.326	0.319	0.331	0.428
426.72				0.376	0.393
457.20					
487.68					
518.16					
548.64					
579.12					
609.60					
640.08					
670.56					
701.04					
731.52					
762.00					
792.48					
822.96					
853.45					
883.42					

NEUTRON PROBE DATA  
(MOISTURE CONTENT CM3/CM3)

Tube #: 10

---

Bearing & Distance from central drain : N 190, 36.9 (m)

---

Depth (cm)	Julian date (reference 1/1/86)				
	85	135	177	268	276
30.48	0.373	0.397	0.444	0.336	0.319
60.96	0.265	0.324	0.284	0.267	0.273
91.44	0.165	0.210	0.163	0.161	0.173
121.92	0.102	0.137	0.106	0.100	0.110
152.40	0.101	0.138	0.108	0.100	0.112
182.88	0.122	0.159	0.127	0.123	0.132
213.36	0.126	0.159	0.127	0.120	0.131
243.84	0.122	0.163	0.123	0.120	0.136
274.32	0.080	0.117	0.083	0.086	0.099
304.80	0.124	0.177	0.121	0.126	0.133
335.28	0.256	0.311	0.261	0.249	0.303
365.76	0.135	0.184	0.134	0.142	0.202
396.24	0.393	0.455	0.394	0.386	0.454
426.72	0.345	0.402	0.352	0.349	0.404
457.20					
487.68					
518.16					
548.64					
579.12					
609.60					
640.08					
670.56					
701.04					
731.52					
762.00					
792.48					
822.96					
853.45					
883.42					

NEUTRON PROBE DATA  
(MOISTURE CONTENT CM3/CM3)

Tube #: 11

Bearing & Distance from central drain : N 186, 60 (m)

Depth (cm)	85	Julian date 135	(reference 177	268	1/1/86) 276
30.48	0.340	0.344	0.340	0.298	0.326
60.96	0.110	0.127	0.108	0.105	0.139
91.44	0.138	0.161	0.143	0.134	0.161
121.92	0.091	0.107	0.091	0.090	0.117
152.40	0.134	0.155	0.138	0.137	0.177
182.88	0.109	0.131	0.110	0.109	0.155
213.36	0.077	0.103	0.078	0.077	0.101
243.84	0.123	0.142	0.125	0.121	0.157
274.32	0.066	0.088	0.066	0.066	0.097
304.80	0.089	0.107	0.089	0.086	0.126
335.28	0.128	0.150	0.129	0.126	0.170
365.76	0.147	0.178	0.144	0.144	0.190
396.24	0.219	0.253	0.225	0.220	0.268
426.72	0.199	0.225	0.199	0.196	0.243
457.20					
487.68					
518.16					
548.64					
579.12					
609.60					
640.08					
670.56					
701.04					
731.52					
762.00					
792.48					
822.96					
853.45					
883.42					



APPENDIX JSample statistics from layer 1 and underlying soilLayer 1

Sample statistics for the first layer are listed below. These values (mean and standard deviation) were found to vary greatly from the overlying second layer. The standard deviation values, as a whole, tend to be less in the first layer. This signifies a more uniform media. The mean values of the 3 transects decrease to the north. This is the same pattern that exists along the second layer from the south edge towards the center. Any interpretations made using the sample statistics from the first layer should be done with caution due to the paucity of data from this layer.

TABLE J1Vertical transects statistics: LAYER 1

units: see table 2

<u>Variable, transect</u>	<u># of samples</u>	<u>Mean</u>	<u>Std deviation</u>	<u>Range</u>
log K, V6	11	-5.071	0.455	1.420
" , V47	2	-4.103	0.467	0.934
" , V75	3	-3.179	0.639	1.564
n , V6	3	0.485	0.003	0.007
$\theta_{1.5}$ , V6	3	0.151	0.030	0.074
$\theta_{15}$ , V6	3	0.104	0.032	0.073
$d_{10}$ , V6	3	6.682	2.448	5.306
$d_{16}$ , V6	3	12.838	3.050	7.538
$d_{30}$ , V6	3	26.981	0.629	1.464
$d_{50}$ , V6	3	59.639	13.242	30.885
$d_{60}$ , V6	3	85.594	22.478	50.886
$d_{84}$ , V6	3	172.608	79.084	192.178
GM , V6	3	43.904	6.892	15.685

Soil

The sample statistics from the underlying soil would lead one to believe that a great deal of variability exists in this horizon as well. However, this variability is believed to be due more to sampling error than actual variability in the soil. The soil is very poorly sorted with 0.5 to 2.0 cm diameter pebbles common. These pebbles made sampling quite difficult and often times impossible. Contacting these pebbles during sampling destroyed the shelly tube's cutting edge and severely affected the quality of the sample. Due to this, piping occurred in approximately half of the soil samples during permeability tests. Permeability measurements taken from samples where piping was suspected were discarded. Therefore, it is quite possible that, due to the effects of piping, the actual log K mean value is lower than the calculated value listed.

TABLE J2Vertical transects statistics: SOIL

units: see table 2

<u>Variable</u>	<u># of samples</u>	<u>Mean</u>	<u>Std deviation</u>	<u>Range</u>
log K	8	-4.691	0.994	2.641
n	9	0.467	0.059	0.204
$\theta_{1.5}$	9	0.224	0.066	0.223
$\theta_{15}$	9	0.174	0.064	0.218
$d_{10}$	9	1.429	1.327	4.614
$d_{16}$	9	3.404	1.932	6.177
$d_{30}$	9	17.551	10.415	34.804
$d_{50}$	9	85.996	32.297	102.382
$d_{60}$	9	150.546	44.497	148.186
$d_{34}$	9	628.500	300.387	1050.000
GM	9	44.262	17.910	53.746

## APPENDIX K

Computer code for program: VGRAM

```

00100 C-----
00200 C      THIS PROGRAM COMPUTES THE VARIOGRAM ('RAW VARIOGRAM')
00300 C      FOR EACH SPATIAL VARIABLE (UP TO 7).
00400 C      EXPERIMENTAL VALUES ARE IN 2-DIMENSIONAL SPACE AND MAY
00500 C      BE UNEVENLY SPACED.
00600 C      USUAL STATISTICAL MOMENTS ARE ALSO COMPUTED.
00700 C-----
00800 C      NVR( ):      DUMMY VECTOR
00900 C      X(I),Y(I):   COORDINATES OF THE EXPERIMENTAL VALUE # I
01000 C                  CARTESIAN COORDINATE SYSTEM. ARBITRARY ORIGIN
01100 C                  DOWN LEFT (ALL VALUES IN THE FIRST QUADRANT)
01200 C      Z( , ):     EXPERIMENTAL VALUES OF THE SPATIAL VARIABLES
01300 C      OFF( ):     CUT-OFF VALUES FOR THE VARIABLES. IF Z( , , I)
01400 C                  .LE.OFF(I), THIS VALUE IS DISCARDED FROM THE
01500 C                  ANALYSIS.
01600 C      NCL( ):     # OF COUPLES
01700 C      AL( ):     AVERAGE LENGTHS
01800 C      VG( ):     VARIOGRAM VALUES
01900 C      STEP:     BASIC VALUE OF H. SHOULD BE AROUND 1/100 OF THE
02000 C                  DIAMETER OF THE REGION.
02100 C      NVAR:     # OF VARIABLES (UP TO 7)
02200 C      NEV:     # OF EXPERIMENTAL VALUES (UP TO 200)
02300 C      MNP:     MAXIMUM # OF POINTS ON THE ABSISSA OF THE GRAPH
02400 C                  =# OF STEPS + 1
02500 C-----
02600 C      DIMENSION SAN(10),CAN(10)
02700 C      DIMENSION NVR(7),OFF(7),ALODAT(7,200),VGODAT(7,200)
02800 C      COMMON STEP,MNP,NDI,DA,ALP(10)
02900 C      COMMON /ISABEL/X(200),Y(200)/SYLVIE/Z(200,7)
03000 C      COMMON /JACK/NC(250),ALO(250),VGO(250)
03100 C      DOUBLE PRECISION IFLN
03200 C-----INPUT-----
03300 C      TYPE 1000
03400 1000  FORMAT(1X,'# OF EXPERIMENTAL VALUES (UP TO 200):'$)
03500 C      ACCEPT 1010,NEV
03600 1010  FORMAT(I)
03700 C      TYPE 1020
03800 1020  FORMAT(1X,'# OF VARIABLES (UP TO 7):'$)
03900 C      ACCEPT 1030,NVAR
04000 1030  FORMAT(I)
04100 C      TYPE 1040
04200 1040  FORMAT(1X,'STEP: '/1X,'(BASIC VALUE OF H, AROUND 1/100 DIAM.
04300 1      'OF THE REGION,F FORMAT)')
04400 C      ACCEPT 1050,STEP
04500 1050  FORMAT(F)
04600 C      TYPE 1060
04700 1060  FORMAT(1X,'MAX # OF PTS. ON THE ABSISSA OF THE GRAPH'/
04800 1      '(=# STEPS + 1, INTEGER FORMAT):'$)
04900 C      ACCEPT 1070,MNP
05000 1070  FORMAT(I)
05100 C      TYPE 1080
05200 1080  FORMAT(1X,'WHAT IS THE INPUT FILE NAME:$)
05300 C      ACCEPT 1090,IFLN
05400 1090  FORMAT(A10)
05500 C      TYPE 1091
05600 1091  FORMAT(1X,'INPUT 0 FOR ISOTROPIC CASE, 1 FOR ANISOTROPY:$)
05700 C      ACCEPT 1092,ISOTPY
05800 1092  FORMAT(I)
05900 C      IF(ISOTPY .EQ. 0)GO TO 507
06000 C      TYPE 501

```

```

06100 501  FORMAT(' HOW MANY DIRECTIONS DO YOU WANT:'$)
06200      ACCEPT 502,NDI
06300 502  FORMAT(I)
06400      TYPE 503
06500 503  FORMAT(' WHAT IS DELTA-ALPHA:'$)
06600      ACCEPT 504,DA
06700 504  FORMAT(F)
06800      TYPE 505
06900 505  FORMAT(' INPUT ALPHA VALUES, DECIMAL, SEPARATED BY A SPACE:
07000      ACCEPT 506,(ALP(I),I=1,NDI)
07100 506  FORMAT(10F)
07200 507  CONTINUE
07300      OPEN(UNIT=22,ACCESS='SEQIN',FILE=IFLN)
07400      READ(22,1100)(OFF(I),I=1,NVAR)
07500 1100  FORMAT(7F)
07600      READ(22,1110)(X(I),I=1,NEV) !COORDINATES
07700      READ(22,1110)(Y(I),I=1,NEV)
07800      READ(22,1110)((Z(I,J),I=1,NEV),J=1,NVAR) !VARIABLES
07900 1110  FORMAT(8F)
08000      CLOSE(UNIT=22,FILE=IFLN)
08100      WRITE(3,1120)
08200      WRITE(5,1120)
08300 1120  FORMAT(15X,'COORDINATES OF THE EXPERIMENTAL POINTS'/15X,
08400 1      'POINT NO.          X-AXIS          Y-AXIS'/)
08500      DO 10 I=1,NEV
08600          WRITE(3,1130)I,X(I),Y(I)
08700          WRITE(5,1130)I,X(I),Y(I)
08800 1130  FORMAT(18X,I3,9X,F8.2,6X,F8.2)
08900 10     CONTINUE
09000      WRITE(3,1140)
09100      WRITE(5,1140)
09200 1140  FORMAT(//10X,'EXPERIMENTAL VALUES'/)
09300      DO 20 I=1,NVAR
09400          NVR(I)=I
09500 20     CONTINUE
09600      WRITE(3,1150)(NVR(I),I=1,NVAR)
09700      WRITE(5,1150)(NVR(I),I=1,NVAR)
09800 1150  FORMAT(2X,'VARIABLE NO.',5X,10(7X,I2))
09900      DO 30 I=1,NEV
10000          WRITE(3,1160)I,(Z(I,J),J=1,NVAR)
10100          WRITE(5,1160)I,(Z(I,J),J=1,NVAR)
10200 1160  FORMAT(15X,I3,2X,10(2X,F7.2))
10300 30     CONTINUE
10400 C-----DO VARICGRAM CALCULATIONS-----
10500      DO 50 INDEX=1,NVAR
10600          I=INDEX
10700          IF(ISOTPY .EQ. 0)CALL VRGM(I,NEV,OFF(I)) !VARIOGRAM CO
10800          IF(ISOTPY .EQ. 1)CALL ANISOT(I,NEV,OFF(I))
10900 50     CONTINUE
11000      IF(ISOTPY .EQ. 1)GO TO 52
11100      DO 51 K=1,MNP
11200          ALODAT(I,K)=ALO(K)
11300          VGODAT(I,K)=VGO(K)
11400 51     CONTINUE
11500      GO TO 53
11600 52     CONTINUE
11700      DO 53 K=1,NDI*MNP
11800          ALODAT(I,K)=ALO(K)
11900          VGODAT(I,K)=VGO(K)
12000 53     CONTINUE

```

```

12100 OPEN(UNIT=23,ACCESS='SEQOUT',FILE='VGRAM.PLT')
12200 IF(ISOTPY.EQ.0)WRITE(23,1250)((ALODAT(I,K),VGODAT(I,K)),K-1
12300 1 MNP),I=1,NVAR)
12400 IF(ISOTPY.EQ.1)WRITE(23,1250)((ALODAT(I,K),VGODAT(I,K)),K-1
12500 1 NDI*MNP),I=1,NVAR)
12600 1250 FORMAT(2F)
12700 CLOSE(UNIT=23)
12800 9999 STOP
12900 END
13000 C-----
13100 SUBROUTINE VRGM(I,NEV,CUT)
13200 COMMON/JACK/NC(250),ALO(250),VGO(250)/SYLVIE/Z(200,7)
13300 COMMON/ISABEL/X(200),Y(200)
13400 COMMON STEP,MNP
13500 DOUBLE PRECISION T,U,V,W,DSQRT
13600 U=0.0
13700 V=0.0
13800 C-----COMPUTE STATISTICAL MOMENTS-----
13900 DO 40 J=1,NEV
14000 U=U+Z(J,I)
14100 V=V+(Z(J,I)*Z(J,I))
14200 40 CONTINUE
14300 U=U/NEV !MEAN
14400 V=V/NEV-U*U !VARIANCE
14500 W=DSQRT(V) !STANDARD DEVIATION
14600 T=V/U !VARIATION COEFFICIENT
14700 DO 10 J=1,MNP
14800 NC(J)=0
14900 ALO(J)=0.0
15000 VGO(J)=0.0
15100 10 CONTINUE
15200 HMAX=(MNP-1)*STEP !COMPUTE MAX LENGTH
15300 HMAXS=HMAX*HMAX !OF H
15400 C-----LOOK FOR THE COUPLES AND COUNT THEM-----
15500 NP=NEV-1
15600 DO 20 M=1,NP
15700 L=M+1
15800 DO 20 J=L,NEV
15900 IF(Z(J,I).LE.CUT)GO TO 20
16000 IF(Z(M,I).LE.CUT)GO TO 20
16100 XX=X(J)-X(M)
16200 YY=Y(J)-Y(M)
16300 HS=XX*XX+YY*YY
16400 IF(HS+1.E-20-HMAXS)15,15,20
16500 15 H=SQRT(HS)
16600 LFO=H/STEP+1.0
16700 NC(LFO)=NC(LFO)+1 !COUNTING (CLASSES)
16800 ALO(LFO)=ALO(LFO)+H !CUMULATING]
16900 DZ=Z(J,I)-Z(M,I) !LENGTHS ]
17000 VGO(LFO)=VGO(LFO)+0.5*DZ*DZ !LOOK AT VARIOGRAM FORMULA
17100 20 CONTINUE
17200 C-----AVERAGE VALUES-----
17300 DO 30 J=1,MNP
17400 A=AMAX0(1,NC(J))
17500 ALO(J)=ALO(J)/A
17600 VGO(J)=VGO(J)/A
17700 30 CONTINUE
17800 C-----OUTPUT-----
17900 WRITE(3,1170)I,NEV,U,V,W,T
18000 WRITE(5,1170)I,NEV,U,V,W,T

```

```

18100      1170      FORMAT(1H1,50('*'),'VARIABLE NO.',I3,50('*')/5X,'NO. OF'
18200      1      ' DATA:',I4//5X,'**STATISTICAL MOMENTS**'/3X,'MEAN=',E11.4
18300      2      /3X,'VARIANCE=',E11.4/3X,'STANDARD DEVIATION=',E11.4/3X,
18400      3      'VARIATION COEFFICIENT=',E11.4)
18500      WRITE(3,1180)STEP
18600      WRITE(5,1180)STEP
18700      1180      FORMAT(//7X,'RAW VARIOGRAM'/7X,'ALL DIRECTIONS'/7X,
18800      1      'STEP=',F7.2)
18900      WRITE(3,1190)
19000      WRITE(5,1190)
19100      1190      FORMAT(1H0,'ALL DIRECTIONS'/1H0,10X,'STEP NO. OF',
19200      1      ' COUPLES AVERAGE DISTANCE VARIOGRAM'/1H )
19300      DO 31 K=1,MNP
19400      WRITE(3,1200)K,NC(K),ALO(K),VGO(K)
19500      WRITE(5,1200)K,NC(K),ALO(K),VGO(K)
19600      1200      FORMAT(1H ,I12,I10,5X,F14.2,5X,E17.4)
19700      31      CONTINUE
19800      RETURN
19900      END
20000      SUBROUTINE ANISOT(KKK,ND,CUT)
20100      C-----
20200      C      SEMI-VARIOGRAM IN TWO DIMENSIONS.
20300      C      IRREGULAR GRID. THERE MAY BE MISSING DATA.
20400      C      CALCULATION BY ANGLE AND DISTANCE.
20500      C      OBTAINED FROM "MINING GEOSTATISTICS" BY JOURNEL AND
20600      C      HUIJBREGTS.
20700      C-----
20800      C      PARAMETERS-----
20900      C      Z(ND,KKK):          DATA ARRAY
21000      C      X(ND),Y(ND):      X AND Y COORDINATES OF POINTS
21100      C      ND:              NUMBER OF POINTS
21200      C      MNP:            MAXIMUM NUMBER OF COMPUTATION LAGS
21300      C      STEP:          LENGTH OF STEP
21400      C      NDI:           NUMBER OF DIRECTIONS
21500      C      ALP(NDI):       ANGLES DEFINING DIRECTIONS WRT X-AXIS (DEGREE)
21600      C      DA:            WIDTH OF ANGLES. IF DA=0, 45 DEGREES IS ASSUMED
21700      C      NC(MNP*NDI):    NUMBER OF COUPLES/LAG/DIRECTION
21800      C      VGO(MNP*NDI):    VARIOGRAM VALUES/LAG/DIRECTION
21900      C      ALO(MNP*NDI):    AVERAGE DISTANCE/LAG/DIRECTION
22000      C      U:             AVERAGE OF VALID DATA
22100      C      V:             VARIANCE OF VALID DATA
22200      C      N:             NUMBER OF VALID DATA
22300      C-----
22400      C      CAPACITY: 10 DIRECTIONS-----
22500      C      DIMENSION CAN(10),SAN(10)
22600      C      COMMON STEP,MNP,NDI,DA,ALP(10)
22700      C      COMMON/JACK/NC(250),ALO(250),VGO(250)/SYLVIE/Z(200,7)
22800      C      COMMON/ISABEL/X(200),Y(200)
22900      C      DATA IA/' '/
23000      C-----
23100      C      INITIALIZE-----
23200      C      PI=3.14159265
23300      C      DALPHA=DA
23400      C      IF(DA .LE. 0.0)DALPHA=45.0
23500      C      DO 1 KD=1,NDI
23600      C          ALPHA=PI*ALP(KD)/180.0
23700      C          CAN(KD)=COS(ALPHA)
23800      C          SAN(KD)=SIN(ALPHA)
23900      C      1      CONTINUE
24000      C      THETA=PI*DALPHA/180.0
24100      C      CDA=COS(THETA)
24200      C      DO 10 IK=1,MNP*NDI
24300      C          NC(IK)=0

```

```

24100          ALO(IK)=0.0
24200          VGO(IK)=0.0
24300 10      CONTINUE
24400          IF(Z(ND, KKK)-CUT)12,12,13
24500 12      CONTINUE
24600          N=0
24700          U=0.0
24800          V=0.0
24900          GO TO 11
25000 13      CONTINUE
25100          N=1
25200          U=Z(ND, KKK)
25300          V=Z(ND, KKK)*Z(ND, KKK)
25400 11      CONTINUE
25500 C-----COMPUTE SEMI-VARIOGRAM, NEW POINT-----
25600          NDI=ND-1
25700          DO 2 I=1, NDI
25800              VR1=Z(I, KKK)
25900              IF(VR1 .LE. CUT)GO TO 2
26000              N=N+1
26100              U=U+VR1
26200              V=V+VR1*VR1
26300              I1=I+1
26400 C-----NEW LAG-----
26500          DO 21 J=I1, ND
26600              IF(Z(J, KKK) .LE. CUT)GO TO 21
26700              DX=X(J)-X(I)
26800              DY=Y(J)-Y(I)
26900              H=SQRT(DX*DX+DY*DY)
27000              IF(H .LT. 1.0E-03)GO TO 25
27100              K=INT(H/STEP+0.5)+1
27200              HS=H*H
27300              HMAX=(MNP-1)*STEP
27400              HMAXS=HMAX*HMAX
27500              IF((K .GT. MNP) .OR. ((HS-HMAXS) .GT. 1.0E-20))
27600 1          GO TO 21
27700 C-----NEW DIRECTION-----
27800          DO 22 KD=1, NDI
27900              COSD=(DX*CAN(KD)+DY*SAN(KD))/H
28000              IF(ABS(COSD) .GE. CDA)GO TO 23
28100 22      CONTINUE
28200          GO TO 21
28300 23      CONTINUE
28400          IK=K+MNP*(KD-1)
28500          NC(IK)=NC(IK)+1
28600          ALO(IK)=ALO(IK)+H
28700          VRR=Z(J, KKK)-VR1
28800          VGO(IK)=VGO(IK)+0.5*VRR*VRR
28900          GO TO 21
29000 25      CONTINUE
29100          WRITE(3, 2000)I, X(I), Y(I), J, X(J), Y(J)
29200          WRITE(3, 2000)I, X(I), Y(I), J, X(J), Y(J)
29300 21      CONTINUE
29400 2        CONTINUE
29500 333     CONTINUE
29600 C-----RESULTS-----
29700          IF(N .EQ. 0)GO TO 3
29800          V=(V-U*U/FLOAT(N))/FLOAT(N)
29900          U=U/FLOAT(N)
30000          DO 30 IK=1, MNP*NDI

```

```

30100      A=AMAX0(1,NC(IK))
30200      ALO(IK)=ALO(IK)/A
30300      VGO(IK)=VGO(IK)/A
30400  30    CONTINUE
30500  3     CONTINUE
30600  C-----PRINT RESULTS-----
30700      IMP=(NDI-1)/5+1
30800      IDM=FLOAT(NDI)/FLOAT(IMP)+0.9999
30900      DO 42 IM=1,IMP
31000          WRITE(3,2001)IM
31100          WRITE(5,2001)IM
31200          WRITE(3,2002)U,V,N
31300          WRITE(5,2002)U,V,N
31400          ID1=1+IDM*(IM-1)
31500          ID2=MIN0(ND1,IDM*IM)
31600          WRITE(3,2003)DALPHA,STEP,(IA,ID,ID=ID1,ID2)
31700          WRITE(5,2003)DALPHA,STEP,(IA,ID,ID=ID1,ID2)
31800          WRITE(3,2004)(ALP(ID),ID=ID1,ID2)
31900          WRITE(5,2004)(ALP(ID),ID=ID1,ID2)
32000          WRITE(3,2005)(IA,ID=ID1,ID2)
32100          WRITE(5,2005)(IA,ID=ID1,ID2)
32200          IKO=MNP*(ID1-1)
32300          IKM=IKO+MNP*(ID2-ID1)
32400          DO 43 K=1,MNP
32500              IK1=K+IKO
32600              IK2=K+IKM
32700              WRITE(3,2006)K,(NC(IK),ALO(IK),VGO(IK),IK=IK1,IK2,MN
32800              WRITE(5,2006)K,(NC(IK),ALO(IK),VGO(IK),IK=IK1,IK2,MN
32900  43    CONTINUE
33000  42    CONTINUE
33100  41    CONTINUE
33200  2000  FORMAT(1H,'**DOUBLY DEFINED POINT**DATUM',I4,' X=',
33300  1      F9.4,' Y=',F9.4,' DATUM',I4,' X=',F9.4,' Y=',F9.4)
33400  2001  FORMAT(1H1,53X,'SEMI-VARIOGRAM ',38X,'***PAGE:',I2,/54X,
33500  1      '*****',10X,'(IRREGULAR GRID 2 DIMENSIONS)'/)
33600  2002  FORMAT(1H,' AVERAGE=',F10.5,6X,'VARIANCE=',E11.5,
33700  1      ' NUMBER OF DATA=',I5)
33800  2003  FORMAT(1H,' DIRECTION TOLERANCE=',F4.1,' DEGREES, STEP=',
33900  1      F7.2,/1H,5X,'!',5(A1,5X,'DIRECTION',I2,6X,'!'))
34000  2004  FORMAT(1H,5X,'!',5(3X,F7.1,' DEGREES',5X,'!'))
34100  2005  FORMAT(1H,' LAG !',5(A1,'NC DISTANCE VARIOGRAM!'))
34200  2006  FORMAT(1H,1X,I3,'!',5(I3,1X,F7.2,1X,E11.5,'!'))
34300      RETURN
34400      END

```



APPENDIX L

Variograms of detrended log K values

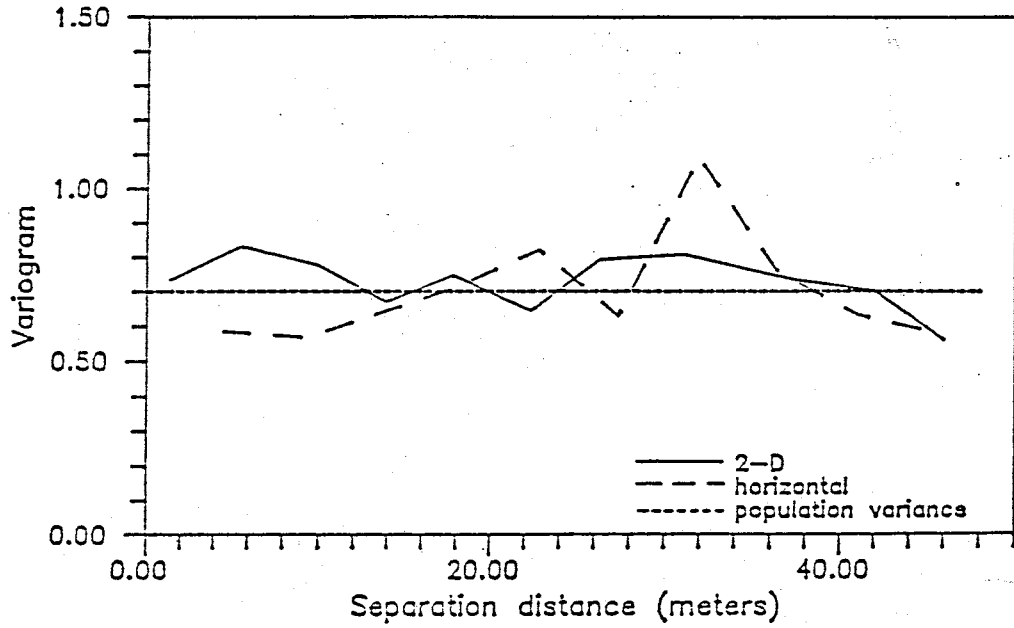


Figure L1. Variograms of detrended log K values from the cross section (0-50 cm depth).

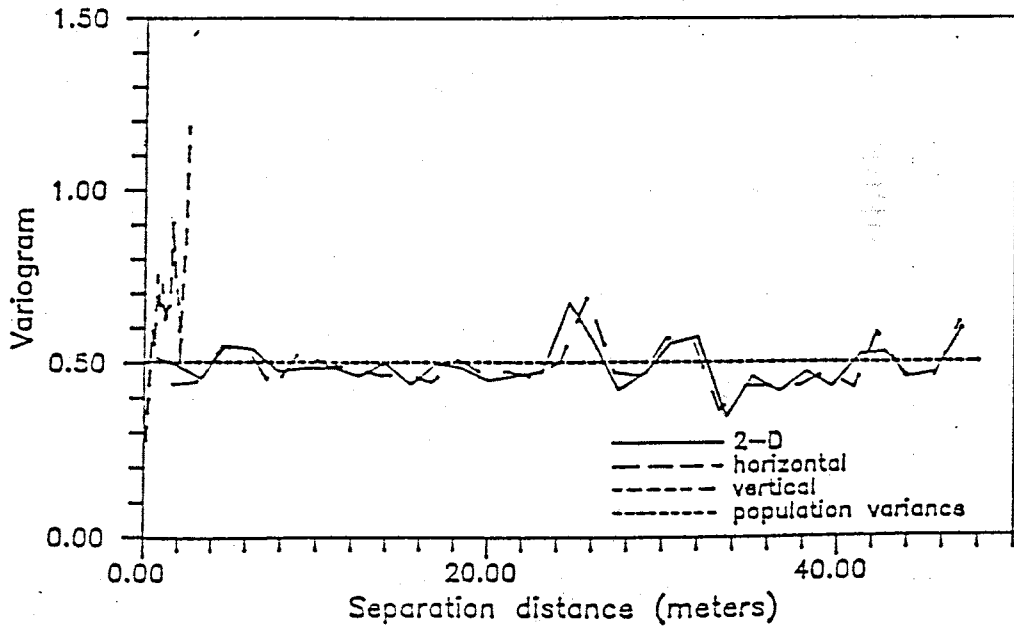


Figure L2. Variograms of detrended log K values from the cross section (50-400 cm depth).

## APPENDIX M

Computer code for program: KRIG

```

C-----
C      THIS PROGRAM SOLVES FOR "KRIGING WEIGHTS" ,LAMBDA(I,J),
C      IN THE SYSTEM GX=Y WHERE G,X AND Y ARE MATRICES.
C      GAMMA(I,J) ARE THE ELEMENTS OF MATRIX 'G'
C      GAMSTA(I,J) ARE THE ELEMENTS OF MATRIX 'Y'
C      WE THEN MAKE PREDICTIONS AND GIVE PREDICTION VARIANCES
C-----
C      VARIABLES:
C      A,B: PARAMETERS TO THE VARIOGRAM FUNCTIONS
C      C: MEASUREMENT ERROR
C      N: THE NUMBER OF X-Y PAIRS (<125)
C      IFLN: CONTAINS THE INPUT DATA FILE NAME
C      FORM1-FORM5: DATA FORMATS FOR THE X,Y AND Z VALUES
C      M1: THE NUMBER OF XP POINTS,<21
C      M2: THE NUMBER OF YP POINTS,<21
C      IFORM: CONTAINS THE ABBREVIATION FOR THE FUNCTIONAL FORM OF
C            THE VARIOGRAM
C      M: THE TOTAL NUMBER OF PREDICTION POINTS (=M1*M2)
C      COPSTA,GAMSTA: CONTAINS THE ELEMENTS OF THE 'Y' MATRIX IN
C            THE GX=Y SYSTEM
C      GAMMA: CONTAINS THE ELEMENTS OF THE G MATRIX IN THE GX=Y
C            SYSTEM. AFTER THE SYSTEM IS SOLVED, GAMSTA CONTAINS
C            THE KRIGING WEIGHTS.
C      ZP: ARRAY CONTAINING THE ESTIMATES
C      VP: ARRAY CONTAINING THE ESTIMATE VARIANCES
C      NOX,NOY: SAME AS M1,M2
C      ZZ: THE 2-DIMENSIONAL BREAKDOWN OF THE ZP ARRAY
C      XYZ,YYY: DUMMY ARRAY USED FOR WRITING OUTPUT TO FILE
C-----
C      DIMENSION X(150),Y(150),XP(450),YP(450),FORM1(15),FORM2(15)
C      DIMENSION FORM5(15),COPSTA(150,450)
C      DIMENSION X1(20),Y1(20),ZZ(20,20)
C      DIMENSION GAMMA(150,150),GAMSTA(150,450),Z(150),ZP(450),VP(450)
C      DIMENSION ICHNG(300),DET(150),SYMSTO(11000)
C      DOUBLE PRECISION IFLN
C      OPEN(UNIT=23,DIALOG)
C      WRITE(5,*)'THIS PROGRAM WRITES TO UNIT 10. YOU MUST DEFINE '
C      WRITE(5,*)'UNIT 10 WHILE IN THE EXEC MODE'
C      TYPE 1050
1050  FORMAT(1X,'WHAT IS THE INPUT FILE NAME: '$)
      ACCEPT 1060,IFLN
1060  FORMAT(A10)
      TYPE 1030
1030  FORMAT(1X,'HOW MANY X-Y PAIRS DO YOU HAVE: '$)
      ACCEPT 1130,N
      WRITE(5,1040)N
1040  FORMAT(1X,'N=',I3)
      TYPE 1070
1070  FORMAT(1X,'WHAT IS THE DATA FORMAT FOR THE X AND Y VALUES?')
      ACCEPT 1170,FORM1
      TYPE 1160
1160  FORMAT(1X,'WHAT IS THE FORMAT FOR THE OBSERVED (Z) VALUES: '$)
      ACCEPT 1170,FORM5
      TYPE 1090
1090  FORMAT(1X,'HOW MANY XP VALUES DO YOU WANT? '$)
      ACCEPT 1130,M1
      TYPE 1091
1091  FORMAT(1X,'WHAT IS THE MINIMUM XP AND THE XP-SPACING?')
      ACCEPT 1131,XPMIN,XPSP

```

```

1131   FORMAT(2F)
      TYPE 1100
1100   FORMAT(1X,'HOW MANY YP VALUES DO YOU WANT?')$)
      ACCEPT 1130,M2
      TYPE 1092
1092   FORMAT(1X,'WHAT IS THE MINIMUM YP AND THE YP-SPACING?')
      ACCEPT 1131,YPMIN,YPSP
      TYPE 1110
1110   FORMAT(1X,'HOW MANY CONTOUR LEVELS DO YOU WANT(<21)?')
      ACCEPT 1130,NOC
1130   FORMAT(I)
1170   FORMAT(15A5)
      TYPE 1180
1180   FORMAT(1X,'CHOOSE THE FUNCTIONAL FORM FOR THE VARIOGRAM'//
1     1X,'LV=LINEAR VARIOGRAM'/1X,'SV=SPHERICAL VARIOGRAM'/1X,
2     'EV=EXPONENTIAL VARIOGRAM'/1X,'GV=GAUSSIAN VARIOGRAM'/
3     1X,'EVM=EXPONENTIAL VARIOGRAM WITH MEASUREMENT ERROR'//
4     1X,'FUNCTIONAL FORM: '$)
      ACCEPT 1190,IFORM
      IF(IFORM .EQ. 'EV')WRITE(3,5500)
      IF(IFORM .EQ. 'EVM')WRITE(3,5505)
      IF(IFORM .EQ. 'GV')WRITE(3,5600)
      IF(IFORM .EQ. 'LV')WRITE(3,5700)
      IF(IFORM .EQ. 'SV')WRITE(3,5800)
      IF(IFORM .EQ. 'EV')WRITE(5,5500)
      IF(IFORM .EQ. 'EVM')WRITE(5,5505)
      IF(IFORM .EQ. 'GV')WRITE(5,5600)
      IF(IFORM .EQ. 'LV')WRITE(5,5700)
      IF(IFORM .EQ. 'SV')WRITE(5,5800)
1190   FORMAT(A3)
      TYPE 1000
1000   FORMAT(1X,'WHAT IS THE VALUE OF A: '$)
      ACCEPT 1020,A
      TYPE 1010
1010   FORMAT(1X,'WHAT IS THE VALUE OF B: '$)
      ACCEPT 1020,B
      TYPE 1015
1015   FORMAT(1X,'WHAT IS THE VALUE OF C: '$)
      ACCEPT 1020,C
1020   FORMAT(F)
1999   TYPE 2000
2000   FORMAT(1X,'DO YOU WANT THE G AND Y MATRICES PRINTED?')
      ACCEPT 1210,IMAT
      TYPE 2001
2001   FORMAT(1X,'DO YOU WANT THE WEIGHTS PRINTED?')
      ACCEPT 1210,IWT
      TYPE 1200
1200   FORMAT(1X,'DO YOU WANT TO CHANGE ANY OF THE ABOVE INFORMATION?')
      ACCEPT 1210,IREP
1210   FORMAT(A1)
      IF(IREP .EQ. 'Y')GO TO 1
5500   FORMAT(/1X,'EXPONENTIAL VARIOGRAM USED: B*(1-EXP(-R/A))')
5505   FORMAT(/1X,'EXPONENTIAL VARIOGRAM W/ ERROR USED: B*(1-EXP(-R/A))+C
1     ')
5600   FORMAT(/1X,'GAUSSIAN VARIOGRAM USED: B*(1-EXP(R*R/(A*A)))')
5700   FORMAT(/1X,'LINEAR VARIOGRAM USED: B*(ABS(R)**A)')
5800   FORMAT(/1X,'SPHERICAL VARIOGRAM USED: B*(1.5*R/A-.5*(R/A)**3')
      WRITE(3,5900)A,B,C
      WRITE(5,5900)A,B,C
5900   FORMAT(/2X,'A=',F10.5,2X,'B=',F10.5,2X,'C=',F10.5)

```

```

C-----INPUT-----
OPEN(UNIT=22,ACCESS='SEQIN',FILE=IFLN)
READ(22,FORM1)(X(I),I=1,N)
READ(22,FORM1)(Y(I),I=1,N)
READ(22,FORM5)(Z(I),I=1,N)
CLOSE(UNIT=22,FILE=IFLN)
M=M1*M2
WRITE(3,1280)
WRITE(5,1280)
1280 1  FORMAT(/1X,70('-')/1X,'OBSERVED (X,Y,Z) VALUES'///,
        1  12X,'X-LOC.',4X,'Y-LOC.',4X,'Z-VALUE')
        DO 120 I=1,N
            WRITE(3,1290)X(I),Y(I),Z(I)
            WRITE(5,1290)X(I),Y(I),Z(I)
120    CONTINUE
1290  FORMAT(10X,3(F10.4))
C-----SET UP THE X1 Y1 ARRAYS-----
DO 7000 IK1=1,M1
        X1(IK1)=XPMIN+(IK1-1)*XPSP
7000  CONTINUE
        DO 7010 IK2=1,M2
            Y1(IK2)=YPMIN+(IK2-1)*YPSY
7010  CONTINUE
C-----CONSTRUCT AND SOLVE THE GX=Y SYSTEM-----
CALL COMPUT(A,B,C,N,M1,M2,M,X,Y,X1,Y1,XP,YP,COPSTA,GAMSTA,GAMMA,
1  SYMSTO,IFORM,IMAT,IWT)
C-----MAKE ESTIMATES AND GIVE ESTIMATE VARIANCES-----
CALL PREDIC(N,M,GAMSTA,COPSTA,VP,ZP,Z)
C-----OUTPUT THE RESULTS-----
CALL GRAPH(M1,M2,X1,Y1,ZP,ZZ,NOC,SCALE,NAMES,1,IMAP)
CALL GRAPH(M1,M2,X1,Y1,VP,ZZ,NOC,SCALE,NAMES,2,IMAP)
9999  STOP
      END

```

```

SUBROUTINE COMPUT(A,B,C,N,M1,M2,M,X,Y,X1,Y1,XP,YP,COPSTA,GAMSTA,
1 GAMMA,SYMSTO,IFORM,IMAT,IWT)
DIMENSION X1(20),Y1(20),XP(450),YP(450),COPSTA(150,450)
DIMENSION GAMMA(150,150),SYMSTO(150),ICHNG(300),DET(150),X(150)
DIMENSION GAMSTA(150,450),Y(150)
ALINVA(A,B,R)=B*ABS(R)**A
SPEVAR(A,B,R)=B*((3*ABS(R))/(2*A)-ABS(R)**3/(A*A*A*2))
EVAR(A,B,R)=B*(1-EXP(-ABS(R)/A))
EMVAR(A,B,C,R)=B*(1-EXP(-ABS(R)/A))+C
GASVAR(A,B,R)=B*(1-EXP(-(ABS(R)*ABS(R))/(A*A)))
C-----CONSTRUCT THE XP-YP VECTORS-----
L=0
DO 5 I=1,M1
DO 5 J=1,M2
    II=I
    JJ=J
    L=L+1
    XP(L)=X1(II)
    YP(L)=Y1(JJ)
5 CONTINUE
C-----CONSTRUCT THE 'G' AND 'Y' MATRICES-----
DO 10 J=1,M
DO 10 I=1,N+1
    COPSTA(I,J)=0.0
    GAMSTA(I,J)=0.0
10 CONTINUE
DO 15 I=1,N+1
DO 15 J=1,N+1
    GAMMA(I,J)=0.0
15 CONTINUE
DO 20 J=1,M
DO 20 I=1,N+1
    II=I
    JJ=J
    R=((X(II)-XP(JJ))*(X(II)-XP(JJ))+(Y(II)-YP(JJ))*
1 (Y(II)-YP(JJ)))**.5
    IF(IFORM.EQ.'LV')GAMSTA(I,J)=ALINVA(A,B,R)
    IF(IFORM.EQ.'SV')GAMSTA(I,J)=SPEVAR(A,B,R)
    IF((IFORM.EQ.'SV').AND.((A-R).LT.0.0))
1 GAMSTA(I,J)=B
    IF(IFORM.EQ.'EV')GAMSTA(I,J)=EVAR(A,B,R)
    IF(IFORM.EQ.'EVM')GAMSTA(I,J)=EMVAR(A,B,C,R)
    IF(IFORM.EQ.'GV')GAMSTA(I,J)=GASVAR(A,B,R)
    IF(I.EQ.N+1)GAMSTA(I,J)=1.0
    IF(IFORM.EQ.'LV')COPSTA(I,J)=ALINVA(A,B,R)
    IF(IFORM.EQ.'SV')COPSTA(I,J)=SPEVAR(A,B,R)
    IF((IFORM.EQ.'SV').AND.((A-R).LT.0.0))
1 COPSTA(I,J)=B
    IF(IFORM.EQ.'EV')COPSTA(I,J)=EVAR(A,B,R)
    IF(IFORM.EQ.'EVM')COPSTA(I,J)=EMVAR(A,B,C,R)
    IF(IFORM.EQ.'GV')COPSTA(I,J)=GASVAR(A,B,R)
    IF(I.EQ.N+1)COPSTA(I,J)=1.0
20 CONTINUE
DO 25 J=1,N+1
DO 25 I=1,N+1
    II=I
    JJ=J
    R=((X(II)-X(JJ))*(X(II)-X(JJ))+(Y(II)-Y(JJ))*(Y(II)-
1 Y(JJ)))**.5
    IF(IFORM.EQ.'LV')GAMMA(I,J)=ALINVA(A,B,R)

```

```

      IF(IFORM .EQ. 'SV')GAMMA(I,J)=SPEVAR(A,B,R)
      IF((IFORM .EQ. 'SV').AND.((A-R) .LT. 0.0))
1      GAMMA(I,J)=B
      IF(IFORM .EQ. 'EV')GAMMA(I,J)=EVAR(A,B,R)
      IF(IFORM .EQ. 'EVM')GAMMA(I,J)=EMVAR(A,B,C,R)
      IF((I .EQ. N+1).OR.(J .EQ. N+1))GAMMA(I,J)=1.0
      IF(I .EQ. J)GAMMA(I,J)=0.0
25      CONTINUE
C-----CONSTRUCT THE SYMMETRIC STORAGE VECTOR-----
      CALL VCVTFS(GAMMA,N+1,150,SYMSTO)
35      CONTINUE
C-----OUTPUT-----
      IF(IMAT .NE. 'Y') GO TO 55
      WRITE(3,1220)
      WRITE(5,1220)
1220      FORMAT(25X,'SOLVING GX=Y SYSTEM',/,1X,70('-'),/,1X,
1      'G MATRIX',/)
      DO 40 I=1,N+1
          WRITE(3,1270)(GAMMA(I,J),J=1,N+1)
          WRITE(5,1270)(GAMMA(I,J),J=1,N+1)
40      CONTINUE
      WRITE(3,1230)
      WRITE(5,1230)
1230      FORMAT(/1X,70('-')//1X,'Y MATRIX'//)
      DO 50 I=1,N+1
          WRITE(3,1270)(GAMSTA(I,J),J=1,M)
          WRITE(5,1270)(GAMSTA(I,J),J=1,M)
50      CONTINUE
C-----SOLVE THE SYSTEM AND OUTPUT THE RESULTS-----
55      CALL LEQLS(SYMSTO,N+1,GAMSTA,M,150,0,ICHNG,DET,IER)
      IF(IWT .NE. 'Y') GO TO 65
      WRITE(3,1250)
      WRITE(5,1250)
1250      FORMAT(/70('-')/1X,'X MATRIX (KRIGING WEIGHTS)'//)
      DO 60 I=1,N+1
          WRITE(3,1270)(GAMSTA(I,J),J=1,M)
          WRITE(5,1270)(GAMSTA(I,J),J=1,M)
60      CONTINUE
1270      FORMAT(1X,200(F10.4))
65      RETURN
      END

```

```
SUBROUTINE PREDIC(N,M,GAMSTA,COPSTA,VP,ZP,Z)
DIMENSION GAMSTA(150,450),COPSTA(150,450),VP(450),ZP(450),Z(150)
DO 110 J=1,M
  SUM1=0.0
  SUM2=0.0
  DO 100 I=1,N
    SUM1=SUM1+GAMSTA(I,J)*Z(I)
    SUM2=SUM2+GAMSTA(I,J)*COPSTA(I,J)
100  CONTINUE
    ZP(J)=SUM1
    VP(J)=SUM2+GAMSTA(N+1,J)
    IF(VP(J).LT.0.)VP(J)=0.0
    VP(J)=SQRT(VP(J))
110  CONTINUE
    RETURN
    END
```

```

SUBROUTINE GRAPH(NOX,NOY,X,Y,ZP,ZZ,NOC,SCALE,NAMES,K,IMAT)
DIMENSION X(12),Y(12),ZZ(20,20),NZ(20,20),ZP(450),XYZ(0:19)
2000 IF(K.EQ.2) GO TO 5000
WRITE(3,1010)
WRITE(5,1010)
1010 FORMAT(/5X,'X-PREDICTION LOCATIONS'//)
WRITE(3,1030)(X(I),I=1,NOX)
WRITE(5,1030)(X(I),I=1,NOX)
WRITE(3,1020)
WRITE(5,1020)
1020 FORMAT(/5X,'Y-PREDICTION LOCATIONS'//)
WRITE(3,1030)(Y(I),I=1,NOY)
WRITE(5,1030)(Y(I),I=1,NOY)
WRITE(3,1040)
WRITE(5,1040)
1040 FORMAT(1H1,/5X,'CONTOURED PREDICTED VALUES. THESE AND THE KRIGING
1 VARIANCES ARE OUTPUT IN A 2-D ARRAY WITH THE USUAL KIND OF
1 CO-ORDINATE SYSTEM--MINIMUM X-Y VALUES AT THE LOWER LEFT.//)
IF(IK.LT.2)GO TO 3100
5000 WRITE(3,1050)
WRITE(5,1050)
1050 FORMAT(1H1,/5X,'CONTOURED KRIGING STANDARD DEVIATIONS'//)
C-----CONSTRUCT THE ZZ ARRAY -----
3100 ZCUT=ZP(1)
ZMIN=ZP(1)
DO 20 I=2,NOX*NOY
IF(ZP(I).GT.ZCUT)ZCUT=ZP(I)
IF(ZP(I).LT.ZMIN)ZMIN=ZP(I)
20 CONTINUE
DELZ=(ZCUT-ZMIN)/(FLOAT(NOC)-1.0)
WRITE(3,2300)DELZ
WRITE(5,2300)DELZ
2300 FORMAT(1X,/,/,2X,'DELTA INTERVAL FOR CONTOUR ',F10.5,
1 //,2X,'CODE VALUE')
DO 301 I=1,NCC
CSTEP=ZMIN+(I-1)*DELZ
WRITE(3,1000)I-1,CSTEP
WRITE(5,1000)I-1,CSTEP
C USED VARIABLE 'XYZ' TO SAVE CSTEP INTO AN ARRAY
XYZ(I-1)=CSTEP
301 CONTINUE
1000 FORMAT(5X,I2,2X,E10.4)
XSP=X(2)-X(1)
YSP=Y(2)-Y(1)
WRITE(3,4000)X(1),Y(1),XSP,YSP
WRITE(5,4000)X(1),Y(1),XSP,YSP
4000 FORMAT(/,5X,'LOWER LEFT CO-ORDINATE=',2F15.4,/,
1 5X,'XSPACE=',F10.4,2X,'YSPACE=',F10.4,/)
3000 L=0
DO 10 I=1,NOX
DO 10 J=1,NOY
L=L+1
NZ(I,J)=(ZP(L)+DELZ/2.-ZMIN)/DELZ
10 CONTINUE
WRITE(3,4010)
4010 FORMAT(1H1,2X,60('-'))
WRITE(5,4011)
4011 FORMAT(1H1,1X,60('-'))
DO 30 J=NOY,1,-1
WRITE(3,1031) (NZ(I,J), I=1,NOX)

```



```
WRITE(5,1032) (NZ(I,J) ,I=1,NOX)
30 CONTINUE
WRITE(23,*) ' X Y '
DO 1 J=NOY,1,-1
    DO 2 I=1,NOX
        WRITE(23,1033)X(I),Y(J),XYZ(NZ(I,J))
2 CONTINUE
1 CONTINUE
1030 FORMAT(1X,/,200(F10.4))
1031 FORMAT(2X,'!',/,2X,'!',25(I3))
1032 FORMAT(2X,'!',2X,20(I3))
1033 FORMAT(F17.5,F17.5,F17.5)
RETURN
END
```

## APPENDIX N

Computer code for program: VALID

```

C-----
C      THIS PROGRAM SOLVES FOR "KRIGING WEIGHTS" ,LAMBDA(I,J),
C      IN THE SYSTEM GX=Y WHERE G,X AND Y ARE MATRICES.
C      GAMMA(I,J) ARE THE ELEMENTS OF MATRIX 'G'
C      GAMSTA(I,J) ARE THE ELEMENTS OF MATRIX 'Y'
C      WE THEN MAKE PREDICTIONS AND GIVE PREDICTION VARIANCES
C-----
C      VARIABLES:
C      A,B: PARAMETERS TO THE VARIOGRAM FUNCTIONS
C      N: THE NUMBER OF X-Y PAIRS (<125)
C      IFLN: CONTAINS THE INPUT DATA FILE NAME
C      FORM1-FORM5: DATA FORMATS FOR THE X,Y AND Z VALUES
C      M1: THE NUMBER OF XP POINTS,<21
C      M2: THE NUMBER OF YP POINTS,<21
C      IFORM: CONTAINS THE ABBREVIATION FOR THE FUNCTIONAL FORM OF
C            THE VARIOGRAM
C      M: THE TOTAL NUMBER OF PREDICTION POINTS (=M1*M2)
C      COPSTA,GAMSTA: CONTAINS THE ELEMENTS OF THE 'Y' MATRIX IN
C            THE GX=Y SYSTEM
C      GAMMA: CONTAINS THE ELEMENTS OF THE G MATRIX IN THE GX=Y
C            SYSTEM. AFTER THE SYSTEM IS SOLVED, GAMSTA CONTAINS
C            THE KRIGING WEIGHTS.
C      ZP: ARRAY CONTAINING THE ESTIMATES
C      VP: ARRAY CONTAINING THE ESTIMATE VARIANCES
C      NOX,NOY: SAME AS M1,M2
C      ZZ: THE 2-DIMENSIONAL BREAKDOWN OF THE ZP ARRAY
C-----
      DIMENSION X(150),Y(150),FORM1(15),FORM2(15),XP(150),YP(150)
      DIMENSION FORM5(15),COPSTA(150,150),GAMST1(150,150),ZN(150)
      DIMENSION GAMMA(150,150),GAMSTA(150,150),Z(150),ZP(150),VP(150)
      DIMENSION ICHNG(300),DET(150),SYMSTO(11000),GAMM1(150,150)
      DIMENSION ZZP(1),DIFF(150),VVP(1)
      DOUBLE PRECISION IFLN
1      TYPE 1050
1050     FORMAT(1X,'WHAT IS THE INPUT FILE NAME: '$)
      ACCEPT 1060,IFLN
1060     FORMAT(A10)
      TYPE 1030
1030     FORMAT(1X,'HOW MANY X-Y PAIRS DO YOU HAVE: '$)
      ACCEPT 1130,N
      WRITE(5,1040)N
1040     FORMAT(1X,'N=',I3)
      TYPE 1070
1070     FORMAT(1X,'WHAT IS THE DATA FORMAT FOR THE X AND Y VALUES?')
      ACCEPT 1170,FORM1
      TYPE 1160
1160     FORMAT(1X,'WHAT IS THE FORMAT FOR THE OBSERVED (Z) VALUES: '$)
      ACCEPT 1170,FORM5
1130     FORMAT(I)
1170     FORMAT(15A5)
      TYPE 1180
1180     FORMAT(1X,'CHOOSE THE FUNCTIONAL FORM FOR THE VARIOGRAM'//
1      1X,'LV=LINEAR VARIOGRAM'/1X,'SV=SPHERICAL VARIOGRAM'/1X,
2      'EV=EXPONENTIAL VARIOGRAM'/1X,'GV=GAUSSIAN VARIOGRAM'//
3      1X,'FUNCTIONAL FORM: '$)
      ACCEPT 1190,IFORM
      IF(IFORM .EQ. 'EV')WRITE(3,5500)
      IF(IFORM .EQ. 'GV')WRITE(3,5600)
      IF(IFORM .EQ. 'LV')WRITE(3,5700)
      IF(IFORM .EQ. 'SV')WRITE(3,5800)

```

```

IF(IFORM .EQ. 'EV')WRITE(5,5500)
IF(IFORM .EQ. 'GV')WRITE(5,5600)
IF(IFORM .EQ. 'LV')WRITE(5,5700)
IF(IFORM .EQ. 'SV')WRITE(5,5800)
1190  FORMAT(A2)
      TYPE 1000
1000  FORMAT(1X,'WHAT IS THE VALUE OF A: '$)
      ACCEPT 1020,A
      TYPE 1010
1010  FORMAT(1X,'WHAT IS THE VALUE OF B: '$)
      ACCEPT 1020,B
1020  FORMAT(F)
      TYPE 1200
1200  FORMAT(1X,'DO YOU WANT TO CHANGE ANY OF THE ABOVE INFORMATION?')
      ACCEPT 1210,IREP
1210  FORMAT(A1)
      IF(IREP .EQ. 'Y')GO TO 1
5500  FORMAT(/1X,'EXPONENTIAL VARIOGRAM USED: B*(1-EXP(-R/A))')
5600  FORMAT(/1X,'GAUSSIAN VARIOGRAM USED: B*(1-EXP(R*R/(A*A))')
5700  FORMAT(/1X,'LINEAR VARIOGRAM USED: B*(ABS(R)**A)')
5800  FORMAT(/1X,'SPHERICAL VARIOGRAM USED: B*(1.5*R/A-.5*(R/A)**3')
      WRITE(3,5900)A,B
      WRITE(5,5900)A,B
5900  FORMAT(/2X,'A=',F10.5,2X,'B=',F10.5)
C-----INPUT-----
      OPEN(UNIT=22,ACCESS='SEQIN',FILE=IFLN)
      READ(22,FORM1)(X(I),I=1,N)
      READ(22,FORM1)(Y(I),I=1,N)
      READ(22,FORM5)(Z(I),I=1,N)
      CLOSE(UNIT=22,FILE=IFLN)
1290  FORMAT(10X,3(F10.4))
      DO 7000 IK1=1,N
           XP(IK1)=X(IK1)
           YP(IK1)=Y(IK1)
7000  CONTINUE
      CALL COMPUT(A,B,N,N,X,Y,XP,YP,GAMSTA,GAMMA,IFORM)
      N1=N-1
      LIS=2
      LJS=2
      IAL=2
      JAL=2
      IA2=N+1
      JA2=N+1
      DO 8000 IDEL=1,N
           LI=0
           DO 8100 LIP=LIS,2
                DO 8110 II=IAL,IA2
                     LI=LI+1
                     LJ=0
                     DO 8120 LJP=LJS,2
                          DO 8130 JJ=JAL,JA2
                               LJ=LJ+1
                               GAMM1(LI,LJ)=GAMMA(II,JJ)
C      WRITE(5,10100)(GAMM1(LI,LJ),LI,LJ,II,JJ)
10100  FORMAT(2X,'GAMM1=',F10.5,2X,'LI,LJ,II,JJ:',4I5)
8130  CONTINUE
           JAL=IDEL+1
           JA2=N+1
8120  CONTINUE
      GAMST1(LI,1)=GAMSTA(II,IDEL)

```

```

                                COPSTA(LI,1)=GAMST1(LI,1)
                                ZN(LI)=Z(II)
C      WRITE(5,5000)(ZN(LI),GAMST1(LI,1),LI,II)
5000   FORMAT(2X,'ZN(LI)=',F10.5,2X,'GAMST1=',F10.6,2X,'LI=',I3,
1      2X,'II=',2X,I3)
      IF(IDEL.EQ.1)GO TO 8110
      JAL=1
      JA2=IDEL-1
8110   CONTINUE
      IAL=IDEL+1
      IA2=N+1
8100   CONTINUE
      LIS=1
C      WRITE(5,10000)(ZN(I),I=1,N)
10000  FORMAT(2X,8F8.4)
      LJS=1
      IAL=1
      IA2=IDEL
      JAL=1
      JA2=IDEL
      CALL VCVTFS(GAMM1,N,150,SYMSTO)
      CALL LEQLS(SYMSTO,N,GAMST1,1,150,0,ICHNG,DET,IER)
      CALL PREDIC(N1,1,GAMST1,COPSTA,VVP,ZZP,ZN)
      VP(IDEL)=VVP(1)
      ZP(IDEL)=ZZP(1)
C      WRITE(5,9666)VP(IDEL),ZP(IDEL)
9666   FORMAT(1H1,F10.5,2X,F10.5)
8000   CONTINUE
      WRITE(5,9600)
      WRITE(3,9600)
9600   FORMAT(1H1,2X,'X-CO-ORD',4X,'Y-CO-ORD',4X,'OBSERVED',4X,
1      'PREDICTED',4X,'KRIGING-SIGMA')
      DO 9610 I=1,N
          WRITE(5,9605)X(I),Y(I),Z(I),ZP(I),VP(I)
          WRITE(3,9605)X(I),Y(I),Z(I),ZP(I),VP(I)
9610   CONTINUE
9605   FORMAT(3X,F8.3,4X,F8.3,2X,F10.4,3X,F10.4,4X,F10.5)
      SUM=0
      VAR=0
      DO 9615 I=1,N
          DIFF(I)=ZP(I)-Z(I)
          SUM=SUM+DIFF(I)
          DIFF(I)=DIFF(I)/VP(I)
          VAR=VAR+DIFF(I)*DIFF(I)
9615   CONTINUE
      SUM=SUM/N
      VAR=VAR/N
      WRITE(5,9630)
      WRITE(3,9630)
9630   FORMAT(2X,/,2X,'OBSERVED PREDICTED NORMALIZED-DIFF.')
      WRITE(5,9635)((Z(I),ZP(I),DIFF(I)),I=1,N)
      WRITE(3,9635)((Z(I),ZP(I),DIFF(I)),I=1,N)
      WRITE(5,9620)SUM,VAR
      WRITE(3,9620)SUM,VAR
9620   FORMAT(2X,/,5X,'MEAN OF DIFFERENCE=',F10.5,/,5X,
1      'AVERAGE SQUARED NORMALIZED DIFFERENCES=',F10.5)
9635   FORMAT(2X,F8.4,2X,F8.4,4X,F10.5)
9999   STOP
      END

```

```

SUBROUTINE COMPUT(A,B,N,M,X,Y,XP,YP,GAMSTA,GAMMA,IFORM)
DIMENSION XP(150),YP(150)
DIMENSION GAMMA(150,150),ICHNG(300),DET(150),X(150)
DIMENSION GAMSTA(150,150),Y(150)
ALINVA(A,B,R)=B*ABS(R)**A
SPEVAR(A,B,R)=B*((3*ABS(R))/(2*A)-ABS(R)**3/(A*A*A*2))
EVAR(A,B,R)=B*(1-EXP(-ABS(R)/A))
GASVAR(A,B,R)=B*(1-EXP(-(ABS(R)*ABS(R))/(A*A)))
C-----CONSTRUCT THE 'G' AND 'Y' MATRICES-----
DO 10 J=1,M
DO 10 I=1,N+1
    GAMSTA(I,J)=0.0
10 CONTINUE
DO 15 I=1,N+1
DO 15 J=1,N+1
    GAMMA(I,J)=0.0
15 CONTINUE
DO 20 J=1,M
DO 20 I=1,N+1
    II=I
    JJ=J
    R=((X(II)-XP(JJ))*(X(II)-XP(JJ))+(Y(II)-YP(JJ))*
1 (Y(II)-YP(JJ)))**.5
    IF(IFORM .EQ. 'LV')GAMSTA(I,J)=ALINVA(A,B,R)
    IF(IFORM .EQ. 'SV')GAMSTA(I,J)=SPEVAR(A,B,R)
1 IF((IFORM .EQ. 'SV').AND.((A-R) .LT. 0.0))
    GAMSTA(I,J)=B
    IF(IFORM .EQ. 'EV')GAMSTA(I,J)=EVAR(A,B,R)
    IF(IFORM .EQ. 'GV')GAMSTA(I,J)=GASVAR(A,B,R)
    IF(I .EQ. N+1)GAMSTA(I,J)=1.0
20 CONTINUE
DO 25 J=1,N+1
DO 25 I=1,N+1
    II=I
    JJ=J
    R=((X(II)-X(JJ))*(X(II)-X(JJ))+(Y(II)-Y(JJ))*(Y(II)-
1 Y(JJ)))**.5
    IF(IFORM .EQ. 'LV')GAMMA(I,J)=ALINVA(A,B,R)
    IF(IFORM .EQ. 'SV')GAMMA(I,J)=SPEVAR(A,B,R)
1 IF((IFORM .EQ. 'SV').AND.((A-R) .LT. 0.0))
    GAMMA(I,J)=B
    IF(IFORM .EQ. 'EV')GAMMA(I,J)=EVAR(A,B,R)
    IF(IFORM .EQ. 'GV')GAMMA(I,J)=GASVAR(A,B,R)
    IF((I .EQ. N+1).OR.(J .EQ. N+1))GAMMA(I,J)=1.0
25 CONTINUE
65 RETURN
END

```

```
SUBROUTINE PREDIC(N,M,GAMSTA,COPSTA,VP,ZP,Z)
DIMENSION GAMSTA(150,150),COPSTA(150,150),VP(1),ZP(1),Z(150)
DO 110 J=1,M
    SUM1=0.0
    SUM2=0.0
    DO 100 I=1,N
        SUM1=SUM1+GAMSTA(I,J)*Z(I)
        SUM2=SUM2+GAMSTA(I,J)*COPSTA(I,J)
100    CONTINUE
        ZP(J)=SUM1
        VP(J)=SUM2+GAMSTA(N+1,J)
        IF(VP(J).LT.0.)VP(J)=0.0
        VP(J)=SQRT(VP(J))
110    CONTINUE
        RETURN
        END
```